# POLITECNICO DI TORINO

Dipartimento di Ingegneria Meccanica e Aerospaziale

Corso di Laurea Magistrale in Ingegneria Meccanica



Politecnico di Torino

Master of Science Thesis

## Thermal-hydraulic and thermo-mechanical analysis and design optimization of the neutralizer for the Neutral Beam Injection system of the Divertor Tokamak Test (DTT) facility


**Supervisors:**

Prof. Roberto Zanino
Prof. Giorgio Zavarise
Dr. Roberto Bonifetto
Dr. Andrea Zappatore

**Candidate:**

Schito Fabia



Academic Year 2020/2021

October 2021

*Remember to look up at the stars and not down at your feet. And however difficult life may seem, there is always something you can do and succeed at.*

*(Stephen Hawking)*

# Abstract

Nuclear fusion promises to be a sustainable, reliable and safe energy source. In Italy, the DTT S.c.a.r.l. is actively engaged on this front with a project, proposed by ENEA and supported by EUROfusion, which has as its goal the construction, at the ENEA research center in Frascati, of a tokamak fusion experiment, aimed at testing possible solutions for the divertor, one if not the most critical component of ITER (under construction in Cadarache, France) and of the subsequent European DEMO.

The main objective of the divertor is the mitigation of the power exhaust issue, due to the enormous thermal heat flux carried to the walls by the plasma particles. A key role inside the tokamak is played by the high-energy neutral beam injection system (NBI), necessary to heat the plasma to an operating temperature of about 100 million degrees.

The purpose of this work is the analysis and the design of one of the key components of the NBI: the neutralizer. This component has the task of neutralizing the D+ ion beam, accelerated towards the vacuum chamber of the tokamak, in order to allow the desired penetration of the beam to the central part of the plasma. The thermal loads due to the interaction between the deuterium beam and the walls (in CuCrZr) of the neutralizer make it necessary to have an ad-hoc refrigeration system for the neutralizer. The relatively low cost and the simplicity of supply and management have suggested the use of pressurized demineralized water as the most suitable heat transfer fluid.

Starting from the conceptual model of the neutralizer provided by the *DTT S.c.a.r.l.*, the initially foreseen geometric configuration is first studied, in the reference operating conditions indicated in the technical specifications. Computational Thermal Fluid Dynamics (CtFD) analyses are carried out using the StarCCM+ commercial code.

The thermal load due to electrons and deuterium ions is considered; however, since the load due to the stray magnetic field was not considered so far, as it is not known for the time being, a safety margin was assumed from the boiling condition, likely resulting in a rather conservative design.

The results of the analysis highlight the incompatibility of the proposed configuration in the operating conditions with the requirements imposed on the necessary flow rates and pressure losses. On the other hand, there is a large margin of operation from the thermal point of view, so that a series of optimizations is proposed, related on the one hand to the fluid dynamics of the collectors, on the other to the removal of some turbulence promoters and the reduction of the circulating flow.

The optimized solution, from the thermal-hydraulic point of view, is finally subjected to a further verification: using as input the temperature distribution accurately calculated in the CtFD study, it is possible to compute the expected deformations and the thermomechanical stresses, providing possible hints for further optimization of the component in the future engineering design phase.

# Acronyms

| | |
|---|---|
| **ASME** | American Society of Mechanical Engineers |
| **BCs** | Boundary Conditions |
| **BLCs** | Beam Line Components |
| **CAD** | Computer Aided Design |
| **CFD** | Computational Fluid Dynamic |
| **CtFD** | Computational Thermal Fluid Dynamics |
| **DTT** | Divertor Tokamak Test |
| **DTT S.c.a.r.l.** | Divertor Tokamak Test, Società Consortile a Responsabilità Limitata |
| **FE** | Finite Elements |
| **FEA** | Finite Elements Analysis |
| **FEM** | Finite Elements Method |
| **ITER** | International Thermonuclear Experimental Reactor[1] |
| **LEE** | Leading Edge Element |
| **MITICA** | Megavolt ITER Injector and Concept Advancement[2] |
| **NBI** | Neutral Beam Injection |
| **SDC-IC** | Structural Design Criteria for ITER In-vessel Components |
| **TT** | Twisted Tape |

[1] Information at [29]
[2] Information at [24]

# Contents

# List of Figures

# List of Tables

# 0. Introduction

When Talete was developing his philosophy, while he was looking at the stars, he fell into a well. A servant laughed at him, since he was concerned about things in heaven and did not see what was in front of him. Nowadays, engineers and scientists develop technologies, they look at wells – sometimes – and they fall into the stars. Nuclear fusion steals that magic knowledge of the stars in heaven (the process that occurs in them) to bring it on earth: the result will be a powerful state-of-the-art device, a nuclear fusion reactor which reproduces similar reactions to obtain electricity in a clean, safe, sustainable, controllable and almost unlimited way.

The road is long and impervious and still much research is necessary to reach the goal. Considerable developments in this context will take place thanks to the studies conducted through the Divertor Tokamak Test facility (DTT), which will allow to conceptualize different and advanced solutions for the divertor, a key component of the future fusion nuclear reactors, and highlight and solve problems related especially to the power exhaust [1].

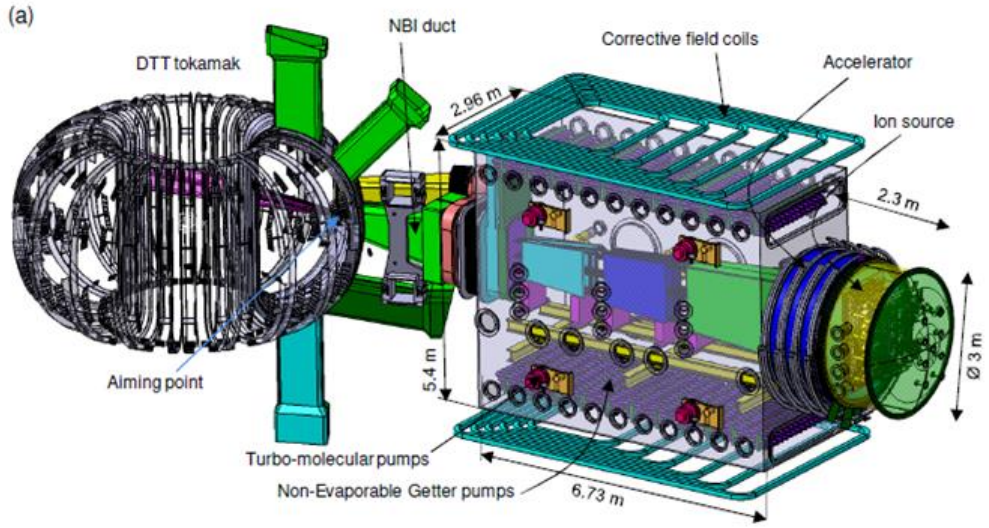


*Figure 1 Overview of the "single source" conceptual design model of DTT facility [2]*

The DTT machine (Figure 1) is equipped with a Neutral Beam Injection System (NBI), which provides deuterium neutrals ($D^0$) with an injected power to the plasma of 10 MW and an energy of 510 keV. Currently, having considered various design solutions, efficiency of the processes, optics of the beam[3] and interaction of fast particles with the plasma and consequent losses, in order to maximize the beam-line performance, DTT

[3] specifically stripping, neutralization and reionization [2].

transport analysis and energetic particles studies have shown that a *single source* NBI with these technical specifications is the best option [2].

From the Ion Source an optimal combination of $D^-$ is conveyed to the Accelerator which provides $D^-$ accelerated beamlets to the Beam Line Components (BLCs). The latter are the main elements of the NBI line: the Neutralizer, the Residual Ion Dump (RID) and the Calorimeter (Figure 2).

In this context, the main purpose of the Neutralizer is to neutralize the accelerated ions received from the Accelerator and it should permit gas injection from 5 points in each slit, similarly to MITICA.

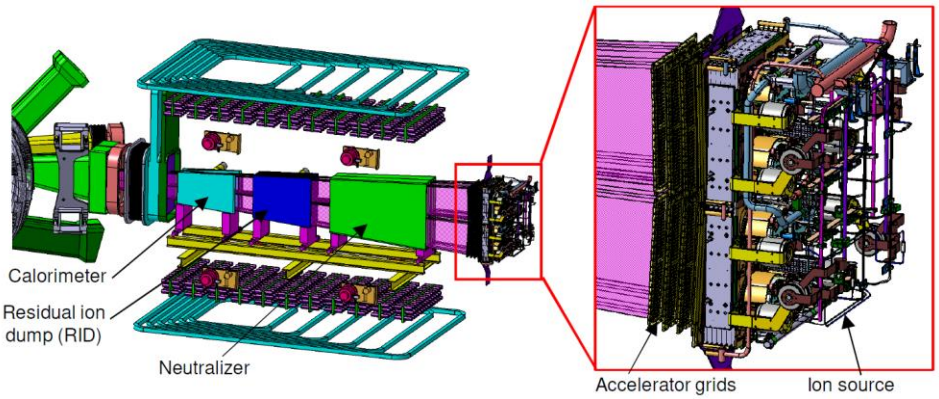


*Figure 2 Ion source, Accelerator and BLCs [2]*

Due to the deuterium beam the whole neutralizer is subjected to a distributed heat flux. The first rudimental conceptual design provided by DTT S.c.a.r.l.[4] is reported in Figure 3.

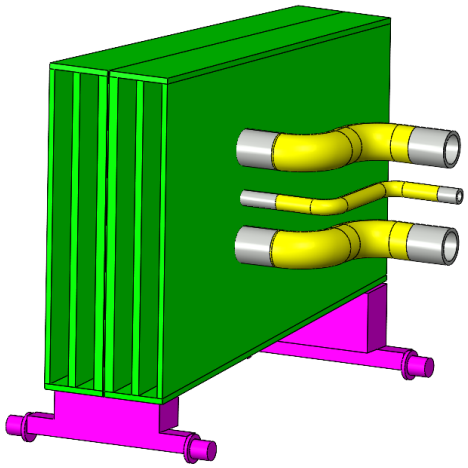

*Figure 3 Rudimental conceptual design provided by DTT S.c.a.r.l.*

[4] Information at [28]

# Aim of the work and methodology

The objective of the present study is to assess the design of the neutralizer of the NBI to:

- cool the system and prevent damage of each component due to non-uniform heat load;
- minimize pressure drop between inlet and outlet of the entire system: according to *DTT S.c.ar.l.* requirements this must not exceed 2 bar;
- minimize the inlet mass flow: according to *DTT S.c.ar.l.* requirements this must not exceed 40 kg/s.

The crucial point of the entire design is the optimization, both of the design itself and of the time required for its development. The work was carried out simultaneously with the latest updates on the study of the thermal loads to which the neutralizer is subjected. Consequently, in the various stages of the design additional information will be progressively added which will allow to recalibrate the results and to conclude the project in the shortest possible time.

The technical roadmap can be summarized in two main steps.

In the first step, only a reference thermal load is known. Starting from the conceptual model provided by *DTT S.c.a.r.l.*, the focus is on the most thermally overloaded component (the Leading Edge Element, LEE) with an accurate Computational Thermal Fluid Dynamic (CtFD) analysis that will indicate the first critical issues of the project. The geometric configuration initially proposed is studied and optimization solutions are provided with particular attention to the fluid dynamics of the manifolds.

In the second phase the thermal load is updated. It is therefore possible to carry out the preliminary optimization of the operational conditions and define the boundary conditions to be applied to the entire neutralizer system, taking into account the fulfillment of the requirements imposed on flow rates and pressure heads. Then the design verification phase follows, ensuring accurate estimation of the temperature distributions and, through Finite Element Method (FEM) analysis, the expected deformations and thermomechanical stresses by analyzing different possible fastening scenarios to provide ideas for the future construction design.

The methodology applied is based on an iterative design. Simulations are performed in StarCCM+: they were fundamental to obtain results without any material construction. Comparisons with experimental correlations from literature, when available, are used to verify their reliability and where possible, common examples borrowed from nuclear engineering applications will be used as a starting point.

# 1. Phase 1 – First analysis with initial overconservative heat load

In the present section initial known heat load is considered. A detailed CtFD study of the LEE is performed, highlighting important results. A CFD analysis of the neutralizer is reported and possible fluid dynamic optimizations are suggested. The initial information on BCs and some specific geometries draw ideas from already existing nuclear engineering designs: MITICA is the main inspiration[5].

## 1.1. LEE sample study

The component initially provided is a sample of the most critical part of the neutralizer: the Leading Edge Element (LEE). The main purpose of the LEE is to absorb the highest heat load and prevent that the delicate structure of the panels behind is deformed or damaged, losing their functionality or, even worst, failing.

Because of the high heat flux due to the neutral beam, according to previous studies conducted on MITICA, a special geometry is adopted at first. A twisted tape insert, with unusual features, is selected for the thermal enhancement.

In principle, since it acts as turbulence promoter, thanks to its geometry it should generate vortices inside the channel and convert the turbulent kinetic energy into thermal energy, enhancing heat transfer both through convection and conduction. A sort of mixing effect is realized and the fluid temperature experiences a lower peak. In fact, the most strenuous challenge in this study is to prevent the coolant from reaching saturation temperature, because, otherwise, localized wear of the material could occur with a consequent reduction in the life of the component. This problem will be taken in consideration also for the other components of the neutralizer in the next chapters.

[5] Several examples can be found analogously in SPIDER and ITER NBI [2].

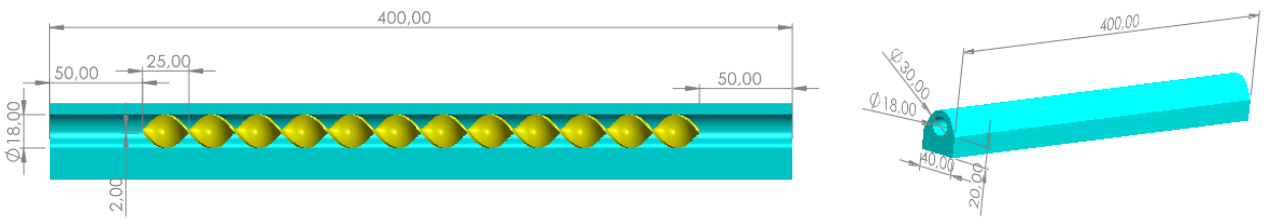


*Figure 4 LEE sample geometry*

| Geometrical input data | | | |
|---|---|---|---|
| L | length of the initial sample | 40 | cm |
| D | inner cylinder diameter | 18 | mm |
| $A_{front}$ | frontal area of the sample where the heat flux is applied | 24886.39 | $mm^2$ |
| **Twisted tape parameters** | | | |
| H | 180 deg twist pitch | 25 | mm |
| d | tape width, coincident with inner cylinder diameter | 18 | mm |
| δ | thickness of twisted tape lamina | 2 | mm |
| y | twist ratio=H/d | 1.389 | |

*Table 1 Geometrical data and definitions of the LEE sample*

In order to accelerate the study, the sample of the LEE (Figure 4), which has a representative geometry (Table 1) with a length of about one quarter with respect to the entire object, is studied first: this is useful not only to understand if, potentially, the entire LEE will have good performance, but also for the successive convergence study. Starting from the Computer Aided Design (CAD) provided, a suitable model for a computational thermal fluid dynamic simulation is realized, after some hypotheses and assumptions.

### 1.1.1. Simulation setup: BCs and materials

The material selected by *DTT S.c.a.r.l.* for the construction of the entire neutralizer, a high heat flux component, is CuCrZr[6], whose thermal properties (i. e. specific heat and thermal conductivity, Table 2) vary with temperature almost linearly, in the considered temperature range (Figure 5). vary with temperature. This choice aims to satisfy the key requirement of exhausting the power loads mitigating temperature levels according to ITER SDC-IC criteria and to guarantee, at the same time, an acceptable mechanical strength. For the sake of simplicity, in this first phase, constant density will be assumed in the solid region.

The relatively low cost and ease of supply and management have suggested the use of pressurized demineralized water as the most suitable heat transfer fluid for the moment. Constant properties are assumed for water in this chapter (Table 2), since, at the considered operative conditions, no significant contribution would be added with a more complex model.

[6] Further specifications for DTT facility can be found in the report [2]. Structural parts and vacuum vessel will be in AISI 304 L, but in this study only CuCrZr is considered.

| CuCrZr | | | | | | | |
|---|---|---|---|---|---|---|---|
| property | symbol | unit | function of | symbol | unit | expression | interval |
| specific heat | $c_p$ | [J/(kg*K)] | temperature | T | [ °C] | 6.32E-06*T$^2$ + 9.49E-02*T + 3.88E+02 | 20 < T < 700°C |
| thermal conductivity | λ | [W/m*K] | temperature | T | [ °C] | 2.11E-07*T$^3$ - 2.83E-04*T$^2$ + 1.38E-01*T + 3.23E+02 | 20 ≤ T ≤ 700°C |
| density | ρ | [kg/m$^3$] | _ | _ | _ | 8940 | |
| Water | | | | | | | |
| specific heat | $c_p$ | [J/(kg*K)] | _ | _ | _ | 4181.72 | |
| thermal conductivity | λ | [W/m*K] | _ | _ | _ | 0.620271 | |
| density | ρ | [kg/m$^3$] | _ | _ | _ | 997.561 | |
| dynamic viscosity | μ | [Pa*s] | _ | _ | _ | 8.89E-04 | |

*Table 2 Materials properties used in Phase 1 for solid and fluid continua modeling*

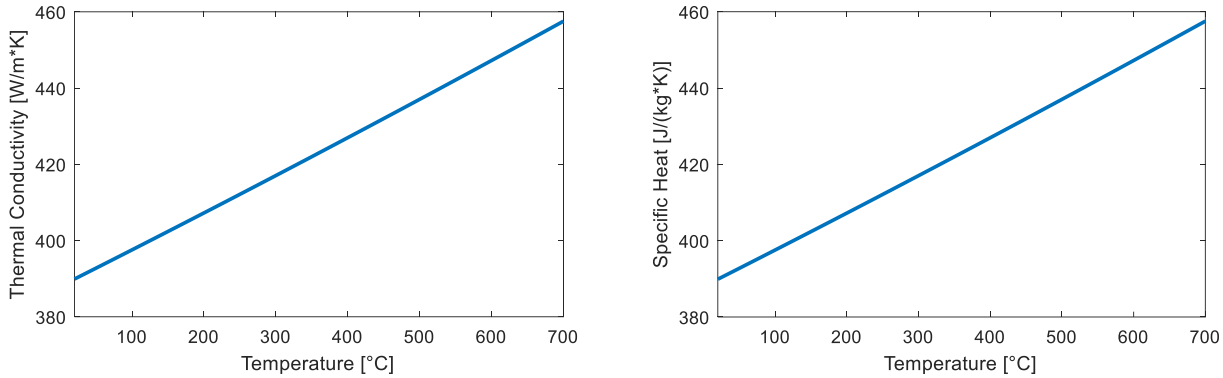


*Figure 5 Specific heat and Thermal conductivity for CuCrZr*

From the fluid dynamic point of view, the nature of the fluid flow is forced convection. This means that, differently from natural convection, heat transfer depends on fluid flow but fluid flow does not depend on the heat transfer and so the two problems can be separated and computational cost reduced by dealing with fluid flow only and adding then the thermal part. This consideration will be relevant not only in this specific part of the study, but also for the successive ones, since lots of simplifications can be made.

Even though the real operation will be pulsed, as it is typical for a tokamak, the problem can be treated conservatively as stationary. Furthermore, thanks to the fact that a liquid is used for the refrigeration system, also considering the operative pressure conditions, incompressible fluid is assumed.

The first, tentative values of pressure and mass flow refer to known data from MITICA [2]. Since high Reynolds are involved, turbulent flow will be considered and, because of the particular geometry and, consequently, of the streamlines, three-dimensional flow simulation is mandatory.

From the thermal point of view, heat flux is applied only to the frontal (curved) surface of the solid, which is directly exposed to the beam and conduction occurs, transferring thermal power to the fluid. At this stage of the study[7], the maximum assumed thermal load (peak of 1.5 MW/m$^2$, [2]) is overconservatively considered as a uniform thermal heat flux applied orthogonally to the surface. Water is supplied at 25°C.

[7] All the known information in this phase is contained in [2].

Boundary conditions are assigned according to these observations[8].

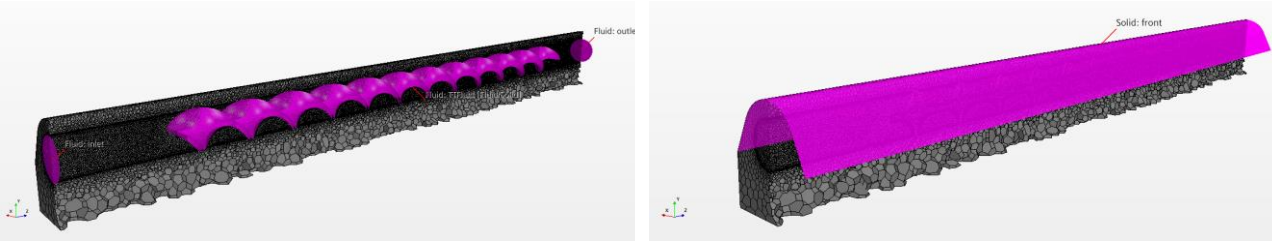


*Figure 6 Boundary regions for the LEE sample*

| Region | Boundary conditions fluid dynamic problem | | | | Boundary conditions thermal problem | | | |
|---|---|---|---|---|---|---|---|---|
| **inlet** | mass flow inlet | $\dot{m}$ | 2 | kg/s | temperature | $T_{in}$ | 25 | °C |
| **outlet** | pressure outlet | $p_{out}$ | 20 | bar | no conduction | | dT/dn=0 | |
| **cylinder, interface** | no slip | $v=v_{wall}$ | 0 | m/s | _ | | | |
| **twisted tape, interface** | no slip | $v=v_{wall}$ | 0 | m/s | _ | | | |
| **frontal surface** | _ | | | | heat flux | $\dot{Q}$ | 1.5 | $MW/m^2$ |
| **other surfaces** | _ | | | | adiabatic | | dT/dn=0 | |

*Table 3 Boundary conditions for fluid dynamic and thermal problem of the LEE sample*

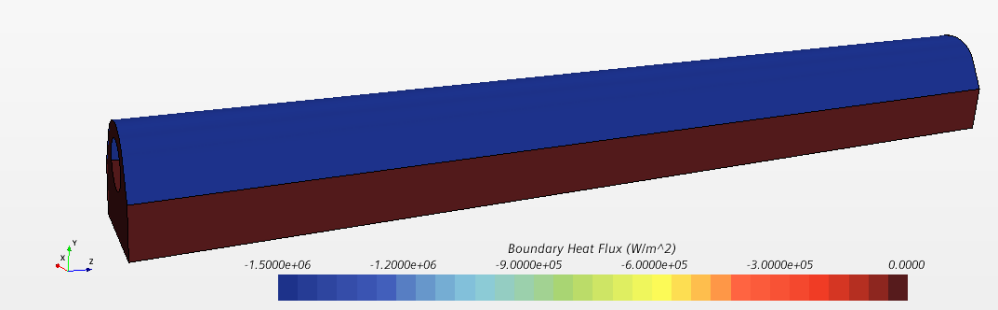


*Figure 7 Boundary heat flux for the LEE sample, given as input*

A coupled numerical model is selected to have robustness and a good convergence rate: this means that continuity, momentum and energy equations are solved together simultaneously as a vector of equations using a pseudo-time-marching approach. By controlling the Courant number, considering the limited geometry of the sample, it is possible to have stability and acceptable simulation time, even a bit faster with respect to segregated model which uses, in general, less memory. With the coupled solver CPU time scales linearly with cell count and so the number of iterations required to solve the flow problem is independent from the mesh size [3], which is very useful in the convergence study.

In addition, the two-equation *k-ω SST Menter* model is chosen, because, due to relevant turbulent phenomena, this model allows a better estimation of wall temperature at the interface between solid and fluid. It solves transport equations for turbulent kinetic energy $k$ and the specific dissipation rate $\omega$ to determine the turbulent eddy viscosity [4]. Differently from the standard version, with the shear-stress transport (SST) Menter suggested as a solution to the sensitivity to free-stream/inlet conditions a blending function to include the cross-diffusion term only far from the walls and not near them [5].

[8] as reported in Table 3, with reference to the surfaces indicated in Figure 6.

In the end, the simulation setup for the LEE sample in StarCCM+ can be summarized as in Table 4.

| Continua Model | |
|---|---|
| Fluid: water | Solid: CuCrZr |
| All y+ Wall Treatment | Constant Density |
| Constant Density | Coupled Solid Energy |
| Coupled Energy | Gradients |
| Coupled Flow | Solid |
| Gradients | Solution Interpolation |
| K-Omega Turbulence | Steady |
| Liquid | Three Dimensional |
| Reynolds-Averaged Navier-Stokes | |
| Solution Interpolation | |
| SST (Menter) K-Omega | |
| Steady | |
| Three Dimensional | |
| Turbulent | |
| Wall Distance | |

*Table 4 Continua Model setup for the LEE sample*

## 1.1.2. Friction factors and Nusselt numbers

To make comparisons with known cases and validate the simulation results, friction factor and Nusselt number are compared to the experimental correlations available in literature[9], with reference to *Manglik* and *Bergles* research [6] in 1991 and 1992.

In the simulation postprocessing, according to [6], the Reynolds number $\boldsymbol{Re}$ referred to inlet values of an empty tube is evaluated using the inner diameter of the tube and surface average velocity at the inlet; The friction factor ($\boldsymbol{f}$) for the twisted tape section is computed from *Blasius* definition [7], [8] using numerical results as

$$f = \frac{\Delta p \left(\frac{D}{\Delta L}\right)}{\rho \frac{v_c^2}{2}} \tag{1.1}$$

where, taken two different sections[10], $\boldsymbol{\Delta p}$ is the pressure difference, $\boldsymbol{\Delta L}$ is the distance, $\boldsymbol{D}$ is the diameter of the plain tube (not hydraulic), $\boldsymbol{\rho}$ is the fluid density and $\boldsymbol{v_c}$ is the velocity in the twisted tape section, evaluated from the inlet velocity $\boldsymbol{v_{inlet}}$ as

$$v_c = v_{inlet} \frac{A_0}{A_c} \tag{1.2}$$

with $\boldsymbol{A_0}$ and $\boldsymbol{A_c}$ empty tube cross-sectional area and axial flow (with twisted tape) cross-sectional area respectively. In general, to consider the characteristic geometry (curvatures and pitches), sections *at least* 7 cm apart must be considered for good evaluations. Anyway, also other distances will be reported.

[9] Several studies have been conducted on similar problems. Other references can be found in [25], [23] and [22].
[10] An example of cross section considered is Fluid: XZcm10 in Figure 8, which stands for a section in the plane XZ taken at 10 cm from the inlet section in the fluid region.

This computed value is compared to friction factors from available correlations evaluated according to *Manglik*, which uses plain tube parameters in formulas. A nonlinear regression obtained after the acquisition of experimental data in 1991 [9], by using the nomenclature in Table 1 gives [6]

$$f_{Fanning}/f_{y=\infty} = 1 + 2.752/y^{1.29} \tag{1.3}$$

$$f_{Fanning} = \frac{0.0791}{Re^{0.25}}\left(\frac{\pi}{\pi - \frac{4\delta}{d}}\right)^{1.75}\left(\frac{\pi + 2 - \frac{2\delta}{d}}{\pi - \frac{4\delta}{d}}\right)^{1.25}\left(1 + \frac{2.752}{y^{1.29}}\right) \tag{1.4}$$

$$Re = \frac{\rho v_{inlet} D}{\mu} \tag{1.5}$$

Another correlation, obtained in 1992 [10] gives

$$f_{Fanning}/f_{y=\infty} = 1 + 2.06(1 + (2y/\pi)^2)^{-0.74} \tag{1.6}$$

where for a straight tape insert ($y = \infty$)

$$f_{y=\infty} = 0.0791 Re^{-0.25}\left(\frac{\pi}{\pi - 4\delta/d}\right)^{1.75}\left(\frac{\pi + 2 - 2\delta/d}{\pi - 4\delta/d}\right)^{1.25} \tag{1.7}$$

Correlation is referred to Fanning friction factor and comparison with Blasius definition $f$ is obtained as [8]

$$f = 4 f_{Fanning} \tag{1.8}$$

For in-tube flows with twisted-tape inserts, the heat transfer behavior is rather complex and different from the hydrodynamic performance, and the twist ratio significantly influence the transition from laminar to turbulent flows. Average computed Nusselt numbers, used to quantify this thermal behavior, are always referred to plain tube diameter. Two definitions are provided for the Nusselt number ($Nu$):

- local Nusselt number [8]

$$Nu = \frac{hD}{k} \tag{1.9}$$

  where $k$ is the thermal conductivity of water, $D$ the plain tube diameter, $h$ the heat transfer coefficient evaluated as

$$h = \frac{q}{T_s - T_b} \tag{1.10}$$

  where, in a fully thermal developed flow given a specific section, $T_s$ is the temperature of the point of the interface fluid-solid in cylindrical area, $T_b$ is the mass flow average temperature, $q$ the local boundary heat flux in the same point[11] of $T_s$.

[11] An example of points where temperature $T_s$ is evaluated is reported in Figure 8 as *Point20cm*, which stands for a point at the interface solid-fluid, taken at 20 cm from the inlet section. Sections for $T_b$ evaluations follow the same notation used for *Fluid: XZcm10*.

- average Nusselt number

$$Nu = \frac{h_p D}{k} \tag{1.11}$$

where the heat transfer $h_p$ is, in general, related to a portion of cylinder where, in ideal conditions, there should be a fully thermal and fluid dynamic developed flow and insert is entirely present. Because of the length of the sample and of the characteristic of the flow, these conditions cannot be entirely realized and the best possible solution is to take only a portion of cylinder as far as possible from the inlet and not disturbed by the outlet region. Considering a stretch between two distinct cross sections in fluid

$$h_p = \frac{q_p}{T_{ps} - T_{pb}} \tag{1.12}$$

$$T_{pb} = \frac{T_{inlet\ portion} + T_{outlet\ portion}}{2} \tag{1.13}$$

where $T_{ps}$ is the surface averaged temperature of the cylinder portion and $T_{pb}$ its mass flow averaged (bulk) temperature.

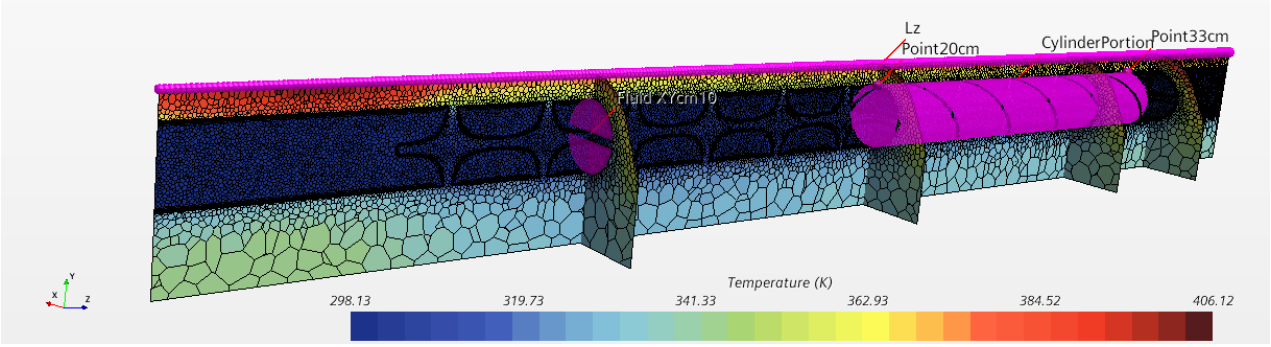


*Figure 8 Example of points considered for Ts, section considered for Tb, cylinder portion for Nu average and Lz line*

Nusselt average number from correlation is referred to inlet Reynolds number and is evaluated, in this specific case (liquid heating) by *Manglik* in 1991 [6] as the straight-line fit

$$Nu/Nu_{y=\infty} = 1 + 0.769/y \tag{1.14}$$

$$Nu_{y=\infty} = 0.023 Re^{0.8} Pr^{0.4} \left(\frac{\pi}{\pi - \frac{4\delta}{d}}\right)^{0.8} \left(\frac{\pi + 2 - \frac{2\delta}{d}}{\pi - \frac{4\delta}{d}}\right)^{0.2} \phi \tag{1.15}$$

$$Pr = \frac{c_p \mu}{k} \tag{1.16}$$

$$\phi = (\mu_0/\mu_w)^n \qquad n = \begin{cases} 0.18\ for\ liquid\ heating \\ 0.30\ for\ liquid\ cooling \end{cases} \tag{1.17}$$

All the experimental correlations are referred to average values and to simpler geometry: cylindrical tube with twisted tape in fully developed flow (thermal and fluid dynamic) and uniform heat load applied on the cylindrical surface. In addition, experimental data were taken for water and ethylene glycole with y=3.0, 4.5 and 6.0: although twist ratio is considered in these equations and no incompatibility can be remarked on the

application to an external interval like the one considered in the LEE, it is important to notice that the precise value of the analyzed case is peculiar. Errors on friction factor predictions are within ±10% and a family of curves is needed for Nu, due to the nonunique nature of laminar-turbulent transition.

Since not all the theorical hypothesis are exactly satisfied in this specific situation (especially for the sample), they should be considered only as rough references. Differences between results obtained from simulations and equations derived from experiments are mainly due to discrepancies in geometries and hypotheses. The observation of the velocity plots (Figure 9) and of normalized temperatures (Figure 10) gives a clear evidence of non-fully developed flow (thermal and fluid dynamic) and comparison between calculated friction factors and Nusselt[12] and those deriving from literature correlations[13] can be carried out by considering, for the computed values, a stretch between 20cm and 33cm and only considering the average values (*CylinderPortion* in Figure 8). From these, percentage errors are calculated.

Anyway, more intervals from the inlet are considered for the computation of the friction factor *fComp* and Nusselt number *NuComp*, and the poor reliable values (with respect to correlations) are reported in graphs to highlight these differences and quantify also non average values for sake of completeness.

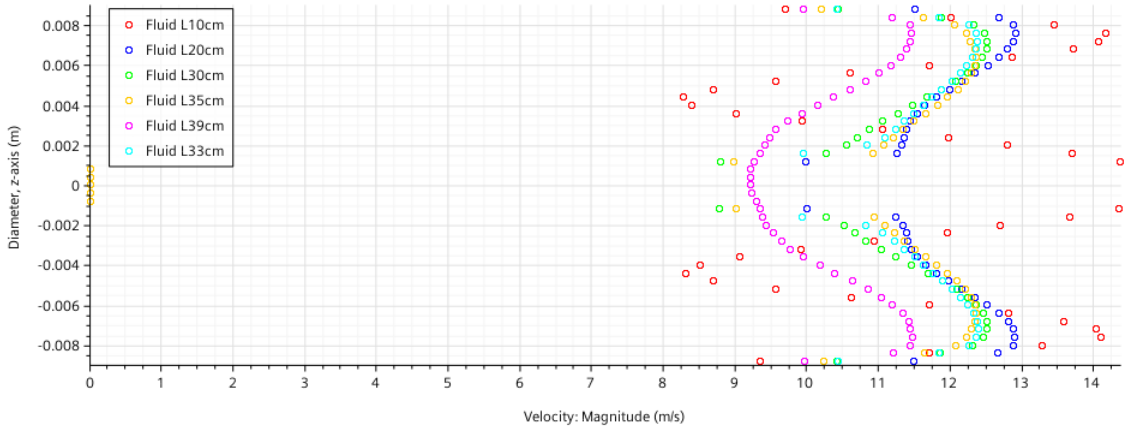


*Figure 9 Velocity plot along distinct lines perpendicular to the main axis of the LEE sample at different distances from the inlet: results obtained after mesh convergence*

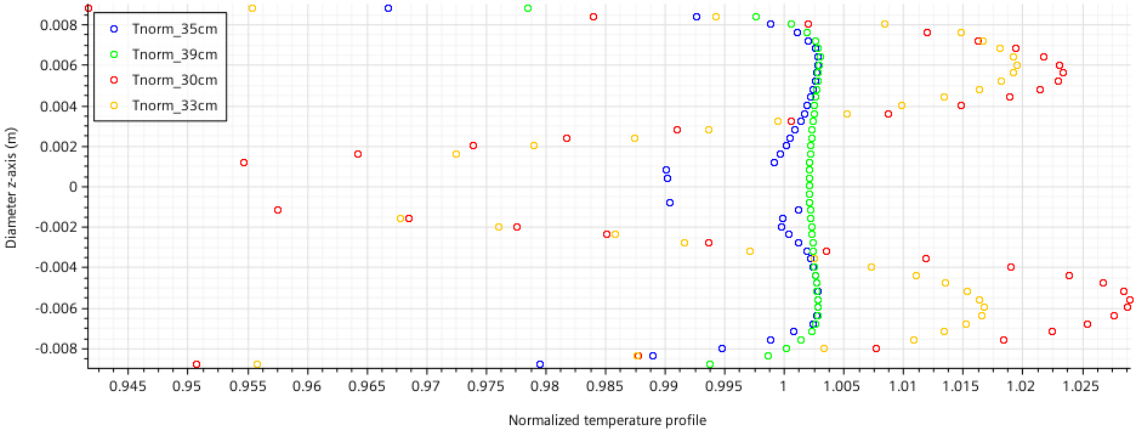


*Figure 10 Normalized temperature along distinct lines perpendicular to the main axis of the LEE sample at different distances from the inlet: results obtained after mesh convergence*

[12] evaluated with the equations (1.1) and (1.11) with data extracted from the simulations. They are also called *computed* values and are indicated in plots with *fComp* and *NuComp*.

[13] evaluated with the equations (1.3) and (1.14) with the known input data. Note that these equations consider always only Reynolds number and so geometry, inlet mass flow and material properties (all known) are sufficient for their calculation.

The definition of normalized temperature is taken from [8]

$$\frac{\partial}{\partial x}\left[\frac{T_s(x)-T(r,x)}{T_s(x)-T_b(x)}\right]_{fd,t}=0 \tag{1.18}$$

where $x$ and $r$ are the axial and radial coordinate, $T_s$ is the temperature of the point of the interface fluid-solid in cylindrical area, $T_b$ is the mass flow average temperature and $T$ is the local fluid temperature. This condition may be reached in a tube for which there is either a uniform surface heat flux or a uniform surface temperature.

## 1.1.3. Stopping criteria

To judge the validity of the simulation, the mere reference of the residuals is not sufficient. Therefore, a series of values are added to the check the convergence of the solution - that is, with a defined mesh -, by taking into account the stability of the numerical solution, the quality of the result and, above all, the physical phenomenon.

Correlations are not used as stopping criteria, (therefore as a constraint) but only and exclusively as an indicative comparison in post processing: this choice derives from the fact that the geometry and the boundary conditions are different from those available in the literature, as clearly evident from the distribution of the heat flux on the outer shell of the case (Figure 7).

The main quantities that can be checked are reported in Table 5. From the first principle of thermodynamics, the expected outlet temperature is

$$T_{out}=\frac{\dot{Q}A_{front}}{\dot{m}c_p}+T_{in} \tag{1.19}$$

| Stopping Criteria | | |
|---|---|---|
| Name | Definition | Type |
| Total Pressure Drop | It must be stable for a certain number of iterations. It is evaluated[14] as difference between mass flow averaged absolute total pressure between inlet and outlet boundary surfaces as $dp=\left[\frac{\sum_f \lvert\dot{m_f}\rvert P_{t,abs_f}}{\sum_f \lvert\dot{m_f}\rvert}\right]_H-\left[\frac{\sum_f \lvert\dot{m_f}\rvert P_{t,abs_f}}{\sum_f \lvert\dot{m_f}\rvert}\right]_L$ | Standard deviation |
| Friction factor (average) | The computed value between two sections at 20 cm and 33 cm from the inlet must be stable | Asymptotic limit |
| Mass flows errors | From the conservation equation, mass flow must be constant along the sample. This means that taking some cross sections, mass flow percentage error between considered section and inlet imposed mass flow rate must be approximately null | Minimum limit |
| Nusselt number (average) | The computed value between two sections at 20 cm and 33 cm from the inlet must be stable | Asymptotic limit |
| Outlet temperature error | First principle must be respected, which means that computed outlet temperature must be coherent with the predicted one | Minimum limit |

*Table 5 Stopping criteria for the LEE sample*

[14] from [27]. In the present study, *total pressure drop* or *pressure drop* will always be referred to this mathematical definition, unless different specifications. *Static pressure difference* will be used with the meaning of surface averaged static pressure difference.

## 1.1.4. Mesh generation and grid independence study

Polyhedral mesh has been chosen as a good compromise between accuracy and computational cost. For the fluid region, at the interface solid-fluid, prism layers are added to better resolve the laminar boundary layer.

Superposition of effects is the main hypothesis used for the mesh independence study, which means that two main steps are followed to decouple the problem and understand separately the effect of each parameter of the mesh.

1) Core convergence: a certain prism layer is selected, ensuring that the wall y+ value was approximately unitary to avoid buffer layer[15] and paying attention to the prism-polyhedral transition on the interface layer. Keeping constant the prism layer parameters only the polyhedral mesh is refined changing the base size. The result of this first convergence study is the final dimension of the polyhedral part of the mesh.
2) Prism layer convergence: the base size in the previous step is kept fixed, and only prism layer parameters are varied. The result is the complete definition of the layer close to the wall and, consequently, of the entire mesh of the sample.

### Core grid independence

Mesh listed in Table 6 are explored. From this first step of the convergence, *case 2* is selected, since it represents a good compromise between accuracy of results and computational cost, quantified also by the number of required iterations (Figure 11): this parameter is relevant to estimate the possible number of cells required in the entire LEE simulation, about four times those required for the sample, considering the total length involved.

| Fixed prism layer | | | | |
|---|---|---|---|---|
| | | total thickness | number of prisms | prism layer near wall thickness |
| TT | | 0.7mm | 15 | 3.6e-6 m |
| cylinder | | 1.2mm | 12 | 4e-6 m |
| Mesh data: variable polyhedral mesh | | | | |
| case | base size | number of cells (total) | number of cells (fluid) | number of cells (solid) |
| 0 | 0.6mm with refinement for TT | 3807709 | 3256997 | 550712 |
| 1 | 0.6mm | 2164165 | 1821448 | 342717 |
| 2 | 0.65mm | 1842967 | 1549467 | 293500 |
| 3 | 0.8mm | 1348637 | 1125328 | 223309 |
| 4 | 1mm | 1132119 | 944505 | 187614 |
| 5 | 2mm | 838836 | 700057 | 138779 |
| 6 | 10mm | 699209 | 586893 | 112316 |

*Table 6 Mesh explored for core grid independence of LEE sample*

With reference to the cases in Table 6, each point of the following graphs corresponds to a specific row progressively numbered, in descending order of number of cells in fluid.

[15] According to the law of the wall developed in 1930 by Hungarian American mathematician, aerospace engineer, and physicist Theodore von Kármán [26].

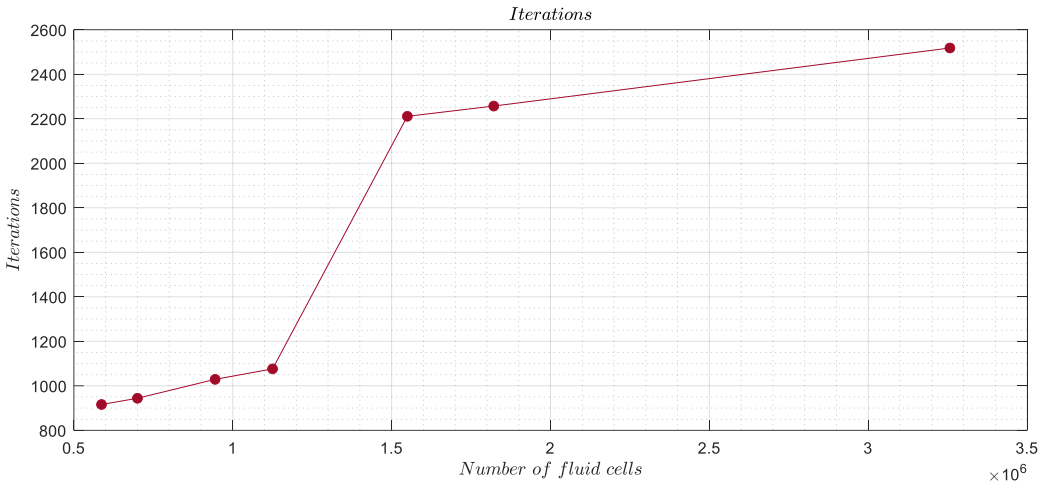


*Figure 11 Core grid independence. Iterations required for each case in core convergence as function of total number of cells in fluid region*

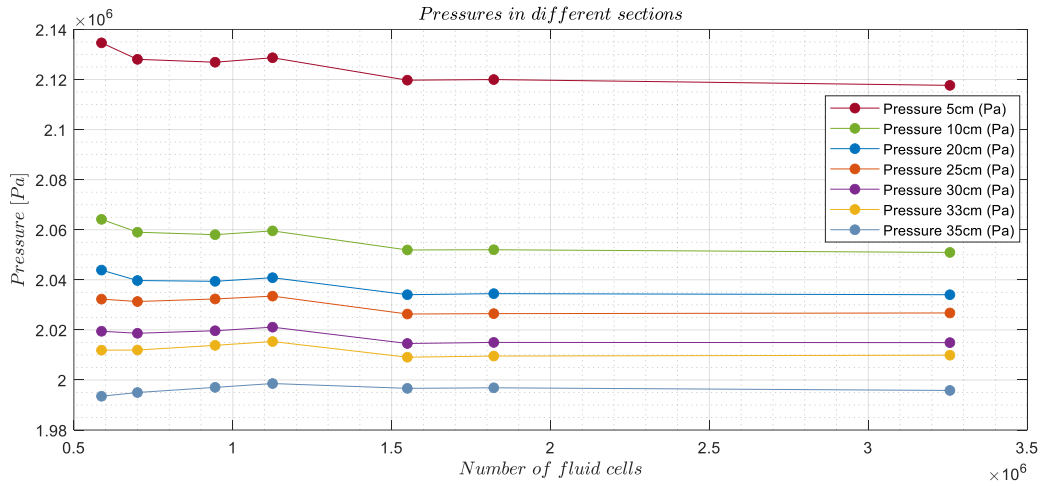


*Figure 12 Core grid independence. Surface averaged static pressure in different sections as a function of the total number of cells in the fluid region. The distance reported is with respect to the inlet cross section.*

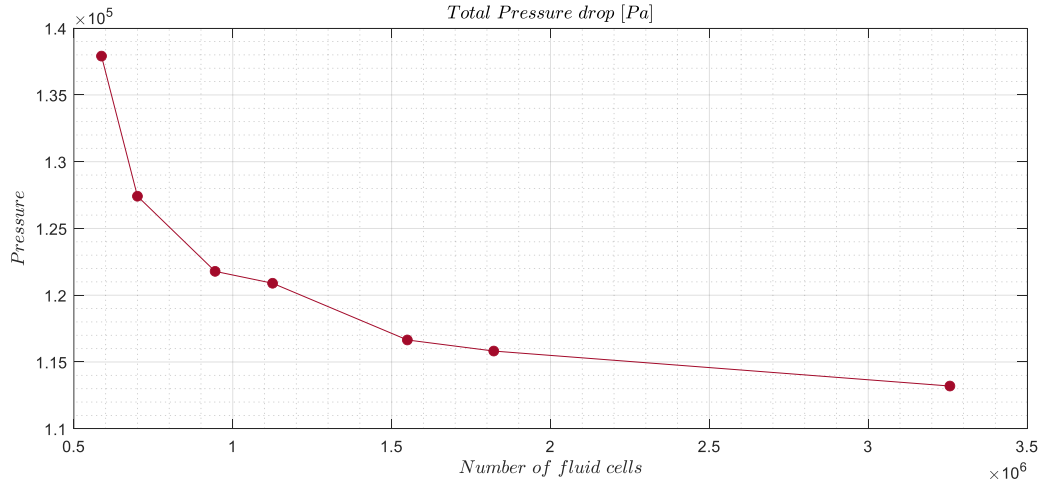


*Figure 13 Core grid independence. Total pressure drop as a function of the total number of cells in the fluid region*

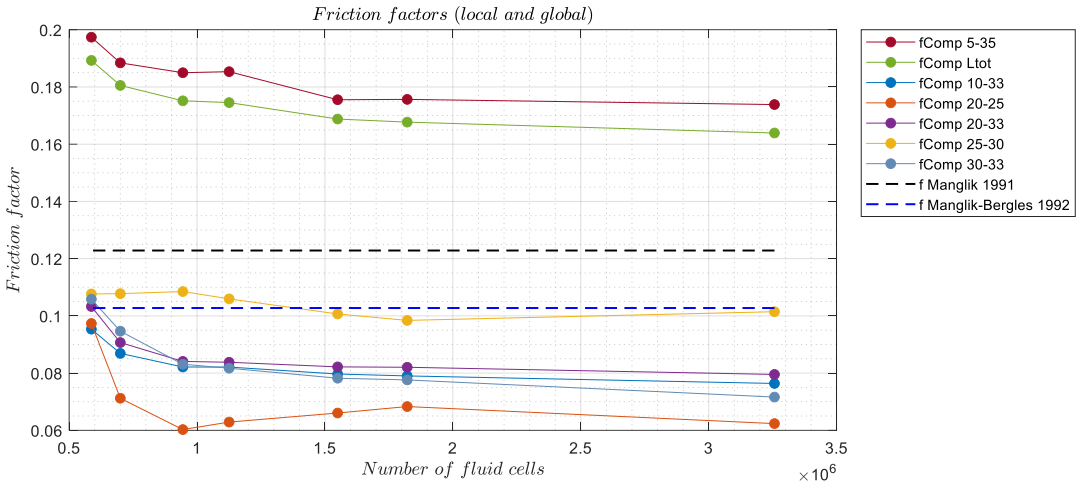


*Figure 14 Core grid independence. Friction factors evaluated with the equation (1.1) between different couples of sections at a distance from the inlet expressed in cm (e.g. fComp 5-35 takes quantities between 5cm and 35cm from the inlet) as a function of the total number of cells in the fluid region*

Relevant quantities to judge the mesh convergence are reported as a function of the number of fluid cells, since all the important phenomena occur in the fluid, while solid mesh does not significantly influence the final results: an asymptotic trend can be seen (Figure 12, Figure 13, Figure 14), which means that further refinement is unnecessary. As anticipated, a certain difference can be highlighted between predictions from experimental correlations and computed values, but the most representative values are in between 20 cm and 33 cm from the inlet.

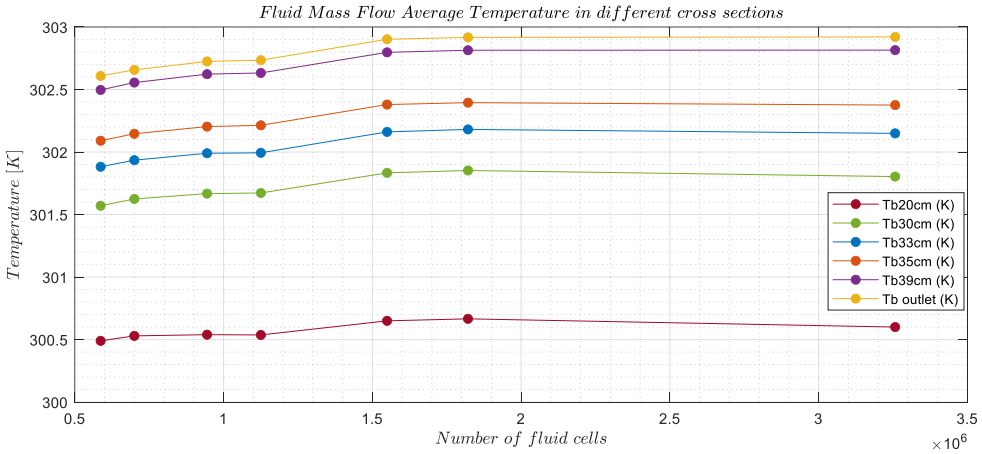


*Figure 15 Core grid independence. Mass flow averaged temperature as a function of the total number of cells in the fluid region*

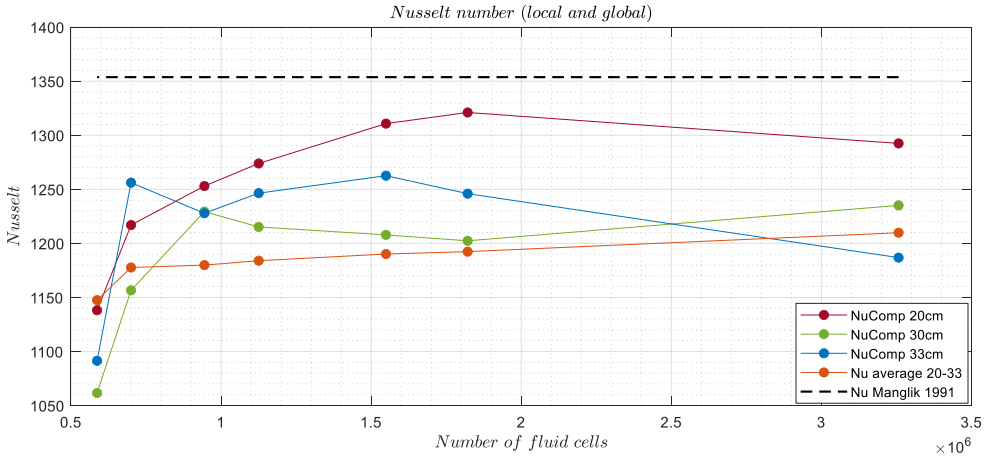


*Figure 16 Core grid independence. Nusselt number as a function of the total number of cells in the fluid region*

To characterize also the thermal phenomena, bulk temperature and Nusselt number are reported in Figure 15 and Figure 16, according to previous definitions. An asymptotic trend can be seen, even if with some oscillations. The real significant value for the Nusselt number is the average one, which has anyway a good match with the correlations.[16] Different quantities have been considered to fully check the mesh: point values, surface integrals and mass flow averaged.

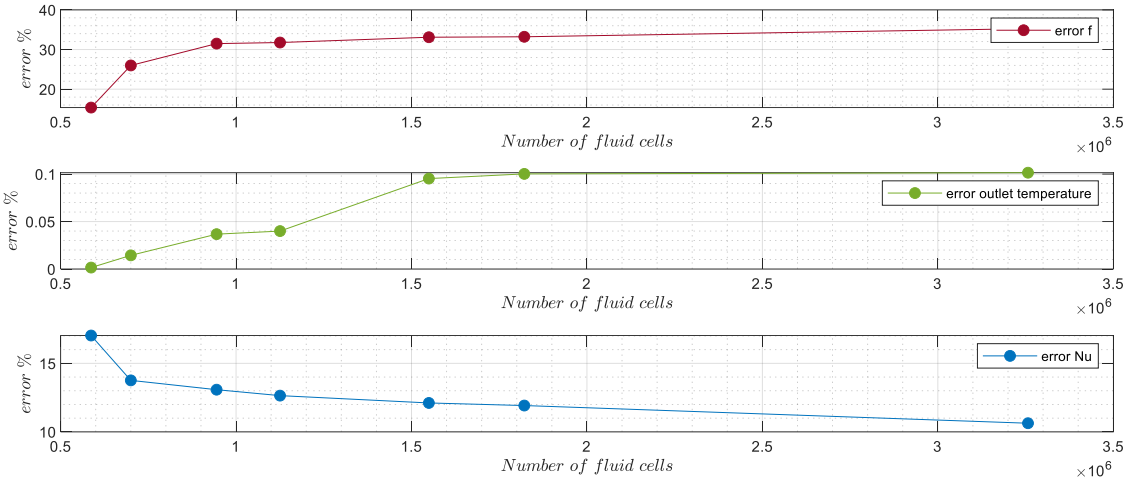


*Figure 17 Core grid independence. Errors between averaged values of friction factors and Nusselt numbers and correlations as functions of the total number of cells in the fluid region*

## Prism grid independence

Keeping fixed the polyhedral parameters of the mesh determined in the previous step, the prism layer is then studied, by analyzing the sensitivity to two main parameters: the number of prisms (pn) and of the total thickness of the prism layer (pltt).

| | case | total thickness | | number of prisms | | number of cells | number of cells (fluid) | number of cells (solid) |
|---|---|---|---|---|---|---|---|---|
| | | TT | cylinder | TT | cylinder | | | |
| Constant prisms number | 8 | 0.9mm | 1.4mm | 15 | 12 | 1820160 | 1526838 | 293322 |
| | 1 | 0.7mm | 1.2mm | 15 | 12 | 1842967 | 1549467 | 293500 |
| | 7 | 0.5mm | 1.0mm | 15 | 12 | 1856532 | 1563308 | 293224 |
| | 9 | 0.4mm | 0.7mm | 15 | 12 | 1876394 | 1582859 | 293535 |
| Constant total thickness of prism layer | 1 | 0.7mm | 1.2mm | 15 | 12 | 1842967 | 1549467 | 293500 |
| | 6 | 0.7mm | 1.2mm | 12 | 15 | 1942254 | 1648754 | 293500 |
| | 3 | 0.7mm | 1.2mm | 17 | 15 | 2099956 | 1806456 | 293500 |
| Changed prisms number and total thickness | 2 | 0.8mm | 1.6mm | 14 | 20 | 2303246 | 2009674 | 293572 |
| | 4 | 0.5mm | 1.0mm | 12 | 15 | 1963621 | 1670397 | 293224 |
| | 1 | 0.7mm | 1.2mm | 15 | 12 | 1842967 | 1549467 | 293500 |
| | 10 | 0.4mm | 0.7mm | 8 | 8 | 1385958 | 1092421 | 293537 |

*Table 7 Meshes studied for prisms grid independence considering as basic case the case 2, which is the result of the core grid independence*

[16] Additional parameters investigated can be found in the *Appendix*, in 1.1. Mesh generation and grid independence study.

Transition from polyhedral mesh to prismatic mesh must be gradual, to correctly transfer information between the two parts. This means that the size of adjacent prisms and polyhedra must be comparable and that the main energy variation should be contained in the prism layer part. Prism layer definition affects mainly the thermal results of the simulation. No relevant difference has been noticed on pressure, mass flows or friction factors by changing both or only one parameter as shown in Figure 18, where, for brevity, only friction factors graphs are reported and show flat curves.

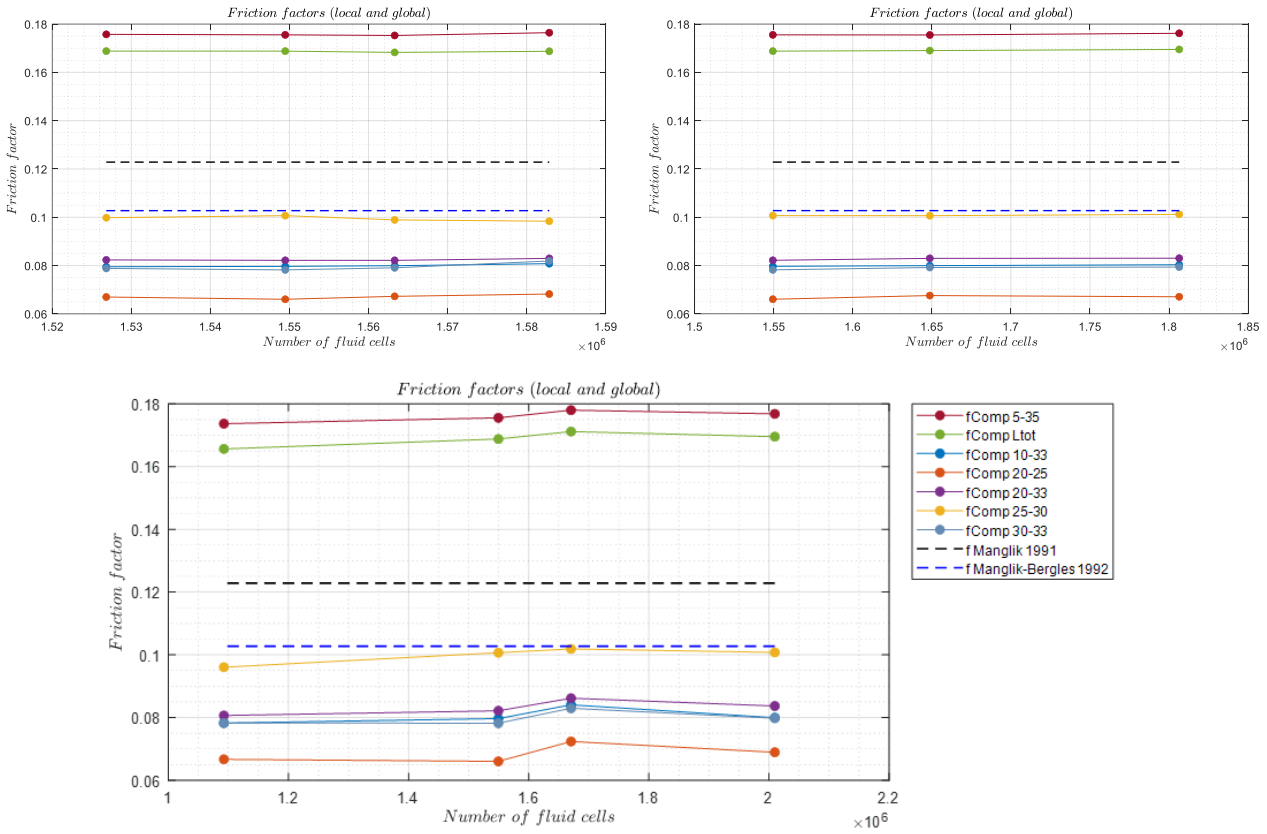


*Figure 18 Prism grid independence. Friction factors with constant prism number (top left), constant prism layer total thickness (top right) and both the variations (bottom). Each point of each graph corresponds to a row of Table 7, consistently with the block indicated therein for constant pn, pltt and both the variation*

Mesh from *case 4* of Table 7 is finally selected to better satisfy the grid independence requirements. In Figure 19 this corresponds to the third point of the last picture. In fact, the two separate effects of the variation of pn and pltt reveal that the main contribution on thermal results accuracy, by considering as reference the average Nusselt number[17], is due to the variation of the prism layer total thickness and to properly consider the proportion of the transition a set of parameters from the case in which both the parameters are varied is taken.

[17] which is the most representative for what previously discussed.

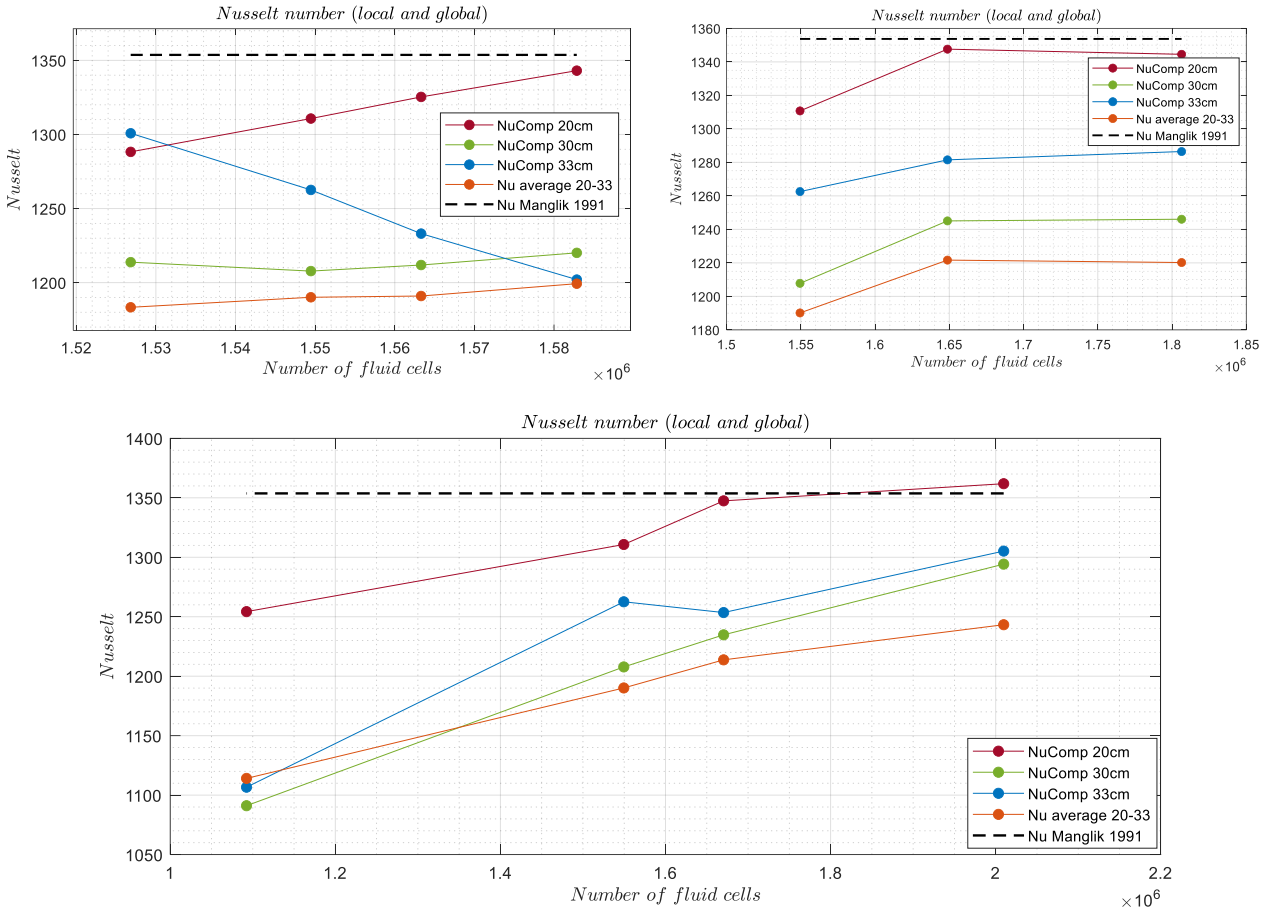


*Figure 19 Prism grid independence. Nusselt numbers with constant prism number (top left), constant prism layer total thickness (top right) and both the variations (bottom). Each point of each graph corresponds to a row of Table 7, consistently with the block indicated therein for constant pn, pltt and both the variation*

Selecting the *case 4* of Table 7, percentage errors between average friction factors and Nusselt number and corresponding literature correlations reduce, approaching the computational- numerical model to the experimental-physical one.

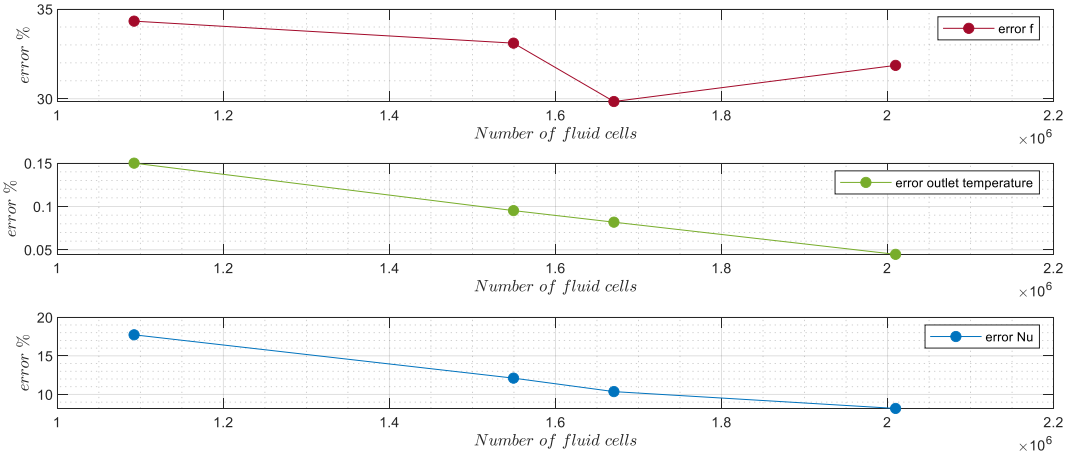


*Figure 20 Prism grid independence. Errors, according to previously definitions between computed and expected temperature, average values of Nu and f and literature correlations, when both prism number and total thickness are changed. Each point of each graph corresponds to a row of Table 7, consistently with the third block of the table*

The effect of the first (wall) layer thickness may be seen in the wall temperature on the external surface of the case. This value, which are interesting to understand if the component is correctly refrigerated, is plotted along a line *Lz* (indicated in Figure 8), parallel to the main axis of the LEE, located in the plane tangent to the external surface, in correspondence to the thinner solid thickness. Because of the twisted tape geometry, the oscillating behavior of the temperature, due to intermittent contact along this line, can be seen. The peak is located where there is no insert: a clear temperature reduction occurs when the flow impacts with the tape.

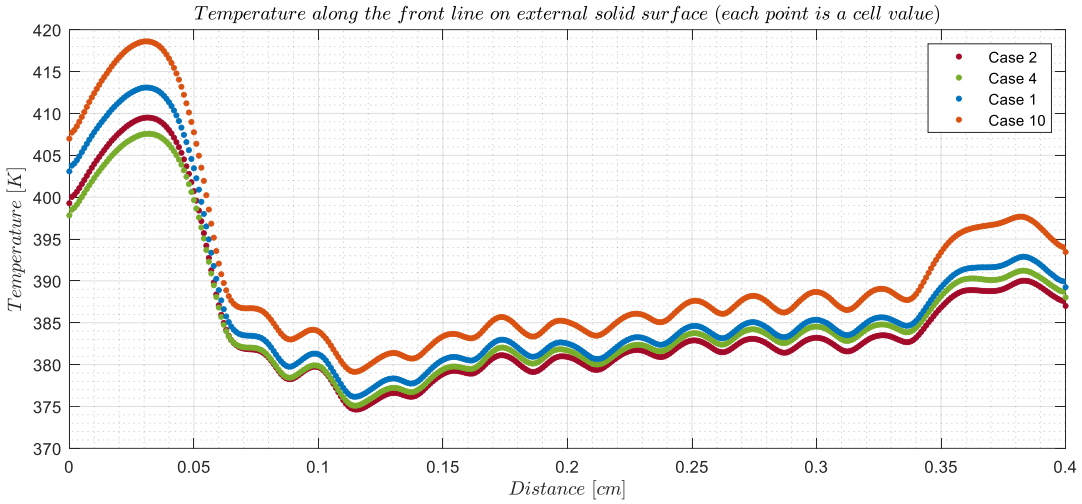


*Figure 21 Temperature along Lz in cases for which both the variations (total thickness and number of prisms) are applied*

The fundamental result of this section is the definition of the mesh parameters for the LEE sample in the conditions described in Table 3. Simulation results and mesh convergence have proven that literature correlations are valid also in the sample case - even if with higher errors with respect to the theoretical values attempted -, where non ideal conditions deviate friction factor and Nusselt number from the available correlations. In the entire LEE model, since more hypotheses will be satisfied consistently with experimental tests, it is reasonable to expect a best match with the predictions.

## 1.2. Entire LEE results

The successive step is to simulate the entire LEE geometry using the same mesh parameters obtained for the representative sample. Boundary conditions and materials remain the same as those of Table 3. All the results are shown on the entire LEE.

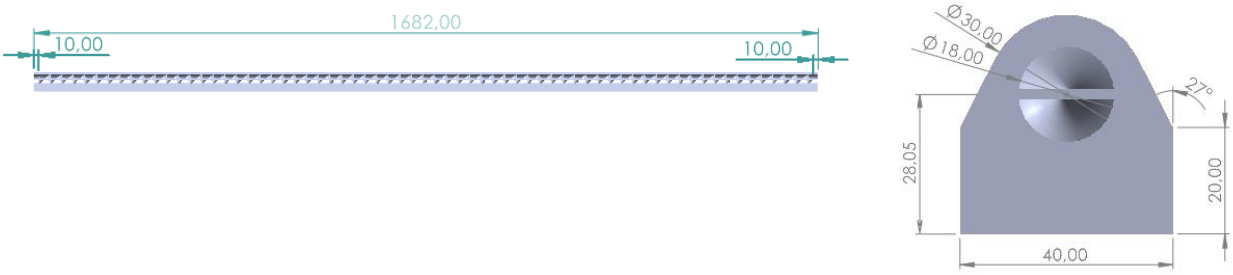


*Figure 22 Geometry of the entire LEE with twisted tape*

| | base size | Prism Layer Total Thickness | Number of Prism Layers | Prism Layer Near Wall Thickness | number of cells | number of cell (fluid) | number of cells (solid) | Iterations |
|---|---|---|---|---|---|---|---|---|
| TT | 0.65mm | 0.5mm | 12 | 3.6e-6 m | | | | |
| cylinder | | 1.0mm | 15 | 4e-6 m | 8795677 | 7484463 | 1311214 | 9055 |

*Table 8 Mesh parameters for the entire LEE with twisted tape*

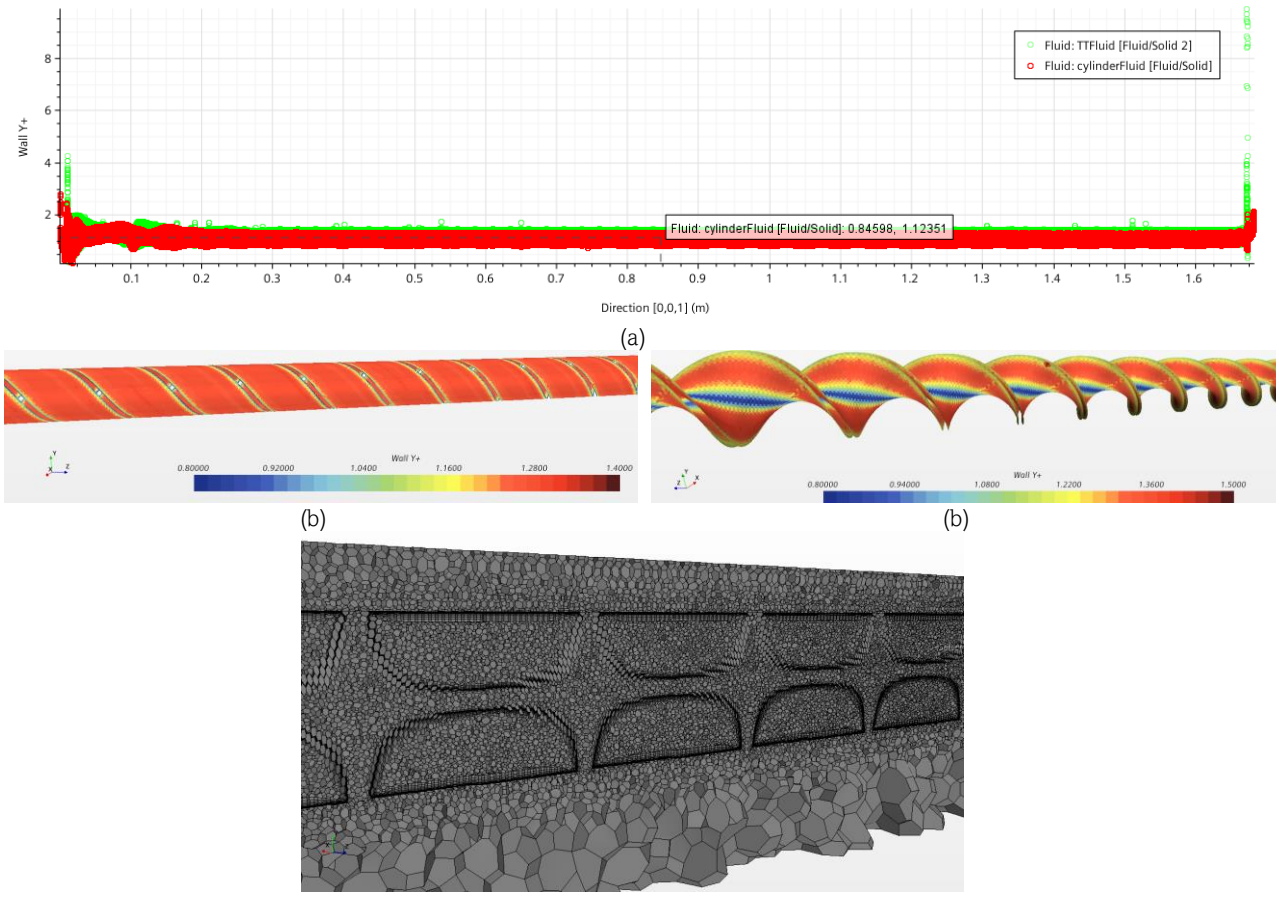


*Figure 23 Y+ along the LEE both for TT and cylindrical interfaces solid-fluid as 2D-plot view (a), detail of the 3D-plot of y+ on the cylindrical interface (b), detail of the 3D-plot of y+ on the cylindrical interface (c), mesh in 3D view for the entire LEE with twisted tape (d)*

In this case, averaged values for Nusselt number and friction factor are taken at a longer distance from the inlet (between 76cm and 166cm), where a fully developed (fluid dynamic and thermal) flow is expected to occur: velocity plots and normalized temperatures in Figure 24 are coincident in this interval. Stopping criteria[18] are consequently updated with these new distances, but they are conceptually the same of Table 5. Asymptotic limit criteria are added for mass flow errors on mass conservation.

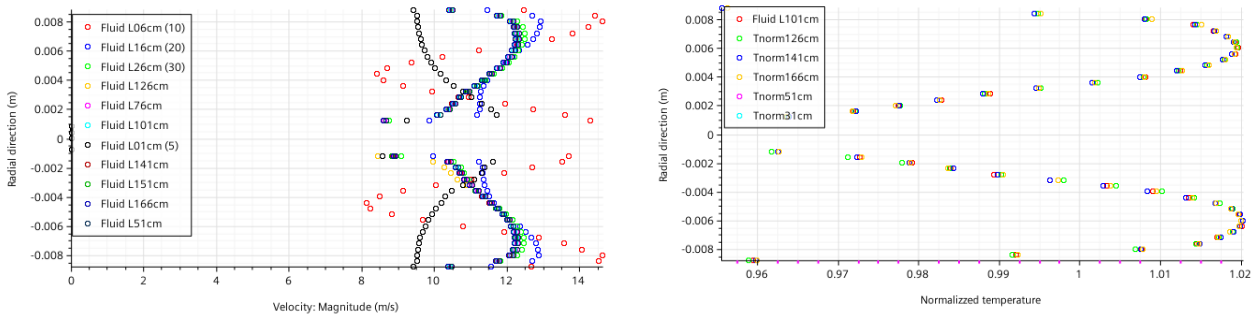


*Figure 24 Velocity plot (on the left) and normalized temperature (on the right) along distinct lines perpendicular to the main axis of the LEE at different distances from the inlet*

[18] Additional graphs are provided in appendix in 1.2. Entire LEE study

## 1.2.1. Fluid dynamics and thermal results

As expected, the turbulence promoter allows to obtain lower temperature peak, if compared to the LEE without twisted tape and the same boundary conditions which is discussed in the following chapter, but pressure drop considerably increases. This is due to the friction realized at the wall and in the fluid and to the increasing of wet perimeter: the vortexes inside the fluid, which follows the curves of the insert, are highlighted by the streamline.

Additional contribution to the high pressure reached at the inlet is given by the entrance region, where the twisted tape starts introducing a sharp change in geometry and turbulent kinetic energy is remarkable. Improving the fluid dynamics of the initial part of the insert, such as by introducing a rounded edge or similar shapes, could reduce this effect.

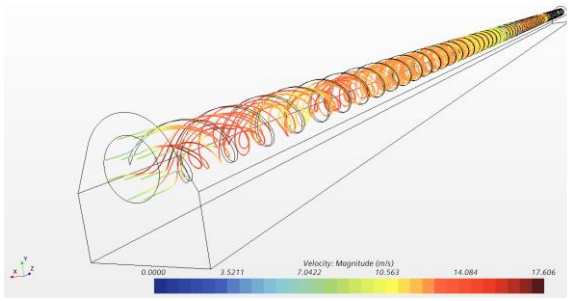


(a)

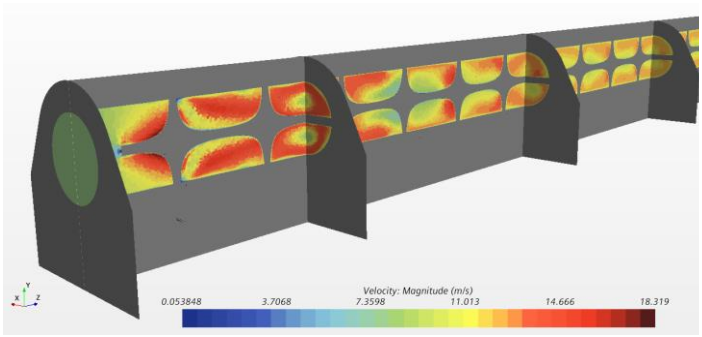


(b)

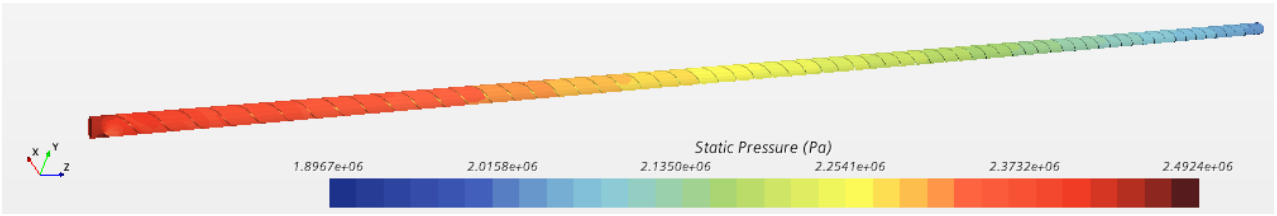


(c)

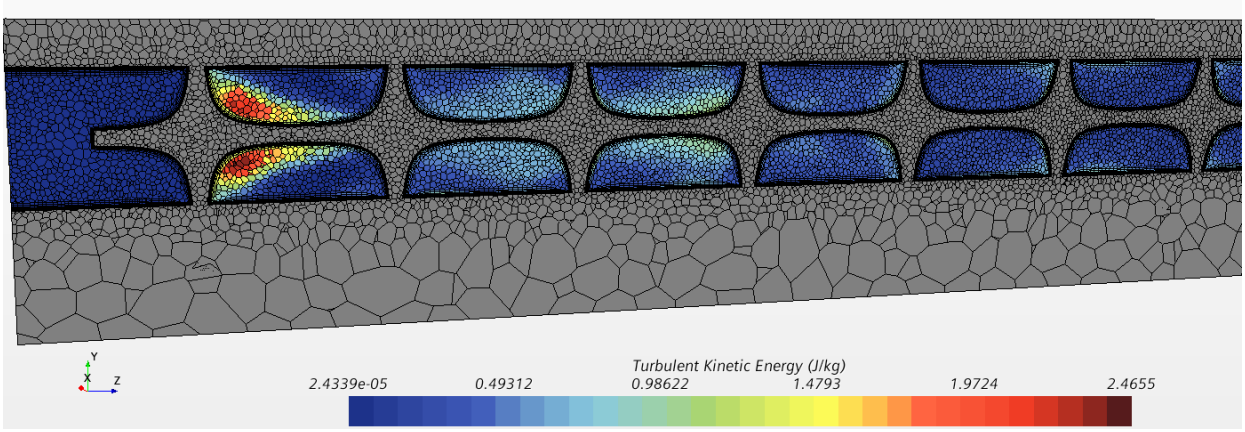


(d)

*Figure 25 Fluid dynamic results: streamlines (a), velocity in the entrance region b), pressure distribution (c), turbulent kinetic energy in the entrance region (d)*

From the thermal point of view, the temperature difference between the wall and the fluid is the responsible of the heat transfer and, consequently, of the refrigeration of the component.

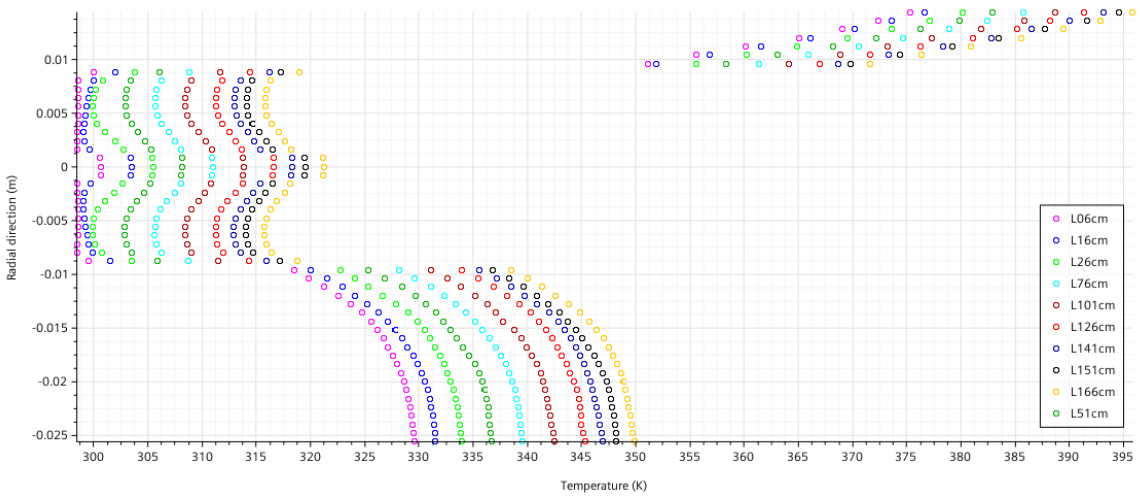


*Figure 26 Temperature along distinct lines perpendicular to the main axis of the LEE at different distances from the inlet*

With the known operative conditions, temperature peaks in solid are far below the acceptable limits, even with the overconservative hypothesis on heat flux: in fact, to prevent material property degradation – and without considering, for the moment, thermomechanical assessment – the maximum temperature must not exceed approximately 400°C [11].

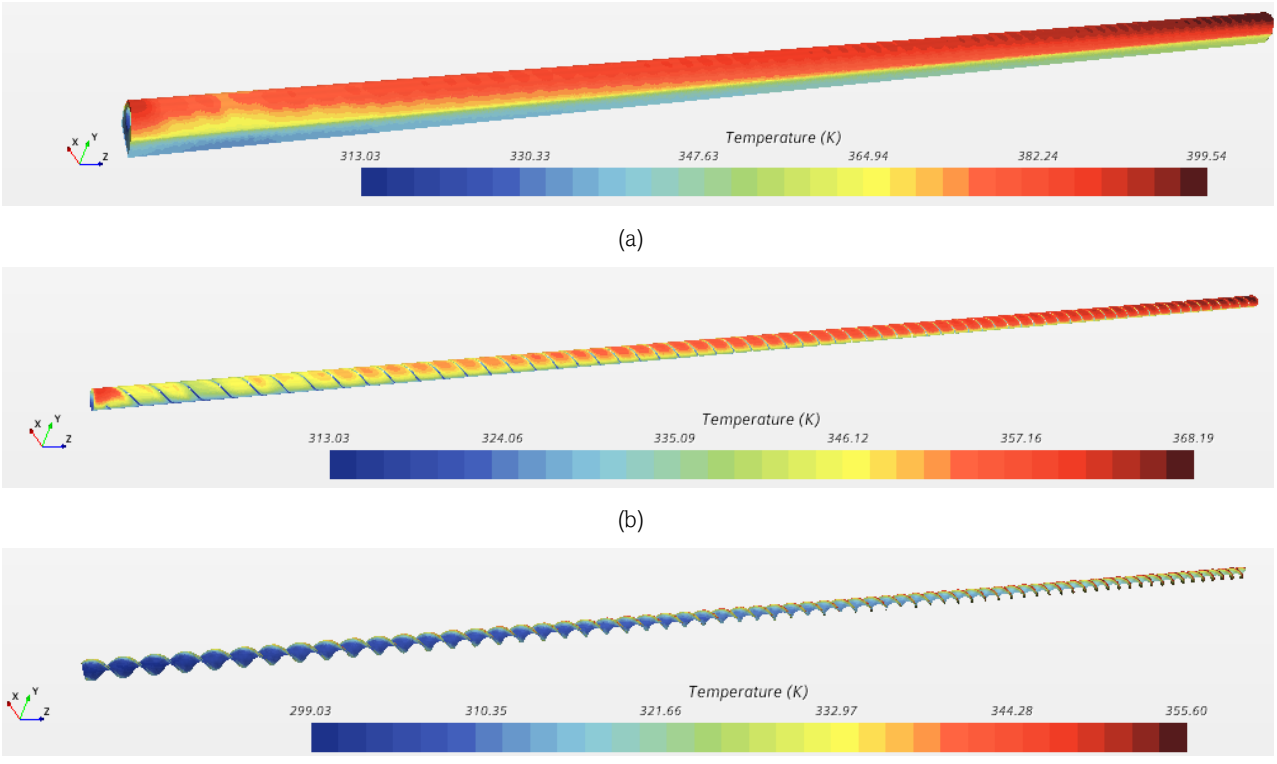


*Figure 27 Temperature distribution on solid surfaces: external case (a), cylinder solid interface (b), twisted tape solid interface (c)*

The strictest constraint is represented by the peak in temperature reached in water at the interface between solid and fluid. At the operative conditions, 20 bar are imposed[19] as surface averaged pressure at the outlet

[19] As in Table 3

but considering the minimum local pressure value reached in fluid region (approximately 19 bar), the saturation temperature is 209°C [12]. This means that, to avoid possible boiling conditions for water and material wear, this limit cannot be achieved and hence, in this case, no saturation problems occur.

Some important parameters, for the performance evaluation of the models, including boundary conditions and geometry, are the total pressure drop[20] between inlet and outlet ($\Delta p$), the static pressure difference between inlet and outlet ($\Delta p_{static}$), the difference between maximum and minimum values of temperature in fluid ($\Delta T$) and the maximum temperature reached in solid and fluid ($T_{max,s}$ and $T_{max,f}$). In this case for a single entire LEE

$$\Delta T \approx 70°C$$

$$T_{max,f} \approx 95°C$$

$$\Delta p \approx 4.1 bar$$

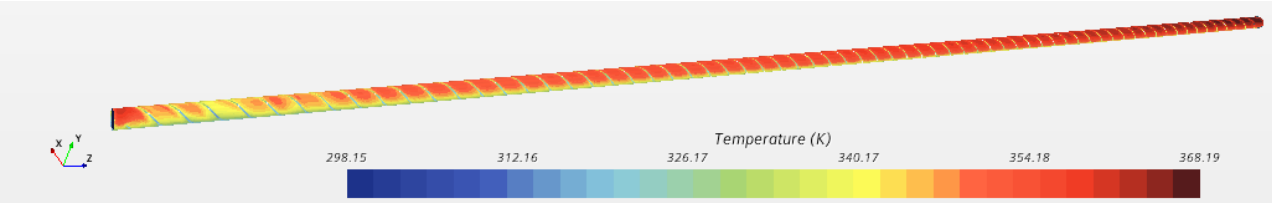


(a)

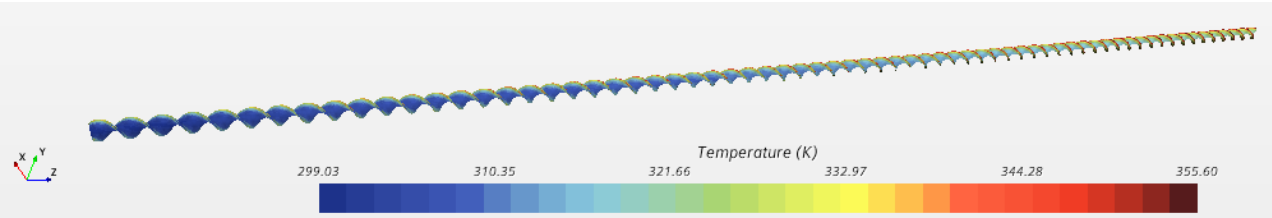


(b)

*Figure 28 Temperature distribution on fluid surfaces: cylinder fluid interface (a), twisted tape fluid interface (b)*

Differently from the sample, the peak for the entire LEE is reached at the outlet on the external surface of the wall. The pseudo-periodic trend of the temperature along the Lz line is given again by the intermittent contact along it, due to twisted tape geometry, which guides it through the pitches.

[20] Introduced before in Table 5

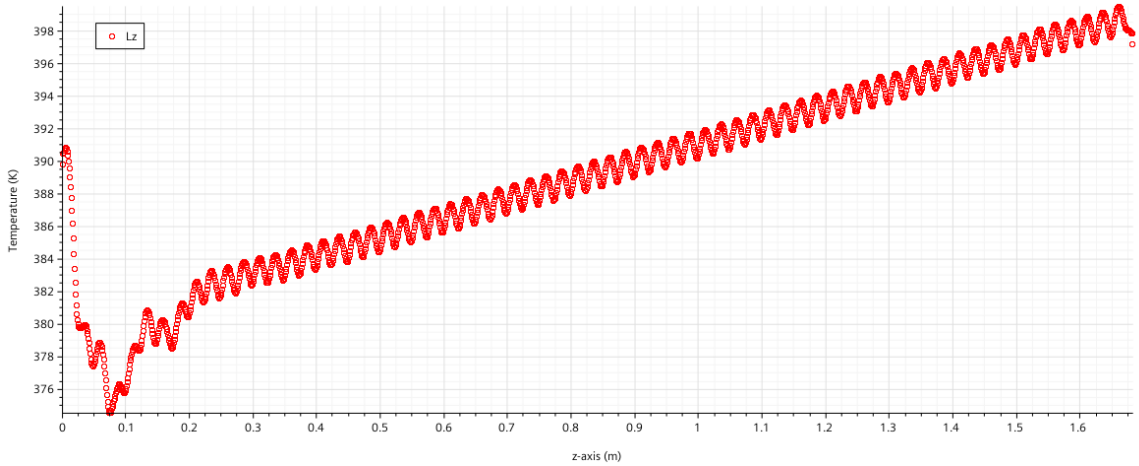


*Figure 29 Temperature along Lz line*

As expected, from the numerical results, errors on friction factor predictions are lower in the entire LEE case than in the sample case, since fluid dynamic conditions are more similar to the ideal conditions recreated by the experiments from which correlations have been derived.

| | | | |
|---|---|---|---|
| | $Re_{inlet}$ | 1.60E+05 | |
| | $v_{inlet}$ | 7.90 | m/s |
| | $v_c$ | 9.19 | m/s |
| | Pr | 5.99 | |
| | f Manglik-Bergles 1992 | 0.103 | |
| | f Manglik 1991 | 0.123 | |
| | Nu Manglik 1991 | 1354.1 | |
| **Pressures** | Pressure 01cm | 2.43E+06 | Pa |
| | Pressure 76cm | 2.21E+06 | Pa |
| | Pressure 101cm | 2.16E+06 | Pa |
| | Pressure 126cm | 2.10E+06 | Pa |
| | Pressure 141cm | 2.07E+06 | Pa |
| | Pressure 151cm | 2.05E+06 | Pa |
| | Pressure 166cm | 2.02E+06 | Pa |
| | Pressure 167.2cm | 2.01E+06 | Pa |
| | **Total Pressure Drop** | **4.10E+05** | **Pa** |
| **Friction factor** | fComp 01-1672 | 0.109 | _ |
| | fComp Ltot | 0.141 | _ |
| | fComp 76-101 | 0.093 | _ |
| | fComp 76-166 | 0.092 | _ |
| | fComp 101-126 | 0.092 | _ |
| | fComp 141-151 | 0.092 | _ |
| | fComp 151-166 | 0.093 | _ |
| **Temperatures (mass flow average)** | Tb76cm | 306.60 | K |
| | Tb101cm | 309.39 | K |
| | Tb126cm | 312.20 | K |
| | Tb141cm | 313.89 | K |
| | Tb166cm | 316.72 | K |
| | Tb outlet | 316.66 | K |
| **Nusselt** | NuComp 101cm | 1266.1 | _ |
| | NuComp 141cm | 1263.5 | _ |
| | NuComp 166cm | 1304.9 | _ |
| | Nu average 76-166 | 1202.0 | _ |
| **error** | error T | 0.08 | % |
| | error Nu | 11.23 | % |
| | error f | 24.76 | % |

*Table 9 Complete report for overconservative case of LEE with twisted tape*

In conclusion, with this first analysis, it is evident that some modifications must be done, even before any thermomechanical assessments. In particular, from material point of view (which means saturations problems for water and material degradation for CuCrZr), even with overconservative hypothesis on the heat load, MITICA operative conditions are not suitable for NBI of DTT: this conspicuous refrigeration is apparently not needed for the LEEs and, above all, the total pressure drop realized (4.1bar) cannot be sustained if all the design requirements are to be met.

In fact, from the conceptual design, which will be introduced in the following chapter, it is known that the hydraulic circuit includes a series of two LEEs. This means that with the actual model and BCs and in a single passage, under the hypothesis that each LEE is loaded in the same way, the temperature difference for the two leading edge elements series is

$$\Delta T_{2LEEseries} \approx 2 \times \Delta T_{singleLEE} \approx 140°C$$

and, therefore, the maximum expected temperature is

$$T_{max,f_{2LEEseries}} \approx T_{water,inlet} + \Delta T_{2LEEseries} \approx 165°C$$

that is far below the limit temperature value to avoid boiling (209°C, at the local minimum pressure reached of 19bar). The total expected pressure drop can be evaluated as

$$\Delta p_{2LEEseries} \approx 2 \times \Delta p_{singleLEE} \approx 8.2bar$$

which is four times greater than the maximum pressure drop imposed as a requirement on total pressure drop (2bar) by *DTT S.c.a.r.l.*.

## 1.3. Comparison with a LEE without twisted tape

Often, in literature a thermal performance factor is defined [13]

$$TPF = \frac{(Nu_{tt}/Nu_p)}{(f_{tt}/f_p)^{1/3}} \tag{1.20}$$

to quantify the potential capability in heat transfer applications with twisted tape. This coefficient compares Nusselt number and friction factor[21] of an empty plain tube (subscript $p$) with an equivalent geometry with the twisted tape insert (subscript $tt$). It can be easily predicted with correlations listed in the previous chapter also for this specific case, because, at least in a restricted range of variation from the BCs used up to now, the geometry seems to have a similar behavior to that of a cylindrical tube with a twisted tape insert described by experimental correlations. For the plain tube, possible formulations are *Petukhov* correlation for friction factor [14]

$$f = (0.790lnRe - 1.64)^{-2} \tag{1.21}$$

valid (as in this case) for

$$3000 \leq Re \leq 5 \cdot 10^6$$

and the *Dittus-Boelter* equation for Nusselt number [15]

$$Nu = 0.023Re^{4/5}Pr^{0.4} \tag{1.22}$$

[21] With definitions previously introduced in 1.1.2. Friction factors and Nusselt numbers.

valid (as in this case) with

$$0.7 \leq Pr \leq 160$$

$$Re \geq 10000$$

$$L/D \geq 10$$

Instead of the TPF definition, which gives average information, a different evaluation method for performance is proposed, applying it to the LEE without twisted tape, by comparing directly the most important parameters already cited. This is not the simpler way to make comparisons, since no analytical expression is available, but it is the most efficient one: simulations are necessary but give an immediate idea of the maximum temperature reached in the fluid, which is the critical variable.

For the single LEE with the same BCs of Table 3 and materials and without TT, using the same mesh determined from the previous grid independence analysis

$$\Delta T \approx 110°C$$

$$T_{max,f} \approx 135°C$$

$$\Delta p \approx 0.44bar$$

which means, in a single passage of the series

$$\Delta T_{2LEEseries} \approx 2 \times \Delta T_{singleLEE} \approx 220°C$$

$$T_{max,f_{2LEEseries}} \approx T_{water,inlet} + \Delta T_{2LEEseries} \approx 245°C$$

$$\Delta p_{2LEEseries} \approx 2 \times \Delta p_{singleLEE} \approx 0.88bar$$

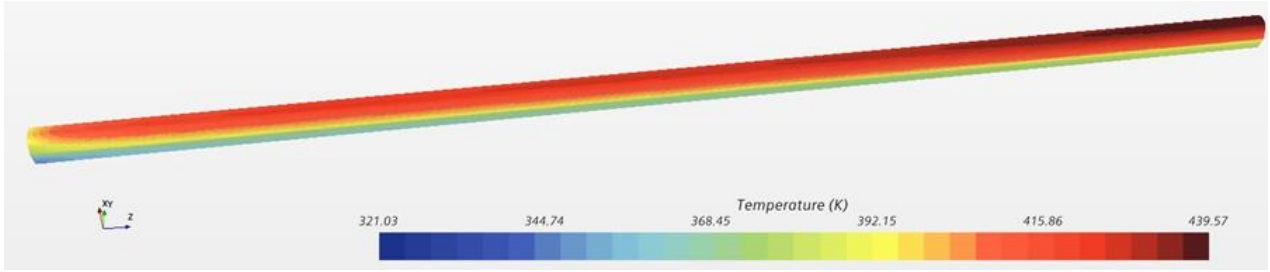


(a)

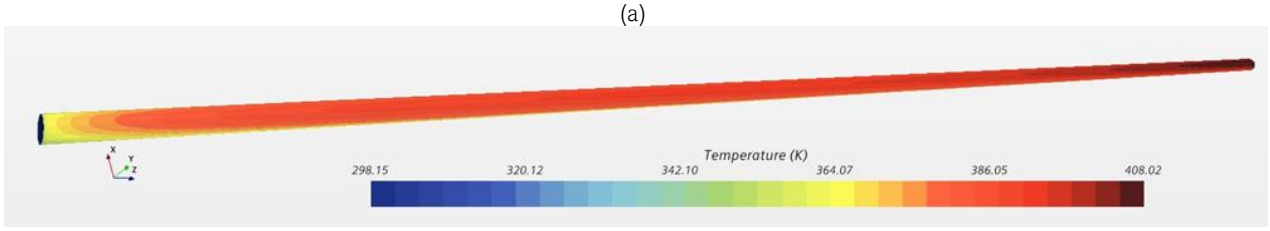


(b)

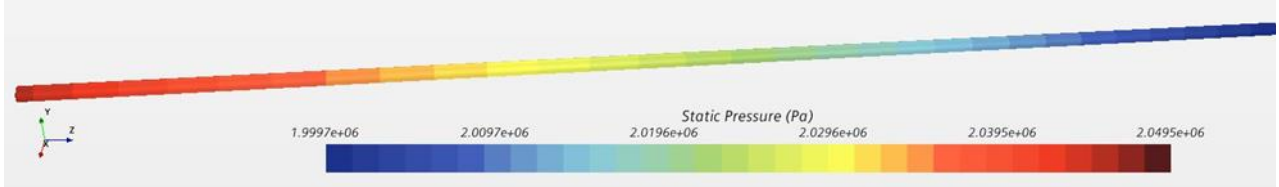


(c)

*Figure 30 Results for a LEE without twisted tape and same BCs: temperature in solid case (a), temperature in fluid (b), pressure (c)*

Hence, considering results in Figure 30, if a LEE without twisted tape is selected, with the heat load of 1.5MW/m$^2$, mass flow should be increased to avoid saturation point for water and this would increase also the pressure drop, which is anyway lower than for the twisted tape solution. The main problem is that it may be not possible to provide water to the LEE in such mass flow conditions; therefore, it is mandatory to

understand if the BCs initially imposed can be satisfied considering the entire hydraulic circuit of the neutralizer and determine how the entire circuit responds to the inlet mass flow rate to select the best option.

## 1.4. First fluid dynamic study of the neutralizer

The development of the rudimental conceptual design[22] (Figure 3) leads to a first possible configuration of the neutralizer. It is not an engineering design, but it allows the feasibility assessments.

The construction - reported in Figure 31 - is composed by two main symmetric blocks (blue): *block 1* on the left and *block 2* on the right. Water is supplied from the inferior duct and exits from the upper duct, running through the hydraulic system by splitting in two subcircuits in parallel: the first one feeding the *LEEs*, the second one feeding the two blocks. The latter are, essentially a set of 6 total panels, 3 per blocks: from the outside to the inside, they are named *lateral, halfway* and *central* respectively. A number will be used to define the block to which they belong.

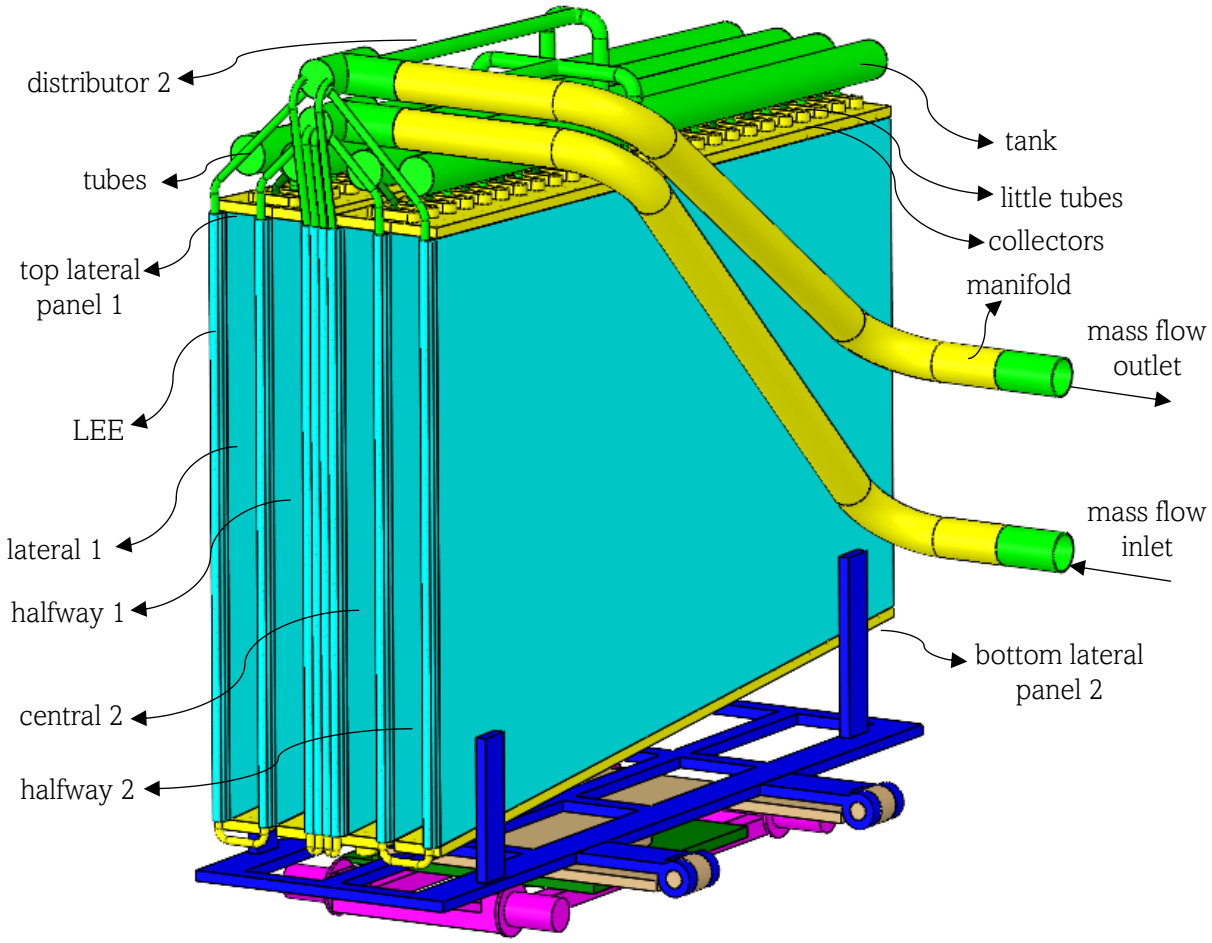


*Figure 31 Conceptual design of the neutralizer*

The LEEs can be seen as four series of two LEEs per passage, which realize U-shapes and are fed by 4 of the 8 inclined *tubes* (green) visible on the top front, while each panel has 26 vertical channels, parallel to the LEEs

[22] Provided by *DTT S.c.a.r.l.*

main axis. Similarly to the LEEs, half of them receive water from the inlet and the remaining ones are the delivery line, in such alternate way that each panel is substantially independent from the others.

Water is conveyed to the panels through the *manifold* (yellow and first T-shape green ducts), which fill the *distributor* system (remaining green part). From the horizontal *tanks* (green) located in the upper part, with a total of 78 *little tubes*, water is driven to the three-way *collectors* at the *top* horizontal *panels* (yellow) and then split, along the single tank, to the inlets of each panel of the two blocks.

A detail of one of the three-way collector which allows the water distribution is given in Figure 32.

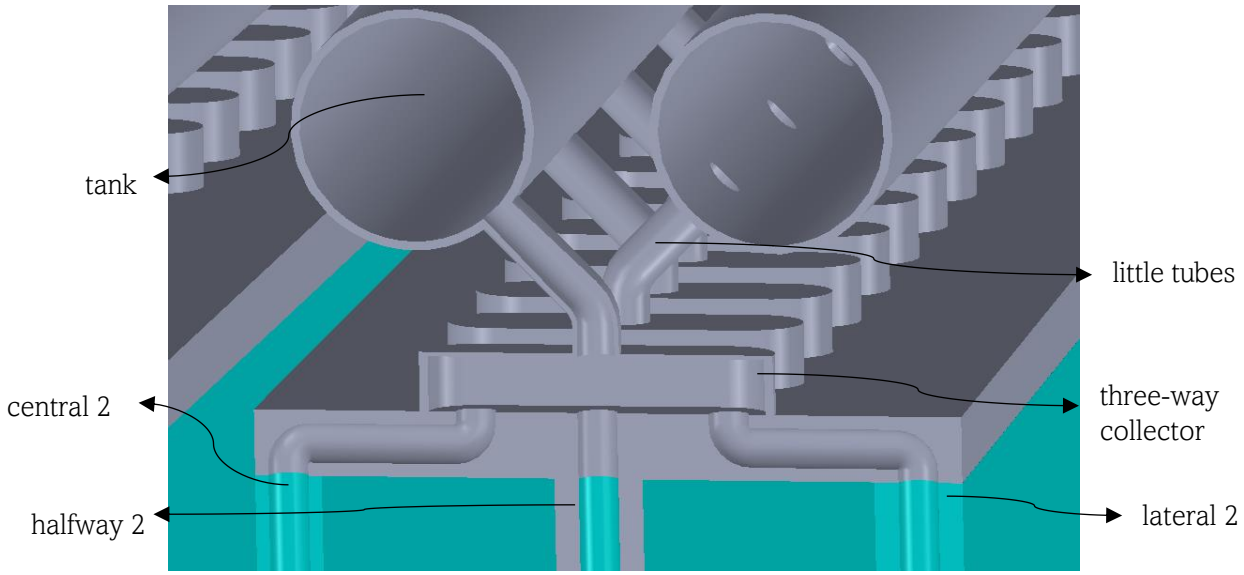


*Figure 32 Detail of the three-way collector and adjacent components*

The original CAD has been adjusted for simulation, without changing the main characteristics[23].

To simulate the entire original model, since the real heat load is not known for the time being, only CFD analysis is performed. This separate study should have been done anyway, because - as already noticed - thanks to the fact that forced convection can be assumed, the fluid dynamic problem does not depend on the thermal one, and the decoupling of the two consequently allows a better understanding of the single phenomena and a simpler optimization of the geometry, taking into account the physical nature of the problem in a more detailed and transparent way by acting directly on the real critical areas and appropriately calibrating the refrigeration system.

The purpose of this study is to understand if at least the most critical component (the LEE) can be fed with the right flow rate and what is the effect on the total pressure drop between the inlet and the outlet of the entire neutralizer (pressure drop IO).

To obtain a mass flow rate of 2kg/s at each LEE, as from the known reference conditions in [2], the maximum available mass flow rate is needed at the inlet of the entire neutralizer.

The entire fluid volume is extracted from the CAD model of the neutralizer in its conceptual shape. Water properties are the same used in the previous chapter (Table 2), while boundary conditions have been imposed as in Table 10. Specific value of the pressure at outlet has no particular meaning, since the relevant quantities for losses evaluation are the pressure differences. For the sake of simplicity, a null value is therefore selected.

[23] Details of main modifications are in *Appendix*, CAD reconstruction.

| Region | Boundary conditions fluid dynamic problem | | | |
|---|---|---|---|---|
| inlet | mass flow inlet | $\dot{m}$ | 40 | kg/s |
| outlet | pressure outlet | $p_{out}$ | 0 | bar |
| other surfaces | no slip | $v=v_{wall}$ | 0 | m/s |

*Table 10 Boundary conditions for CFD simulation for the entire neutralizer*

Due to the size of the model and to the computational cost of the simulation, no mesh convergence has been performed in this case and a big base size is selected for the mesh, which is characterized by a polyhedral part for the inner channel with prism layer at the walls. Results must be considered with poor accuracy, but this does not affect the goal of the simulation, that is to have a qualitative idea of the pressure distribution to highlight potential critical areas and obtain guidelines for optimizations. Attention on y+ value has been made, trying to limit it to unitary values where possible.

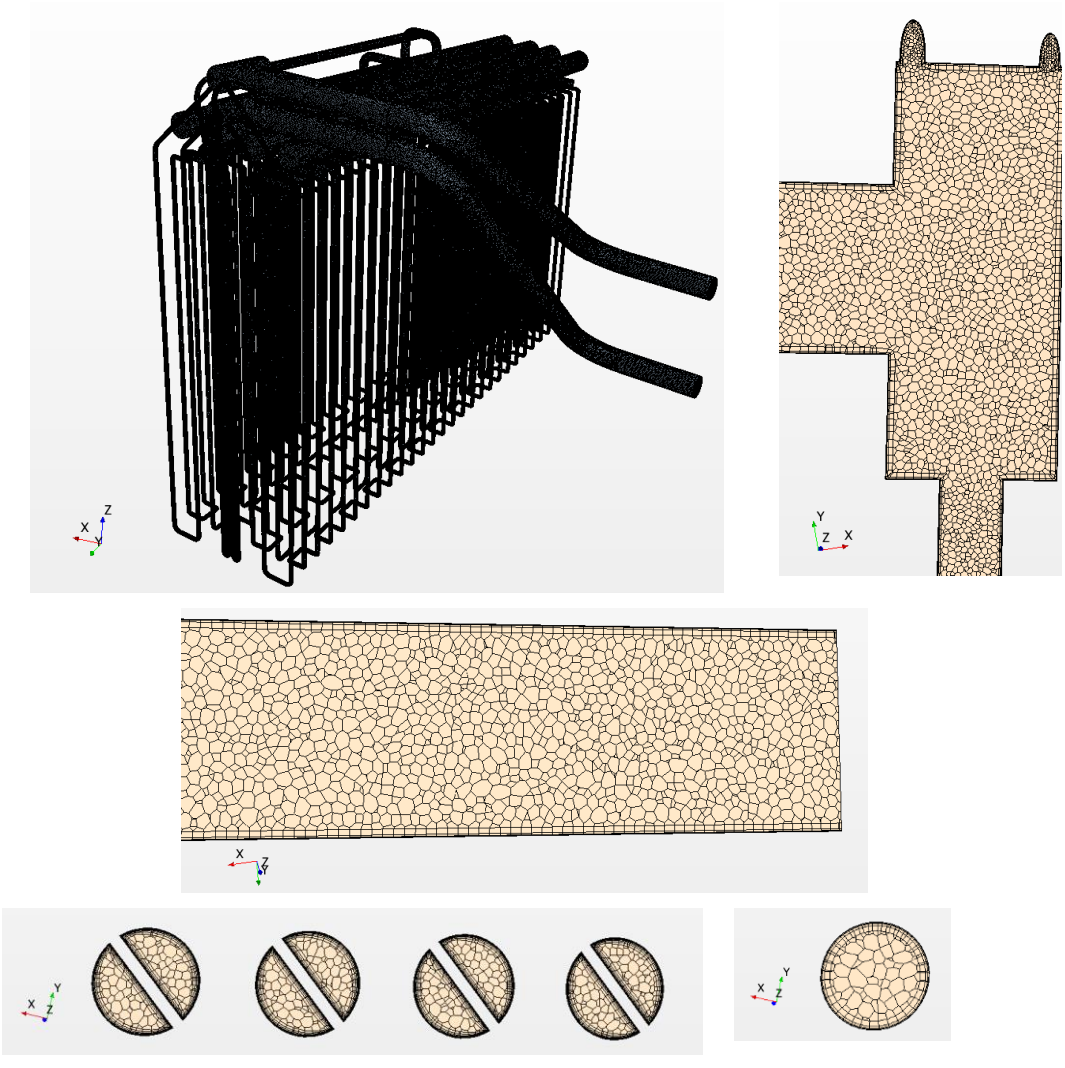

*Figure 33 Mesh of the original CAD: entire mesh (top left), detail of the T-shape manifold (top right), detail of manifold section (middle), detail of central LEEs cross sections (down left) and panels' tube (down right). Total number of cells: 48652293.*

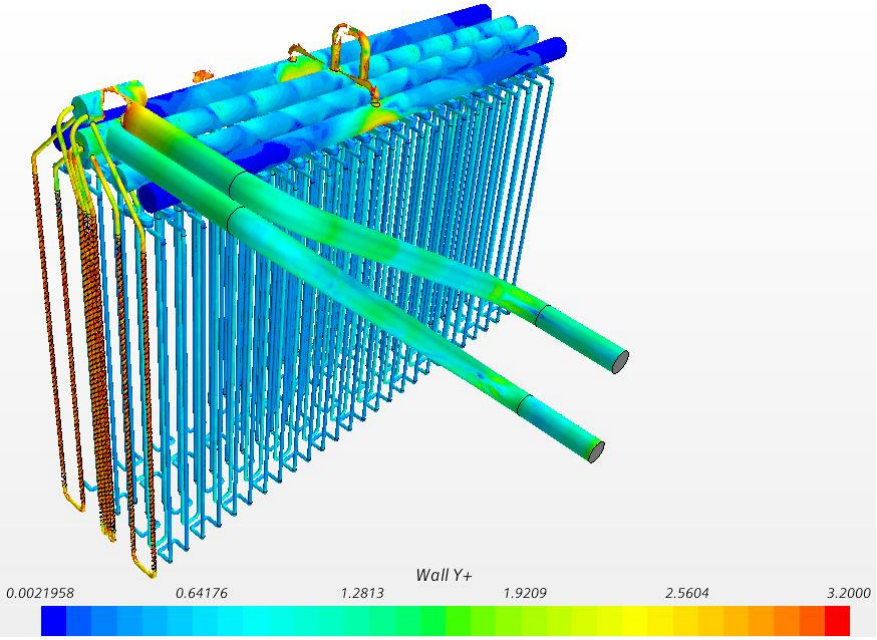


*Figure 34 Wall y+ for CAD original entire with TT*

From the analysis of the LEE, in view of the convergence of the pressure drop on this component as a function of the mesh size (Figure 13), it is reasonable to expect that, with a coarser mesh, with respect to that adopted for the detailed LEE analysis, a higher pressure drop will be modeled in this piece of hydraulic circuit. Consequently, also the total pressure drop IO will be higher than the two LEE series evaluated before (8.2 bar), and will be furtherly increased by the pressure drops that occur in the remaining parts of the circuit. The entire neutralizer analysis can therefore be considered conservative from the pressure drop point of view.

The selected model (Table 11) requires a k-$\varepsilon$ model and a segregated solver to speed up the solution.

| Continua model: water |
|---|
| Gradients |
| Segregated Flow |
| Solution Interpolation |
| Two-Layer All y+ Wall Treatment |
| Wall Distance |
| Realizable K-Epsilon Two-Layer |
| K-Epsilon Turbulence |
| Reynolds-Averaged Navier-Stokes |
| Turbulent |
| Constant Density |
| Liquid |
| Steady |
| Three Dimensional |

*Table 11 Continua model for the entire neutralizer simulation*

To quantify the losses inside the circuit, with this model setup, different sections are considered[24]. With reference to Figure 35, to have 2kg/s at LEE, the total pressure drop realized between inlet and outlet is approximately 13.6bar (Table 12) and the principal cause is the LEE itself, as anticipated. The sums of static pressure differences in the two separate parallel circuits - the one to the LEEs and the one to the panels[25] - coincide, as expected, with the total pressure drop IO.

[24] Further details in *Appendix*, Detailed results for simulation for the original CAD with TT

[25] Sum of static pressure differences in parallel circuit to the LEEs is given by (inlet-tube2,4,5,7) + (tube2,7,4,5-tube1,8,3,6) + (tube1,3,6,8-outlet), where the commas represent all the alternative sections of LEEs for the jump calculation. Sum of

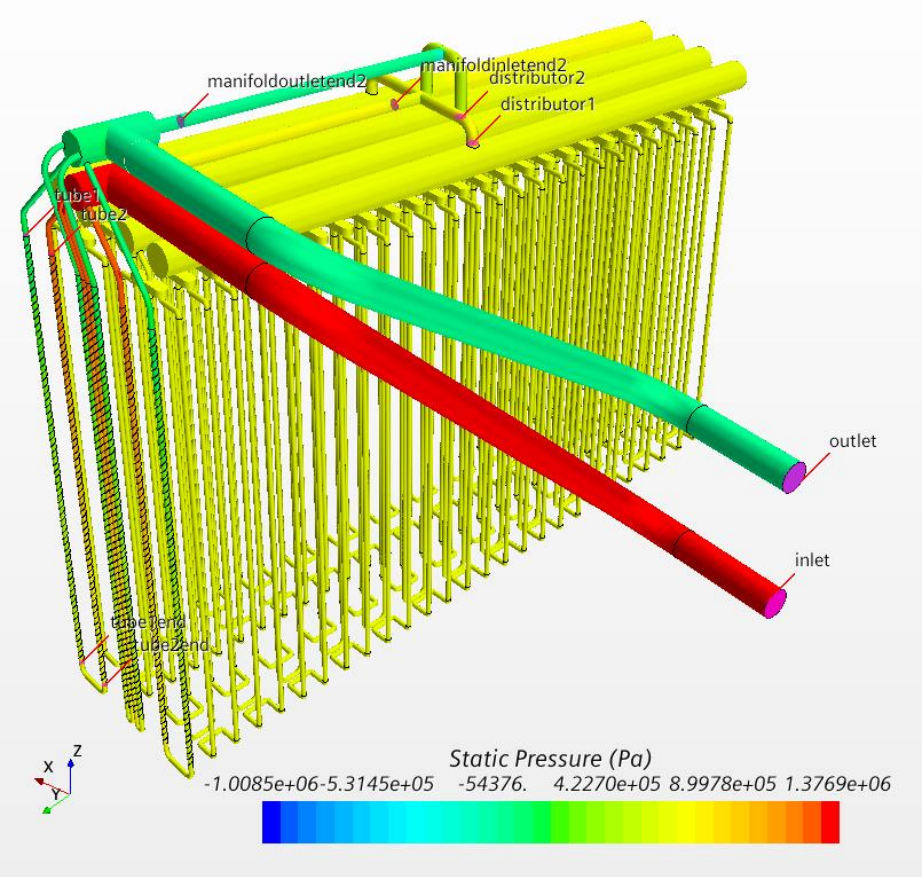


*Figure 35 Pressure distribution for the TT, with total mass flow of 40kg/s: main sections. LEE1 inlet-outlet sections are named as tube1 and tube1end. Similarly and alternatively also other LEEs, numbered progressively from left to right.*

| Static Pressure Differences (Pa) | |
|---|---|
| **Forward circuit Static Pressure differences (Pa)** | |
| inlet-tube2,4,5,7 | 7.69E+04 |
| inlet-manifoldinletend2 | 6.63E+05 |
| manifoldinletend2-distributor1 | 1.33E+03 |
| **Return circuit Static Pressure differences (Pa)** | |
| tube1,3,6,8-outlet | 9.85E+04 |
| distributor2-manifoldoutletend2 | 4.80E+05 |
| manifoldoutletend2-outlet | 4.40E+03 |
| **Pressure drops on panels and LEEs (Pa)** | |
| distributor 1-distributor2 | 2.11E+05 |
| tube2-tube1 | 1.19E+06 |
| tube7-tube8 | 1.19E+06 |
| tube4-tube3 | 1.19E+06 |
| tube5-tube6 | 1.18E+06 |
| sum of pressure difference (parallel circuit to LEEs) | 1.36E+06 |
| sum of pressure difference (parallel circuit to Panels) | 1.36E+06 |
| **Pressure Drop IO** | 1.36E+06 |
| **Mass flows** | |
| Mass Flow Inlet (kg/s) | -40.00 |
| Mass Flow tube 1 (kg/s) | 2.06 |
| Mass Flow distributor1 (kg/s) | -15.70 |

*Table 12 Static pressure differences in the entire original CAD with 40kg/s*

static pressure differences in parallel circuit to the panels is given by (inlet-manifoldinletend2) + (manifoldinletend2-distributor1) + (distributor1-distributor2) + (distributor2-manifoldoutletend2) + (manifoldoutletend2-outlet).

Each LEE has a different mass flow, due to the asymmetric position of the manifold, and the pressure drop is slightly overestimated, due to the coarse mesh. Two main circuits are highlighted: considering the LEEs or panel channels, the *forward circuit* (from the inlet) in the negative direction of z-axis and the *return circuit* (to the outlet) in the positive direction of z-axis.

These two circuits emphasize the critical parts where higher pressure differences occur: as evident from Table 12, excluding the LEEs, additional sources of pressure losses are the abrupt changes in geometry in the flow area of the *T-shape manifold* (Figure 36) and of the *distributor* (Figure 37), respectively delimited by the sections *inlet-manifoldinletend2 (*and *tube2,4,5,7)* and *distirbutor2(*and *2b)-manifoldoutletend2*. This can also be graphically observed from the abrupt discontinuity of colored plot of static pressure and from the velocity field (Figure 38): the latter stresses two points in red where velocity is high. Since the pressure losses scales with the square of velocity, these two points are meaningful to individuate areas where geometry could be adjusted to better convey the fluid and correctly guide the flow.

| FORWARD CIRCUIT | | RETURN CIRCUIT | |
|---|---|---|---|
| Manifold T-shape | | Distributor | |
| PressureInlet (Pa) | 1.36E+06 | PressureOutlet (Pa) | -1.14E-02 |
| Pressure Static manifold inlet end (Pa) | 7.63E+05 | Pressure Static manifold outlet end2 (Pa) | 4.40E+03 |
| Pressure Static manifoldinletend2 (Pa) | 6.97E+05 | Pressure Static manifold outlet end3 (Pa) | 1.50E+04 |
| Pressure Static distributor1 (Pa) | 6.96E+05 | Pressure Static distributor2 (Pa) | 4.84E+05 |
| Pressure Static distributor1b (Pa) | 7.01E+05 | Pressure Static distributor2b (Pa) | 4.84E+05 |
| Mass Flow Inlet (kg/s) | -40.00 | Mass Flow distributor2b (kg/s) | 16.05 |
| Mass Flow tube 1 (kg/s) | 2.06 | Mass Flow distributor2 (kg/s) | 15.66 |
| Tubes | | Tubes | |
| Pressure Static tube 2 (Pa) | 1.28E+06 | Pressure Static tube 1 (Pa) | 9.85E+04 |
| Pressure Static tube 2end (Pa) | 6.65E+05 | Pressure Static tube 1end (Pa) | 6.60E+05 |
| Pressure Static tube 4 (Pa) | 1.29E+06 | Pressure Static tube 3 (Pa) | 1.01E+05 |
| Pressure Static tube 4end (Pa) | 6.89E+05 | Pressure Static tube 3end (Pa) | 6.69E+05 |
| Pressure Static tube 5 (Pa) | 1.28E+06 | Pressure Static tube 6 (Pa) | 1.01E+05 |
| Pressure Static tube 5end (Pa) | 6.89E+05 | Pressure Static tube 6end (Pa) | 6.70E+05 |
| Pressure Static tube 7 (Pa) | 1.29E+06 | Pressure Static tube 8 (Pa) | 9.83E+04 |
| Pressure Static tube 7end (Pa) | 6.91E+05 | Pressure Static tube 8end (Pa) | 6.84E+05 |

*Table 13 Forward and return circuits in the entire neutralizer with TT*

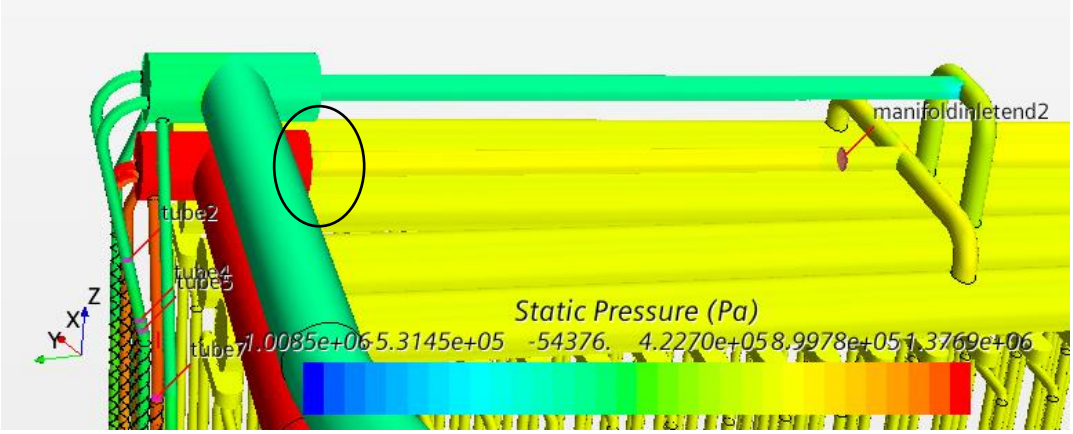


*Figure 36 T-shape manifold (forward circuit) delimited by purple sections and the inlet. The abrupt pressure discontinuity is highlighted by the passage from red to yellow color (indicated by the black circle).*

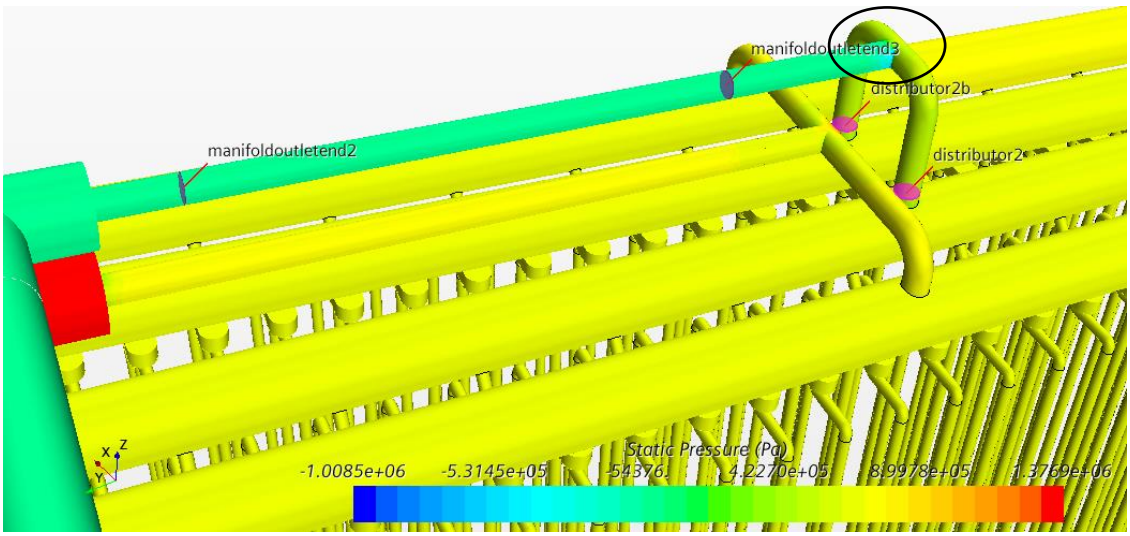


*Figure 37 Distributor (return circuit) delimited by purple sections. The abrupt pressure discontinuity is highlighted by the passage from yellow to green color (indicated by the black circle).*

From Table 13, it is therefore possible to extrapolate two simplified models and decouple the problem to investigate alternative configurations which can reduce the total pressure drop. For the forward circuit, pressure in sections at the inlet of the LEEs' series (tube 2, 4, 5, 7) is approximately the same, while the mass flow directed to the distributor channel is the difference between inlet total mass flow and total mass flow to the LEEs. For the return circuit pressure at disributor2 and 2b is the same. Instead of absolute values of pressures, when they coincide, for the sake of simplicity null values can be imposed, by expressing them as referred to reference values, that means to focus on differences.

The procedure is not immediate since a little variation in geometry breaks the balance of mass flows.

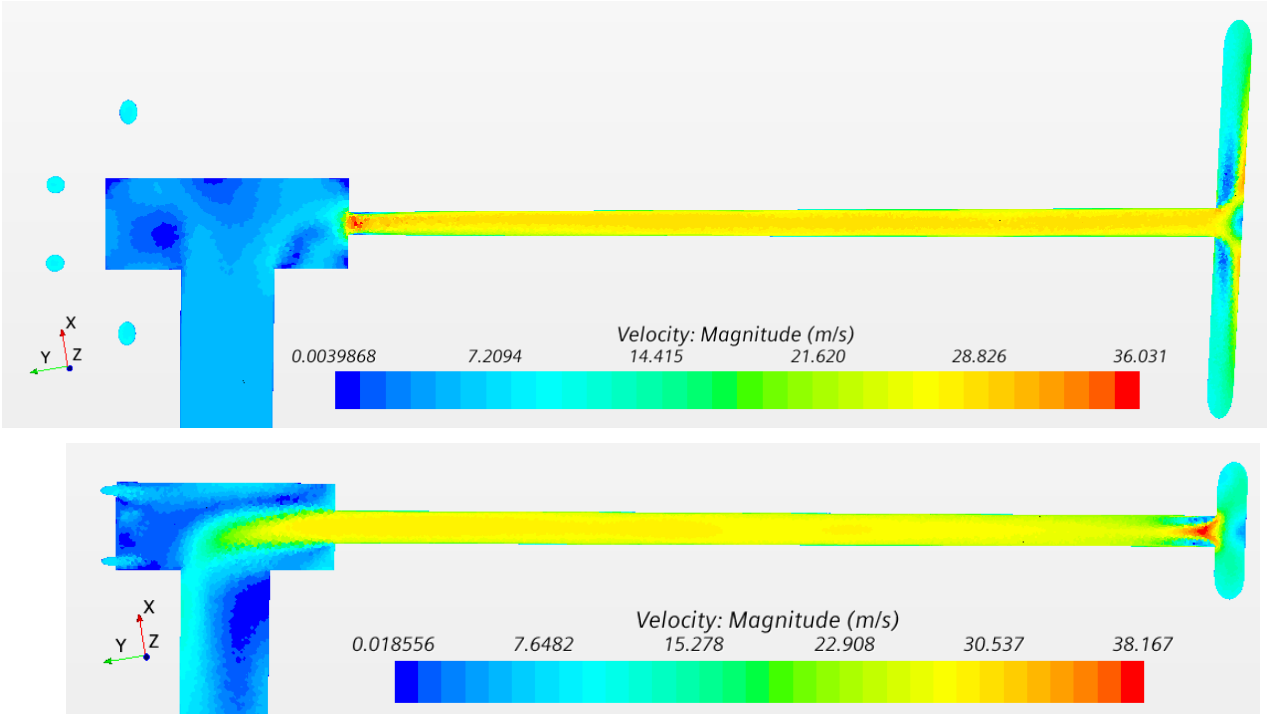


*Figure 38 Velocity field: T-shape manifold from the forward circuit with fluid from left to right (top) and distributor from the return circuit with fluid from right to left (bottom). Top view of the neutralizer.*

# 1.5. CFD optimization of single components: alternative configurations

Critical components from fluid dynamic point of view can be selected and studied to provide possible alternative configurations. The references to known literature cases is of great help for the analysis.

## 1.5.1. T-shape manifold optimization

### Original shape and literature knowledge

From Table 13, for the T-shape manifold the following boundary conditions can be imposed to setup the CFD simulation:

| | | | |
|---|---|---|---|
| pressure outlet | outlet di tutti i tubi ai LEE | 0 | Pa |
| mass flow inlet | inlet | 40 | kg/s |
| outlet, mass flow | outlet del tubo al distributor | 32 | kg/s |

*Table 14 CFD boundary conditions for standalone analysis of T-shape manifold*

To have a better and representative estimation of this part, and to validate the simplified extrapolated model, the original shape of the standalone critical length is tested in a simulation separately and then compared to other geometries. The selected model is the same of the CFD analysis of the entire neutralizer and it is described in Table 11, while material properties for water are listed in Table 2. The velocity field (Figure 39) confirms the possibility of introducing adjustment in the restricted section.

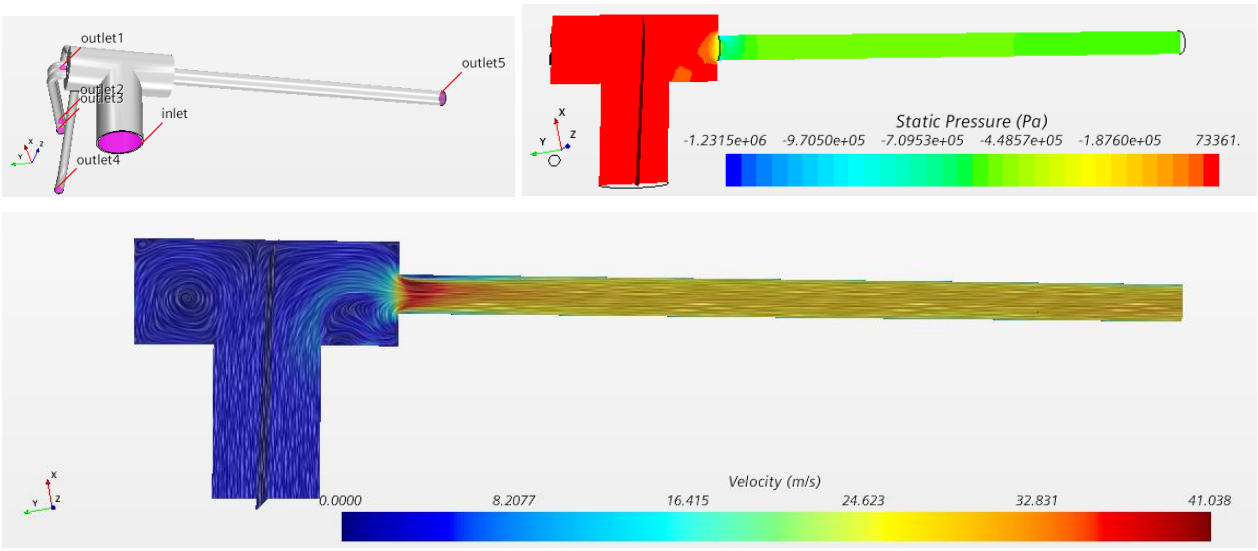


*Figure 39 T-shape manifold standalone, original shape: geometry and BCs sections (top left), section view of static pressure (top right), velocity field (bottom)*

From literature, it is well known that a sudden contraction or reduction in pipe size is the cause of pressure losses and can be estimated analytically by means of a pressure loss equation which is [16]

$$h_f = \left(\frac{1}{C_c} - 1\right)\frac{V_2^2}{2g} \tag{1.23}$$

where $V_2$ is the velocity in correspondence of $A_2$, $A_1$ and $A_2$ are the two cross sectional areas from which the coefficient $C_c$ depends on and is tabulated (Figure 40)

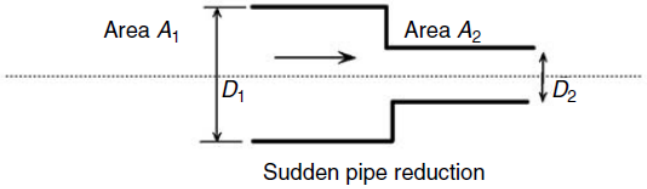


| $A_1/A_2$ | 0.00 | 0.10 | 0.20 | 0.30 | 0.40 | 0.50 | 0.60 | 0.70 | 0.80 | 0.90 | 1.00 |
|---|---|---|---|---|---|---|---|---|---|---|---|
| $C_c$ | 0.585 | 0.624 | 0.632 | 0.643 | 0.659 | 0.681 | 0.712 | 0.755 | 0.813 | 0.892 | 1.000 |

*Figure 40 Sudden pipe reduction [16]*

Many designs are known to reduce the pressure drops, such as rounded contractions or reentrant ducts.

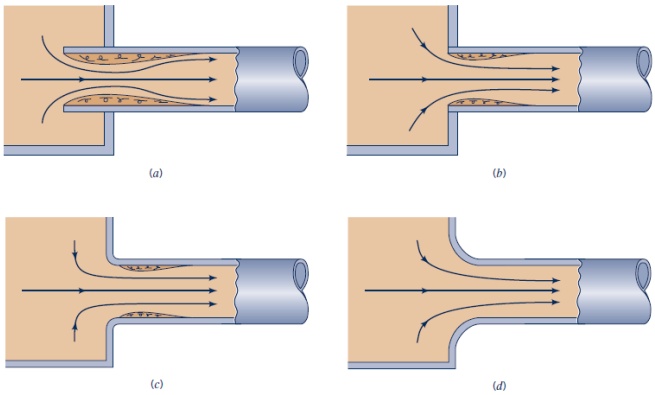


*Figure 41 Entrance flow conditions and loss coefficient: (a) Reentrant, $K_L$=0.8, (b) sharp-edged, $K_L$=0.5, (c) slightly rounded, $K_L$=0.2, well-rounded, $K_L$=0.8 [7]*

By defining the loss coefficient [7] as

$$K_L = \frac{\Delta p}{\frac{1}{2}\rho V} \tag{1.24}$$

in fact, the greater the coefficient $K_L$, the greater the $\Delta p$ losses[26]. As suggested from Figure 42 one possibility for the improvements of the design could be reducing the ratio between the two cross-sectional areas of the

[26] Many ideas are available in [12] and [17].

ducts or adopting less sharp entrance to guide and avoid vortex formation in the corner and consequently reduce friction.

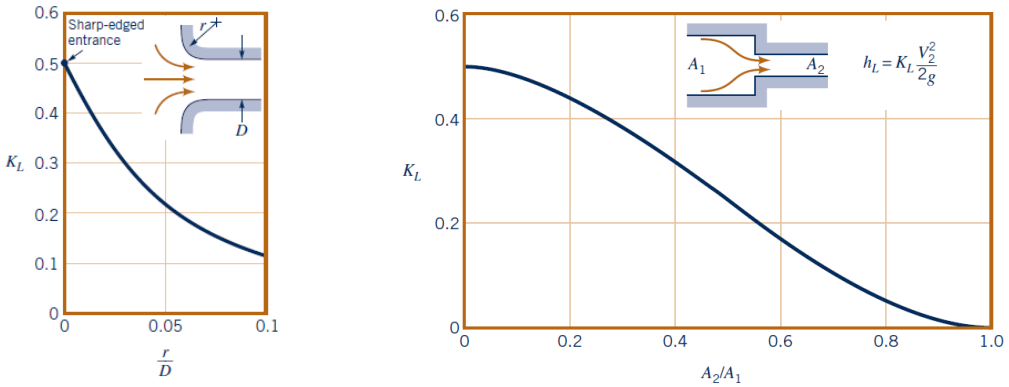


*Figure 42 Entrance loss coefficient for rounded and sharp-edged entrance [7]*

If instead of this sudden contraction a gradual reduction is selected, beneficial effects can be found in the total loss and the gain increases decreasing the cone angle and the ratio between the larger and smaller diameters.

Another loss coefficient parameter (similar to $K_L$) is:

$$h_c' = k_c' \frac{V_2^2}{2g}$$

*Contraction* (for $\theta = 20°$):
$K_L = 0.30$ for $d/D = 0.2$
$K_L = 0.25$ for $d/D = 0.4$
$K_L = 0.15$ for $d/D = 0.6$
$K_L = 0.10$ for $d/D = 0.8$

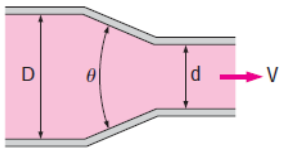


| $D_2/D_1$ | $K_C$ $\theta = 60°$ | $K_C$ $\theta = 180°$ |
|---|---|---|
| 0.0 | 0.08 | 0.50 |
| 0.20 | 0.08 | 0.49 |
| 0.40 | 0.07 | 0.42 |
| 0.60 | 0.06 | 0.27 |
| 0.80 | 0.06 | 0.20 |
| 0.90 | 0.06 | 0.10 |

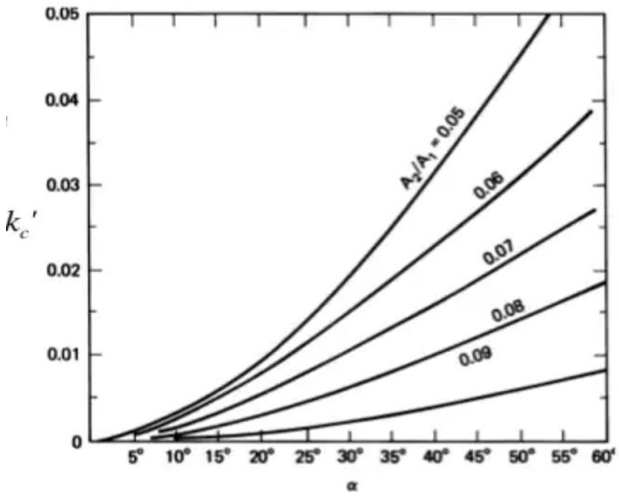


*Figure 43 Loss coefficient for gradual reduction [12]*

For a rounded pipe reducer [17] (a rounded entrance with convex curvature), with the same nomenclature of Figure 40

$$K_L = \left(0.1 + \frac{50}{Re_1}\right)\left[\left(\frac{D_1}{D_2}\right)^4 - 1\right] \tag{1.25}$$

## Manual iterative optimization attempts based on literature knowledge

First possible modification can be a cone-shape section reduction, according to the previous observations.

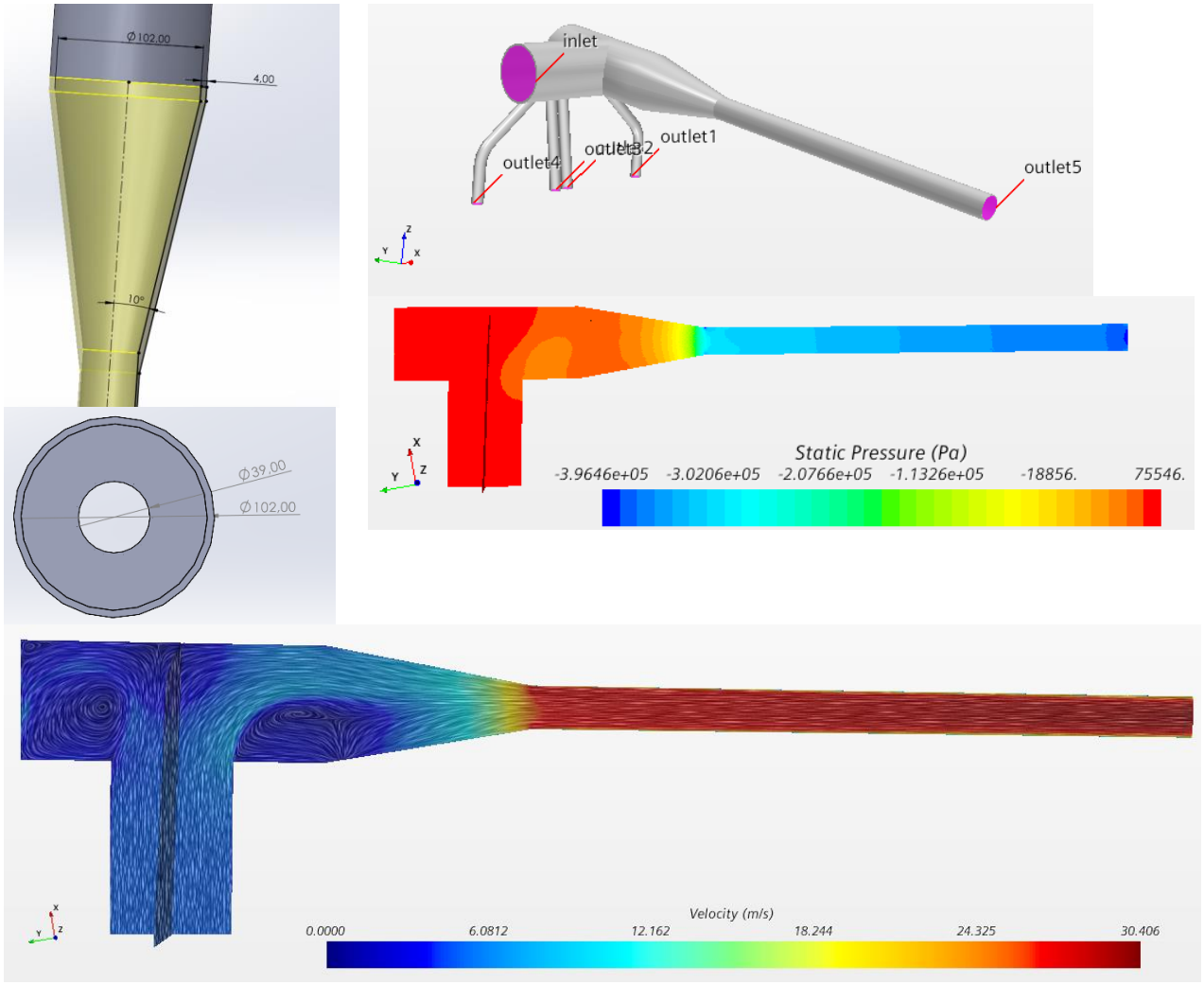


*Figure 44 T-shape manifold optimization, cone 10°: geometry and BCs sections (top left), section view of static pressure (top right), velocity field (bottom)*

All the comparisons are made with section views taken with the same plane. A reduction of maximum value in velocity field can be noticed (approximately 26%), corresponding to a pressure drop decreasing.

From literature, by reducing the cone angle, a further decreasing in pressure drop can be expected. In this case, difference with respect to a 10° cone, from the velocity field observation, is not considerable, but a slight improvement is still visible.

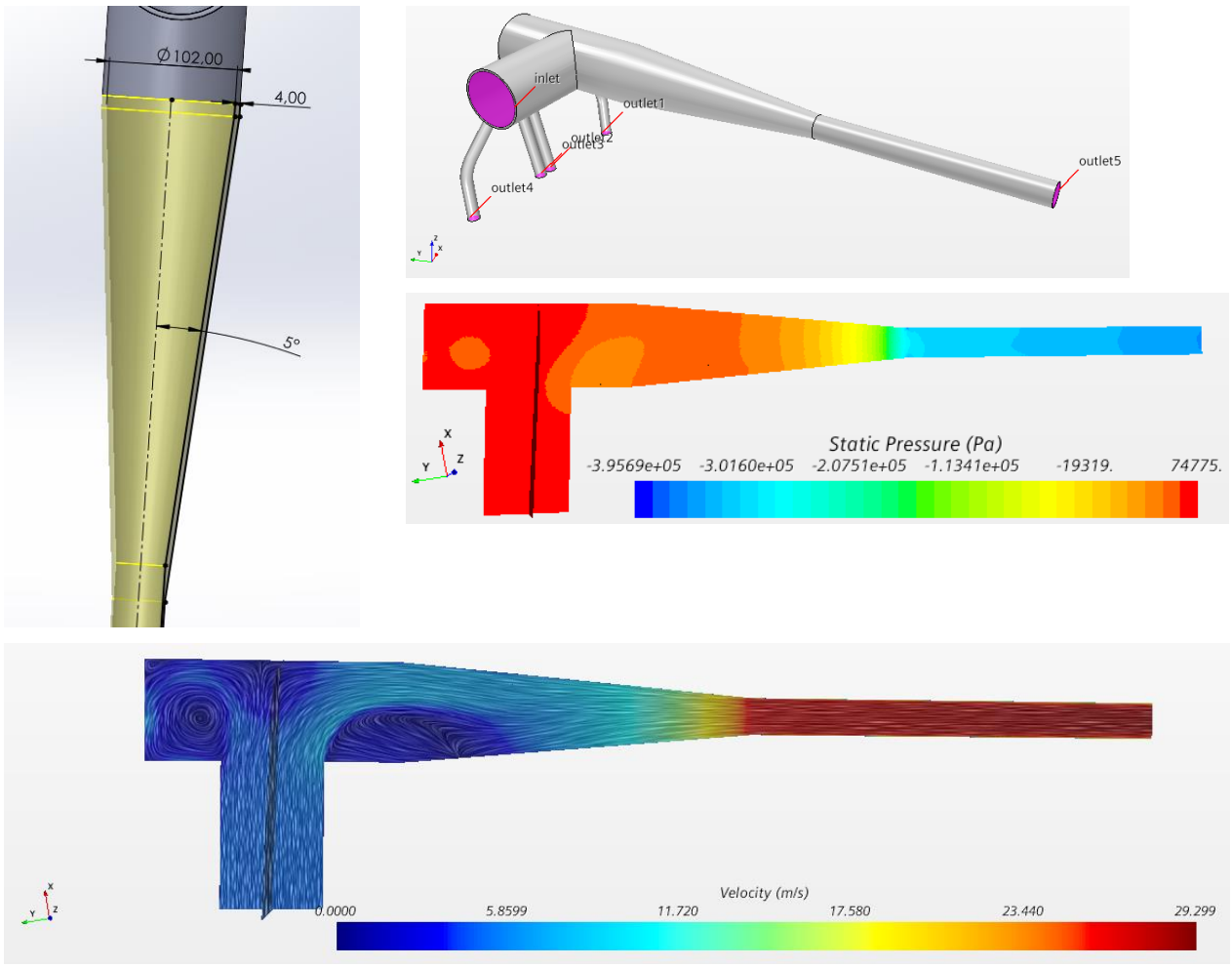


*Figure 45 T-shape manifold optimization, cone 5°: geometry and BCs sections (top left), section view of static pressure (top right), velocity field (bottom)*

Another shape that can be tested is the rounded pipe reducer with a convex filling. In this case, the gain on pressure drop seems to be less convenient with respect to the previous solutions. A higher radius for rounding gives lower maximum velocities: the limit case degenerates in a cone.

The rounded concave entrance (nozzle-like shape) gives better results on speed decreasing with respect to the convex rounding if curvature radius is compared.

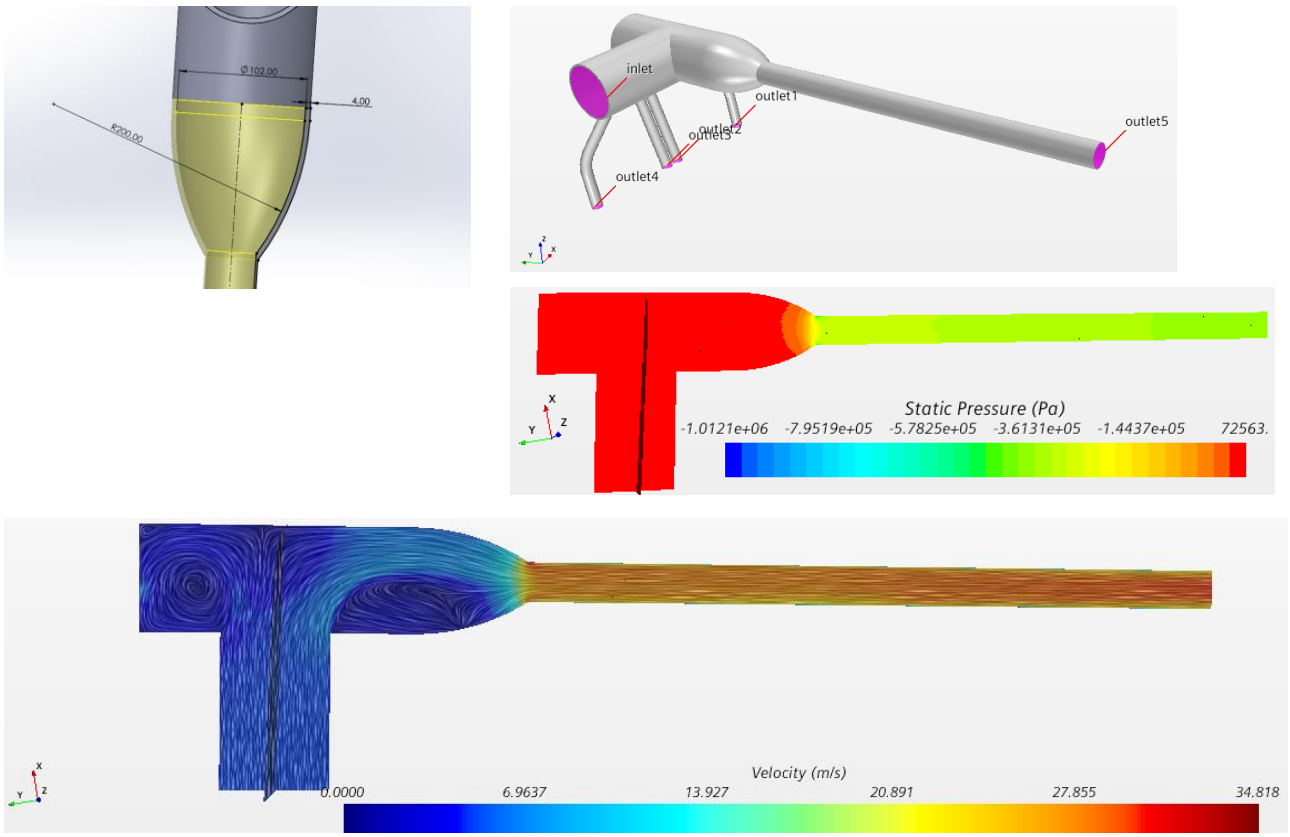


*Figure 46 T-shape manifold optimization, rounded pipe reducer filling R=20cm: geometry and BCs sections (top left), section view of static pressure (top right), velocity field (bottom)*

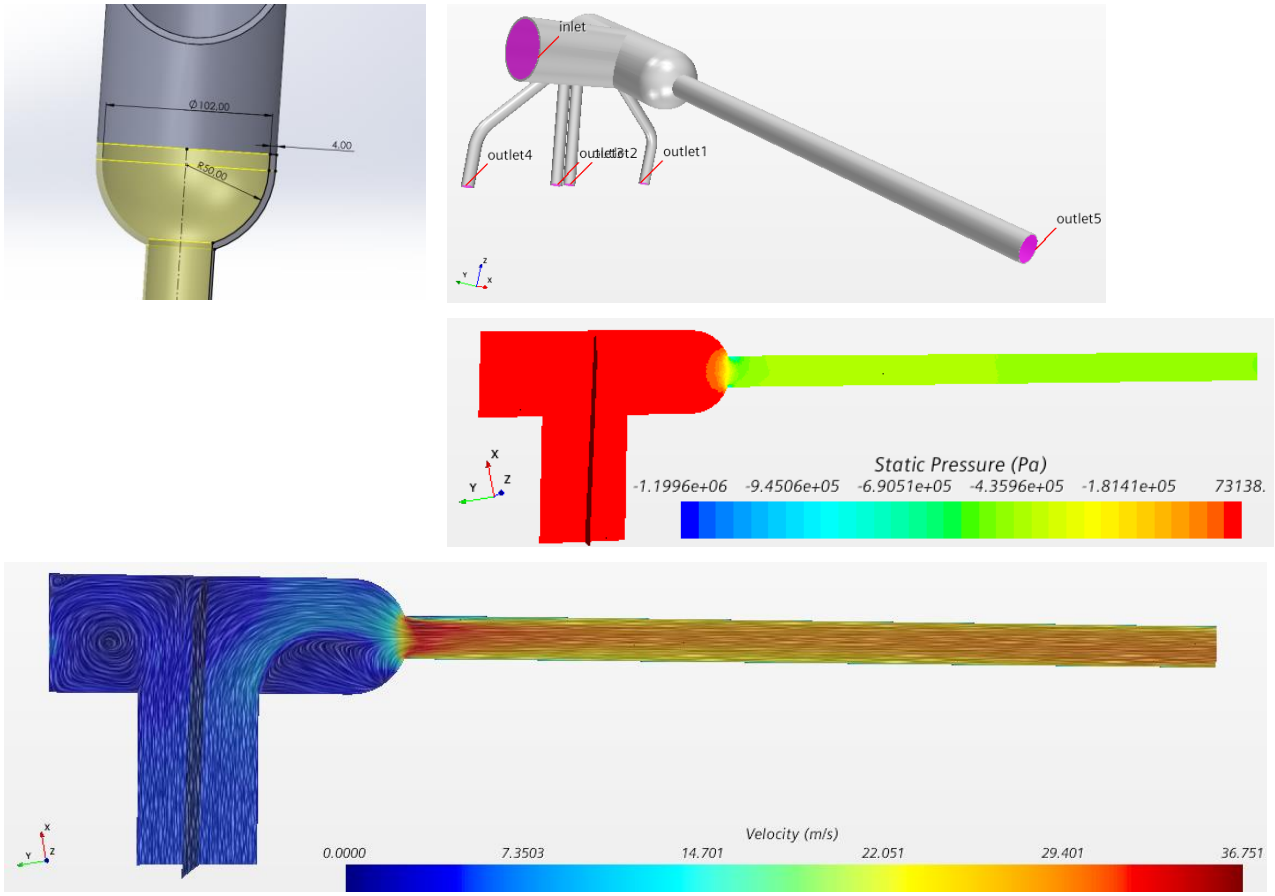


*Figure 47 T-shape manifold optimization, rounded pipe reducer filling R=5cm: geometry and BCs sections (top left), section view of static pressure (top right), velocity field (bottom)*

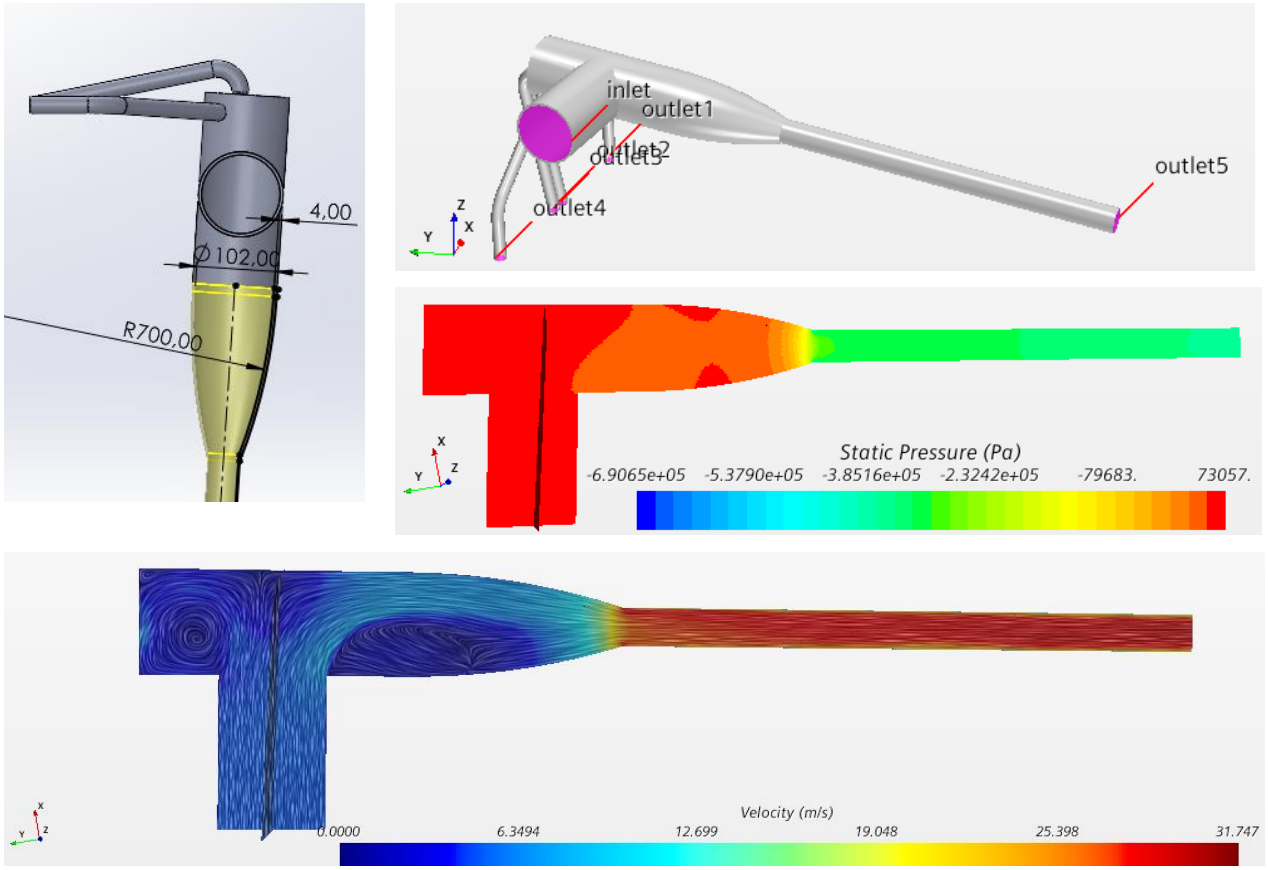


*Figure 48 T-shape manifold optimization, rounded pipe reducer filling R=70cm: geometry and BCs sections (top left), section view of static pressure (top right), velocity field (bottom)*

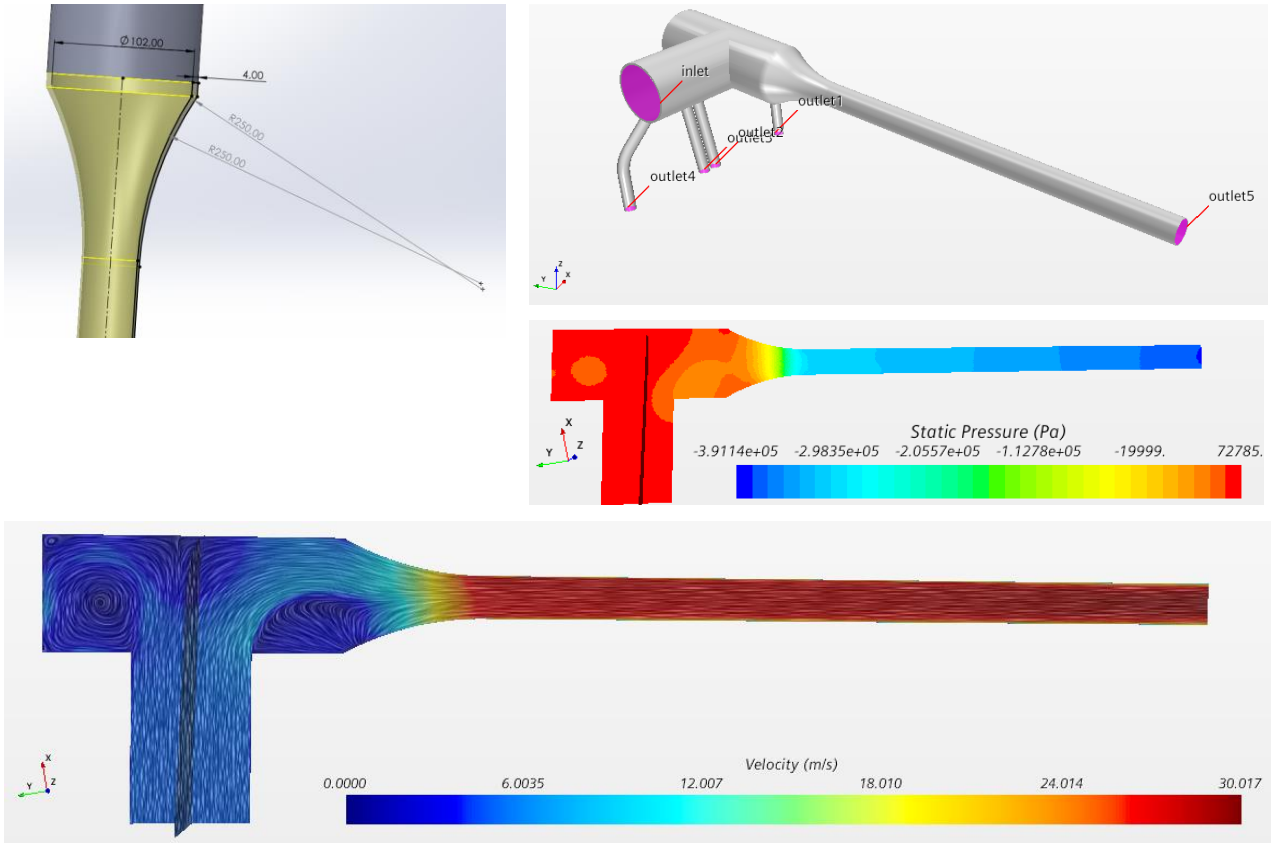


*Figure 49 T-shape manifold optimization, nozzle shape R=25cm: geometry and BCs sections (top left), section view of static pressure (top right), velocity field (bottom)*

## Optimization attempts based on topology

The optimal distribution of material (resulting in the shape of the object) in a specified domain can be determined with a powerful mathematical instrument: adjoint topology optimization. This method is based on the minimization of a predefined field cost function (for example the pressure drop, the maximum temperature etc.) with the use of penalty factors. It allows to study the influence of design parameters and physical inputs on the engineering objective in the simulation [18]. By fixing certain constraints (the minimization of pressure drop in this case), the solver iteratively finds the shape which leads to their satisfaction. The main advantage is that the computational cost does not depend on the number of design variables. Since it leads to particular shapes - optimal from numerical point of view or in additive manufacturing, but not suitable for conventional production – in this context this solution is proposed as a verification of the iterative manual procedure applied before. Material properties are selected as in previous chapter, but the continua model is corrected substituting the segregated model with the coupled to activate the adjoint. The key procedure is to solve the material distribution, so a large design space must be prepared to give freedom to the flow to reach areas at minimum pressure drop guided by the pressure gradient, in this case, and other parameters. The design space is prepared as CAD, volume is then extracted and coarsely meshed.

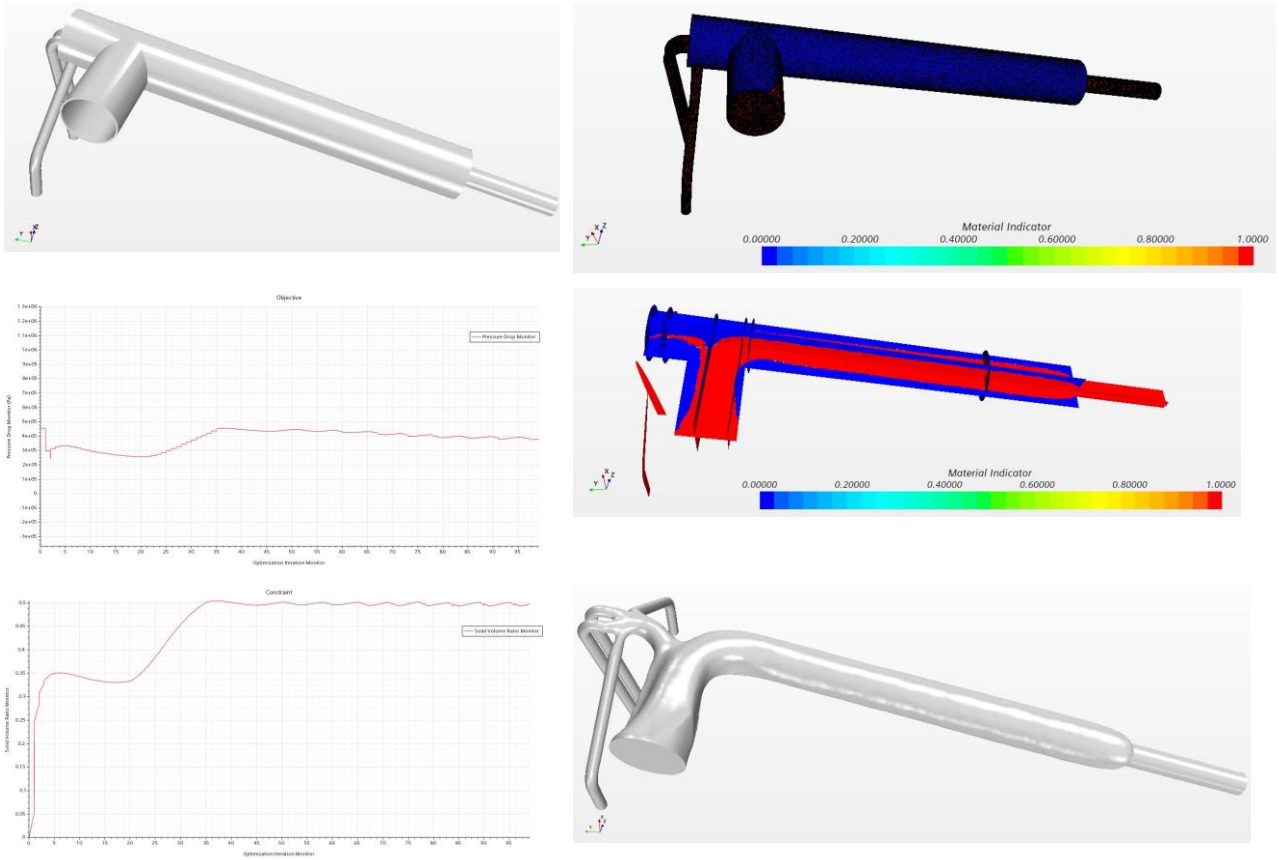


*Figure 50 CAD design preparation (top left), design space at the beginning (top right), design space after solution (middle right), final results for fluid volume after topology optimization (bottom right), Objective function (middle, left) and Constraint function (bottom left)*

At the beginning the entire design space is filled with fluid. During the topology process, solid fraction grows and at the end of the procedure all the inlets and outlets defined should be, at least, connected by the fluid, represented by a material indicator value 1.0. Two important graphs can be reported: the objective and the constraint functions. The first one is represented in this case by the pressure drop, while the second one by the solid volume ratio, which expresses the fraction of solid volume with respect to the fluid volume. Both are given as function of optimization iterations.

At first, since the algorithm is iterating to meet the objective and the constraint, pressure drop significantly varies over the optimization iterations until, after a certain number of iterations, constraint oscillates on a fixed value (it was imposed in this case that no more than 50% must become solid as a design choice), while objective tends asymptotically to a minimum: that is the target solution.

Qualitatively, this solution goes in a direction which is very similar to the proposed manual optimizations: mainly, a gradual reduction of the section should be adopted to decrease the pressure drop, possibly with a reduction of the diameter near the tubes which goes to the LEEs. This suggestion could be deducted also intuitively, since having a duct with the same cross-sectional area of the sum of the areas of the single tubes would reduce the ratio between the two equivalent diameters and, consequently the pressure drop. Similarly, reducing the diameter to the distributor would have the effect of reducing the ratio of the two diameter of the contraction and again would reduce the pressure drop on the other side of the circuit.

The model used for this simulation is reported in Table 15.

| Continua model: water |
|---|
| Gradients |
| Coupled Flow |
| Solution Interpolation |
| Two-Layer All y+ Wall Treatment |
| Wall Distance |
| Realizable K-Epsilon Two-Layer |
| K-Epsilon Turbulence |
| Reynolds-Averaged Navier-Stokes |
| Turbulent |
| Constant Density |
| Liquid |
| Steady |
| Three Dimensional |
| Topology Physics |
| Topology Optimization |
| Adjoint Frozen Turbulence |
| Adjoint Flow |
| Adjoint |
| Adaptive Mesh |

*Table 15 Continua model for adjoint topology optimization*

The code developed for the simulation can be summarized in the steps shown in Figure 51.

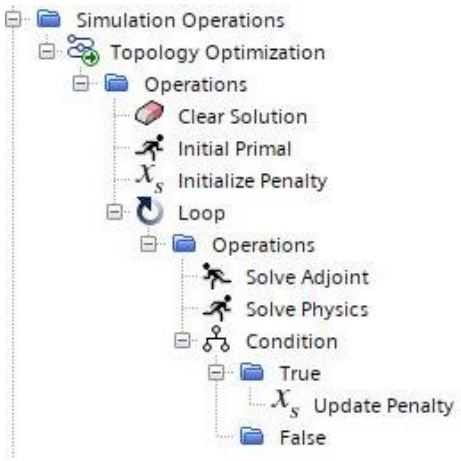


*Figure 51 Simulation Operations for adjoint topology optimization*

## Results

Final results are presented in Table 16. Pressure drop 1, 2 and 3 are the mass flow averaged absolute total pressure differences between inlet and outlet 1, 2, 5 respectively. Shape variation impacts mainly on outlet 5, which is the section that goes to the distributor and where the reduction was desired.

| | original shape | cone 10° | cone 5° | filling R200mm | filling R50mm | filling R700mm | nozzle R250mm |
|---|---|---|---|---|---|---|---|
| Pressure Drop 1 (Pa) | 3.84E+04 | 4.15E+04 | 4.03E+04 | 3.71E+04 | 3.84E+04 | 3.79E+04 | 3.86E+04 |
| Pressure Drop 2 (Pa) | 3.87E+04 | 4.11E+04 | 3.98E+04 | 3.80E+04 | 3.85E+04 | 3.85E+04 | 3.78E+04 |
| Pressure Drop 3 (Pa) | 2.64E+05 | 7.07E+04 | 4.90E+04 | 8.22E+04 | 1.75E+05 | 6.26E+04 | 7.10E+04 |
| Pressure inlet (Pa) | 6.14E+04 | 6.37E+04 | 6.28E+04 | 6.06E+04 | 6.12E+04 | 6.10E+04 | 6.08E+04 |
| Pressure outlet 1 (Pa) | 0.00E+00 | 0.00E+00 | 0.00E+00 | 0.00E+00 | 0.00E+00 | 0.00E+00 | 0.00E+00 |
| Pressure outlet 2 (Pa) | -5.73E-03 | -1.99E-02 | -6.43E-03 | -9.09E-03 | -2.85E-03 | -5.22E-03 | -3.19E-03 |
| Pressure outlet 3 (Pa) | -3.44E-03 | -1.60E-02 | -3.12E-03 | -4.67E-03 | -4.32E-03 | -4.37E-03 | -3.42E-03 |
| Pressure outlet 4 (Pa) | -9.62E-03 | -2.53E-02 | -1.16E-02 | -9.74E-03 | -9.58E-03 | -5.57E-03 | -6.37E-03 |
| Pressure outlet 5 (Pa) | -5.68E+05 | -3.74E+05 | -3.50E+05 | -3.87E+05 | -4.81E+05 | -3.65E+05 | -3.75E+05 |
| Mass Flow inlet (kg/s) | -40.00 | -40.00 | -40.00 | -40.00 | -40.00 | -40.00 | -40.00 |
| Mass Flow outlet 1 (kg/s) | 2.04 | 2.03 | 2.04 | 2.05 | 2.04 | 2.05 | 2.04 |
| Mass Flow outlet 2 (kg/s) | 2.02 | 2.03 | 2.03 | 2.02 | 2.02 | 2.02 | 2.03 |
| Mass Flow outlet 3 (kg/s) | 1.89 | 1.95 | 1.91 | 1.90 | 1.90 | 1.89 | 1.89 |
| Mass Flow outlet 4 (kg/s) | 2.05 | 1.99 | 2.03 | 2.02 | 2.05 | 2.05 | 2.03 |
| Mass Flow outlet 5 (kg/s) | 32.00 | 32.00 | 32.00 | 32.00 | 32.00 | 32.00 | 32.00 |
| Volume (m^3) | 4.60E-03 | 5.15E-03 | 5.70E-03 | 5.09E-03 | 4.84E-03 | 5.51E-03 | 4.85E-03 |
| Weight (kg) | 4.59E+00 | 5.14E+00 | 5.68E+00 | 5.08E+00 | 4.83E+00 | 5.50E+00 | 4.84E+00 |

*Table 16 Final results of optimization for T-shape manifold*

The static pressure difference between outlet 5 and outlet 1 (Pressure outlet 5 - Pressure outlet 1 = 5.68bar) is coherent with that predicted on the entire CFD model in Table 12 (inlet-manifoldinletend2 = 6.63bar), unless the presence of errors due to the mesh and additional loss due to the s-bend shape manifold of the remaining duct not considered in the simplified version of the original model.

The solution finally selected as the best possible optimization is the cone with 5°, since it gives the higher pressure drop reduction[27]. The weight variation is not relevant; therefore the choice does not substantially influence the load conditions on the structure. As predicted, a very little angle of the cone maximizes the performance of the design and the attempted gain on pressure drop can be evaluated as

$$Gain = Pressure\ Drop\ 3\ of\ orignal\ shape - Pressure\ Drop\ 3\ of\ orignal\ shape = 2.15bar$$

[27] Always according to definition of mass flow averaged pressure difference between two sections.

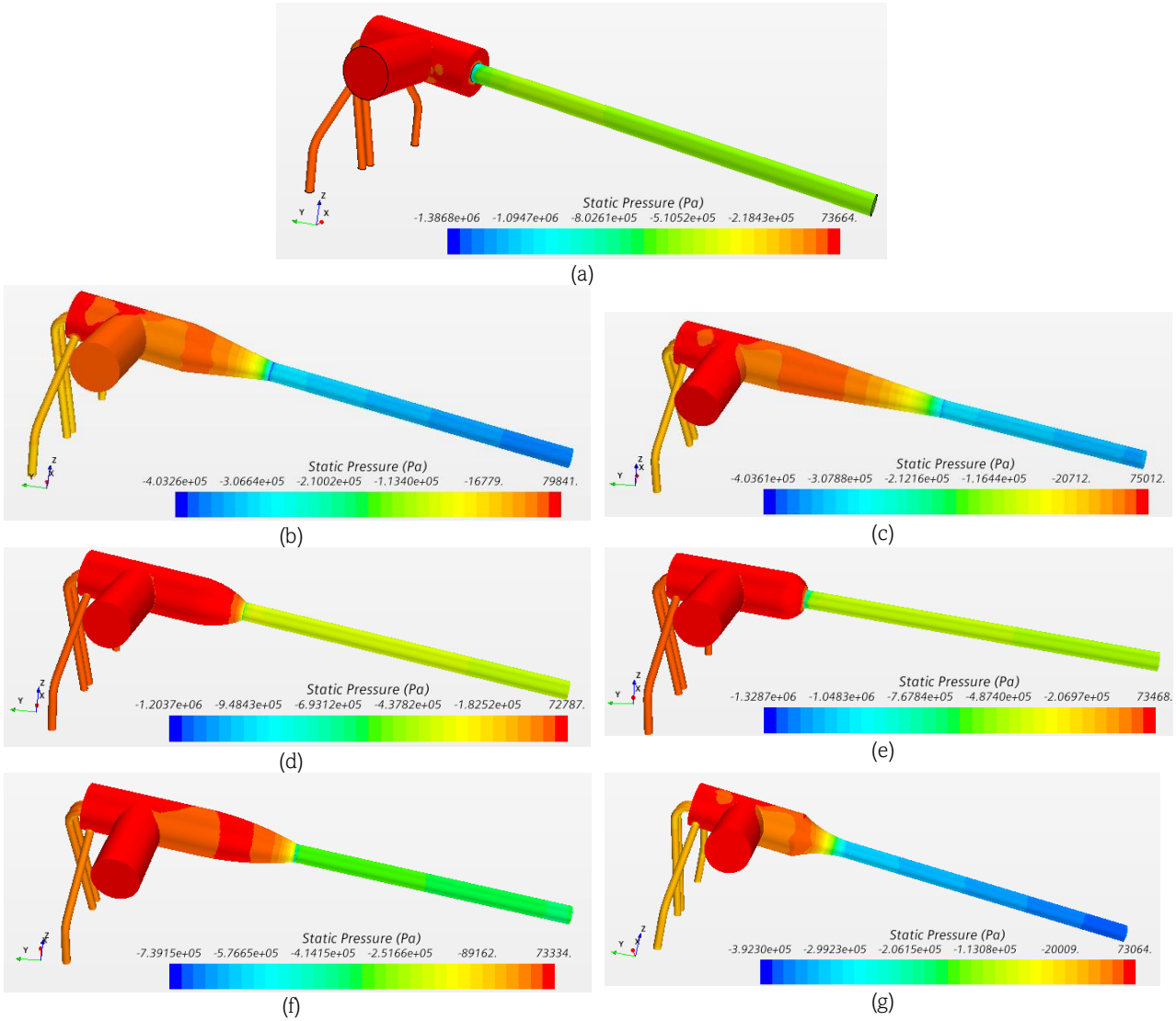


*Figure 52 T-shape manifold optimization, static pressure distribution: original shape (a) , cone 5° (b), cone 10° (c), filling R200mm (d), filling R50mm (e), filling R700mm (f), nozzle R250mm (g)*

## 1.5.2. Distributor optimization

### Original shape and literature knowledge

A similar approach can be adopted also for the distributor optimization. In particular, with the same material properties in Table 2 and model in Table 11, the following BCs are adopted with reference to the cross-sections in Figure 53:

| | | | |
|---|---|---|---|
| pressure outlet | outlet | 0 | Pa |
| mass flow inlet | inlet1 | 16 | kg/s |
| mass flow inlet | inlet2 | 16 | kg/s |

*Table 17 CFD boundary conditions for standalone analysis of distributor*

As for previous optimization, distributor original shape is studied standalone first to validate the simplified treatment. Model has been adjusted by extruding the fluid volume in the *inlet1* and *inlet2* sections to improve convergence. The outlet is at the interface with the terminal part of the *T-shape manifold* of the *return circuit*.

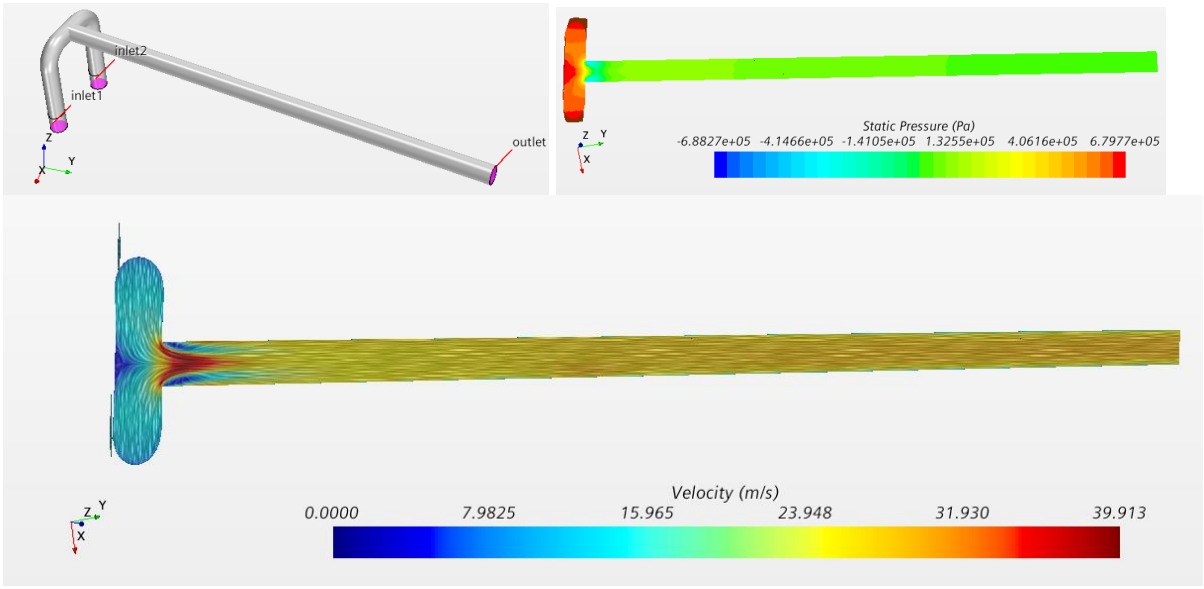


*Figure 53 Distributor standalone, original shape: geometry and BCs sections (top left), section view of static pressure (top right), velocity field (bottom)*

T- junctions are often used in nuclear power plants [19]. From literature in two dimensions, it is known that alternative devices for fluid confluence are the Y-junction and Arc-junction. In the first case, the pressure loss mainly consists of friction loss, curved loss and confluence loss [20], while the second is generally used when large eddy and velocity shock occur in traditional T-junction and Y-junction, depending on operative conditions and continua involved.

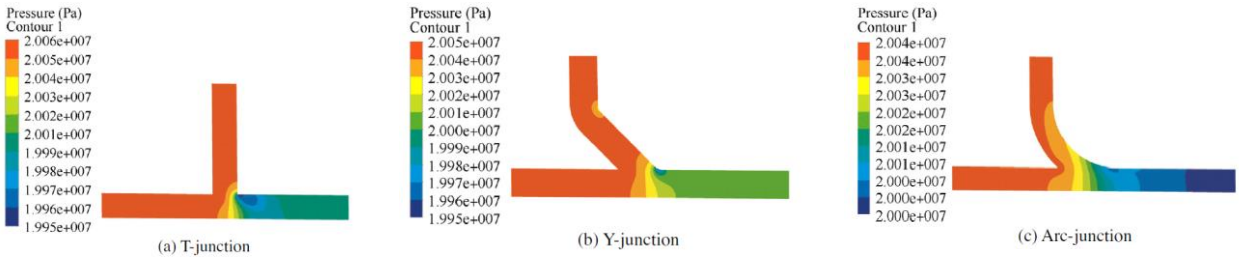


*Figure 54 Literature example of pressure field of three junctions studied in [20]*

The following optimization attempts to take their cue from the examples just mentioned, adapting the two-dimensional design into the 3D connection for the case at hand.

## Manual iterative optimization attempts based on literature knowledge

The first explored shape is a direct derivation of the 2D Y-junction: symmetry is applied to adapt the design to the two inlet sections. The tested angle between the two branches – which is only an example - is approximately 22° and the diameter of each branch, confluence tube to outlet section included, is the same of the original design. This Y-shape basic design shows a reduction in maximum magnitude of the velocity field throughout the horizontal length: this results in a drastic reduction of the pressure drop (Table 18). All the comparisons are made with section views taken with the same plane.

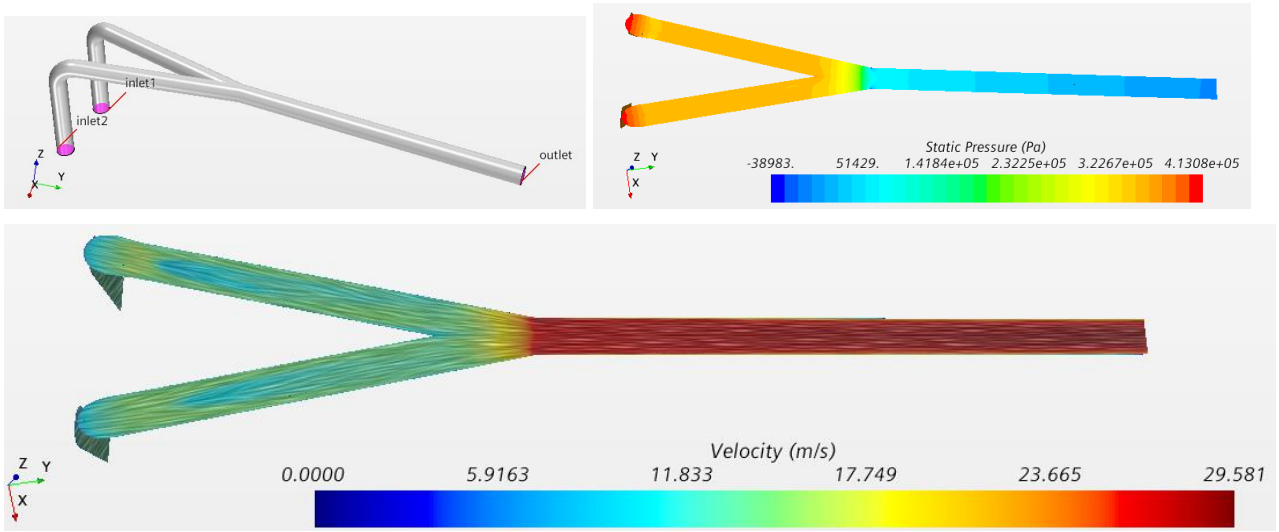


*Figure 55 Distributor optimization, Y-shape: geometry and BCs sections (top left), section view of static pressure (top right), velocity field (bottom)*

As proposed from literature, Arc-shape is a second possible solution. Diameters are not varied with respect to the original geometry to consider only the shape variation effect of the arc. The construction tries to connect the two inlets to the outlet with a curve as smooth as possible: an arc of circumference tangent to the straight duct. In this way, the streamlines of the two fluxes should gradually converge, resulting in a decrease of the pressure drop.

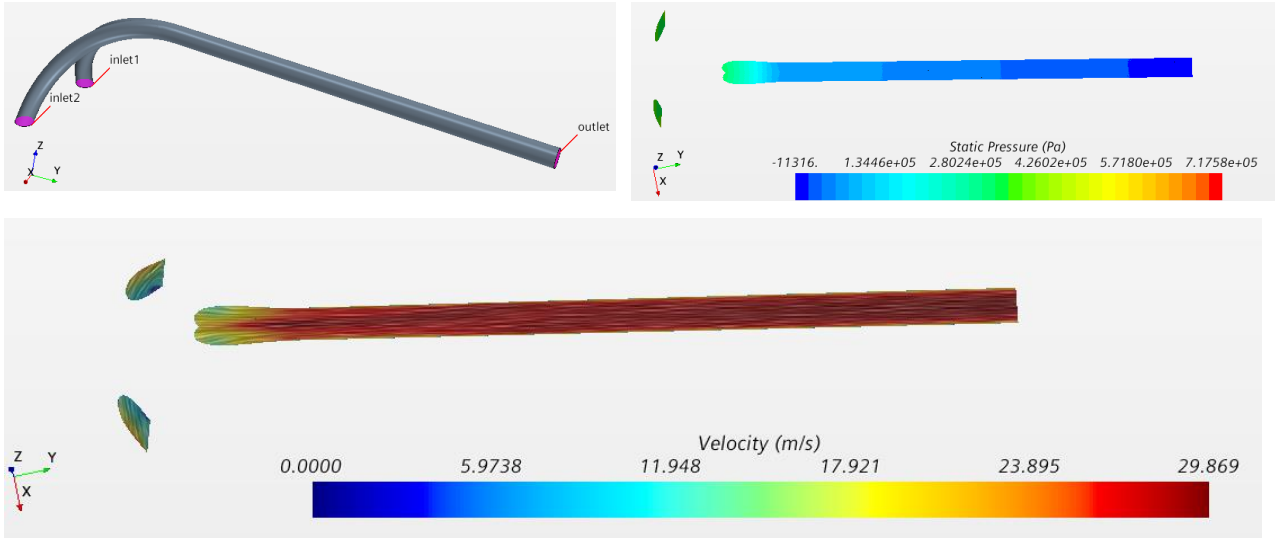


*Figure 56 Distributor optimization, Arc-shape: geometry and BCs sections (top left), section view of static pressure (top right), velocity field (bottom)*

These first two examples seem to induce similar effects on velocity fields and pressure drop. No significant modification can be done for the Arc-shape, but for the Y-shape different fillets can be explored. A mild improvement seems to be provided by a minor fitting.

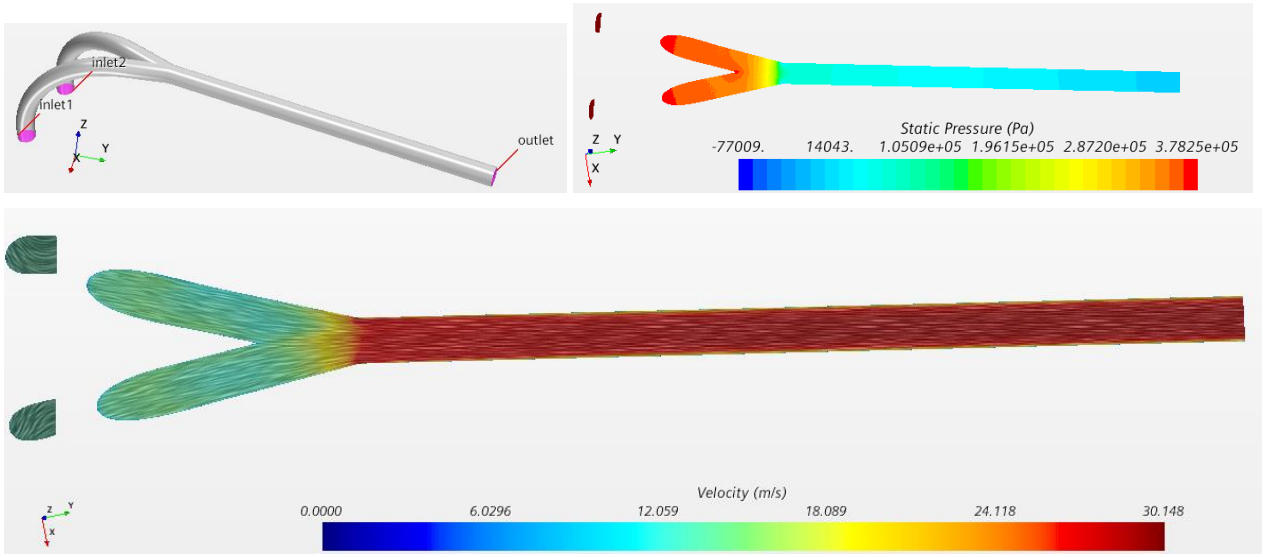


*Figure 57 Distributor optimization, Y-shape with big fillet: geometry and BCs sections (top left), section view of static pressure (top right), velocity field (bottom)*

Reducing the ratio between the two cross sections of a pipe reduction decreases the loss coefficient (Figure 40): thinking in terms of equivalent diameters or total cross-sectional areas, this is equivalent to realize a passage from the bifurcation to the straight pipe such that there is a total area, at the meeting point, at least equal to the sum of the cross-sectional areas of the two bifurcations. This can be practically obtained by increasing the diameter of the straight tube.

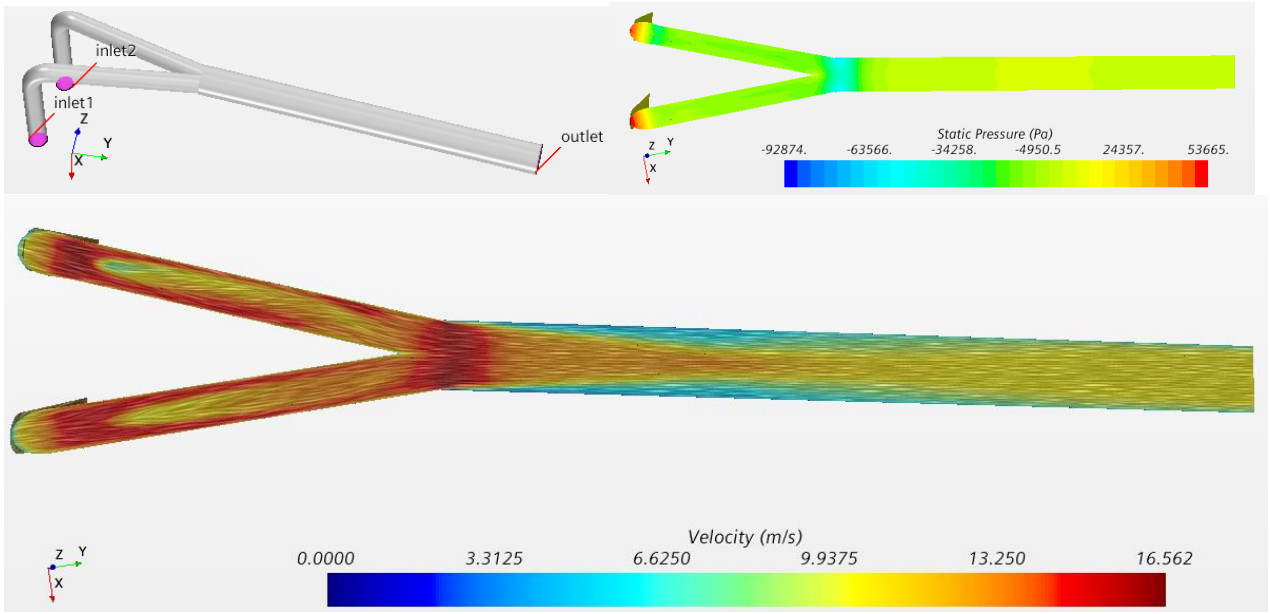


*Figure 58 Distributor optimization, Y-shape with medium cylinder: geometry and BCs sections (top left), section view of static pressure (top right), velocity field (bottom)*

The effect on the velocity field reduction is much more evident in this case, since the maximum velocity value is almost halved with respect to the original condition. Furthermore, the peak is shifted to the smaller diameter zone, in the bifurcations. With a more radical modification (i. e. bigger cylinder) no relevant changes occur.

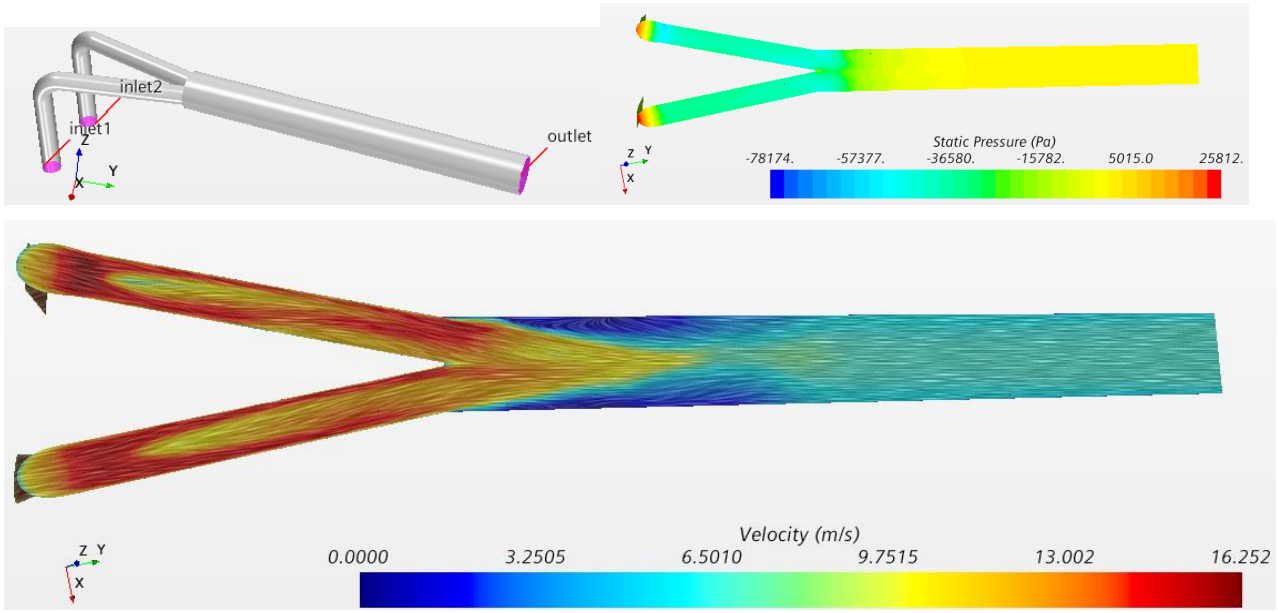


*Figure 59 Distributor optimization, Y-shape with big cylinder: geometry and BCs sections (top left), section view of static pressure (top right), velocity field (bottom)*

The CFD simulations give similar results for all these optimizations: this may be useful for the successive production to evaluate which alternative is more convenient from the economic point of view.

## Optimization attempts based on topology optimization

Topology optimization can be applied as before, starting from a design space. Materials and models are the same described in the previous adjoint topology optimization. BCs are described in Table 17.

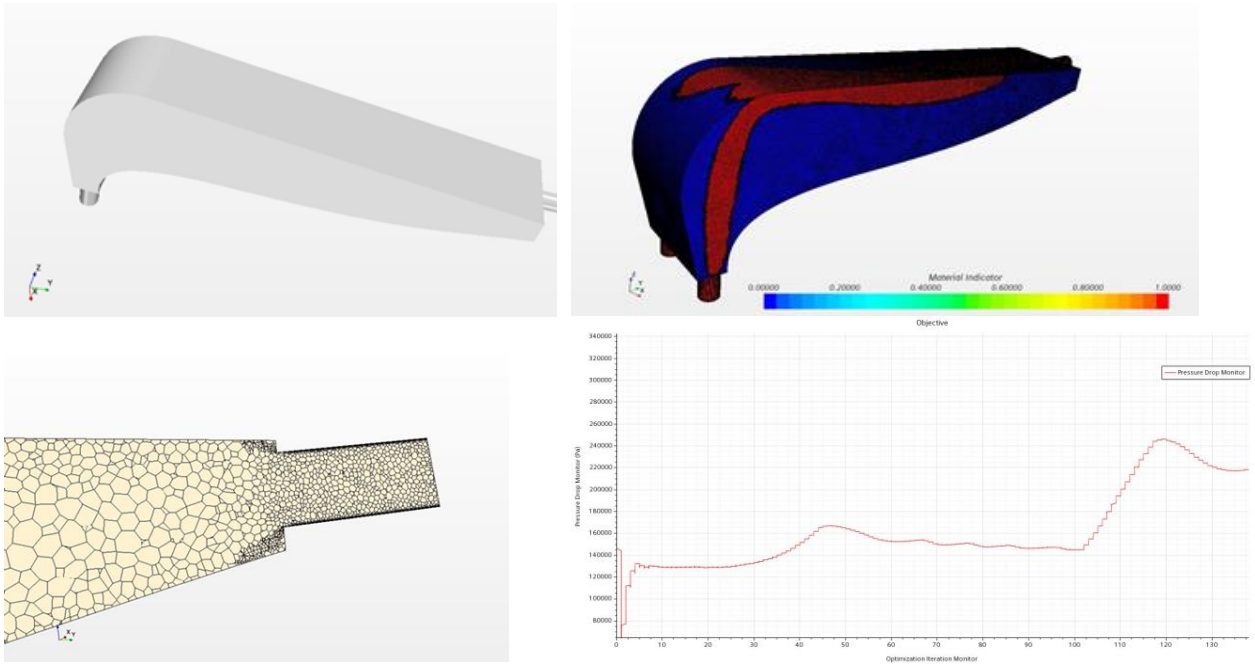

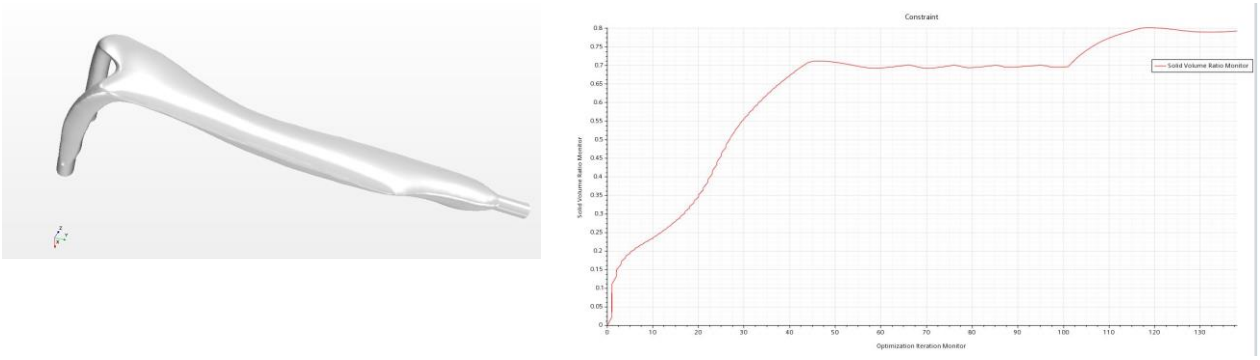


*Figure 60 CAD design preparation (top left), design space after solution (top right), mesh of the design space (middle left), final results for fluid volume after topology optimization and smoothing (bottom left), Objective function (middle right) and Constraint function (bottom right)*

As before, the shape is complex and could not be realized with traditional production, but gives another guideline for the direction to be followed to reach the goal.

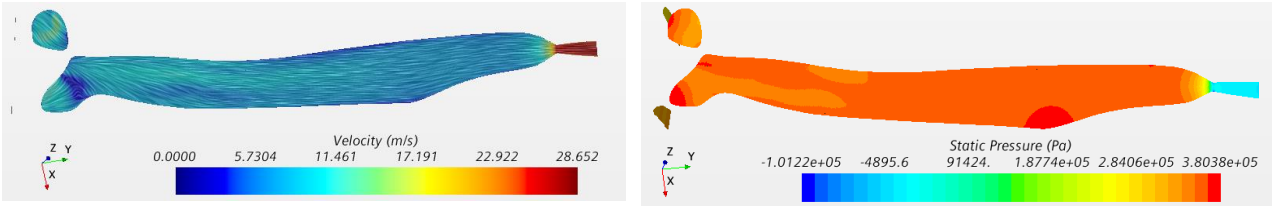


*Figure 61 Velocity field and static pressure for topology optimization solution of distributor*

## Results

Results are presented in table form:

| | original | Y-shape | Arc-shape | Y-shape big fillet | medium cylinder | big cylinder | topology optimization |
|---|---|---|---|---|---|---|---|
| Pressure Drop 1 (Pa) | 3.26E+05 | 8.56E+04 | 1.03E+05 | 8.60E+04 | 5.30E+04 | 5.53E+04 | 4.53E+04 |
| Pressure static inlet1 (Pa) | 6.14E+05 | 3.75E+05 | 4.03E+05 | 3.68E+05 | 1.53E+04 | -1.24E+04 | 3.25E+05 |
| Pressure static inlet2 (Pa) | 6.12E+05 | 3.68E+05 | 4.03E+05 | 3.70E+05 | 1.26E+04 | -1.58E+04 | 3.28E+05 |
| Pressure static outlet (Pa) | -4.96E-03 | -2.08E-03 | -5.75E-03 | -6.71E-03 | -4.16E-04 | 0.00E+00 | -6.58E-04 |
| Volume (m^3) | 2.02E-03 | 2.38E-03 | 1.92E-03 | 2.09E-03 | 3.97E-03 | 5.27E-03 | 5.09E-03 |
| Weight (kg) | 2.02 | 2.38 | 1.92 | 2.08 | 3.96 | 5.25 | 5.07 |

*Table 18 Final results of optimization for distributor*

Static pressure is evaluated as surface average. Pressure difference in the standalone model (pressure static inlet 1-pressure static outlet = 6.1bar) is coherent with the whole neutralizer simulation (from Table 12, distributor2-manifoldoutletend2 = 4.8bar), again, as before, unless errors due to the coarser mesh of entire neutralizer and additional loss due to ducts extrusions of the simplified model done to improve the convergence.

The quantity to be considered for minimization is the absolute total pressure difference between section inlet1 or inlet2 (they are the same) and outlet (pressure drop 1). The solution, from manual iterative optimization procedure, which gives the higher reduction is the Y-shape with medium cylinder. This is finally selected. The attempted gain on total pressure drop can be estimated as

$$Gain = Pressure\ Drop\ 1\ of\ orignal\ shape - Pressure\ Drop\ 1\ of\ orignal\ shape = 2.74bar$$

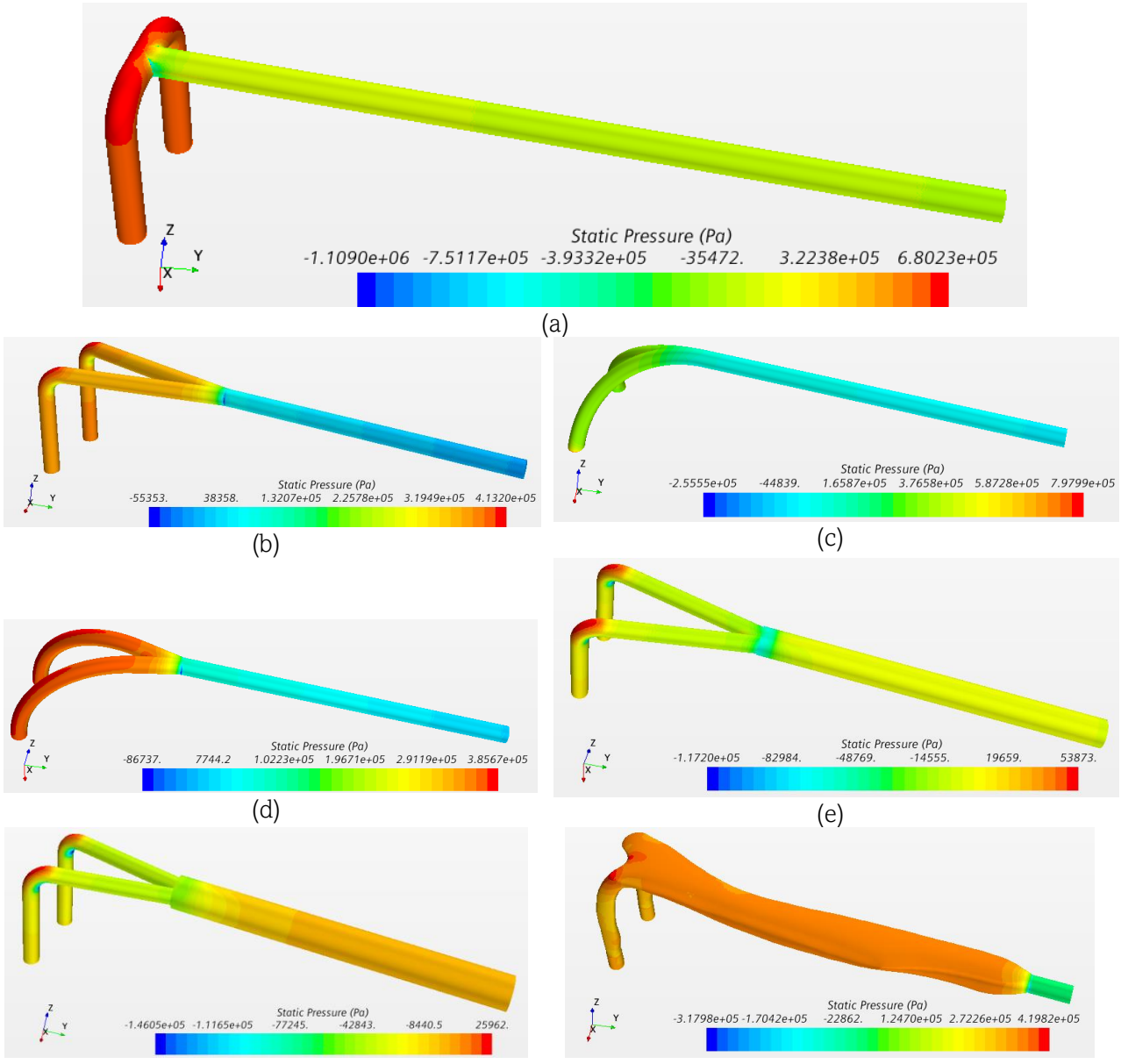


*Figure 62 Distributor optimization, static pressure distribution: original shape (a), Y-shape (b), Arc-shape (c), Y-shape with big fillet (d), Y-shape with medium cylinder (e), Y-shape with big cylinder (f), topology optimization (g)*

## Conclusion

In the end the attempted total pressure drop reduction, if both the two selected shapes are substituted in the original model is

$$Total\ Gain = Gain_{T-shape\ manifold} + Gain_{distributor} = 2.15bar + 2.74bar \sim 4.9bar$$

# 1.6. Optimized neutralizer designs

Starting from the single component optimizations, the selected designs are substituted in the entire model of the neutralizer, to validate the total pressure drop reduction estimated (***Total Gain***). Different possible optimizations are presented in a qualitative way. No mesh convergence has been done for these models and coarse mesh (but similar in each case) has been used. The purpose of this chapter is to understand the global effect in the whole neutralizer of the developed designs of critical parts and, essentially, how the mass flows are distributed in the various solutions: this is particularly interesting for the successive thermal evaluations and for the future development of accuracy on heat flux, so that, depending on the thermal heat load, mass flows can be calibrated as desired starting, at least, from the qualitative observations developed in this study. Material, model and BCs in all the following optimizations are the same of the original model (Table 10, Table 11).

## 1.6.1. Optimization 1

The previous analysis has suggested the substitution of the *T-shape manifold* with a *cone of 5°* and of the *distributor* with a *Y-shape with a medium cylinder*. This is implemented in the *Optimization 1*.

From Table 12, with the actual mesh of the whole model (rather coarser to speed up the simulations) it is estimated 13.6bar of total pressure drop IO of which 11.9bar occur only in crossing the LEEs[28].

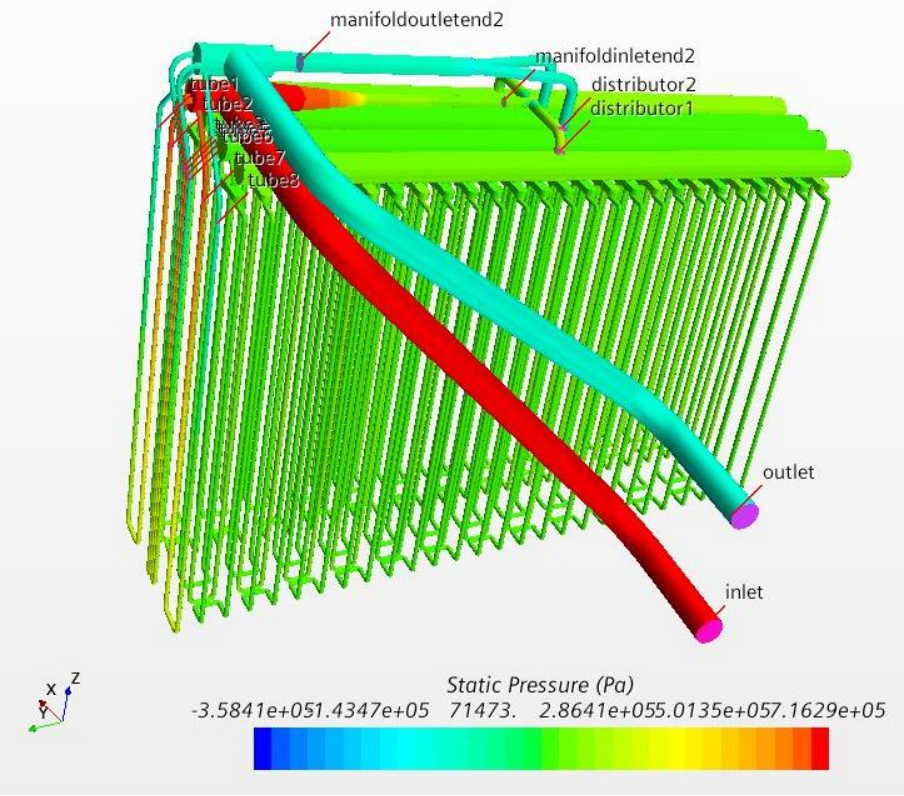


*Figure 63 Optimization 1: pressure distribution*

It can be observed that, if the same mass flow (40kg/s) is imposed at the inlet, for the total pressure drop IO, the maximum recovery desirable in the remaining circuit - if 2kg/s are to be guaranteed to the LEEs as in

[28] Thanks to the detailed study for LEEs, it was noticed that this value is a bit overestimated, but this is not relevant for the qualitative evaluations.

MITICA –, therefore, remains very low: approximately 1.7bar. This derives from the observation of the parallel circuit to the LEEs only. Such a condition is, apparently, in contrast with the ***Total Gain*** predicted in the previous chapter (4.9bar), where optimizations, actually, focus only on the parallel circuit to the panels.

The reason of this apparent inconsistency is that the reduction on total pressure drop IO theoretically predicted just before will be satisfied with a consequential flow rate adjustment to the LEEs: since pressure drop will be reduced on the optimized components (of the circuit to the panels), less resistance will be seen by the fluid in this direction and so pressure drop IO will decrease because a lower flow rate will flow into the LEEs. This is what happens in the *Optimization 1*. Cross sectional areas follow the same nomenclature previously used.

| Static Pressure Differences (Pa) | |
|---|---|
| **Forward circuit Static Pressure differences (Pa)** | |
| inlet-tube2,4,5,7 | 4.16E+04 |
| inlet-manifoldinletend2 | 5.01E+05 |
| manifoldinletend2-distributor1 | -2.66E+04 |
| **Return circuit Static Pressure differences (Pa)** | |
| tube1,3,6,8-outlet | 3.95E+04 |
| distributor2-manifoldoutletend2 | -2.52E+04 |
| manifoldoutletend2-outlet | 1.62E+04 |
| **Pressure drops on panels and LEEs (Pa)** | |
| distributor 1-distributor2 | 2.45E+05 |
| tube2-tube1 | 6.29E+05 |
| tube7-tube8 | 6.33E+05 |
| tube4-tube3 | 6.25E+05 |
| tube5-tube6 | 6.28E+05 |
| sum of pressure difference (parallel circuit to LEEs) | 7.10E+05 |
| sum of pressure difference (parallel circuit to Panels) | 7.10E+05 |
| **Pressure Drop IO** | **7.10E+05** |
| **Mass flows** | |
| Mass Flow Inlet (kg/s) | -40.0 |
| Mass Flow tube 1 (kg/s) | 1.47 |
| Mass Flow distributor1 (kg/s) | -17.0 |

*Table 19 Static pressure differences and mass flows in the entire Optimization 1 CAD with 40kg/s*

It is evident from Figure 63 that, especially for the *Y-shape* of the *distributor* pressure difference has been substantially zeroed[29] (distributor2-manifoldoutletend2). The effect on the total pressure drop IO is of a significant reduction: approximately 6.5bar are recovered.

Pressure drop on LEEs is almost coincident with total pressure drop IO: this means, again, that the losses are mainly due to them and that the recovery is caused by a decreasing of mass flow (27% of reduction) in their channels.

## 1.6.2. Optimization 2

By substituting the *T-shape manifold* with a *cone of 5°* and the *distributor* with a *Y-shape* (with the cylinder of the same diameter of the original design, Figure 55) a lower recovery on total pressure drop IO should be

[29] Further details in Appendix in Detailed results for simulation for Optimization 1

expected, but, since in this case diameters are preserved also in the splitting junction of the T-shape manifold of the *return circuit* mass flow distribution between panels and LEEs should be more similar to the original design. This is implemented in the *Optimization 2*.

The results are a pressure drop recovery of 3.5bar and a mass flow reduction to the single LEE of 11%.

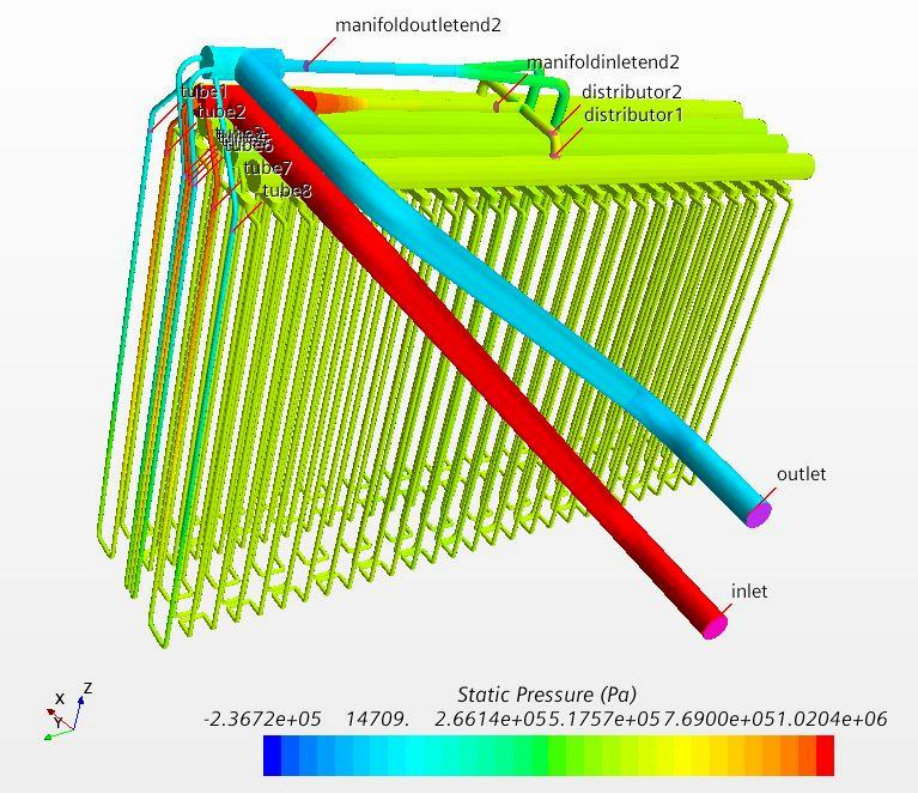


*Figure 64 Optimization 2: pressure distribution*

| Static Pressure Differences (Pa) | |
|---|---|
| Forward circuit Static Pressure differences (Pa) | |
| inlet-tube2,4,5,7 | 5.01E+04 |
| inlet-manifoldinletend2 | 4.54E+05 |
| manifoldinletend2-distributor1 | -2.78E+04 |
| Return circuit Static Pressure differences (Pa) | |
| tube1,3,6,8-outlet | 9.11E+04 |
| distributor2-manifoldoutletend2 | 3.42E+05 |
| manifoldoutletend2-outlet | 8.43E+03 |
| Pressure drops on panels and LEEs (Pa) | |
| distributor 1-distributor2 | 2.32E+05 |
| tube2-tube1 | 8.68E+05 |
| tube7-tube8 | 8.68E+05 |
| tube4-tube3 | 8.58E+05 |
| tube5-tube6 | 8.69E+05 |
| sum of pressure difference (parallel circuit to LEEs) | 1.01E+06 |
| sum of pressure difference (parallel circuit to Panels) | 1.01E+06 |
| **Pressure Drop IO** | **1.01E+06** |
| Mass flows | |
| Mass Flow Inlet Monitor 2 (kg/s) | -40.00 |
| Mass Flow tube 1 Monitor (kg/s) | 1.78 |
| Mass Flow distributor1 Monitor (kg/s) | -16.43 |

*Table 20 Static pressure differences and mass flows in the entire Optimization 2 CAD with 40kg/s*

The mass flow in this version of the optimized *distributor* is reduced with respect to *Optimization 1*: however, in the component the pressure increases (distributor2-manifoldoutletend2). This means that this solution is less performing, since it develops more friction in the duct. On the other hand, the pressure decrease - with respect to previous optimization - that can be seen in the *T-shape manifold with a cone of 5°* (inlet-manifoldinletend2) is due to the same decreased mass flow and compensates a bit the minor gain.

## 1.6.3. Optimization 3

Further improvement may occur by substituting in the *Optimization 1* a cone with a smaller angle, according to literature knowledge. In the *Optimization 3* this is realized by selecting a *T-shape manifold* with a *cone of 2°* and a *distributor* with *a Y-shape with a medium cylinder.*

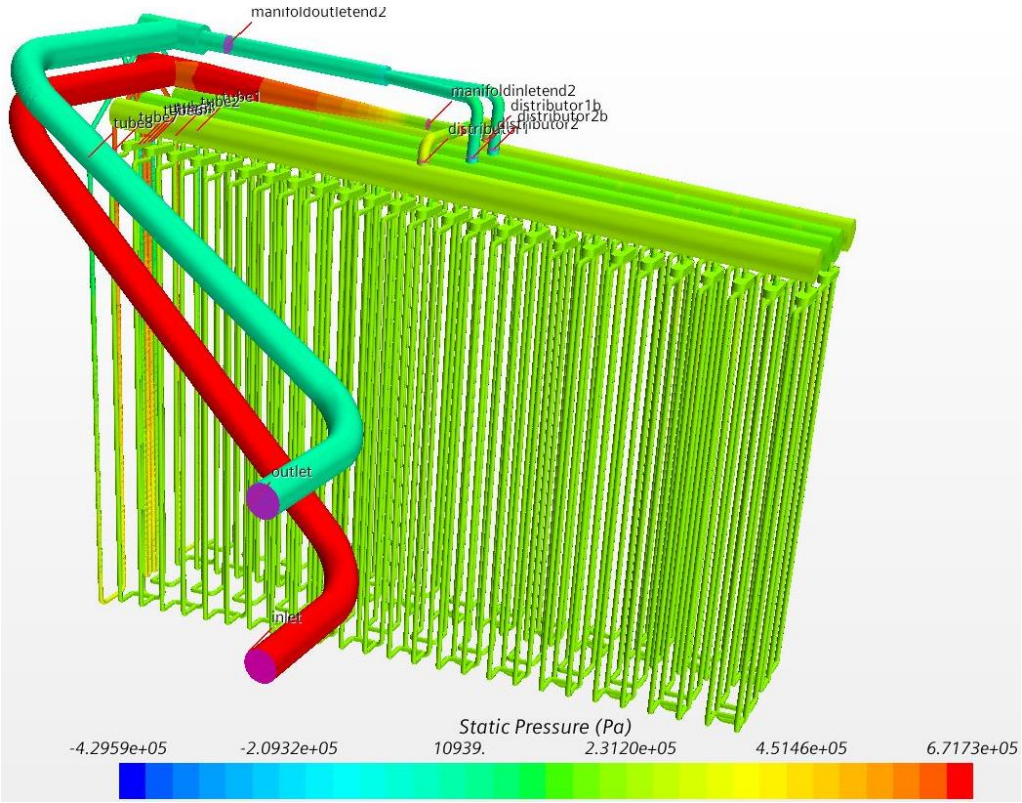


*Figure 65 Optimization 3: pressure distribution*

The results confirm the pressure drop IO reduction, with a higher gain of 7bar with respect to the original model. Mass flow to the single LEE is even smaller, as expected, because the more pushed cone design acts as a driver of mass flow and attracts more fluid subtracting it from the LEEs. A 29% reduction in flow rate to the single LEE can be noticed.

| Static Pressure Differences (Pa) | |
|---|---|
| Forward circuit Static Pressure differences (Pa) | |
| inlet-tube2,4,5,7 | 3.54E+04 |
| inlet-manifoldinletend2 | 4.53E+05 |
| manifoldinletend2-distributor1 | -2.51E+04 |
| Return circuit Static Pressure differences (Pa) | |
| tube1,3,6,8-outlet | 3.30E+04 |
| distributor2-manifoldoutletend2 | -8.31E+03 |
| manifoldoutletend2-outlet | 8.32E+03 |
| Pressure drops on panels and LEEs (Pa) | |
| distributor 1-distributor2 | 2.34E+05 |
| tube2-tube1 | 5.93E+05 |
| tube7-tube8 | 5.95E+05 |
| tube4-tube3 | 5.88E+05 |
| tube5-tube6 | 5.89E+05 |
| sum of pressure difference (parallel circuit to LEEs) | 6.62E+05 |
| sum of pressure difference (parallel circuit to Panels) | 6.62E+05 |
| Pressure Drop IO | 6.61E+05 |
| Mass flows | |
| Mass Flow Inlet (kg/s) | -40.00 |
| Mass Flow tube 1 (kg/s) | 1.42 |
| Mass Flow distributor1 (kg/s) | -17.13 |

*Table 21 Static pressure differences and mass flows in the entire Optimization 3 CAD with 40kg/s*

## 1.6.4. Optimization 4

With a more sophisticated design of the *T-shape manifold* another possible solution is proposed. The key idea is that the $\boldsymbol{Total\ Gain}$ sees beneficial effect if both the two parallel circuits are improved.

A gradual contraction (cones shapes) develops less friction and reducing the ratio between the cross sectional areas of a tube variation - such as from the T-shape manifold to the tubes directed to the LEEs - decreases the pressure drop, since geometrical discontinuity is less evident. These observations are applied in *Optimization 4* (Figure 66).

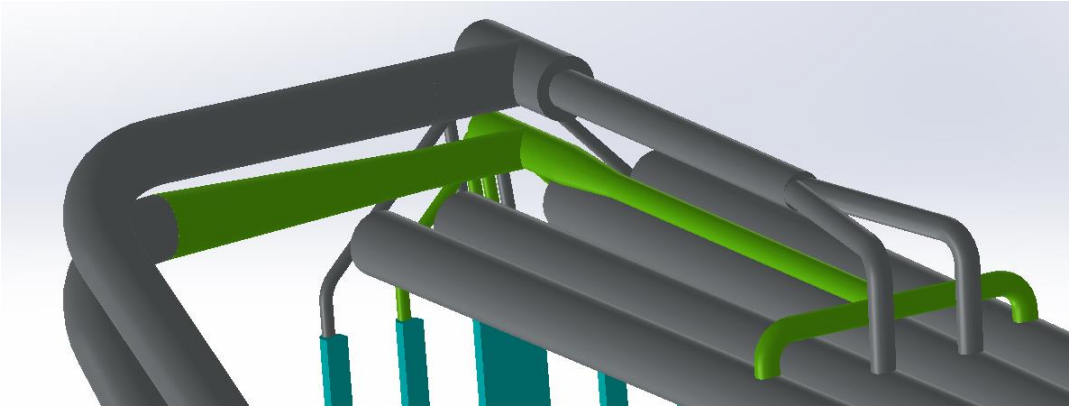

*Figure 66 Optimization 4: detail of the advanced shape for T-shape manifold (green)*

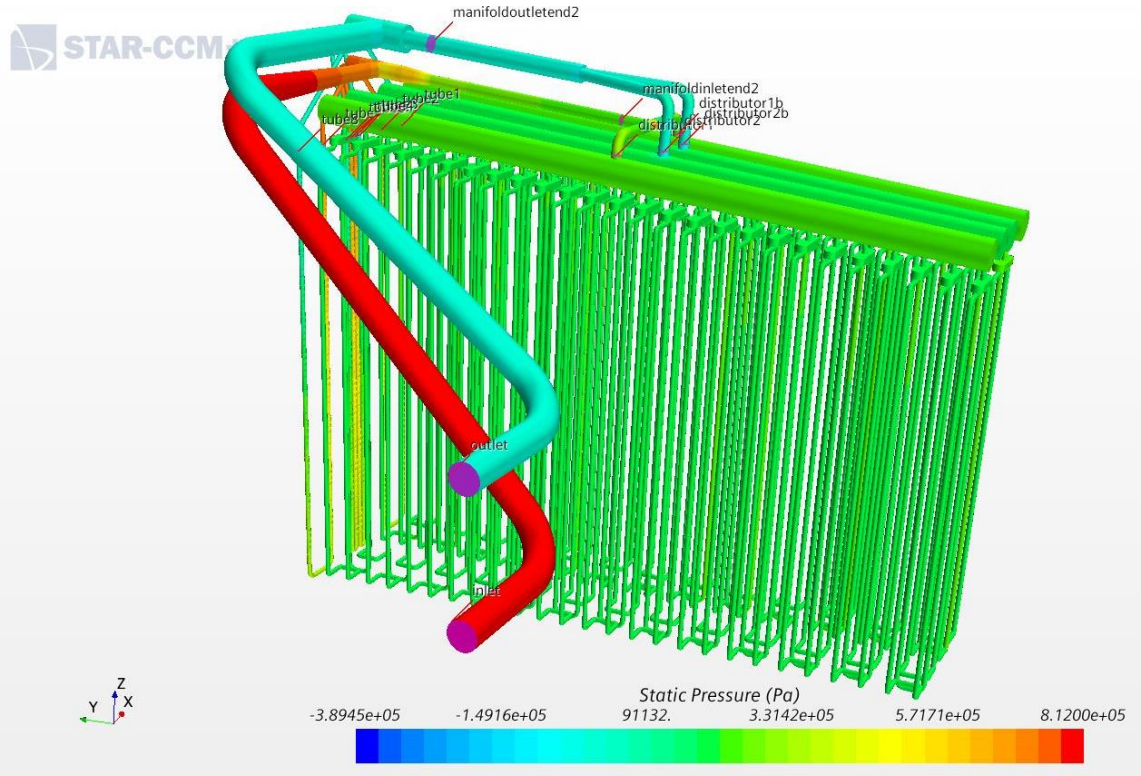


*Figure 67 Optimization 4: pressure distribution*

With respect to the *Optimization 1* and *3,* which have the same *Y-shape design* for the distributor part, a small increase in the pressure drop is visible from the side of the parallel LEE circuit, due to the adoption of the smaller diameter cylinder. This design rebalances a bit the flows altered by the cone in the direction of the panels and results in a higher mass flow to the single LEE. With respect to the original design a 24% reduction can be seen to the LEE's single channel and a total gain on pressure drop IO of 5.6 bar. An advantage of this solution is the reduction of materials required for the construction.

| Static Pressure Differences (Pa) | |
|---|---|
| **Forward circuit Static Pressure differences (Pa)** | |
| inlet-tube2,4,5,7 | 1.09E+05 |
| inlet-manifoldinletend2 | 5.85E+05 |
| manifoldinletend2-distributor1 | -1.23E+04 |
| **Return circuit Static Pressure differences (Pa)** | |
| tube1,3,6,8-outlet | 3.38E+04 |
| distributor2-manifoldoutletend2 | -1.37E+04 |
| manifoldoutletend2-outlet | 1.37E+04 |
| **Pressure drops on panels and LEEs (Pa)** | |
| distributor 1-distributor2 | 2.31E+05 |
| tube2-tube1 | 6.62E+05 |
| tube7-tube8 | 6.62E+05 |
| tube4-tube3 | 6.68E+05 |
| tube5-tube6 | 6.67E+05 |
| sum of pressure difference (parallel circuit to LEEs) | 8.04E+05 |
| sum of pressure difference (parallel circuit to Panels) | 8.04E+05 |
| **Pressure Drop IO** | **8.04E+05** |
| **Mass flows** | |
| Mass Flow Inlet (kg/s) | -40.00 |
| Mass Flow tube 1 (kg/s) | 1.52 |
| Mass Flow distributor1 (kg/s) | -16.89 |

*Table 22 Static pressure differences and mass flows in the entire Optimization 4 CAD with 40kg/s*

## 1.6.5. Conclusions

Proposed optimization must be considered as qualitative results: they show that the concept of optimization cannot be subjected only to a pressure drop IO minimization. More parameters must be considered, such as the ratio between the total mass flow rate and a mass flow which is critical (i. e. to the LEEs). Optimization solution, only by considering pressure drop minimization, in this sense, is not unique. What can be summarized, anyway, and can be eventually used when heat load will be uploaded or corrected for other reasons, is that:

- pressure drops act as drivers for mass flows: by adopting one of these optimizations with the same mass flow at the inlet of the neutralizer, it is therefore possible to increase or to decrease refrigeration in the direction where it is needed. This depends on heat flux, so a calibration is needed on the results with a realistic heat flux distribution;
- the optimum point lies in the balance between total mass flow rate provided, pressure drop IO and ratio between total mass flow rate and mass flow rate in the thermally critical ducts: these three quantities must be minimized together;
- total pressure drop IO is mainly given by the pressure difference at LEEs with a parallel configuration like those proposed: specifically, it is at least equal to the pressure drop on these components. In order to reduce the pressure drop IO, it is mandatory to reduce the pressure drop at LEEs;
- small variations in the flow rate circulating in the LEEs lead to large variations in the pressure drop IO: this is particularly true for the design with twisted tape insert, since friction factor curves as function of the mass flow rate are very steep, as it will be shown in the following section;
- a *cone shape* for *T-shape manifold* of the *forward circuit* drastically decreases the pressure drop IO, but reduces the mass flow to the LEEs. This effect is emphasized by the reduction of the cone angle;
- similarly, the *Y-shape* for the bifurcation of the *distributor* of the *return circuit* has the effect of a reduction of the pressure drop IO and of the mass flow to the LEEs. About this observation, a smaller cylinder for the straight tube of confluence of the distributor results in a milder effect.

As a summary, for the proposed geometries, some quantities (figures of merit) can be defined to numerically quantify the price to be paid (Pressure Drop IO, $P_{IO}$) to have a desired mass flow in a specific direction.

LEEs and panels will be subjected to thermal heat load. Assuming that no modification is made for the design of LEEs or panels (top, bottom and vertical) and tanks, the pressure losses due to the remaining parts of the hydraulic system can be described by:

- $\Delta P_{LEE} = 1 - \frac{P_{2LEEseries}}{P_{IO}}$, for the parallel LEEs circuit. This must be *minimized*, which would mean that almost all the losses are due only to the LEEs and no friction occur in the remaining part of this parallel circuit;
- $\Delta P_{Y+cone} = \frac{P_{Y+cone}}{P_{IO}}$, for the circuit of the parallel panels. This represents the losses in the part of panel circuit that is modified and in an ideal case this should be *minimized*.

Since pressure drops act as drivers of mass flows, previous two points should be considered also with reference to the mass flow that they involve:

- $\Delta P_{LEE}/\dot{m}_{LEE} = \frac{1-\frac{P_{2LEEseries}}{P_{IO}}}{\dot{m}_{LEE}}$, which express the price to be paid (in terms of pressure) to obtain the useful effect (kg/s) for the single LEE. This should be *minimized;*
- $\Delta P_{Y+cone}/\dot{m}_{Y+cone} = \frac{P_{Y+cone}}{P_{IO}\cdot\dot{m}_{Y+cone}}$, which express the price to be paid (in terms of pressure) to obtain the useful effect (kg/s) for the single block of panels. This should be *minimized*;

- $coeff = \left(1 - \frac{P_{2LEEseries}}{P_{IO} \cdot \dot{m}_{LEE}}\right) / \frac{P_{Y+cone}}{P_{IO} \cdot \dot{m}_{distributor}}$, which represent the ratio between the price paid for the LEEs and for the single block of panels.
- $mass\ flow\ ratio = \frac{\dot{m}_{Y+cone}}{\dot{m}_{LEE}}$, which gives an idea of the distribution of mass flow between a single LEE and a single block (1 or 2) of panels.

| | symbol | Original design | Optimization 1 | Optimization 2 | Optimization 3 | Optimization 4 |
|---|---|---|---|---|---|---|
| **Pressure Drop IO** | $\boldsymbol{P_{IO}}$ | **1.36E+06** | **7.10E+05** | **1.01E+06** | **6.61E+05** | **8.04E+05** |
| tube2-tube1 | $P_{2LEEseries}$ | 1.19E+06 | 6.29E+05 | 8.68E+05 | 5.93E+05 | 6.62E+05 |
| inlet-manifoldinletend2 | $P_{cone}$ | 6.63E+05 | 5.01E+05 | 4.54E+05 | 4.53E+05 | 5.85E+05 |
| distributor2-manifoldoutletend2 | $P_Y$ | 4.80E+05 | -2.52E+04 | 3.42E+05 | -8.31E+03 | -1.37E+04 |
| Mass Flow tube 1 (kg/s) | $\dot{m}_{LEE}$ | 2.06 | 1.47 | 1.78 | 1.42 | 1.52 |
| Mass Flow distributor1 (kg/s) | $\dot{m}_{Y+cone}$ | 15.70 | 16.97 | 16.43 | 17.13 | 16.89 |
| **mass flow ratio** | | **7.6** | **11.5** | **9.2** | **12.0** | **11.1** |
| $\Delta P_{LEE}$ | | 13% | 11% | 14% | 10% | 18% |
| $\Delta P_{Y+cone}$ | | 84% | 67% | 79% | 67% | 71% |
| $\Delta P_{LEE}/\dot{m}_{LEE}$ | | 0.062 | 0.077 | 0.078 | 0.072 | 0.116 |
| $\Delta P_{Y+cone}/\dot{m}_{Y+cone}$ | | 0.054 | 0.039 | 0.048 | 0.039 | 0.042 |
| **coeff** | | **1.2** | **2.0** | **1.6** | **1.8** | **2.8** |

*Table 23 Comparison among the different Optimizations*

Considering the proposed solutions, from Table 23, it is evident that, for what concern the mass flow ratio, the design which allows to obtain the highest mass flow to the LEEs is the O*riginal* one, while the *Optimization 3* allows to obtain the maximum possible mass flow (and therefore refrigeration) to the panels. These two designs give also the lower cost of mass flow to a single series of LEEs ($\Delta P_{LEE}/\dot{m}_{LEE}$) and to the block of panels ($\Delta P_{Y+cone}/\dot{m}_{Y+cone}$) respectively. The last coefficient gives an idea of the proportion, on the price paid, between one LEEs series and a block of panels and, ideally, it should be unitary, that would mean that the cost of mass flow to reach every part of the circuit is the same. However, it is important that, not only the cost is equal, but it is low, therefore all these parameters must be considered together. In general, with these designs, if the LEEs are the thermally critical components the *Original* solution is the most adequate. If the panels are the critical components, it would be much more convenient to select the *Optimization 3*. The final decision, anyway, is sensible to the real effective mass flow required for the refrigeration and so depend on the heat flux deposited.

# 2. Phase 2 – New heat load: electrons and deuterium

In this second phase of the study a realistic heat load distribution is provided. Only electrons and deuterium contributions are considered, while the stray field effect is neglected. The most energetically charged particles are responsible for a non homogeneous distribution of heat load, which is applied on the inner side of the panels and on the LEEs (Figure 68). The total peak, considering the sum of the two contributions (deuterium and electrons), is 0.72 MW/m$^2$, located on the LEEs.

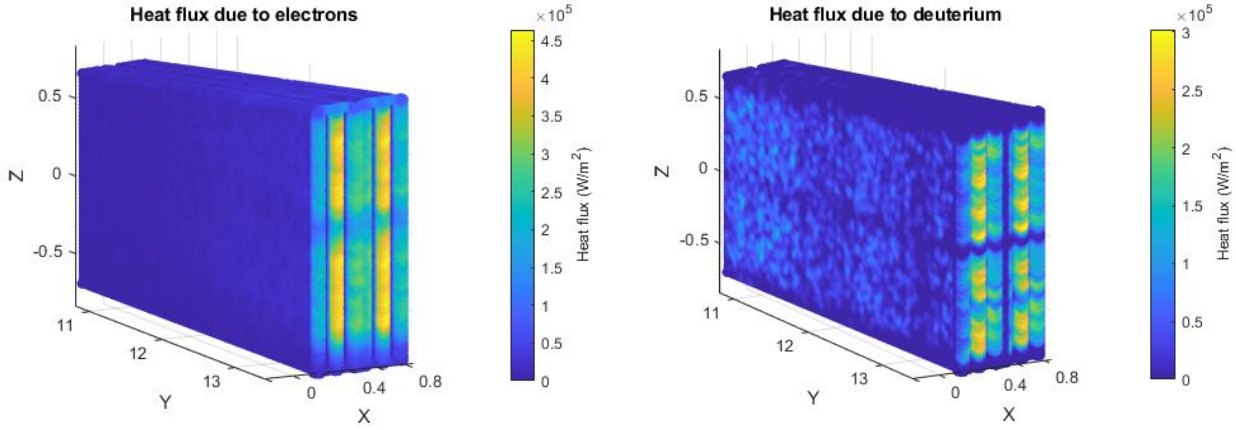


*Figure 68 Electrons (a) and deuterium (b) heat loads provided by DTT S.c.a.r.l.*

The total heat flux has been calculated starting from the data provided[30] and applied to the neutralizer. Data were evaluated on a simplified version of the neutralizer CAD and with another mesh, so they have been adapted with three dimensional interpolation to be applied to the complex CAD which has been analyzed up to now and which will be studied in the following chapters. The final result is shown in Figure 69.

Total power deposited on the neutralizer surfaces of the complex CAD is evaluated with an error of 5.38% and it is estimated to be 1.51MW[31].

[30] with a MATLAB script. For details see *Appendix*, MATLAB script for heat load evaluation

[31]Since the mesh where the results for electrons and deuterium was not known and the CAD were a bit different, also the total power evaluated is given with an error. To verify that not only the distribution but also the total power is

Considering the total heat power deposited for each single component and the peak reached with this heat load, the most critical elements are LEE2, Halfway2, Central2 and Lateral1. Only these components will be analyzed in detail, since they represent the worst cases.

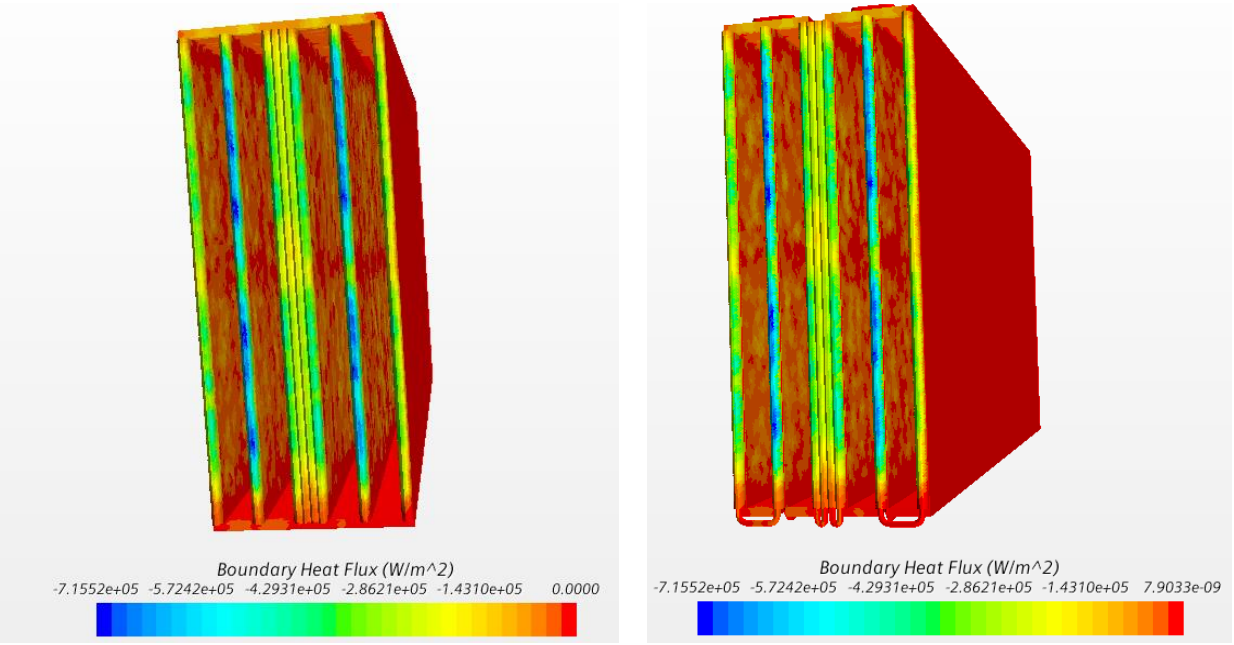


*Figure 69 Heat flux: Simplified CAD (left), Complex CAD (right)*

## 2.1. Optimization of the operational conditions

As it was highlighted from the optimization studies in section 1.6. Optimized neutralizer designs, it is very important to define exactly the amount of mass flow strictly necessary to the refrigeration, otherwise the pressure drop would overcome the possible range or, even worse, the mass flow distribution could be not adequate to preserve the single components, causing not only an economic loss during the operation but also damage, failure or unnecessary additional maintenance.

The stricter constraint is the saturation temperature of water. To avoid problems related to local boiling and local wear of the material at the interface solid-fluid, due to high temperatures reached by the fluid because of the high heat load, maximum temperature of the water, in each part of the hydraulic circuit, must be limited below the saturation value at the operative pressure condition considered.

With an iterative procedure, the minimum mass flows required for the refrigeration of LEEs and panels are separately determined: first, only boiling condition constraints will be considered, then a preliminary thermomechanical analysis will partially confirm the validity of the values found. For the sake of brevity, the latter is not reported in the study since an in-depth discussion on thermomechanical assessment will be held

correctly applied to the model currently studied, a full check is performed and reported in a table in Appendix, Check on heat load

directly in the verification phase. In the end, the entire neutralizer is studied again to provide, for each component, at least the minimum necessary mass flow computed.

To speed up the process, even if the BCs are varied, no mesh convergence or changes are made in the iterative research of minimum mass flows, since the procedure should only provide a reference possible value that must be verified at the end of the study.

## 2.1.1. Minimum mass flow for LEEs

### Model setup and BCs

From Figure 69 it can be seen that LEEs are subjected to a distributed heat load.

A conservative hypothesis is made: since only electrons and deuterium loads are known (no stray field have been considered or roughly quantified), and being the thermal stresses that will arise unknown, a good margin on the thermal heat load is kept. Instead of a distributed load, a heat load uniformly applied to the orthogonal surface of the infinitesimal elements is considered and slightly increased from the peak (evaluated as $0.72 MW/m^2$): a constant value of $1 MW/m^2$ is therefore considered on the entire curved surface of the LEE. This is also useful for the application of the successive step, where literature correlation will be used. From the technical report [2], at the outlet of the most critical LEE[32] it is possible to guarantee 20bar.

The boundary conditions are imposed as in Table 24.

| Region | Boundary conditions fluid dynamic problem | | | | Boundary conditions thermal problem | | | |
|---|---|---|---|---|---|---|---|---|
| inlet | mass flow inlet | $\dot{m}$ | variable | kg/s | temperature | $T_{in}$ | 25 | °C |
| outlet | pressure outlet | $p_{out}$ | 20 | bar | no conduction | | dT/dn=0 | |
| cylinder, interface | no slip | $v=v_{wall}$ | 0 | m/s | _ | | | |
| twisted tape, interface | no slip | $v=v_{wall}$ | 0 | m/s | _ | | | |
| frontal surface | _ | | | | heat flux | $\dot{Q}$ | 1 | $MW/m^2$ |
| other surfaces | _ | | | | adiabatic | | dT/dn=0 | |

*Table 24 BCs for determination of minimum mass flow required at LEE*

The minimum local pressure obtained in the detailed analysis of the LEE with the twisted tape was 18.9bar: this represents the worst possible case, since mass flow should be reduced with respect to the initial value of (2kg/s), according to the observations already made, and so minimum local pressure should not decrease. In fact, in that case, even with a constant $1.5 MW/m^2$ heat load on the frontal surface, refrigeration was more than necessary. At this pressure (18.9bar) the saturation temperature is 209°C and must not be exceeded. Considering the two LEEs series and the inlet temperature this means that, on a single LEE, in the fluid region

$$T_{max,fluid} - T_{min,fluid} < \frac{209°C\ saturazione\ -25°C\ inlet}{2\ LEE\ in\ serie} = 92°C \tag{2.1}$$

[32] Which is the LEE2, with the notation previously introduced. In the Figure 69 (right) it is the second LEE from the left.

Mass flow is therefore iteratively changed to satisfy this constraint.

Material properties are the same of Table 2 and continua model selected to speed up the simulation is described in Table 25. The mesh adopted has the same parameters determined in the grid independence analysis of the LEE sample.

| Continua Model | |
|---|---|
| Fluid: water | Solid: CuCrZr |
| All y+ Wall Treatment | Constant Density |
| Constant Density | Segregated Solid Energy |
| Segregated fluid temperature | Gradients |
| Segregated Flow | Solid |
| Gradients | Solution Interpolation |
| K-Omega Turbulence | Steady |
| Liquid | Three Dimensional |
| Reynolds-Averaged Navier-Stokes | |
| Solution Interpolation | |
| SST (Menter) K-Omega | |
| Steady | |
| Three Dimensional | |
| Turbulent | |
| Wall Distance | |

*Table 25 Continua model for minimum mass flow determination in the LEE*

## Development of a predictive model starting from literature knowledge

To reduce as much as possible the number of required simulations, literature knowledge can provide a valid support, thanks to the fact that, from previous studies, the LEE behavior (in conditions like those in Table 24) is well approximated by the correlations. In a very approximate way, it is possible to calculate the maximum fluid temperature ($T_{max}$) expected as the flow rate ($\dot{m}$) and the corresponding pressure drop ($\Delta p$) vary, from the experimental correlations available and already presented.

From friction factor (Blasius definition) it can be obtained the $\Delta p(\dot{m})$, since

$$\begin{cases} \Delta p = f \dfrac{\rho \dfrac{v_{inlet}^2}{2}}{\left(\dfrac{D}{\Delta L}\right)} \\ v_{inlet} = \dfrac{\dot{m}}{\dfrac{\pi D^2}{4}\rho} \end{cases} \tag{2.2}$$

where $\Delta L$ is the total length and $\Delta p = p_{out} - p_{in}$ the pressure drop between inlet and outlet sections of the LEEs, $\rho$ the density of the fluid, $v_{inlet}$ the inlet velocity of the fluid, $D$ the diameter of the empty pipe.

From average Nusselt number it can be obtained $T_{max}(\dot{m})$, since

$$\begin{cases} Nu = \dfrac{hD}{k} \\ h = \dfrac{q}{T_s - T_b} \\ T_b = \dfrac{T_{b,\,inlet} + T_{b,outlet}}{2} \\ T_{b,outlet} = \dfrac{A_{front} q}{c_p \dot{m}} + T_{b,inlet} \end{cases} \tag{2.3}$$

where$T_s$ is the surface average temperature (on cylinder surface of the inner tube), $T_{b,inlet}$ the mass flow average temperature at inlet cross section known from BCs, $q$ the known heat flux from BCs.

By using simulations as calibration tools, it can be estimated a $\Delta T^*$, different for twisted tape and plain tube designs, constant for a certain range of mass flows and variable with the heat flux $q$, which allows to predict in an indicative and rough way

$$T_{max} = T_s + \Delta T^* \tag{2.4}$$

From the two previous systems, all variables are known, except for Nusselt number and friction factor, which are actually known from literature. In this way, the system is grossly predictable[33].

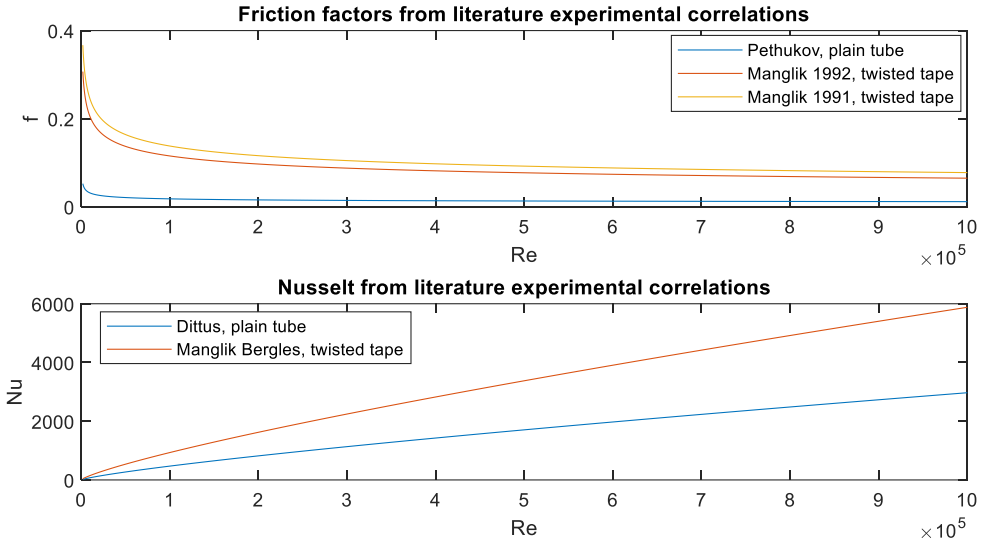


*Figure 70 Friction factors and Nusselt number: curves for the specific geometry and fluid model of the LEE studied*

Given the geometry, for any mass flow the pressure drop $\Delta p(\dot{m})$ and $T_s(\dot{m})$ can be estimated directly (unless a percentage error) from the graph of these two functions, before doing any simulation. Above all, the pressure drop can be predicted for different types of twisted tapes and it can be easily noticed that, unless strictly necessary – presence of very high heat load, especially if constant, and poor mass flow - it is not convenient the choice of twisted inserts if the main objective is the reduction of the pressure drop of the neutralizer.

For the determination of the maximum temperature, which is the real challenge, $\Delta T^*$ must be determined. The method followed requires two passages:

- running a simulation of first attempt with a certain mass flow and extract $T_{max}$ and $T_s$
- evaluate the $\Delta T^* = T_{max} - T_s$

This is not a correlation, but gives, at least, an idea of the working point to understand how to setup the following simulation and reduce the number of attempts to find the limit temperature.

[33] Friction factors and Nusselt number from experimental correlations are the same cited used in the LEE sample studied. The complete simple code developed has been developed in MATLAB. See script in Appendix, MATLAB code developed for Tmax and pressure drop evaluation in the LEE

For twisted tape and plain tube design, in this condition, the $\Delta T^*$has been estimated, respectively, 33K and 27K. Since the interesting variable is the $T_{max,fluid} - T_{min,fluid}$, this quantity[34] has been directly reported in Figure 72.

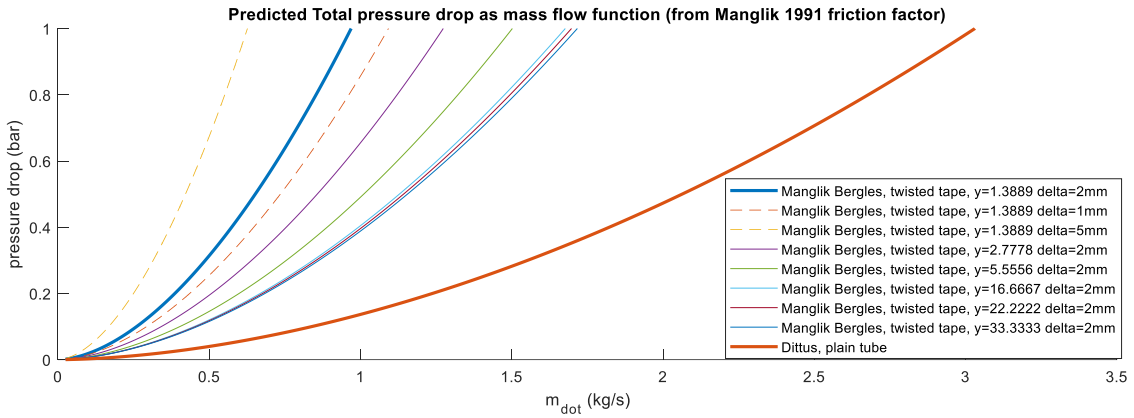


*Figure 71 Predicted total pressure drop for LEE as plain tube geometry (friction factor from Pethukov correlation) and with different type of twisted tape (friction factor from Manglik-Bergles 1991 correlation), where y=twist ratio and delta=thickness of the lamina*

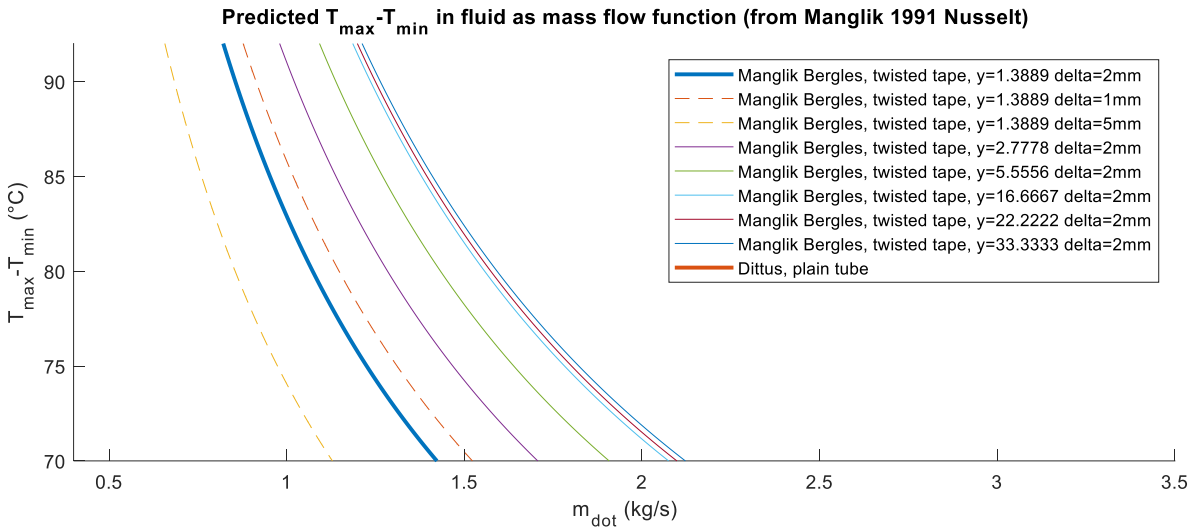


*Figure 72 Predicted temperature difference in fluid for LEE as plain tube geometry (friction factor from Dittus Boelter correlation) and with different type of twisted tape (Manglik-Bergles), where y=twist ratio and delta=thickness of the lamina*

## Results

To satisfy the constraint of (2.1)

$$T_{max,fluid} - T_{min,fluid} < 92K$$

if a plain tube design for the LEE is selected at least 1.5kg/s are required, while with a twisted tape design only 0.85kg/s are needed. On the other hand, the pressure drop is higher with the twisted tape (0.9bar) than with the plain tube (0.25bar), for the respective mass flow rates.

[34] Minimum temperature in fluid is the inlet temperature (known from BCs)

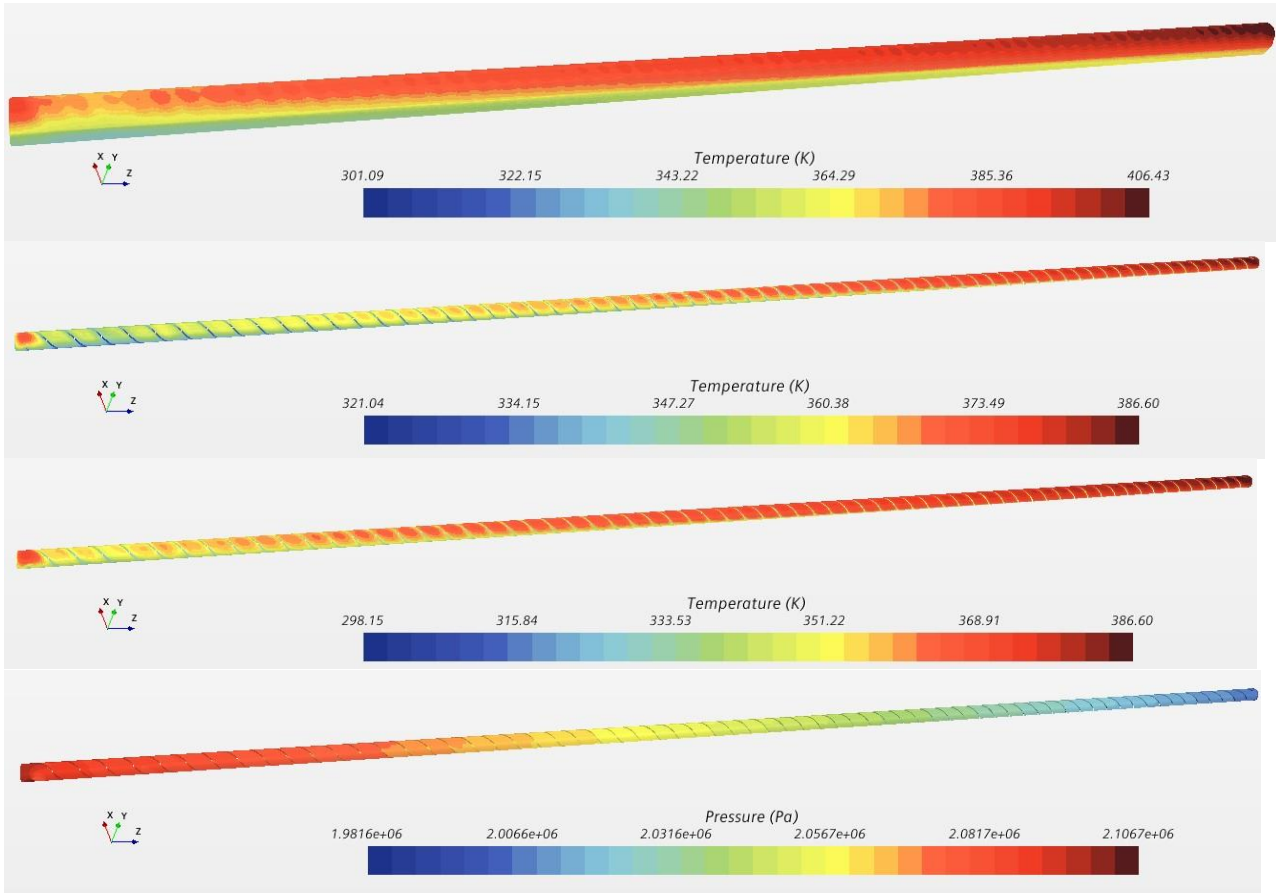


*Figure 73 LEE with TT with mass flow 0.85kg/s, from the top: temperature distribution for solid (case), solid (cylinder), fluid (cylinder), pressure distribution in fluid*

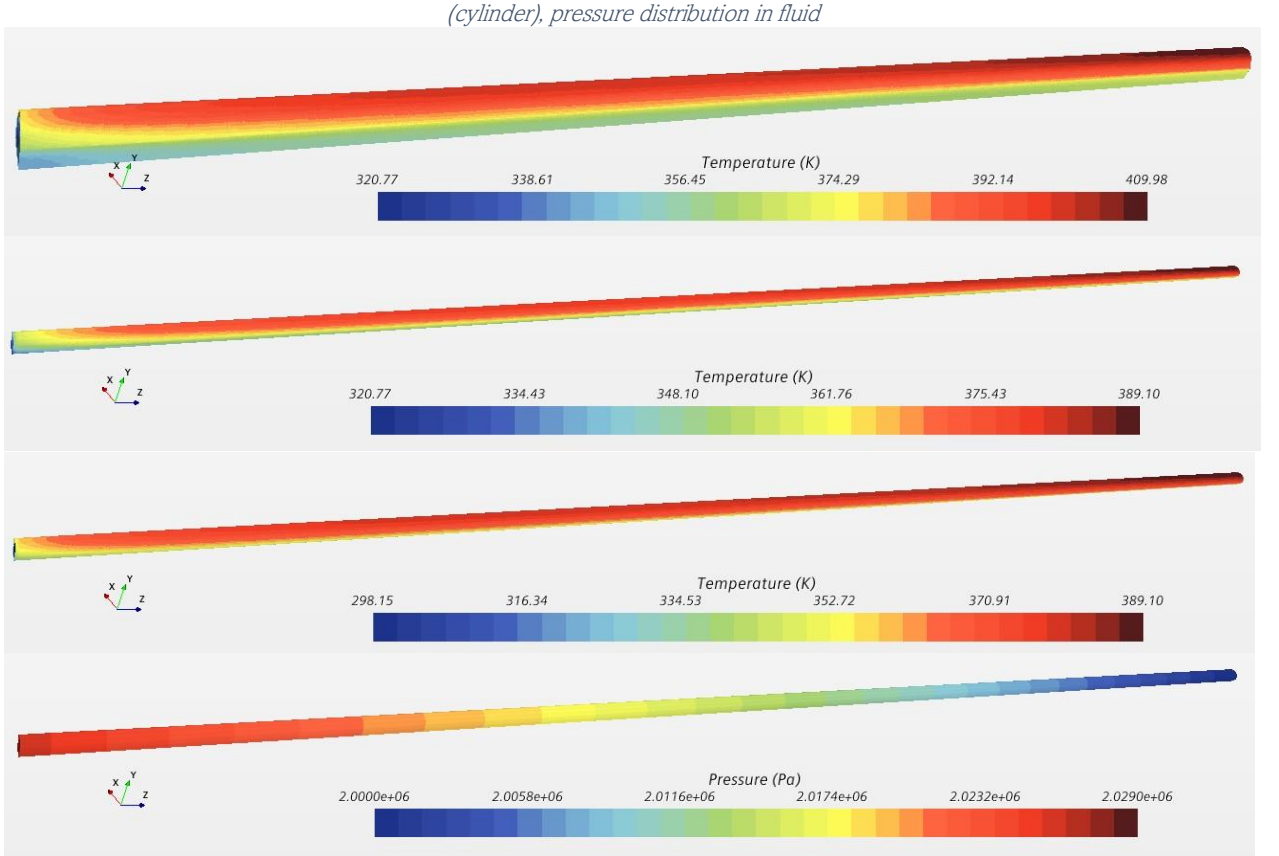


*Figure 74 LEE without TT (plain tube) with mass flow 1.5kg/s, from the top: temperature distribution for solid (case), solid (cylinder), fluid (cylinder), pressure distribution in fluid*

Finally the selected design is the LEE without the twisted tape, with a minimum mass flow required of 1.5kg/s.

In this condition, no boiling phenomena should occur and, since also temperature on the solid wall surface is very low, according to the limit fixed to prevent material properties decay (673K [11]), no relevant problem can be highlighted, but thermomechanical assessment must be performed. Mass flow distribution in the neutralizer should confirm the possibility to obtain such a mass flow at each LEE, considering also the required mass flow to the panels and the total mass flow available.

| | without TT | | with TT | | | observations |
|---|---|---|---|---|---|---|
| | 2kg/s | 1.5kg/s | 0.9kg/s | 0.85kg/s | 0.75kg/s | |
| Iteration | 1338 | 1282 | 2301 | 3453 | 2300 | |
| **Total Pressure Drop (Pa)** | **4.19E+04** | **2.52E+04** | **1.00E+05** | **9.05E+04** | **7.26E+04** | mass flow averaged absolute total pressure |
| **Tmax (K)** | **370.96** | **389.10** | **382.94** | **386.60** | **395.30** | Maximum temperature reached in the fluid region |
| T_outlet (K) | 310.68 | 314.86 | 325.38 | 326.95 | 330.80 | mass flow averaged at outlet |
| Tsurface media_totale (K) | 349.44 | 363.54 | 353.80 | 356.26 | 362.18 | Evaluated at the interface solid-fluid of the cylinder |
| fComp_Ltot | 0.014 | 0.015 | 0.170 | 0.172 | 0.178 | Evaluated between inlet and outlet (total length) |
| NuComp_Ltot | 709 | 560 | 645 | 618 | 559 | Evaluated between inlet and outlet (total length) |
| errorftot (%) | 11.58 | 10.94 | 13.42 | 13.38 | 13.22 | Error between fComp_Ltot and experimental correlations |
| errorNutot (%) | 3.75 | 3.10 | 9.71 | 9.56 | 9.46 | Error between NuComp_Ltot and experimental correlations |
| fComp_section76_166 | 0.015 | 0.016 | 0.115 | 0.117 | 0.121 | Friction factor evaluated between two sections at 76cm e 166cm from the inlet |
| Nu medio76-166 | 717 | 566 | 649 | 621 | 563 | Nusselt number evaluated between two sections at 76cm e 166cm from the inlet |
| f_errorfriction (%) | 10.22 | 9.54 | 23.18 | 23.10 | 23.01 | Error between fComp_section76_166 and experimental correlations |
| errorNu (%) | 4.93 | 4.24 | 9.25 | 9.03 | 8.94 | Error between NuComp_section76_166 and experimental correlations |
| errorT (%) | 0.04 | 0.06 | 1.10 | 1.17 | 1.22 | Error between outlet temperature and predicted from first principle of thermodynamics |
| T_max-T_min nel fluido (K) | 72.81 | 90.95 | 84.79 | 88.45 | 97.15 | In a single LEE it must be below 92K to avoid saturation temperature |

*Table 26 Results for the determination of minimum mass flow in LEEs: simulations required*

## Updating the model: definitive conceptual design of the LEEs

The model of the LEE without TT is finally updated by correcting the material properties as in Table 27 and adding the real heat load, in order to verify if, with the minimum mass flow determined (1.5kg/s) and all the hypothesis previously exposed, it is still valid. The thermal load is applied also on the lateral surfaces as shown in the first picture of Figure 75.

| CuCrZr | | | | | | |
|---|---|---|---|---|---|---|
| property | symbol | unit | function of | symbol | unit | expression |
| specific heat | $c_p$ | [J/(kg*K)] | temperature | T | [ °C] | 6.32E-06*T$^2$ + 9.49E-02*T + 3.88E+02 |
| thermal conductivity | λ | [W/m*K] | temperature | T | [ °C] | 2.11E-07*T$^3$ - 2.83E-04*T$^2$ + 1.38E-01*T + 3.23E+02 |
| density | ρ | [kg/m$^3$] | _ | _ | _ | ρ = 8900*(1 - 3 x10$^{-6}$ (7.20 x10$^{-9}$ T$^3$ - 9.05x10$^{-6}$T$^2$ + 6.24 x10$^{-3}$T + 16.6)x(T - 20)) |
| Thermal expansion coefficient | $\alpha$ | | | | | -3.1212e-17T$^4$+ 8.8090e-14T$^3$ -9.1206e-11T$^2$+ 4.3244e-08T+ 9.8884e-06 |
| Zero thermal strain reference temperature | | | | | K | 293.15 |
| Poisson's ratio | | | | | | 0.33 |
| Young modulus | | | | | | E = 128- 2.59x10-2 T - 4.87x10-5 T$^2$ |
| Water | | | | | | |
| specific heat | $c_p$ | IAPWS | | | | |
| thermal conductivity | λ | | | | | |
| density | ρ | | | | | |
| dynamic viscosity | μ | | | | | |

*Table 27 Properties for complete definitive conceptual design of the LEEs. The last 4 parameters of the solid model are not used for CtFD analysis but for the following FEM analysis*

The continua model must be upgraded with the correction of non constant density for the continua model and of non constant[35] properties of the materials both for liquid and solid (Table 28).

| Continua model | |
|---|---|
| Water | CuCrZr |
| IAPWS-IF97 (Water) | Polynomial density |
| Segregated Fluid Temperature | Gradients |
| Gradients | Segregated Solid Energy |
| Segregated Flow | Solution interpolation |
| Solution Interpolation | Solid |
| All y+ Wall Treatment | Steady |
| Wall Distance | Three dimensional |
| SST (Menter) K-Omega | |
| K-Omega Turbulence | |
| Reynolds-Averaged Navier-Stokes | |
| Turbulent | |
| Liquid | |
| Steady | |
| Three Dimensional | |

*Table 28 Complete continua model: non constant properties for water and solid*

[35] properties are taken from [11]. For the coefficient of thermal expansion, only some values were given, without any polynomial function. To obtain an expression that could be used in StarCCM+, an interpolation of the available data has been performed with the MATLAB script reported in *Appendix,* MATLAB code for alpha extrapolation from DTT data.

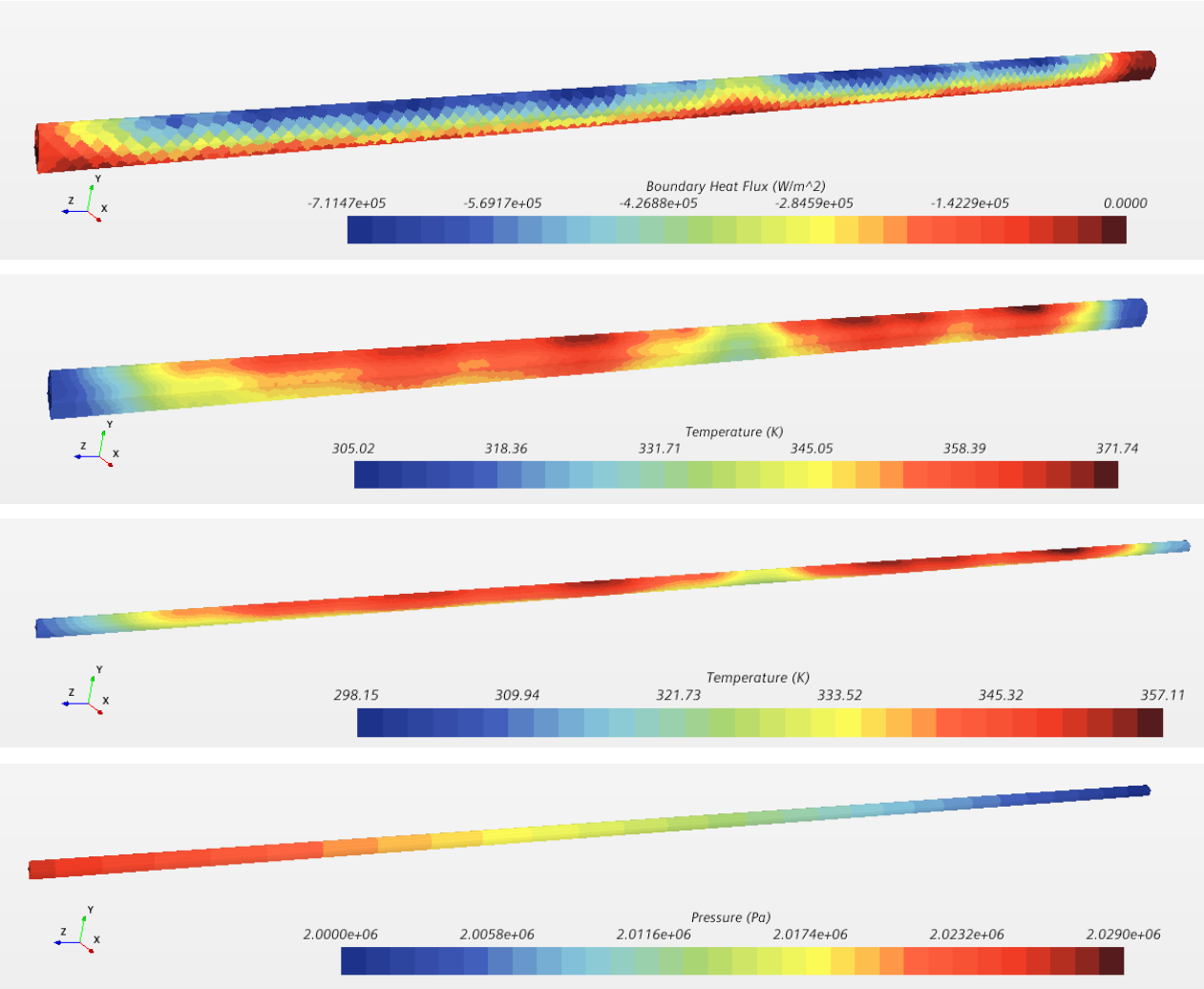


*Figure 75 Minimum mass flow determination results. LEE without twisted tape, 1.5kg/s, variable properties and distributed heat load: boundary heat flux, temperature on the case, temperature on the fluid, pressure distribution*

In the end, minimum mass flow results for the LEE to avoid boiling phenomena are:

$$\dot{m} = 1.5kg/s$$

$$\Delta p = 0.25bar$$

$$T_{max,fluid} - T_{min,fluid} = 59K$$

Thermomechanical assessment must then be performed.

This model is called *definitive*, because it considers all real conditions in terms of heat flux and material properties. It is also defined *preliminary*, because it is a reference model: it should be verified with thermomechanical assessment and, above all, the effective mass flow must be determined after the calculation of the entire model distribution, since it is a consequence of the whole neutralizer design and flux splitting components. Nevertheless, accuracy of results must be improved with grid independence analysis.

## 2.1.2. Panels: minimum mass flow

### Model setup and BCs

For what concerns the panels, materials and models are the same described in Table 2 and Table 25.

With the hypothesis that the target pressure drop IO of 2bar will be satisfied, the pressure in correspondence of the inlet mass flow sections for each hole of the panels should not vary significantly from the value imposed also for LEEs. This means that the same saturation temperature (482K) can be taken as reference and as constraint. In particular for the panels, it is imposed that in the fluid region, to avoid boiling phenomena

$$T_{max,fluid} < 482K$$

As a conservative approach, the real heat load is considered in this case but a good margin from the saturation temperature is kept: this choice allows to consider appropriately the heat load without excessive overestimations like the one that would occur imposing a constant heat load on a huge surface as that of the panels.

Boundary conditions are expressed in Table 29, with reference to the notation like the geometry reported in Figure 76. A zero pressure has been imposed at all the outlets since the important result is the pressure drop.

| Region | Boundary conditions fluid dynamic problem | | | | Boundary conditions thermal problem | | | |
|---|---|---|---|---|---|---|---|---|
| top hole 1:2:25 | mass flow inlet | $m_{dot}$ | variable | kg/s | temperature | $T_{in}$ | 25 | °C |
| top hole 2:2:26 | pressure outlet | $p_{out}$ | 0 | bar | no conduction | | dT/dn=0 | |
| lateral surfaces | | | | | heat flux | $Q_{dot}$ | distributed | $MW/m^2$ |
| other surfaces | | | | | adiabatic | | dT/dn=0 | |

*Table 29 BCs for the determination of the minimum mass flow required for the panels*

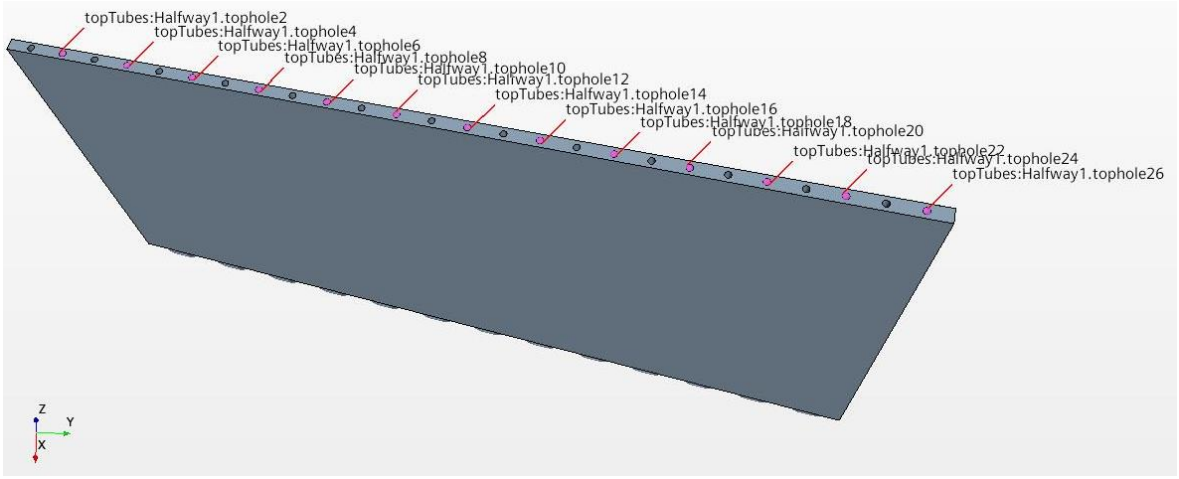


*Figure 76 Halfway 1 sections for BCs: in the entire study "top hole" referred to a panel stands for a section in the upper part of the panel. The numeration goes from 1 (the farthest tube hole from the LEE) to 26 (the closest to the LEE). Odd numbers stand for inlet, even numbers for outlet.*

Halfway panel 1 and 2, Central panel 2 and Lateral panel 1 are considered: they are the most critical panels, since higher heat load is deposited on their surfaces, with higher peaks. All the three typologies of panels are analyzed since the heat load is not symmetric.

A coarse mesh is selected for panels to speed up the process, since many simulations are required. A rapid grid independence analysis[36] is performed on halfway panel 1, with a mass flow rate of 0.25kg/s imposed at each channel. This value comes from a first explorative attempt of individuation of a minimum mass flow required for halfway panel 1.

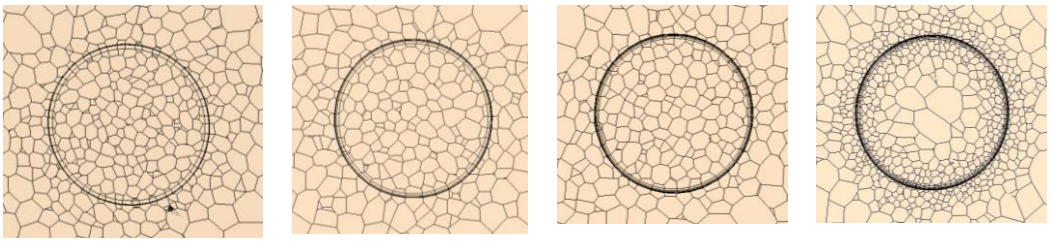

*Figure 77 Rapid mesh convergence for halfway 1. From left to right: 3 prism layers, 5 prism layers, 7 prism layers, 8 prism layers*

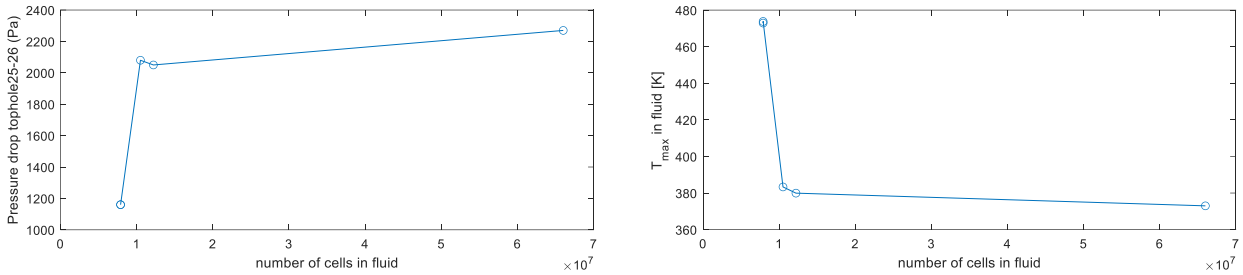


*Figure 78 Rapid mesh convergence analysis on halfway panel 1*

The mesh finally selected for each critical panel, in this stage, is represented in Figure 79 and it is derived from the parameters of the third mesh in Figure 77.

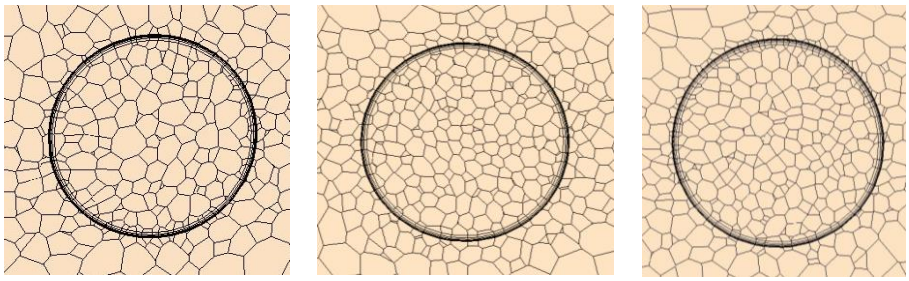

*Figure 79 Mesh used for the panels for the determination of minimum mass flow: Halfway 2 (16366724 cells), Lateral1 (25837691 cells), Central2 (25443584 cells)*

After several simulations, the minimum mass flow required for each channel of each panel is determined, so that the constraint on the maximum temperature in fluid is satisfied[37]:

$$\dot{m}_{min,Halfway2} = 0.15kg/s$$

$$\dot{m}_{min,Central2} = 0.07kg/s$$

$$\dot{m}_{min,Lateral1} = 0.07kg/s$$

[36] Complete data from which the graphs have been taken are reported in *Appendix* Rough convergence analysis on halfway panel 1.

[37] The complete numerical results are detailed in *Appendix* Panels: results for minimum mass flow determination

## Updating the model: definitive preliminary model of the panels

After the selection, the model is updated by correcting the material model with properties listed in Table 27, variable with temperature, and the continua with Table 28. To properly consider also pressure dependence of properties of water, instead of a zero pressure, for the top hole 2:2:26 (outlet BCs), 20 bar are considered.

The final results for the minimum mass flows of panels are summarized in the following figures and tables.

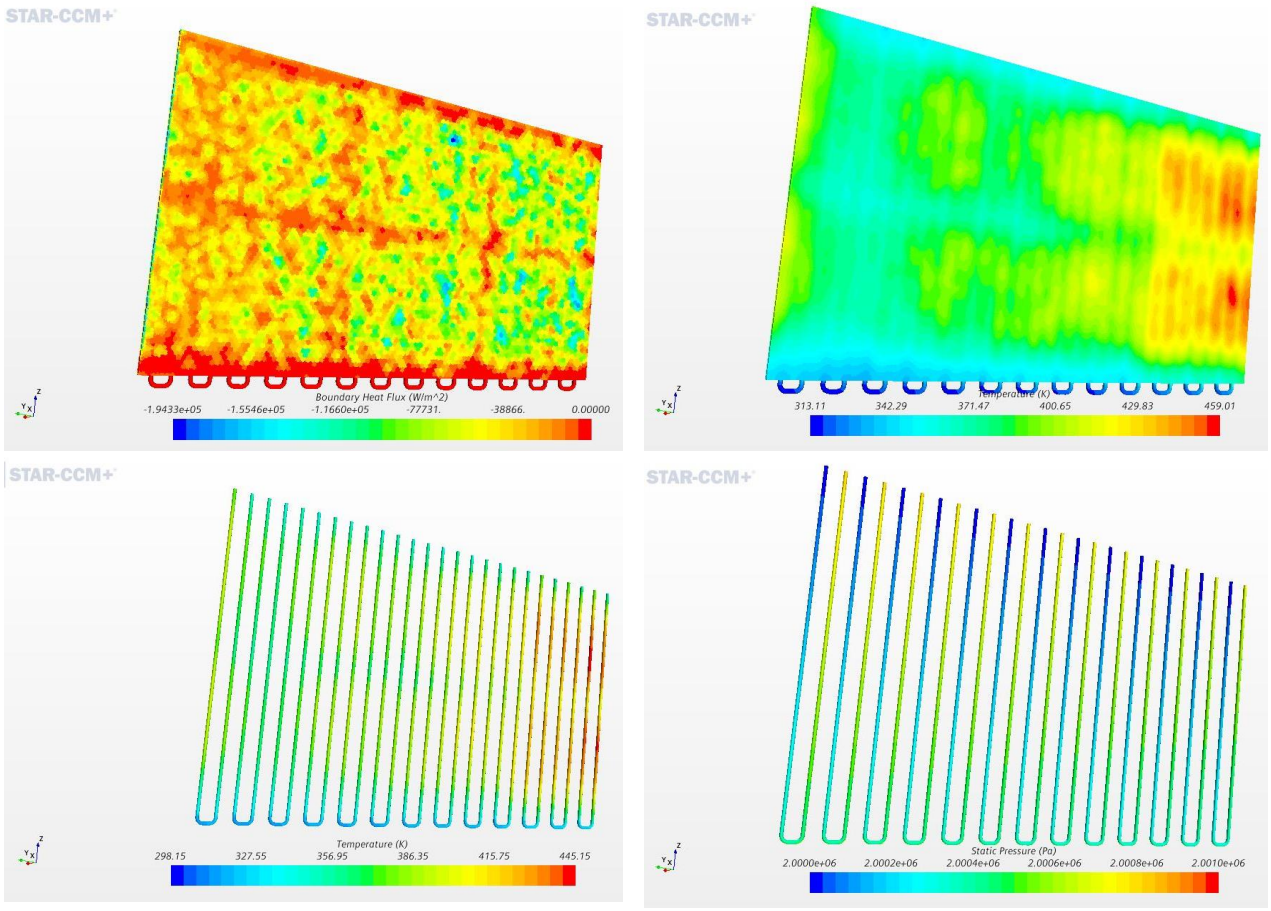


*Figure 80 Halfway 2, variable material properties, minimum mass flow 0.15kg/s, distributed heat load: boundary heat flux, temperature distribution on solid surface, temperature in fluid, pressure distribution*

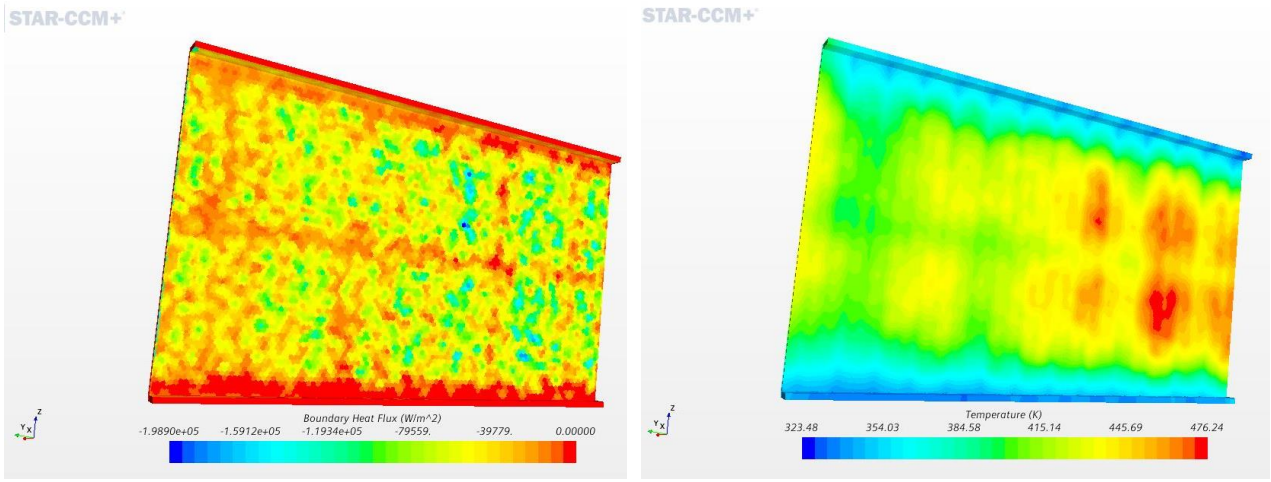

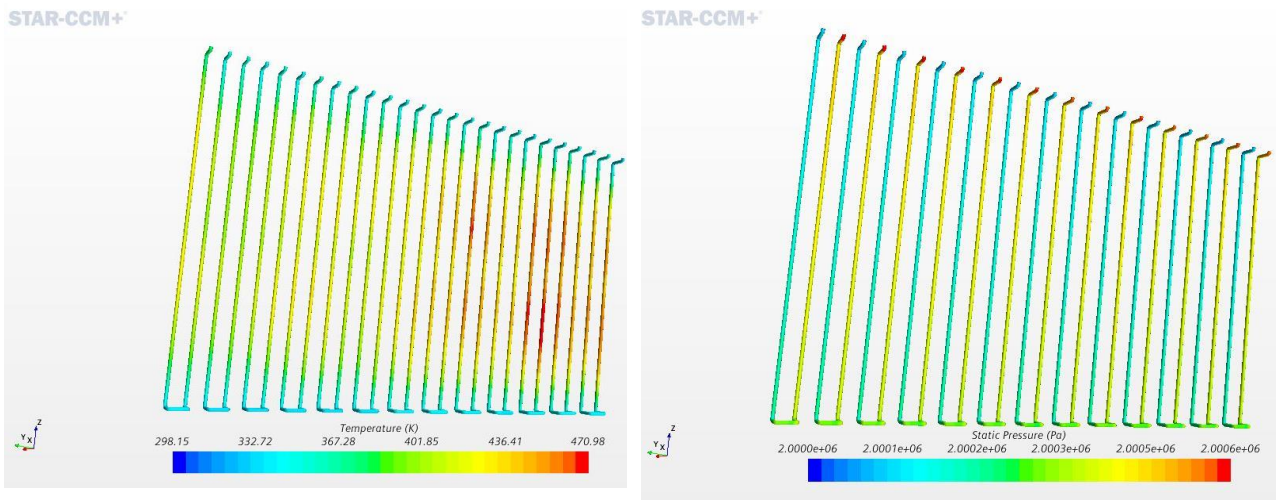


*Figure 81 Central 2, variable material properties, minimum mass flow 0.07kg/s, distributed heat load: boundary heat flux, temperature distribution on solid surface, temperature in fluid, pressure distribution*

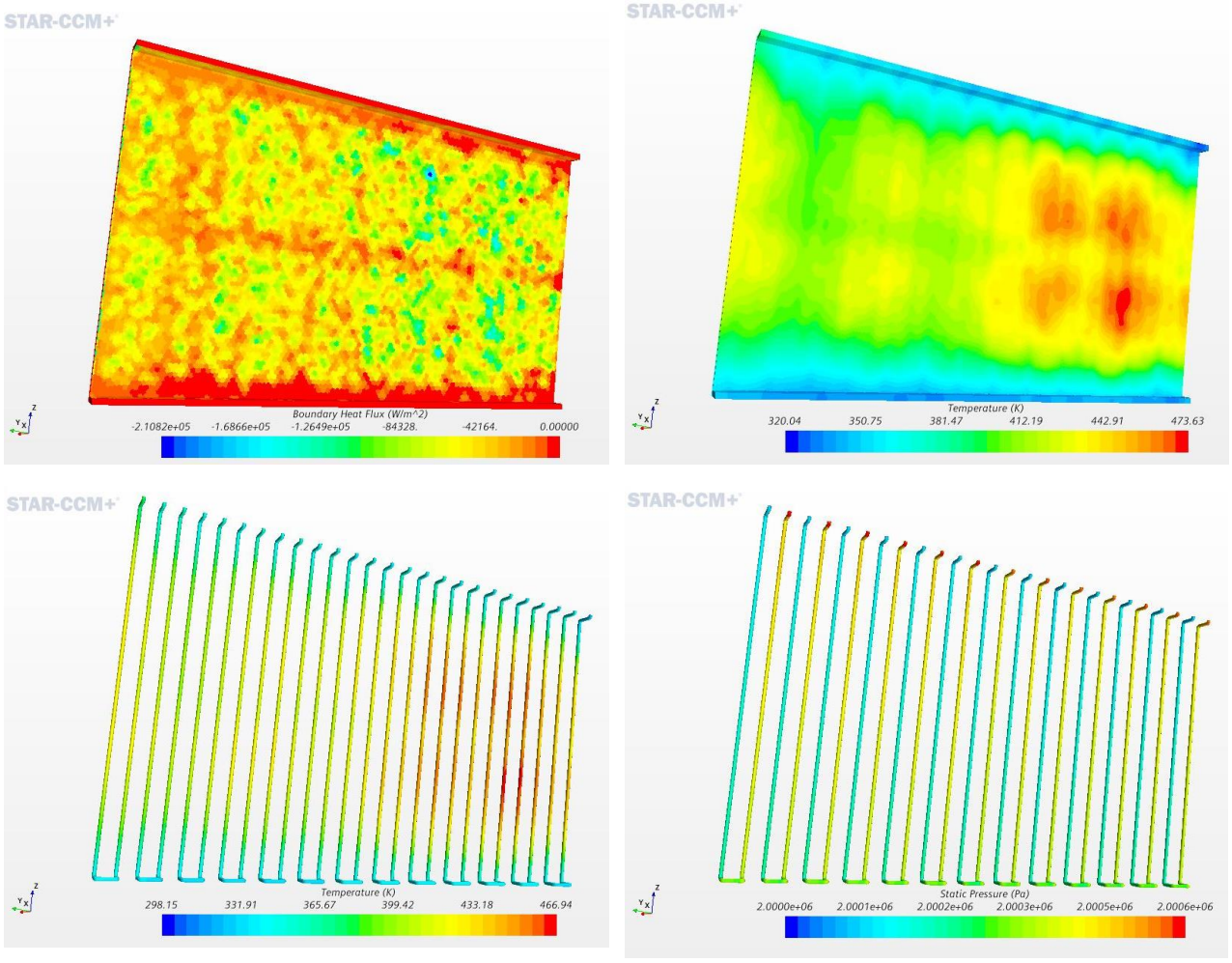


*Figure 82 Lateral 1, variable material properties, minimum mass flow 0.07kg/s, distributed heat load: boundary heat flux, temperature distribution on solid surface, temperature in fluid, pressure distribution*

With the nomenclature of Figure 76, pressure drop (mass flow averaged of absolute total pressure) for each couple of channels is indicated as Pressure Drop followed by the number of the couple from the shorter tube

to the longest one[38]. As it can be seen, attempted values are very small, which means that, with these minimum mass flow rates to the panels, refrigeration is guaranteed for the solid, no boiling phenomena should occur and target pressure drop IO limit (<2bar) should be satisfied, as from requirements.

| | HALFWAY 2 | LATERAL 1 | CENTRAL 2 |
|---|---|---|---|
| | **0.15 kg/s** | **0.07 kg/s** | **0.07 kg/s** |
| cells | 1.64E+07 | 2.58E+07 | 2.54E+07 |
| cells fluid | 1.22E+07 | 1.95E+07 | 1.97E+07 |
| cells solid | 4.18E+06 | 6.31E+06 | 5.75E+06 |
| Iteration | 930 | 1944 | 1983 |
| Pressure Drop 1 (Pa) | 6.69E+02 | 4.60E+02 | 4.64E+02 |
| Pressure Drop 2 (Pa) | 6.81E+02 | 4.64E+02 | 4.69E+02 |
| Pressure Drop 3 (Pa) | 6.87E+02 | 4.68E+02 | 4.68E+02 |
| Pressure Drop 4 (Pa) | 6.97E+02 | 4.59E+02 | 4.69E+02 |
| Pressure Drop 5 (Pa) | 7.08E+02 | 4.73E+02 | 4.78E+02 |
| Pressure Drop 6 (Pa) | 7.19E+02 | 4.75E+02 | 4.77E+02 |
| Pressure Drop 7 (Pa) | 7.29E+02 | 4.63E+02 | 4.71E+02 |
| Pressure Drop 8 (Pa) | 7.43E+02 | 4.86E+02 | 4.83E+02 |
| Pressure Drop 9 (Pa) | 7.51E+02 | 4.82E+02 | 4.85E+02 |
| Pressure Drop 10 (Pa) | 7.61E+02 | 4.89E+02 | 4.87E+02 |
| Pressure Drop 11 (Pa) | 7.72E+02 | 4.94E+02 | 4.91E+02 |
| Pressure Drop 12 (Pa) | 7.82E+02 | 4.84E+02 | 4.99E+02 |
| **Pressure Drop 13 (Pa)** | **791.62** | **501.24** | **500.17** |
| Temperature2 (K) | 344.87 | 340.69 | 345.93 |
| Temperature4 (K) | 342.85 | 345.89 | 346.70 |
| Temperature6 (K) | 343.06 | 347.20 | 349.25 |
| Temperature8 (K) | 336.30 | 345.20 | 343.42 |
| Temperature10 (K) | 334.97 | 347.98 | 347.47 |
| Temperature12 (K) | 334.34 | 343.89 | 345.75 |
| Temperature14 (K) | 331.77 | 341.35 | 343.66 |
| Temperature16 (K) | 330.62 | 338.82 | 341.19 |
| Temperature18 (K) | 331.80 | 340.24 | 342.08 |
| Temperature20 (K) | 331.68 | 341.39 | 343.04 |
| Temperature22 (K) | 328.39 | 338.48 | 340.01 |
| Temperature24 (K) | 327.39 | 338.37 | 338.01 |
| Temperature26 (K) | 333.51 | 345.32 | 344.19 |
| **Tmax in fluid (K)** | **445.15** | **466.94** | **470.98** |
| **Tmax in solid (K)** | **459.01** | **476.24** | **474** |

*Table 30 Minimum mass flow required for panels: final results*

All the maximum temperatures in fluid are below the limit of 482K, and maximum temperature in solids is far from critical conditions of material property degradation (approximately 673K, [11]). Thermomechanical assessment must be performed as a verification, and accuracy of results must be improved. These models, in this sense, are called *definitive* and *preliminary*, with the same meaning used in LEE's definition of the previous chapter, therefore they are only a reference limit condition.

[38] i.e. Pressure Drop 1 = mass flow averaged absolute total pressure in top hole 1 - mass flow averaged absolute total pressure in top hole 2 and so on.

## 2.1.3. Entire neutralizer: total mass flow and real BCs calculation

The real challenge now is to understand how the design of the neutralizer should be arranged to obtain such optimized mass flows distribution. Thanks to the optimization solutions discussed, more alternatives are available.

One of the requirements is to minimize the total mass flow at the inlet, which means to have lower water and energy consumptions. If the mass flow coming from the distributor is equivalently split through the channels of the six panels, the maximum of the minimum mass flows, previously determined as necessary for each single channel of the six panels, must be taken as reference. With this hypothesis two possibilities are exposed.

| | WITHOUT TT | | WITH TT | |
|---|---|---|---|---|
| minimum mass flow required for the single LEE | 1.50 | kg/s | 0.85 | kg/s |
| total mass flow available at inlet | 40 | | | kg/s |
| number of inlet tubes to the LEEs | 4 | | | |
| number of inlet tubes to the panels (13 inlet holes x 6 panels) | 78 | | | |
| **minimum mass flow required for all the LEEs** | **6.00** | **kg/s** | **3.40** | **kg/s** |
| maximum mass flow available for the panels | 34.00 | kg/s | 36.60 | kg/s |
| maximum mass flow available for each single channel of the panels if mass flow from distributor is equally split | 0.44 | kg/s | 0.47 | kg/s |
| minimum mass flow required for the single tube of a halfway panel | 0.15 | | | kg/s |
| minimum mass flow required for the single tube of a central or lateral panel | 0.07 | | | kg/s |
| **minimum mass flow required for all the panels (considering the halfway constraint)** | **11.70** | | | **kg/s** |
| **Total minimum mass flow required** | **17.70** | **kg/s** | **15.10** | **kg/s** |
| Pressure drop attempted on panels | 0.01 | | | bar |
| Pressure drop attempted at the 2 LEEs series (from Table 26) | 0.50 | bar | 1.82 | bar |

*Table 31 Computation of minimum total mass flow required at the neutralizer*

As anticipated, if the twisted tape is selected, the total pressure drop would be much higher with respect to plain tube solution. It would not be possible to consider also other losses in the circuit, since only the LEEs requires almost the total available pressure drop (2 bar).

In general, since the selected solution is that without twisted tape for the LEEs, less resistance will be seen by the fluid in this direction. This means that a huge mass flow (with respect to the models with TT and considering the same mass flow at the inlet of the neutralizer) should be here conveyed. As a first attempt, the original CAD design, without TT inserts, is tested. This will be the selected solution, and no more attempts are required, since the mass flow distribution satisfies the *desiderata*.

### CFD simulation of the entire neutralizer

The distribution of pressure and mass flows is studied with a CFD simulation of the entire neutralizer with the new boundary conditions. Water properties that have been used can be found in Table 2 (constant properties), and continua model in Table 11. BCs, with reference to the sections Figure 84, are as follows:

| Region | Boundary conditions fluid dynamic problem | | | |
|---|---|---|---|---|
| **inlet** | mass flow inlet | $\dot{m}$ | 17.7 | kg/s |
| **outlet** | pressure outlet | $p_{out}$ | 0 | bar |
| **other surfaces** | no slip | $v=v_{wall}$ | 0 | m/s |

*Table 32 BCs for the neutralizer with minimum total mass flow*

More meshes are tested for the model. Here is directly proposed, as a result, the selected one, with 175 million cells, which is the best refinement that has been obtained. Especially for the panels, as a possible future improvement, the mesh could be further refined by adding more prism layers to better solve the turbulent flow.

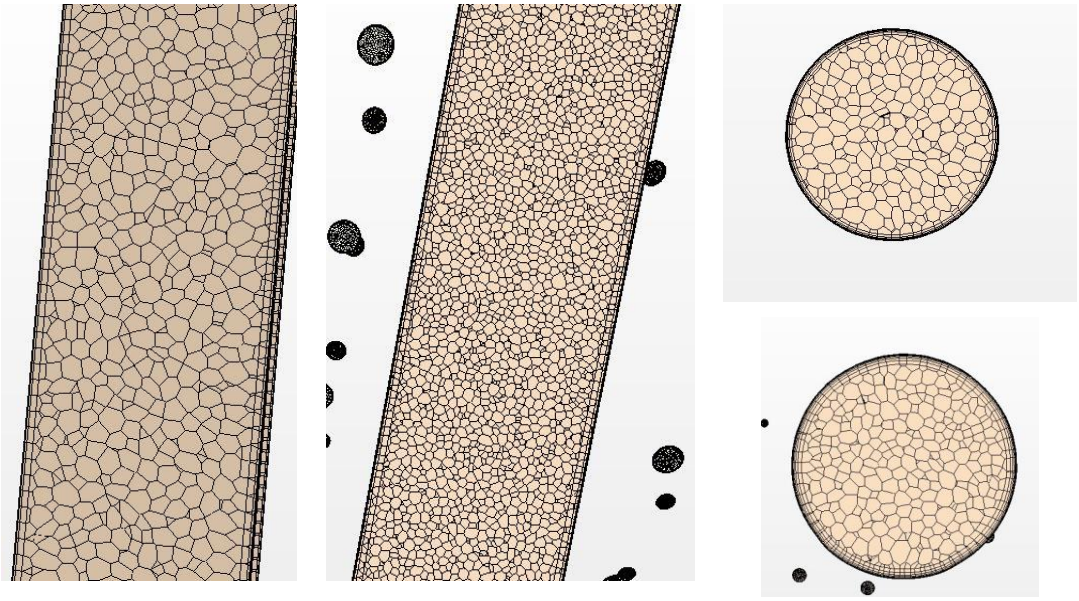

*Figure 83 Final CFD mesh with 175 million cells of the entire neutralizer: manifold (left), distributor (right), panels (top right), LEE (bottom right)*

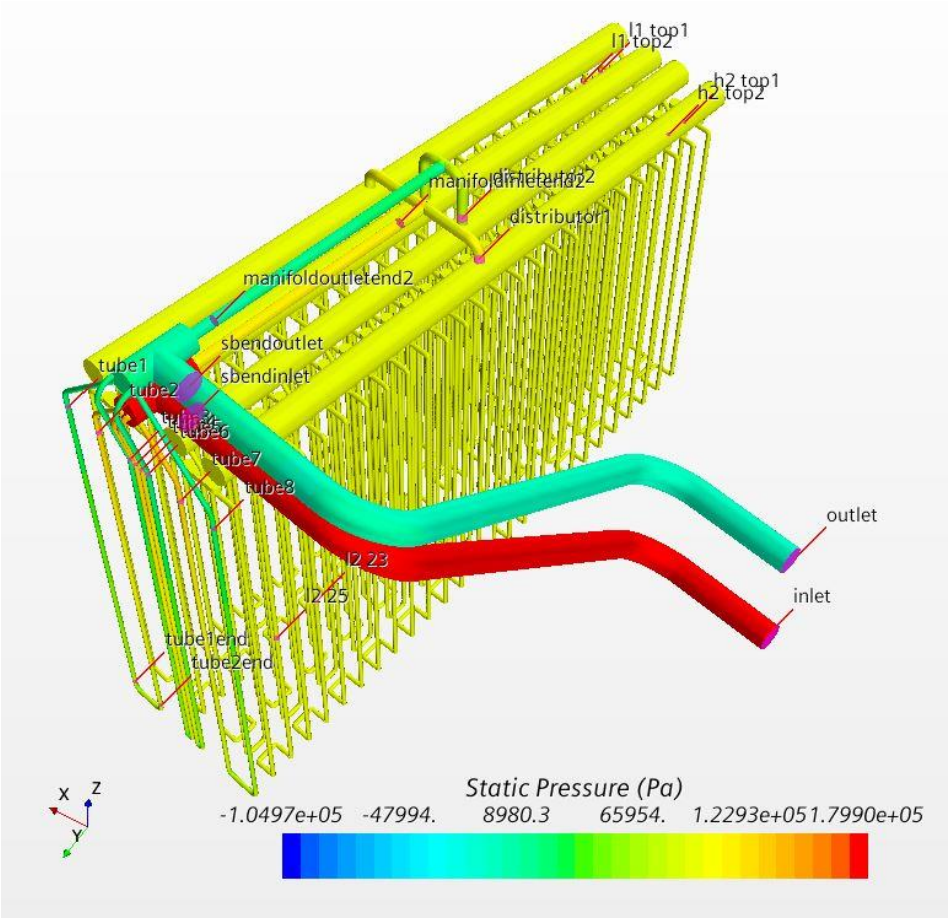


*Figure 84 CFD pressure distribution for neutralizer, 175 million cells in fluid, 17.7kg/s at inlet, 0bar pressure at outlet*

Results can be summarized[39] as in Table 33.

Sections used in all the tables of this study are reported in purple: h=halfway, l=lateral, c=central, 1,2 are the blocks (left and right) to which each panel belongs.

| STATIC PRESSURE DIFFERENCES (bar) | | |
|---|---|---|
| inlet-sbendinlet | 0.02 | Parallel circuit to the panels |
| sbendinlet-manifoldinletend2 | 0.68 | |
| manifoldinletend2-distributor1 | 0.11 | |
| distributor1-distributor2 | 0.23 | |
| distributor2-manifoldoutletend2 | 0.67 | |
| manifoldoutletend2-sbendoutlet | 0.07 | |
| sbendoutlet-outlet | 0.02 | |
| sbendinlet-tube2 | 0.52 | Parallel circuit to the LEEs |
| tube2-tube1 | 0.96 | |
| tube1-sbendoutlet | 0.27 | |
| | | |
| sum of pressure differences from parallel circuit to the panels | 1.79 | |
| sum of pressure differences from parallel circuit to the LEEs | 1.79 | |
| pressure drop IO | 1.79 | |
| MASS FLOWS (kg/s) | | |
| mass flow inlet | 17.70 | |
| minimum mass flow to the LEEs (tube 3, 4, 5 and 6) | 1.80 | They vary between 1.78 and 1.91 kg/s |
| minimum mass flow for a single channel of halfway 2 (h2 13 and h2 15) | 0.19 | They vary between 0.19 and 0.24 kg/s |
| minimum mass flow for a single channel of lateral 1 (l1 13 and l1 15) | 0.08 | They vary between 0.08 and 0.09 kg/s |
| minimum mass flow for a single channel of central 2 (c2 13 and c2 15) | 0.08 | They vary between 0.08 and 0.09 kg/s |

*Table 33 Static pressure differences and mass flows from CFD simulation of the entire neutralizer with 17.7kg/s*

Due to the asymmetric position of the inlet and outlet of the neutralizer, mass flow is different for each LEE. This is true also for the different channels in a single panel and for each panel, because of the different length of the internal channels.

All the simulations have shown that the main losses are due to the components already highlighted as critical, the *T-shape manifold* from the *forward circuit* and the *distributor* from the *return circuit*. These losses (which are the highest in the parallel circuit to the panels) allow to guide the water flow with the desired mass flow ratio between LEEs and panels and so are necessary and beneficial.

The proportion – just as a reference – can be adjusted in future re-designs if the heat load increases at the panels surfaces by using the optimizations described in 1.6. Optimized neutralizer designs. In particular, by changing the ratio between pressure differences for the sections *sbendinlet-tube2* (here 0.52 bar) and

[39] Sections used in all the tables of this study have been already described. Others derived parts are reported in purple in Figure 84: for the panels, h=halfway, l=lateral, c=central; 1 and 2 after the letter are the blocks (left and right) to which each panels belongs. The numeration of the panel holes starts from the farthest tube with respect to the LEE (1) up to the nearest tube to the LEE (26). Without any specification (i.e. h1) the hole is taken at middle height of the channel. With the specification "top" (i.e. h1 top, the hole is taken on the top of the panel). Numeration for the LEEs' holes (called "tube") on the top is given from the left to right, progressively numbered from 1 to 8. The "end" added (i.e. tube1end) refers to the LEE final part of the channel.

*sbendinlet-distributor1* (here 0.79 bar), the flow can be guided[40]. In fact, this increase (i.e. stray effect) could arise and could be more problematic for the panels then for the LEEs, so that for the first it is possible that a higher mass flow is required. This because margin on temperature limits for LEEs will be higher than the one selected for the panels for two main reasons:

- first, since a more conservative hypothesis was used in the preliminary optimization of the operational conditions for the LEEs margin on boiling temperature is higher in this case
- second, a higher margin with respect to the minimum mass flows evaluated for the critical components occur at the LEEs instead of panels with this CFD[41] simulation prediction

For what concerns the parallel circuit to the panels, excluding the mentioned components, other losses are substantially negligible.

For the parallel circuit to the LEEs, the higher pressure drop is due to the LEEs itself: this is a bit overestimated, due to the coarser mesh adopted for them in this model, but it highlights anyway that the current configuration is a good solution in terms of performance, since there is a good flow distribution and total pressure drop IO is mainly due to mostly unchangeable (refrigerated) components.

To validate the hydraulic model selected, the grid independence plot that can be obtained from the results from the other meshes that have been built[42] is also reported. It cannot be strictly defined as a grid independence analysis, since adopting a rigorous method for the entire CAD simulation would require much time and resources and obtaining a mesh too complex to be managed. Convergence of the results, assuming as valid the finest CFD simulation will be detailed and systematically discussed in the following chapters.

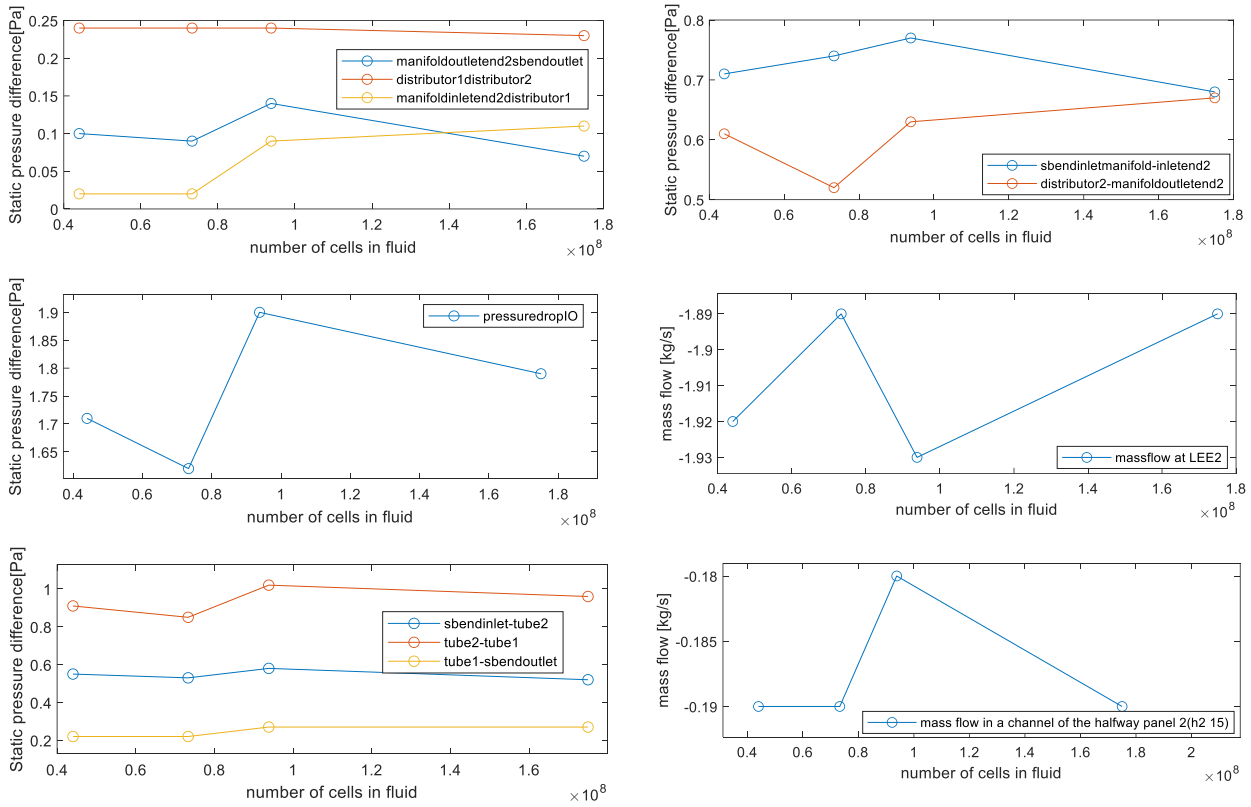


*Figure 85 Rough grid independence analysis for 4 entire CAD model of the neutralizer*

[40] Another possible solution to easily obtain the same result can be that of reducing the diameter of the inner channels of the LEEs to convey greater flow rate to the panels.
[41] 175 million cells in fluid
[42] Detailed results in Appendix, Mesh convergence for 4 entire models of the neutralizer

Last point of the graphs in Figure 85 is finally selected, since it is the finest mesh that has been obtained. The distribution of mass flow oscillates between values of the two or three decimal places, an unrealistic accuracy level, so that the values obtained can be considered practically similar. Also total pressure drop oscillates in a certain range, which is of the order of tenths of bar. Further refinements are advisable, but the selection made takes the best possible option in terms of compromise between computational cost and accuracy of results.

## 2.2. Design verification

Starting from the CFD results[43] on the most accurate model that has been developed, the BCs can be now defined, assuming as correct this hydraulic model. In particular, if a pressure 20bar must be guaranteed at LEE1 (which is the LEE that follows LEE2, the most charged and critical) as from MITICA reference and from hypothesis done up to now, by considering the total pressure drop realized, the minimum theoretical pressure at the outlet can be calculated as the difference between this attempted value and the actual estimated difference between pressure at outlet section of LEE1 and outlet:

$$p_{out,th} = p_{LEE} - (p_{LEE1} - p_{out}) \tag{2.5}$$

The theoretical pressure at the inlet can be estimated from total pressure drop

$$p_{in,th} = p_{out} + \Delta p_{IO} \tag{2.6}$$

and, supposing that the circuit control is obtained with a hydraulic pump located at the inlet of the neutralizer, this value should be rounded in order to find a suitable commercially available pump. From the real inlet pressure $p_{in}$ estimated, the real outlet pressure to be imposed as boundary condition can be calculated as

$$p_{out} = p_{in} - \Delta p_{IO} \tag{2.7}$$

| | | |
|---|---|---|
| pressure at LEE1 outlet | 20 | bar |
| pressure drop | 1.79 | bar |
| theoretical pressure at system outlet | 19.72 | bar |
| theoretical pressure at system inlet | 21.51 | bar |
| pressure at inlet (with pump) | 22 | bar |
| pressure at outlet (attempted) | 20.21 | bar |

*Table 34 Determination of the new realistic operative pressure for the neutralizer*

From this calculation and from results of the CFD with 175 million cells, the new BCs for each component (i.e. LEE2, halfway2, central2, lateral1) can be defined by scaling each pressure drop previously extrapolated

[43] In Appendix CFD 175 million cells 17.7kg/s at inlet, 0bar outlet

to the new pressure outlet. The extrapolation is obtained considering the sections *l1top1*, *tube1*, *tube1end* and similar.

First, standalone components are analyzed. Then, a comparison with a complete CtFD model is proposed to validate the results. In the end three models will be available and all of them should be equivalent and with a different grade of detail and/or quantity and quality of information provided:

- CFD entire model of the neutralizer
- CtFD standalone critical components models
- CtFD entire model of the neutralizer

Each model aims at maximizing CPU available resources and time required for obtaining (and post-processing) the results.

## 2.2.1. Standalone components CtFD verification

Detailed models for LEEs and panels are developed separately. This choice allows to obtain a detailed overview on the critical components with accuracy of results, thanks to the fact that the geometry is simplified and a better quality for the single meshes can be adopted.

To speed up the grid independence analysis only a sample of the LEE2 and a sample of the panel with the highest heat load (halfway 2) are considered. For the grid independence analysis and the final models presented as results after (i.e. all the simulations in this chapter) the grid independence study, continua model and material properties used are listed in Table 27 and Table 28.

### LEE2: grid independence study

Being all the BCs different, the grid independence study must be repeated also for the leading edge element. A piece of LEE2 is selected. This is the most charged LEE in terms of total power and peaks, but not the one with the minimum mass flow. It represents anyway the worst thermal condition for LEEs, as it will be shown, because the difference in mass flow is not so relevant with respect to the difference in the distributed heat load. Since a distributed heat load is deposited on the surface, the most critical piece is considered (Figure 86), with a length of about a quarter of the entire LEE2.

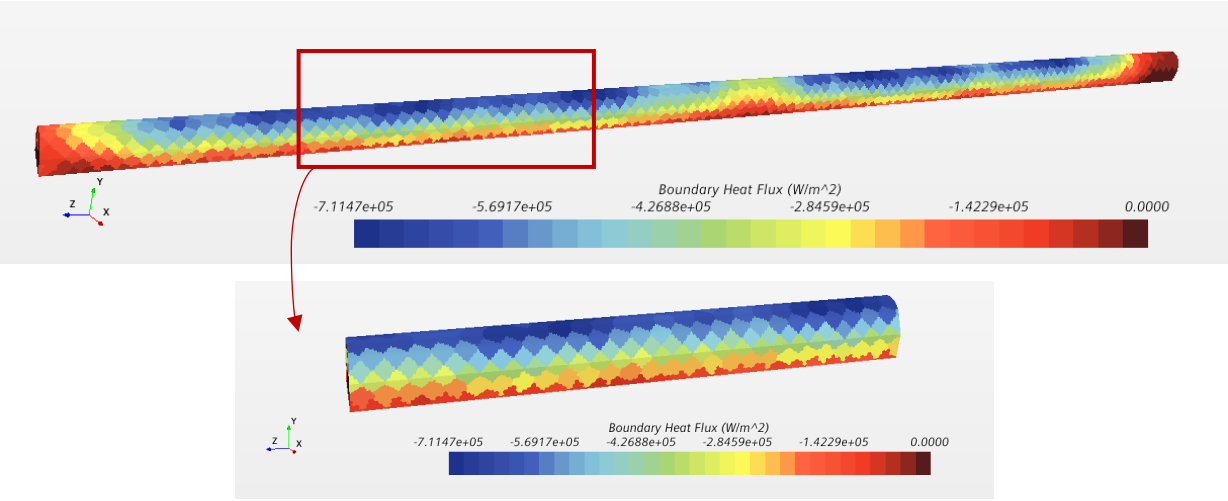


*Figure 86 Boundary heat flux for the extrapolated sample of LEE2*

BCs are imposed considering as inlet mass flow rate the value obtained with an extrapolation from the entire CFD model with 175 million cells (Table 33). For the sake of simplicity, the expected outlet pressure of 20bar is considered, even if the real value in this section will be slightly different.

| Region | Boundary conditions fluid dynamic problem | | | | Boundary conditions thermal problem | | | |
|---|---|---|---|---|---|---|---|---|
| inlet | mass flow inlet | $m_{dot}$ | 1.89 | kg/s | temperature | $T_{in}$ | 25 | °C |
| outlet | pressure outlet | $p_{out}$ | 20 | bar | no conduction | | dT/dn=0 | |
| frontal, rear and left surface | | | | | heat flux | $Q_{dot}$ | distributed | $MW/m^2$ |
| other surfaces | | | | | adiabatic | | dT/dn=0 | |

*Table 35 BCs for the sample of LEE2 analysis*

Grid independence analysis considers first the polyhedral part and then the prism layer part.

Keeping fixed the initial prism layer with a near wall thickness of 5e-6m, a prism layer total thickness of 1.5mm and 15 prism layers, the polyhedral part is studied. Base sizes are reported for increasing number of cells in the fluid. Each mesh corresponds to a point of the mesh convergence graph. As a result, the 1mm base size is selected.

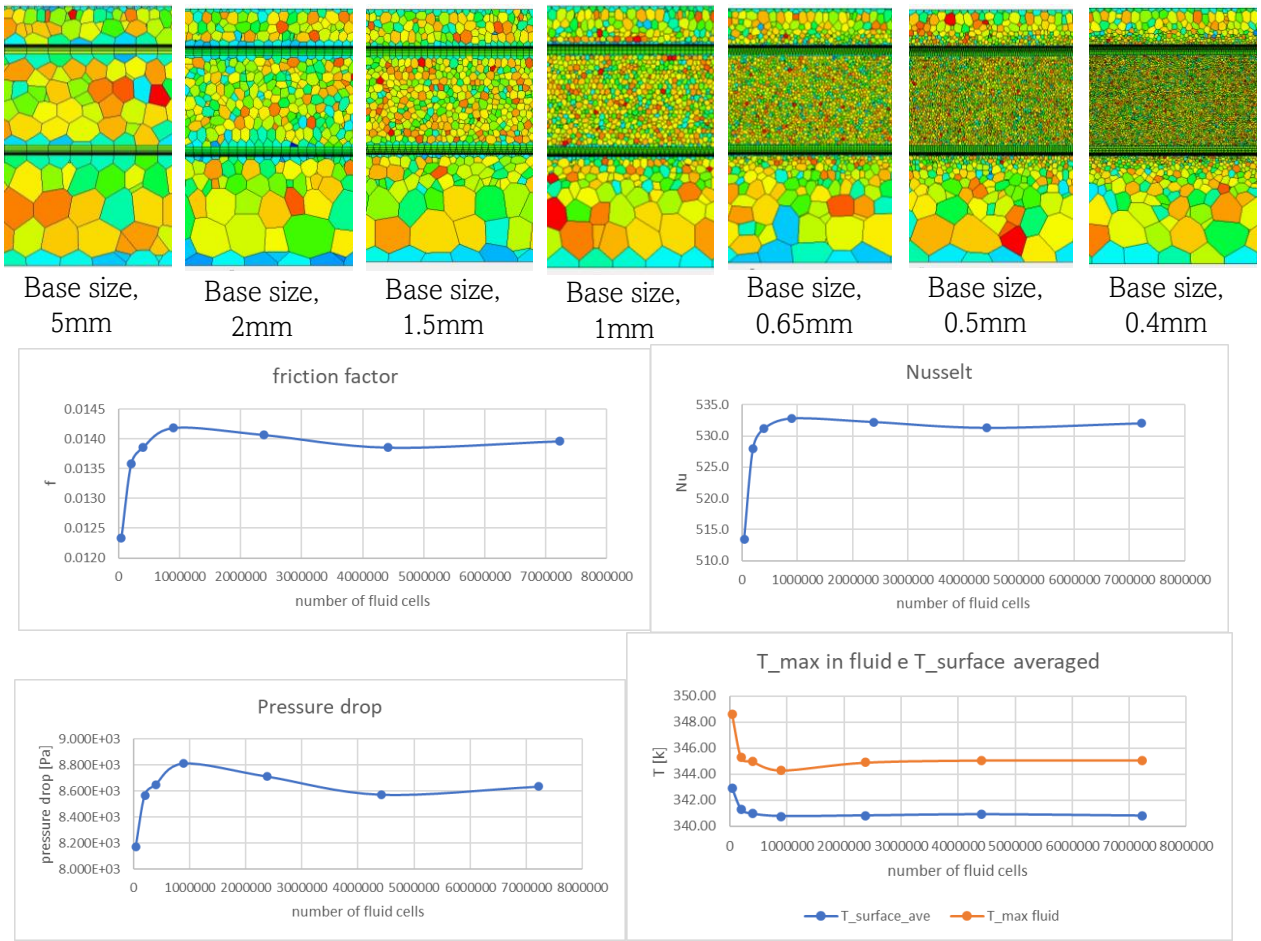


*Figure 87 LEE2 sample grid independence analysis, variable polyhedral mesh: mesh considered (top), graphs (bottom)*

Keeping fixed the base size, prism layer is analyzed. The combinations of prism layer total thickness (pltt) and prism number (pn) are reported for increasing number of cells in the fluid. Turbulent kinetic energy as reported as colored map to qualitatively show the mesh and the energetic variation contained inside the layer.

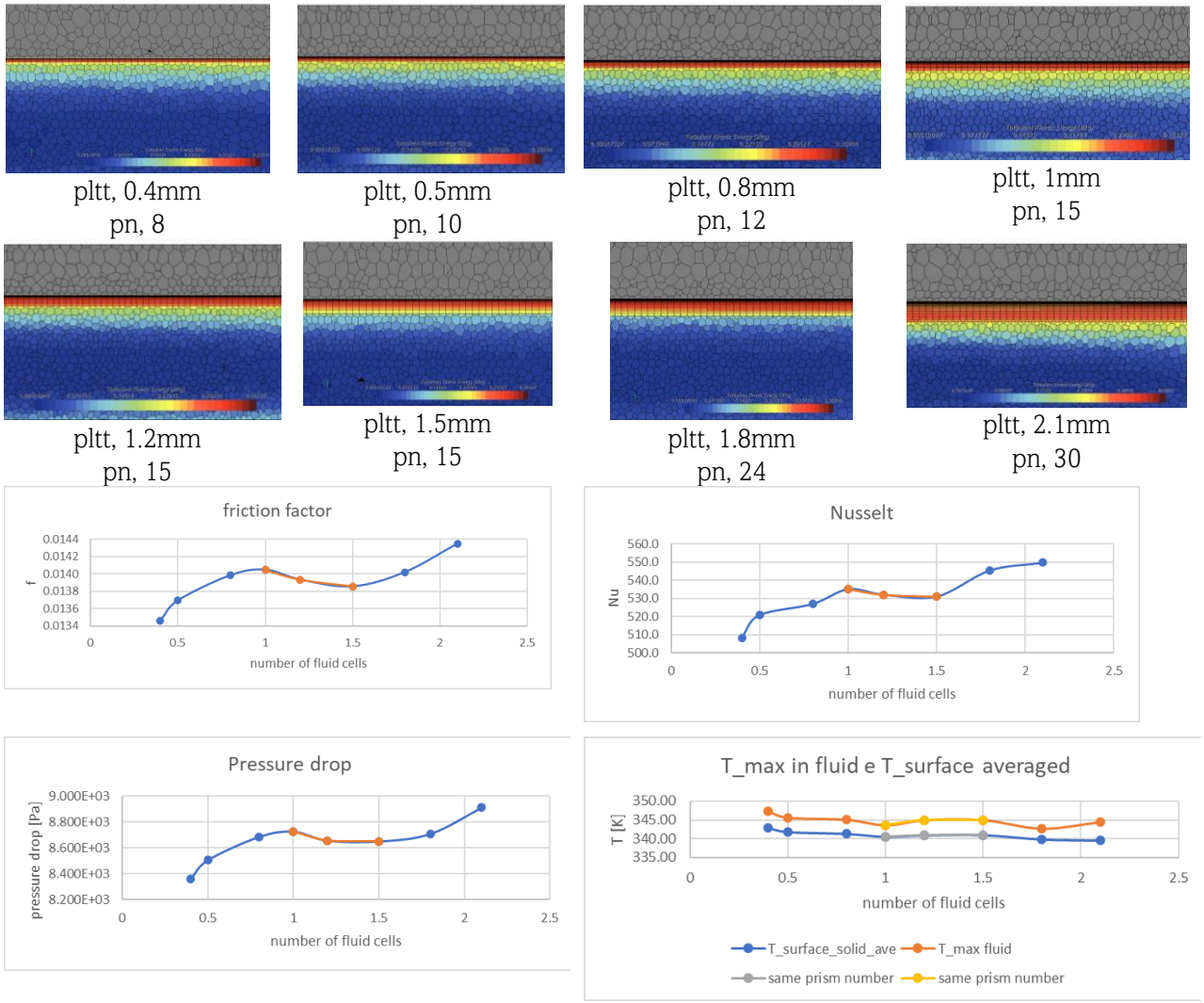


*Figure 88 LEE2 sample grid independence analysis, variable prism layer mesh: mesh considered (top), graphs (bottom)*

Int the end, the final parameters selected for the LEE2 sample mesh and consequently for the entire LEE2's model are

| Mesh for the LEE2: results of grid independence | |
|---|---|
| prism layer  near wall thickness | 5e-6m |
| prism layer total thickness | 1.2mm |
| number of prism layers | 15 |
| base size | 1mm |

*Table 36 Mesh for standalone LEE2 model*

## Halfway panel 2: mesh convergence study

For what concerns the panels, a piece of the halfway panel 2 (the worst case) is considered. The geometry should be as representative as possible, so a U-shape channels series is considered, corresponding to the last part of the panel, where the higher temperatures will occur, according to the temperature map obtained previously for the halfway 2 – that means in correspondence of the highest total power deposited -: the key idea is to predict with a unique mesh with the best accuracy at least the area which can be more problematic.

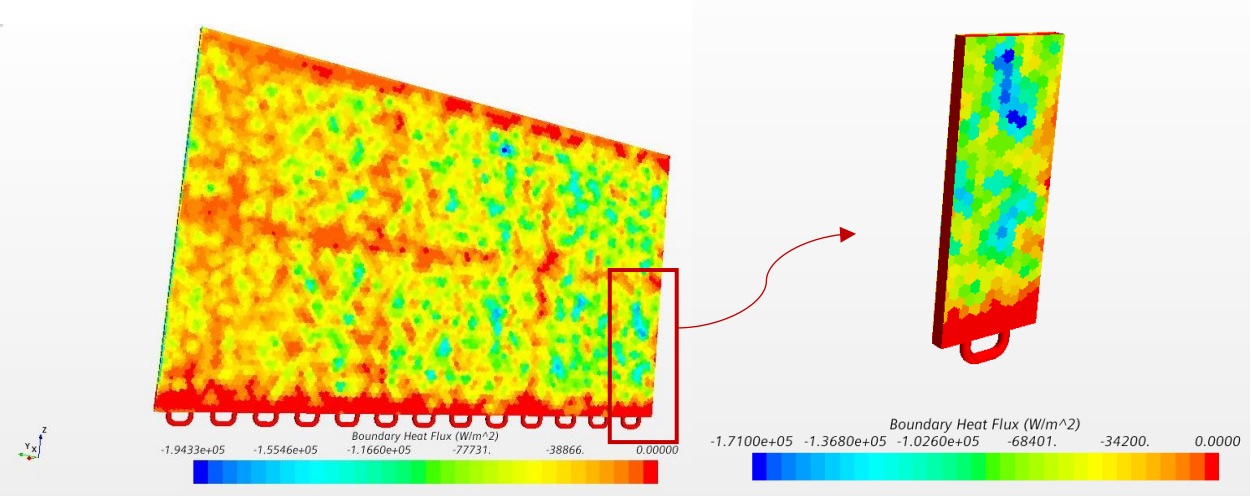


*Figure 89 Boundary heat flux for the extrapolated sample of Halfway panel 2*

Again, as before, BCs are imposed considering as inlet mass flow rate the value obtained with an extrapolation from the entire CFD model with 175 million cells (Table 33). The reference sections used, from which mass flow values are taken, with the known nomenclature, are *h2 1* and *h2 2.*

| Region | Boundary conditions fluid dynamic problem | | | | Boundary conditions thermal problem | | | |
|---|---|---|---|---|---|---|---|---|
| Inlet (h2 1) | mass flow inlet | $m_{dot}$ | 0.238 | kg/s | temperature | $T_{in}$ | 25 | °C |
| Outlet (h2 2) | pressure outlet | $p_{out}$ | 20 | bar | no conduction | | dT/dn=0 | |
| lateral surfaces | | | | | heat flux | $Q_{dot}$ | distributed | $MW/m^2$ |
| other surfaces | | | | | adiabatic | | dT/dn=0 | |

*Table 37 BCs for the sample of LEE2 analysis*

By applying the same procedure used for the sample of the LEE2, first polyhedral mesh is studied. Keeping fixed the initial prism layer with a near wall thickness of 3e-5m, a prism layer total thickness of 0.5mm and 7 prism layers, base size is iteratively varied.

More quantities are considered: pint value (i.e. maximum temperature in fluid an solid), integral value (i. e. mass flow averaged total pressure) and also value for intermediate sections (bulk temperature in section 3, which is in the middle between inlet and outlet holes).

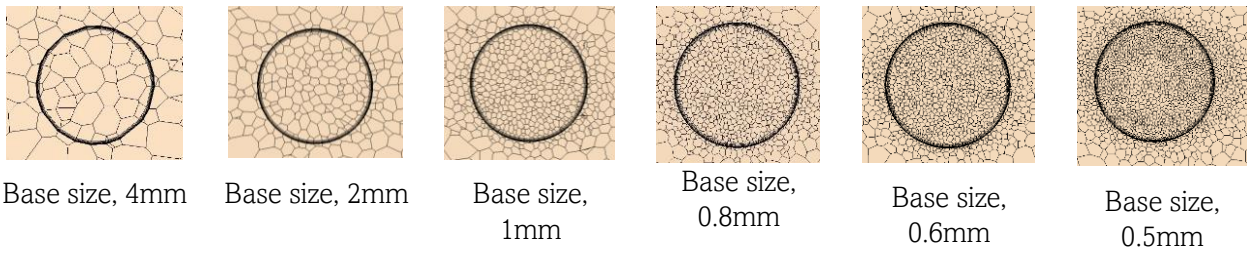

Base size, 4mm | Base size, 2mm | Base size, 1mm | Base size, 0.8mm | Base size, 0.6mm | Base size, 0.5mm

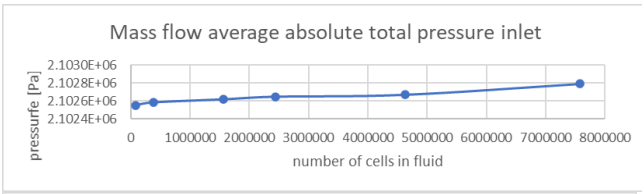


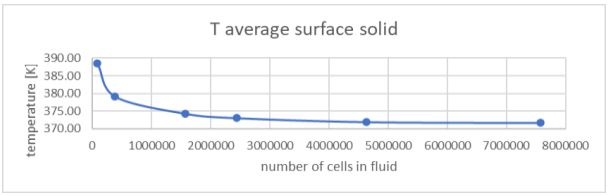


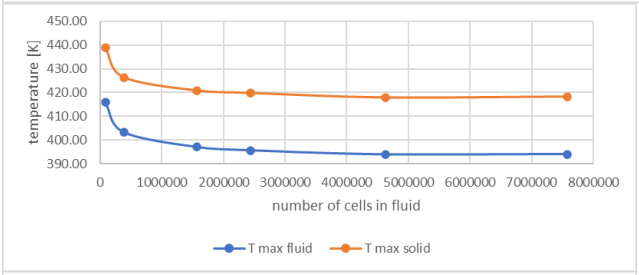


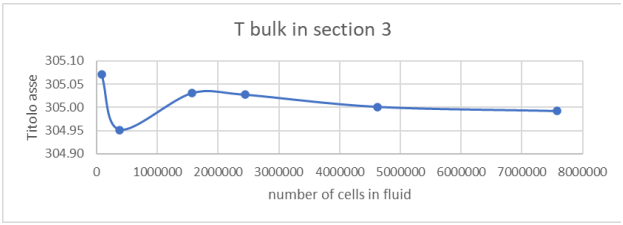


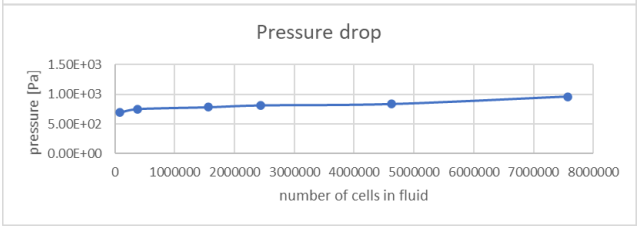


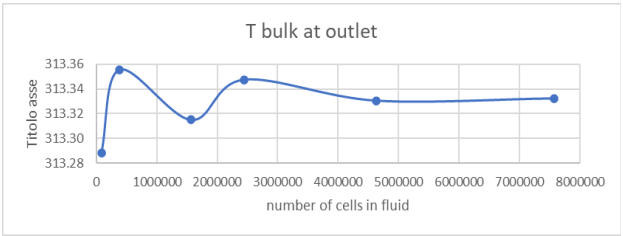


*Table 38 Halfway panel 2 sample grid independence analysis, variable polyhedral mesh: mesh considered (top), graphs (bottom)*

From this graphs, the mesh with a 1mm base size is selected. Keeping fixed the latter, prism layer parameters are varied.

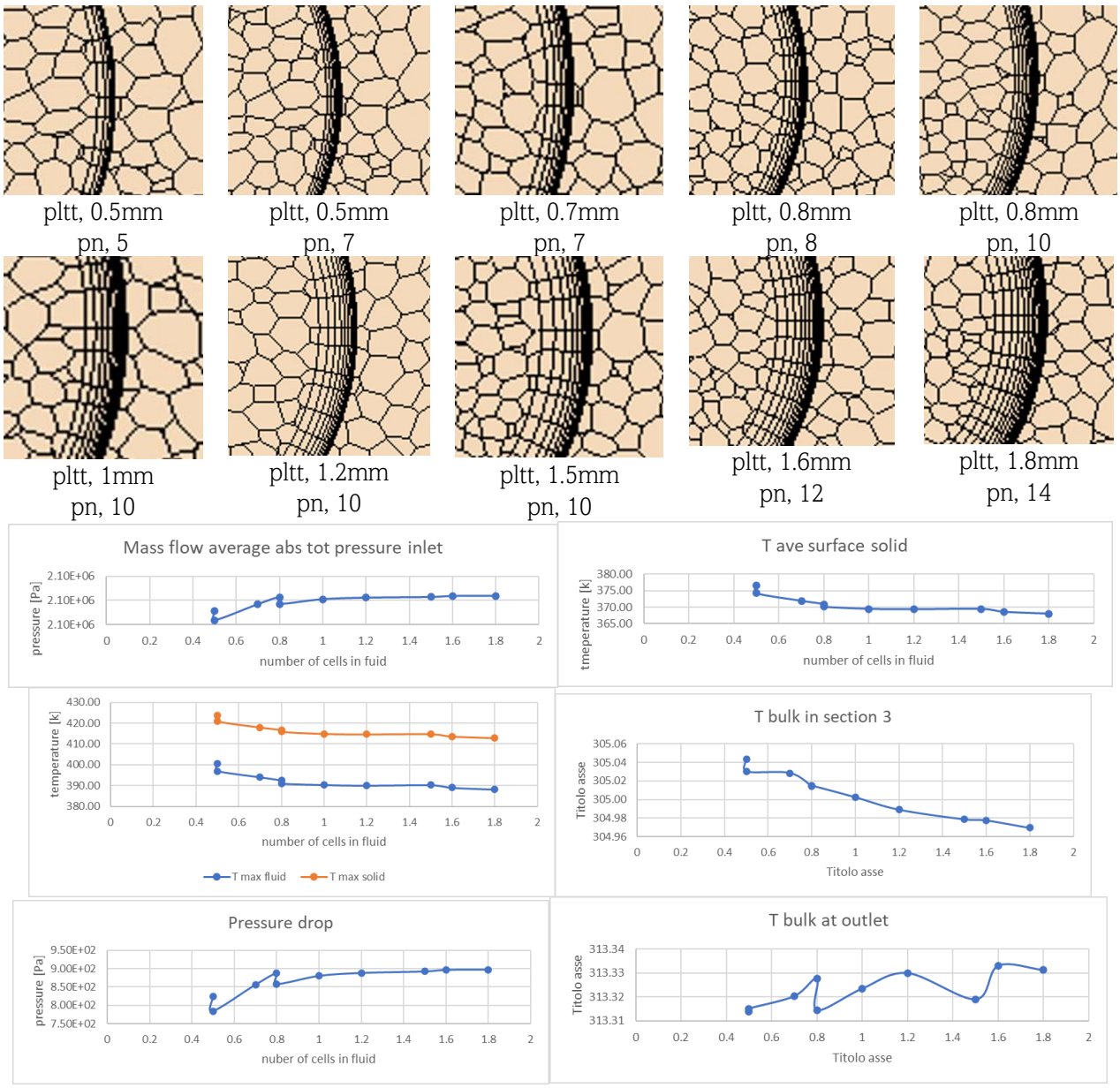


*Figure 90Halfway 2 sample grid independence analysis, variable prism layer mesh: mesh considered (top), graphs (bottom)*

In the end the final mesh selected for the halfway 2 panel is

| Mesh for the panels: results of grid independence | |
|---|---|
| prism layer near wall thickness | 3e-5m |
| prism layer total thickness | 1mm |
| number of prism layers | 10 |
| base size | 1mm |

*Table 39 Mesh for standalone halfway 2 panel sample model*

This mesh will then be adopted, with the same parameters also for the final mesh of the standalone models of the three panels analyzed.

## LEE2 standalone: CtFD final results

With the mesh parameters previously determined, the final simulation is set up[44], correcting also the expected pressure at the outlet as from the entire CFD simulation.

| Region | Boundary conditions fluid dynamic problem | | | | Boundary conditions thermal problem | | | |
|---|---|---|---|---|---|---|---|---|
| inlet | mass flow inlet | $m_{dot}$ | 1.89 | kg/s | temperature | $T_{in}$ | 25 | °C |
| outlet | pressure outlet | $p_{out}$ | 21.06 | bar | no conduction | | dT/dn=0 | |
| frontal, rear and left surface | | | | | heat flux | $Q_{dot}$ | distributed | MW/m$^2$ |
| other surfaces | | | | | adiabatic | | dT/dn=0 | |

*Table 40 BCs for standalone complete model of LEE2*

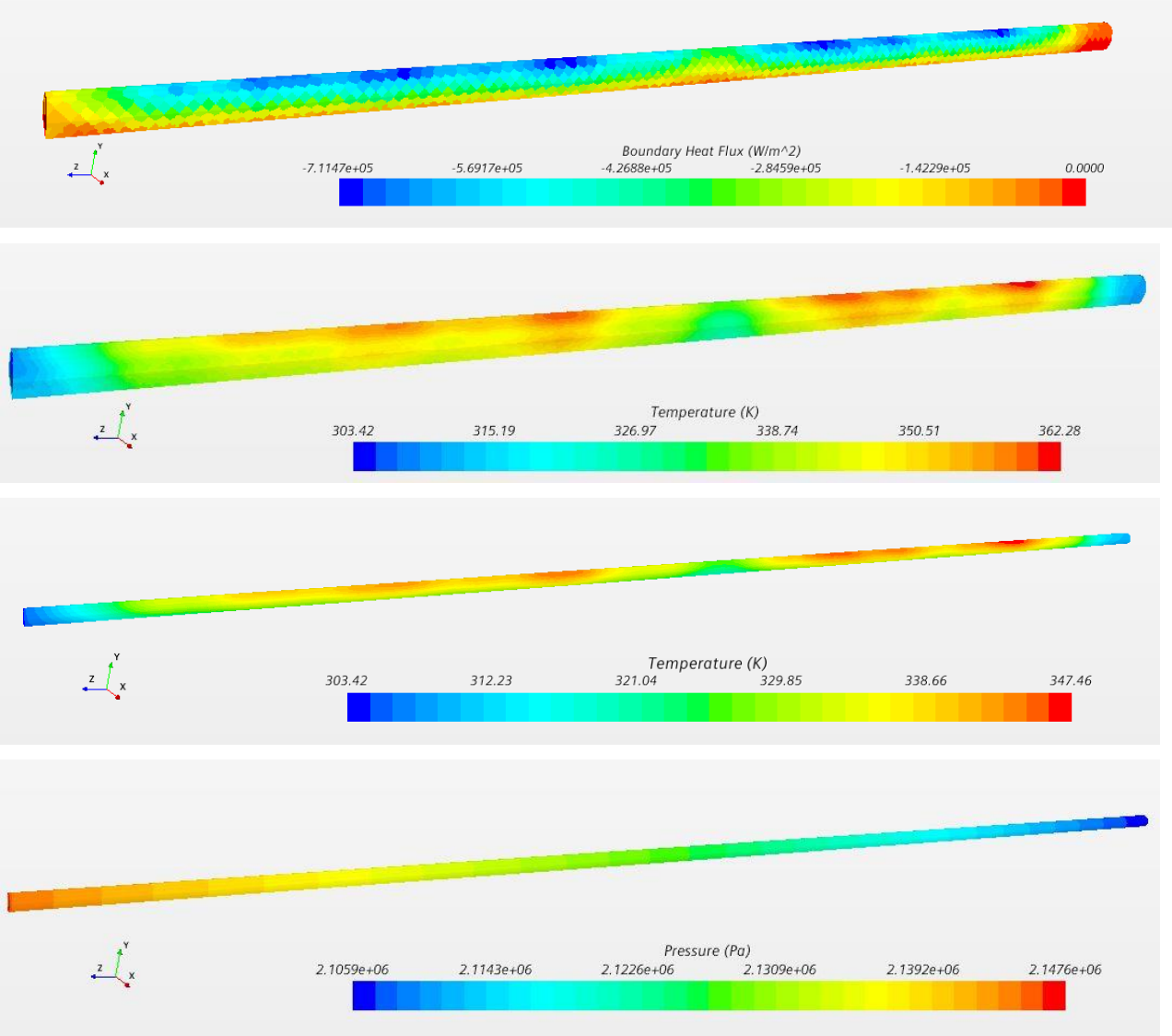


*Figure 91 LEE2, standalone results: number of total cells 4600532, number of fluid cells 3801003*

[44] Inlet and outlet sections regions of the fluid in these results (also for panels) are not considered: this is done to obtain a direct comparison (for the values of temperature) with results on the entire CtFD model developed at the end of the study.

Final results confirm that the temperature both for liquid and solid is below the limit for water saturation and property degradation of CuCrZr, respectively, with particular reference to thermal conductivity. A thermomechanical assessment must be performed to verify that the refrigeration is effectively sufficient also from a structural point of view. Numerical results will be reported directly in the successive chapters, in comparison with the entire model of the neutralizer (Table 51).

## Halfway panel 2 standalone: CtFD final results

The final CtFD detailed results that can be consider valid for the BCs, obtained from entire CFD model, indicated in Table 41 are reported in graphic form in (Figure 92, Figure 95 and Figure 96).

| Region | Boundary conditions fluid dynamic problem | | | | Boundary conditions thermal problem | | | |
|---|---|---|---|---|---|---|---|---|
| top hole 1:2:5 | mass flow inlet | $m_{dot}$ | 0.24 | kg/s | temperature | $T_{in}$ | 25 | °C |
| top hole 7:2:11 | | | 0.23 | | | | | |
| top hole 13 | | | 0.20 | | | | | |
| top hole 15 | | | 0.19 | | | | | |
| top hole 17:2:25 | | | 0.22 | | | | | |
| top hole 2:2:26 | pressure outlet | $p_{out}$ | 21.17 | bar | no conduction | | dT/dn=0 | |
| lateral surfaces | | | | | heat flux | $Q_{dot}$ | distributed | $MW/m^2$ |
| other surfaces | | | | | adiabatic | | dT/dn=0 | |

*Table 41 BCs for standalone complete model of Halfway panel 1*

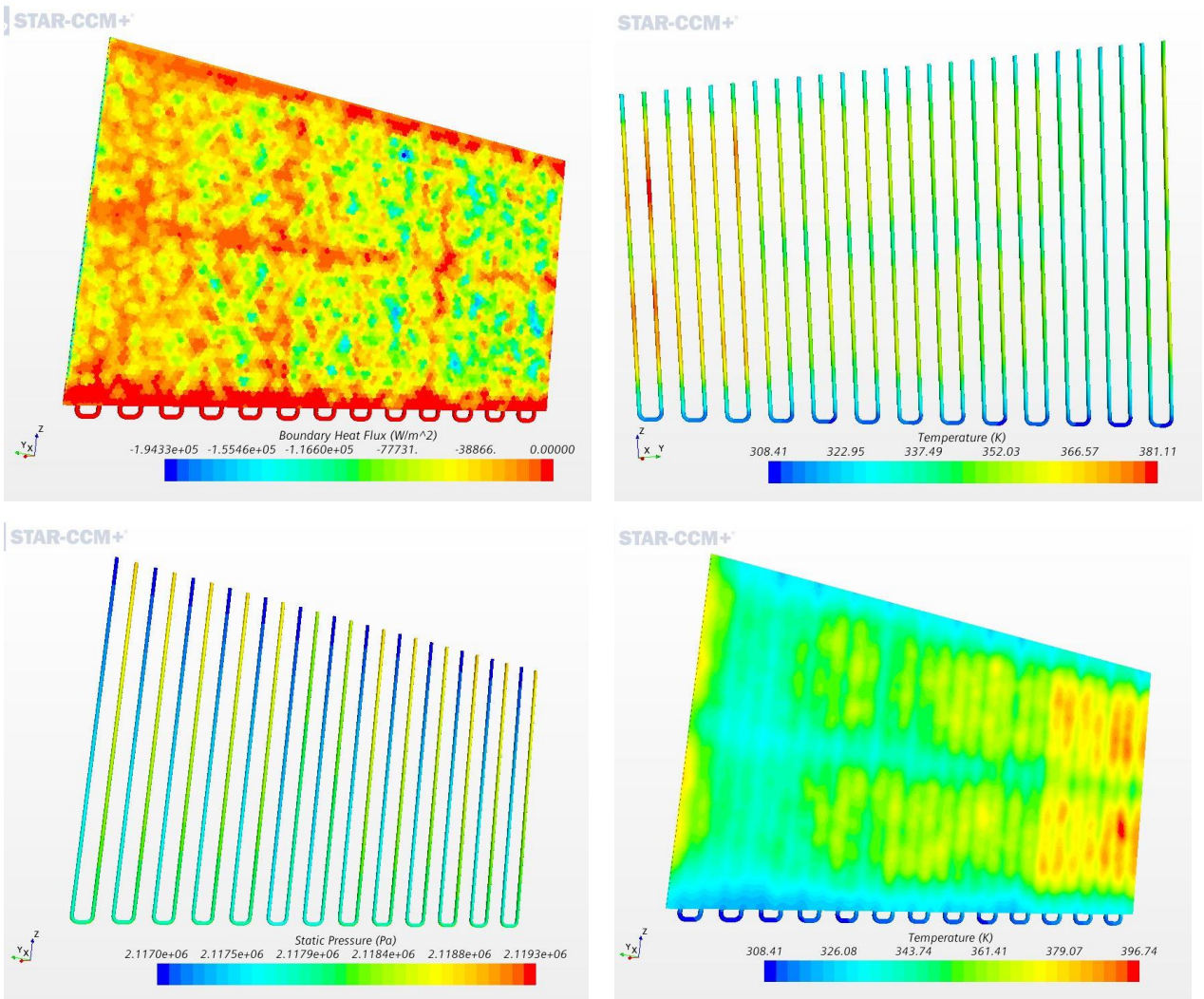


*Figure 92 Halfway 2, standalone results*

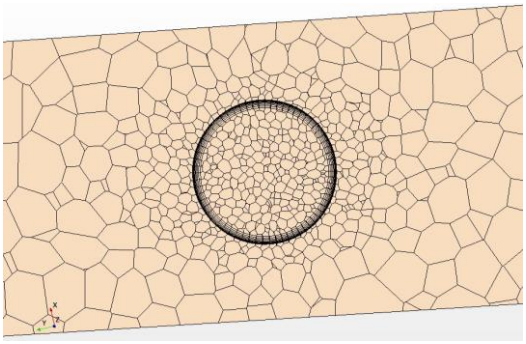

*Figure 93 Mesh used for Halfway panel 2. Total number of cells 38236436. Number of fluid cells 30708228*

## Central panel 2: standalone: CtFD final results

Similar BCs are applied also to central panel 2, where the mass flow rate inside the channels is, in general, smaller. Also in this case, each single channel has a slightly different mass flow. Pressure at outlet is derived directly from the entire CFD with 175 million cells as a sum of the static pressure difference between the value at the single outlet holes of the panel and the expected pressure outlet (as it has been done with the LEE2).

| Region | Boundary conditions fluid dynamic problem | | | | Boundary conditions thermal problem | | | |
|---|---|---|---|---|---|---|---|---|
| top hole 1:2:11 | mass flow inlet | $m_{dot}$ | 0.09 | kg/s | temperature | $T_{in}$ | 25 | °C |
| top hole 13:2:15 | | | 0.08 | | | | | |
| top hole 17:2:25 | | | 0.09 | | | | | |
| top hole 2:2:26 | pressure outlet | $p_{out}$ | 21.17 | bar | no conduction | | dT/dn=0 | |
| lateral surfaces | | | | | heat flux | $Q_{dot}$ | distributed | $MW/m^2$ |
| other surfaces | | | | | adiabatic | | dT/dn=0 | |

*Table 42 BCs for standalone complete model of Central panel 2*

The mesh uses the same parameters derived from convergence analysis for the sample of the halfway 2 panel, but, since geometry is a bit different and also top and bottom panels are considered, the total number of cells is higher with respect to the halfway.

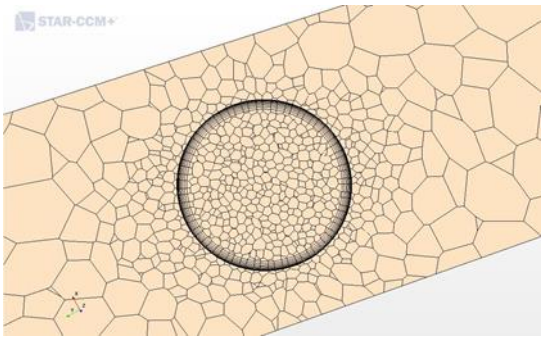

*Figure 94 Mesh used for Central panel 2. Total number of cells 67437426, number of fluid cells 55833371*

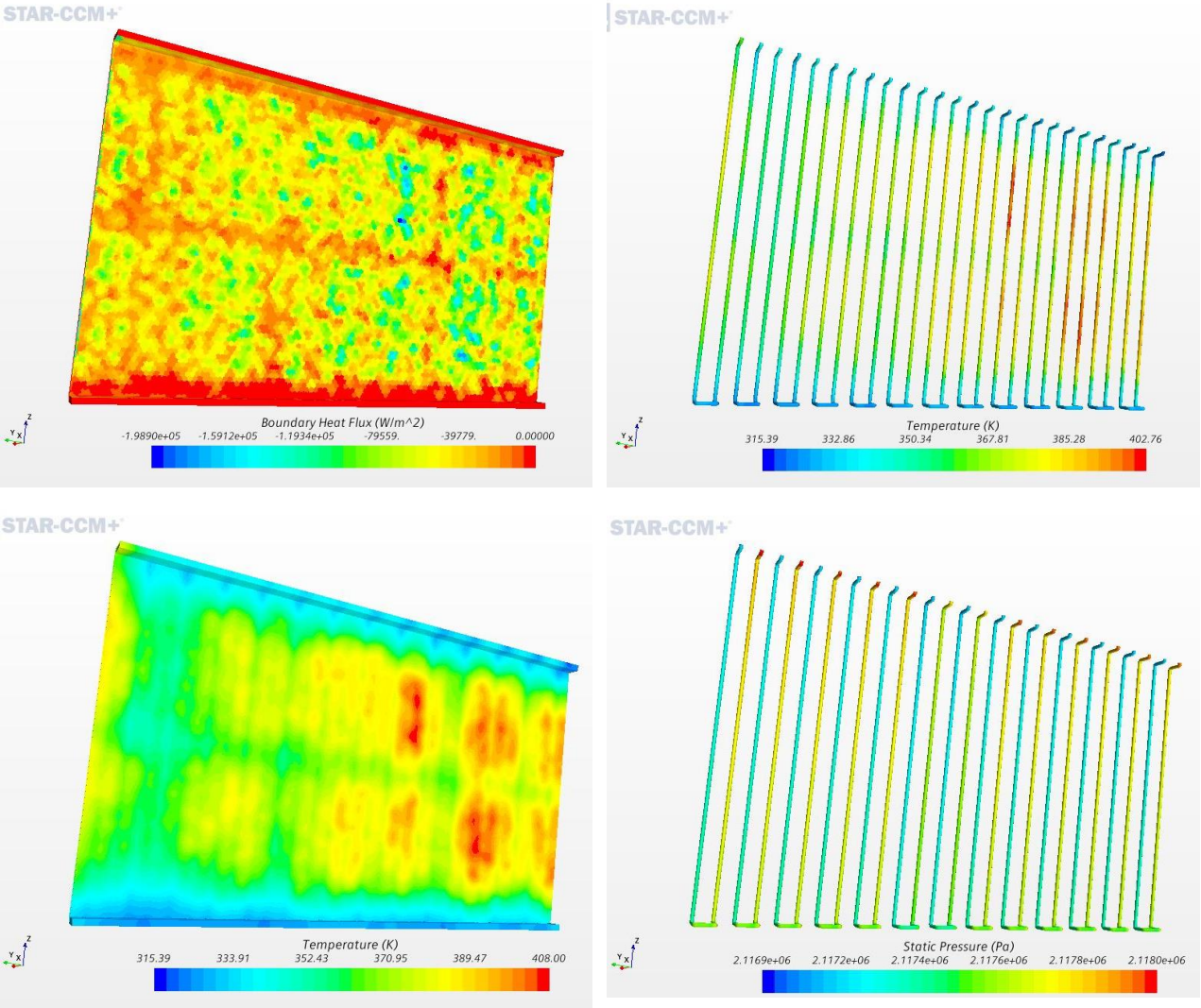


*Figure 95 Central 2, standalone results*

## Lateral panel 1: standalone: CtFD final results

As in the previous cases, the maximum temperature calculated is below the maximum limit and thermal constraints are satisfied.

| Region | Boundary conditions fluid dynamic problem | | | | Boundary conditions thermal problem | | | |
|---|---|---|---|---|---|---|---|---|
| top hole 1:2:11 | mass flow inlet | $m_{dot}$ | 0.09 | kg/s | temperature | $T_{in}$ | 25 | °C |
| top hole 13:2:15 | | | 0.08 | | | | | |
| top hole 17:2:25 | | | 0.09 | | | | | |
| top hole 2:2:26 | pressure outlet | $p_{out}$ | 21.17 | bar | no conduction | | dT/dn=0 | |
| lateral surfaces | | | | | heat flux | $Q_{dot}$ | distributed | $MW/m^2$ |
| other surfaces | | | | | adiabatic | | dT/dn=0 | |

*Table 43 BCs for standalone complete model of Lateral panel 1*

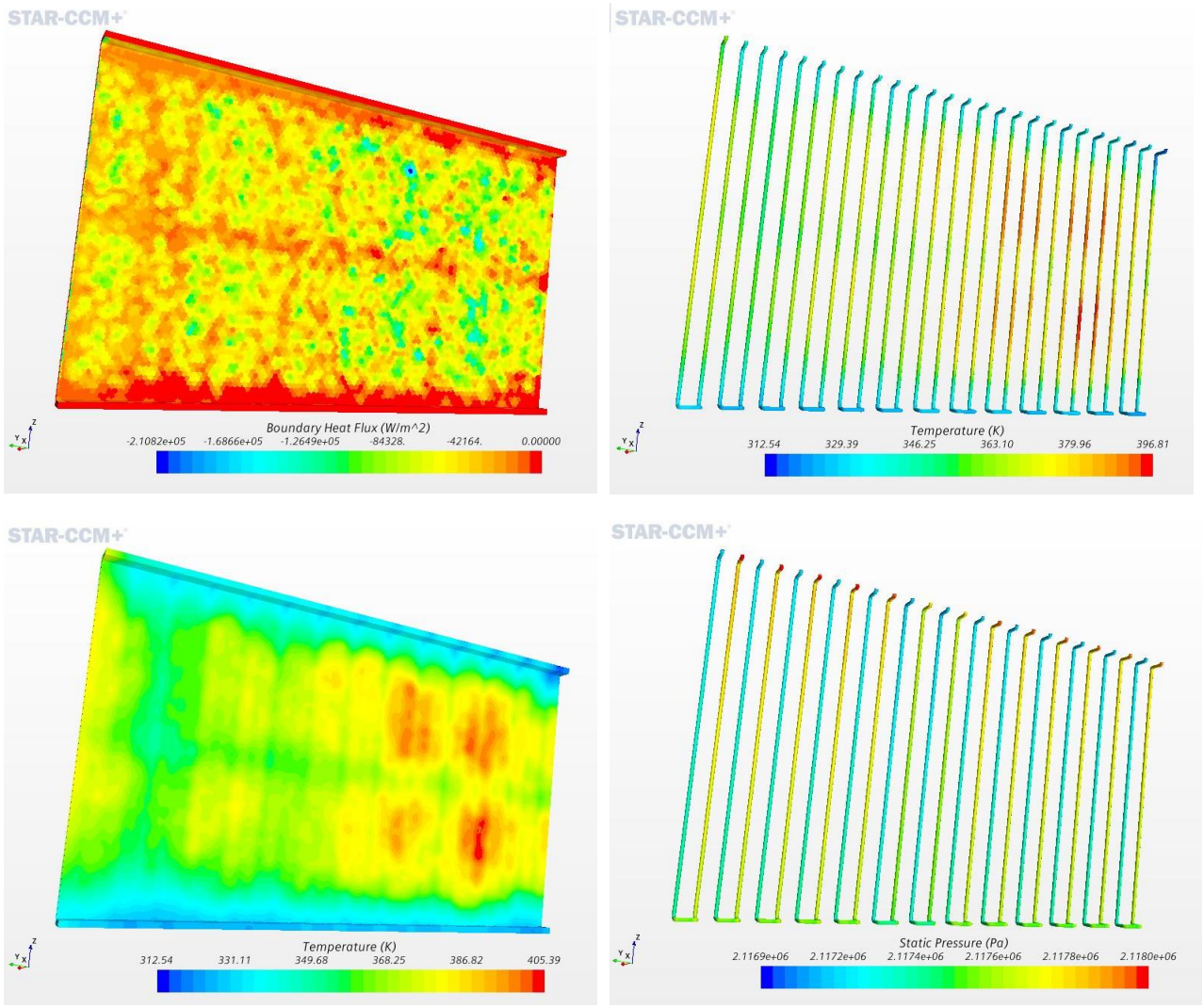


*Figure 96 Lateral 1, standalone results*

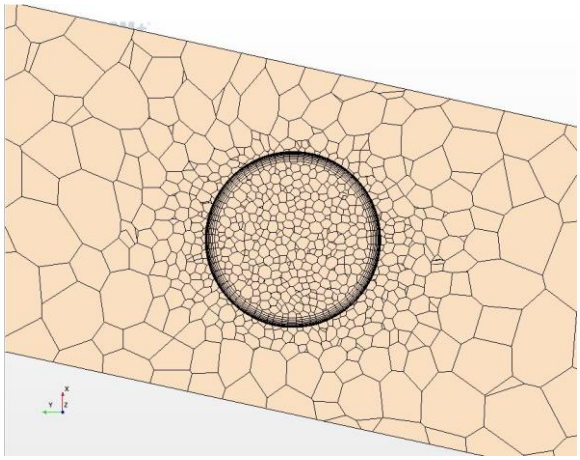

*Figure 97 Mesh used for lateral panel 1. Total number of cells: 69517528, number of fluid cells, 56439034*

Main numerical results also for all these three panels are reported directly as comparisons with the entire two models of the neutralizer[45].

[45] in the *Appendix,* Direct comparison for panels between the 3 models

## 2.2.2. Thermo-mechanical assessment of the critical components: Scenario 1

### Knowledge from the theory, models and assumptions

The geometry of a pipe can be defined by:

- $r_e$, external radius of the pipe
- $r_i$, internal radius of the pipe
- $\beta = \frac{r_i}{r_e}$, ratio of the two pipes
- $s = r_e - r_i$, thickness of the pipe

If the ratio $s/r_i$>0.1, the pipe is defined as radially thick [21]. In the entire neutralizer, the smallest thickness of the cylindrical walls is approximately 2mm, with 18mm inner diameter: this occurs also in panels. The latter have a more complex geometry, since instead of ideal cylinders, grooves are present inside the panel walls. However, if for the sake of simplicity, all the channels are modeled like constant thickness tubes, by considering the mentioned values, they can be considered radially thick and, with simplifying assumptions, some observations can be made, according to the *Lamè's* theory.

For a section of thick pipe with internal pressure, the most stressed point is at the internal edge [21]. In general, in a wedged tube, small uniform variations in temperature generate high axial stresses. However, under the hypothesis that the pipe is axially unloaded, i.e. open, free to expand and subject to internal pressure $p_i$, in this case, for a radially thick pipe

$$\sigma_z = 0 \tag{2.8}$$

$$\sigma_r = -p_i \tag{2.9}$$

$$\sigma_c = p_i \frac{1+\beta^2}{1-\beta^2} \tag{2.10}$$

where $\sigma_z$, $\sigma_r$ and $\sigma_c$ are the axial, radial and circumferential tensions respectively. For ductile materials, with the Von Mises hypothesis, in general, the equivalent ideal tension is

$$\sigma_{id} = \frac{1}{\sqrt{2}}\sqrt{(\sigma_c - \sigma_r)^2 + (\sigma_c - \sigma_z)^2 + (\sigma_r - \sigma_z)^2} \tag{2.11}$$

In this case, if 22bar are considered as internal pressure, it becomes (with the assumptions made on geometry),

$$\sigma_{id} = \frac{1}{\sqrt{2}}\sqrt{(\sigma_c - \sigma_r)^2 - \sigma_c\sigma_r} = p_i \frac{\sqrt{3+\beta^4}}{1-\beta^2} \approx 12MPa \tag{2.12}$$

This means that, as a preliminary observation, by considering *only* the internal pressure, in an ideal case, without the contribution of thermal load and other constraints, the equivalent tension due to internal pressure should have a minority effect on the total stress of the components with respect to the thermal heat load. Therefore, in this context only thermal stress will be considered without any additional load (no weight etc.).

To analyze the thermomechanical effect of the load and the performance of the refrigeration system, the finite element method (FEM) analysis is applied with StarCCM+. The main hypotheses are:

- static analysis
- isotropic linear elasticity
- isotropic thermal expansion
- own weight of components neglected
- no contact interaction between solid and fluid (only solid and thermal field developed are considered)
- isostatic structure

The materials properties considered for all the thermomechanical analysis are the thermal expansion coefficient, the zero thermal strain reference temperature, the Poisson's ratio and the Young modulus defined

in Table 25. Density value is not relevant since no weight contribution is considered and, therefore, mass matrix has no meaning in this context.

The thermal stress model, defined according to the previous hypothesis, is described in Table 44.

| CuCrZr Stress Model |
|---|
| Solution interpolation |
| Specified temperature load |
| Material law models |
| Solid stress |
| Solid |
| Steady |
| Three dimensional |

*Table 44 Solid stress model for FEM analysis*

The meshes used for the analysis are generated with tetrahedral elements for all the components. Mid-side nodes are added to tet4 elements to obtain quadratic tet10 elements and improve accuracy.

Since real constraints are not know, as a hypothesis, the structure is assumed to be free to expand upwards (in the positive direction of the z axis) as it were resting on a support with some gears. Three scenarios are analyzed:

- Scenario 1: isolated components with panels free to expand upwards
- Scenario 2: panels welded to each other free to expand upwards and LEEs screwed to the panels
- Scenario 3: panels and LEEs welded to each other, free to expand upwards

Von Mises stress and displacements will be used as main parameters of interest in FEA. Displacements, in particular, are graphically shown with a scale factor 30, to better visualize also the qualitative effect of the deformations.

## FEM: mesh convergence for LEE2 from standalone results

In this first scenario, the LEEs are screwed to the panels and each vertical panel is welded with the respective top and bottom panel, but free to expand with respect to all the other adjacent components. All the FEM analysis for standalone components of Scenario 1 will be performed using in input the temperature field obtained in the simulation described in *2.2.1. Standalone components CtFD verification*, which are the components in the realistic conditions analyzed with high accuracy of results.

Mesh convergence study is performed to validate FEM results on the LEE2.

First, constraints for the model must be defined. To properly consider only thermomechanical effects, constraints cannot be too restrictive, otherwise they would lead to unrealistic stress concentrations. To prevent rigid body motion and allow free expansion of the solid structure, three points are selected where constraints are applied, that is where and in which direction displacements are locked.

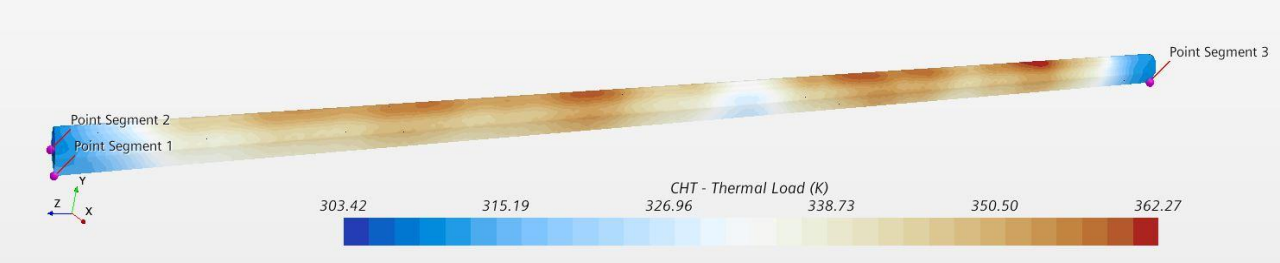


*Figure 98 LEE2: thermal heat load applied for thermal stress analysis and constraints*

For the LEE2 case (and for all the LEEs) it is assumed that it could expand downwards with an appropriate fastening system. It is also assumed that it cannot detach from the panel to which it is bound.

| Point | Constraint |
|---|---|
| Point Segment 1 | X, Y, Z |
| Point Segment 2 | Y, Z |
| Point Segment 3 | Y |

*Table 45 LEE2 constraints: locked displacement directions*

To test the constraint set -as are imposed in Figure 98-, a uniform thermal distribution of 650 K is applied. If the constraints are realistic, which means that the body is free to expand, with such a load, stress levels must be close to zero.

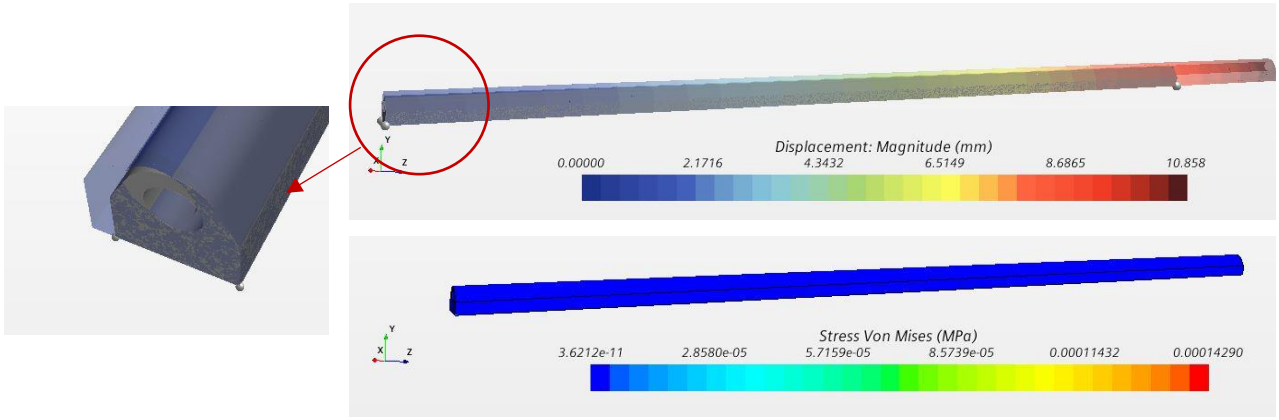


*Figure 99 LEE2: constraints test, 650K uniformly applied to the entire solid surface. Displacement is shown with a scale factor 30.*

As it can be seen from Figure 99, stress levels are close to zero with the uniform heat load, so the constraints are realistic and should provide correct value of stress even with a not uniform load.

In this case, the temperature field computed in the CtFD analysis from Figure 91 is used: in this kind of simulations, temperature data are actually available on the conjugate heat transfer analysis of the finite volume (FV) mesh. To perform a finite element analysis, this field must be mapped, interpolated and transferred to the finite element (FE) mesh. The result for the LEE2 is the thermal load in Figure 98.

Several simulations are run for the LEE2, by varying the FE base size of the mesh (Figure 100).

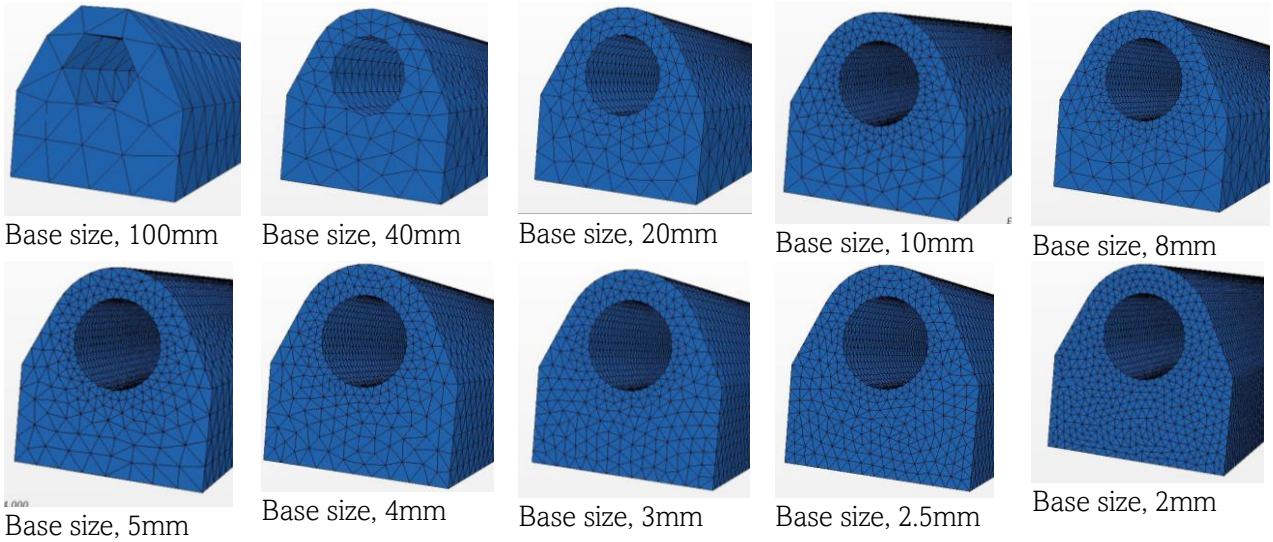


*Figure 100 Mesh convergence FEM for LEE2*

The final selected mesh has a base size of 2.5mm. The computed maximum displacement has a variation of ~0.01mm: this level of accuracy is not realistic and can be substantially considered a flat curve (Figure 101). Von Mises stress has an asymptotic trend, so that also a 20mm base size can predict the stress value accurately. Numerical values are reported also in Table 46 FEM: mesh convergence analysis for LEE2

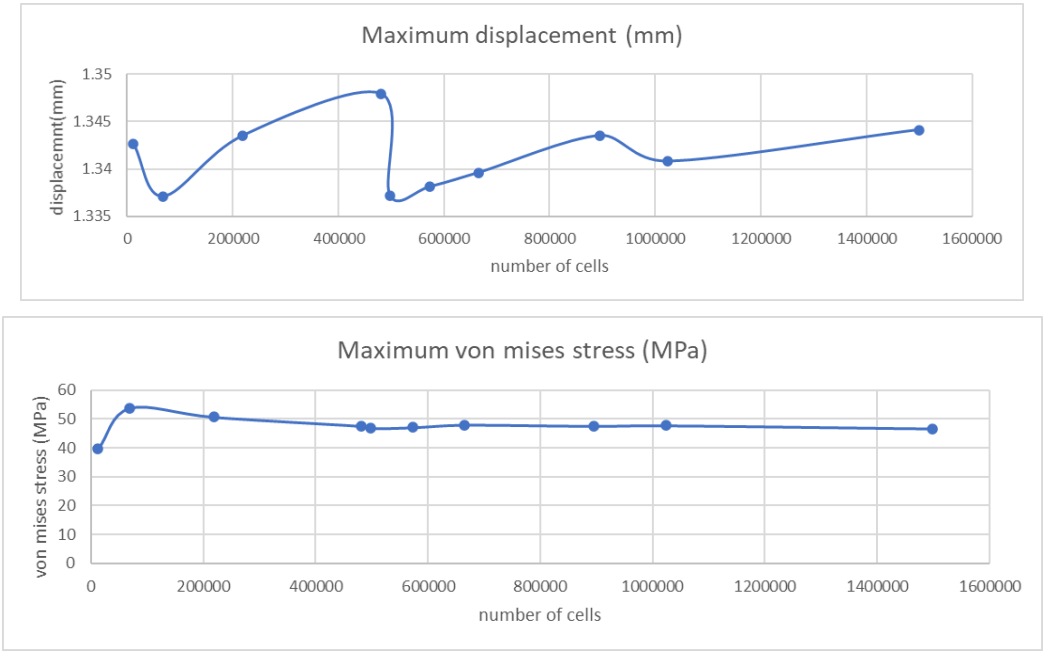


*Figure 101 FEM: mesh convergence analysis for LEE2. Maximum displacement and maximum Von Mises Stress*

| base size | number of cells | Maximum displacement | Maximum Stress (Von Mises) |
|---|---|---|---|
| 100mm | 11802 | 1.3426 | 39.631 |
| 40mm | 68091 | 1.3371 | 53.715 |
| 20mm | 219045 | 1.3435 | 50.592 |
| 10mm | 480242 | 1.3479 | 47.523 |
| 8mm | 497261 | 1.3372 | 46.662 |
| 5mm | 572202 | 1.3381 | 46.974 |
| 4mm | 665566 | 1.3396 | 47.888 |
| 3mm | 895875 | 1.3435 | 47.509 |
| 2.5mm | 1023520 | 1.3408 | 47.658 |
| 2mm | 1498943 | 1.3441 | 46.616 |

*Table 46 FEM: mesh convergence analysis for LEE2*

## LEE2

Final results for the LEE2 are reported in Figure 102 and they are obtained from convergence analysis with the mesh with a 2.5mm base size.

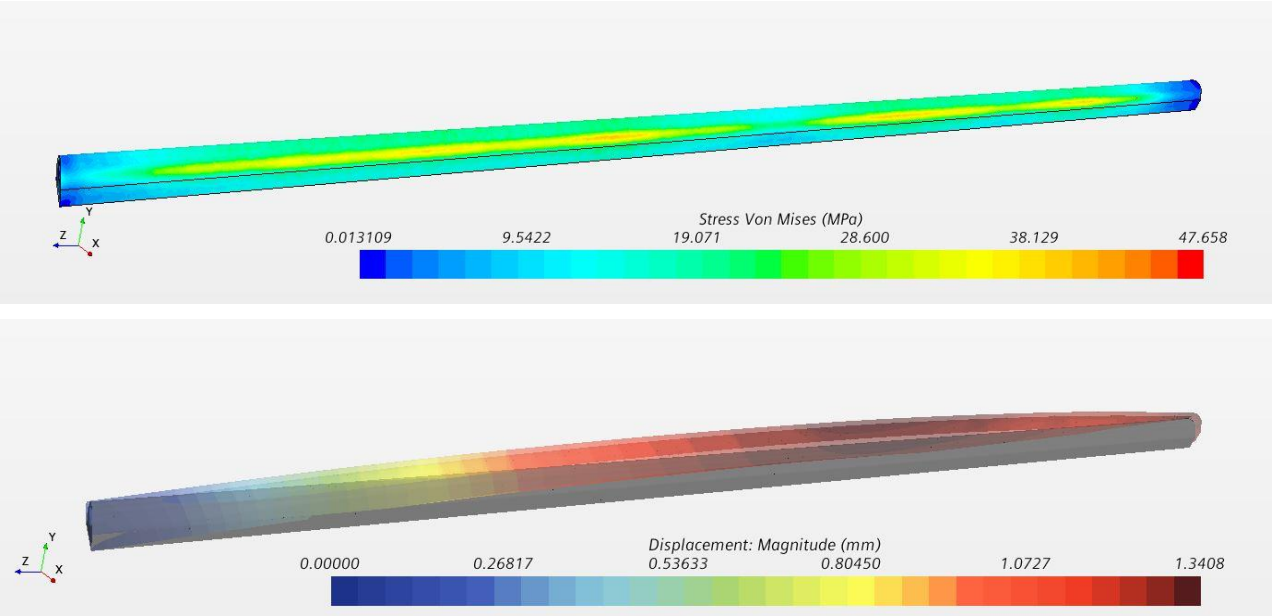


*Figure 102 LEE2: Von Mises stress and Displacement. Displacement is shown with a scale factor 30.*

The computed maximum stress and displacement are

$$\sigma_{max} = 48\ MPa$$

$$displacement_{max} = 1.34mm$$

Since the thermal distribution shows a higher temperature on the frontal surface, even if it is not a uniform distribution, it is similar to the known literature case of a beam subjected to temperature gradient over the depth. The expected effect is that of a bending deflection due to the almost linear variation[46] of tension through the depth. The specific case of the LEE is different, since temperature has not a clear and uniform distribution, but the main concept of flexural behavior is confirmed and the bending deflection occurs in the direction of the highest temperature.

## Halfway panel 2

No grid independence is performed for the panels: the finest FE mesh that can be obtained in StarCCM+ has been chosen for all the models.

Constraints are imposed as in Table 47. In this way the panel can expand upward and in the direction of the ion dump to avoid any approaches to the ion source.

| Point | Constraint |
|---|---|
| Point Segment 1 | X, Y, Z |
| Point Segment 2 | Y, Z |
| Point Segment 3 | Z |

*Table 47 Halfway 2 constraints: locked displacement directions*

By following the same procedure of the LEE2, panels are tested by applying a uniform temperature distribution of 650K. Since Von Mises stress are very low, the constraints are realistic and can predict correctly thermal stress also with the computed temperature distribution.

[46] *thermal butterfly distribution* of the strain diagram

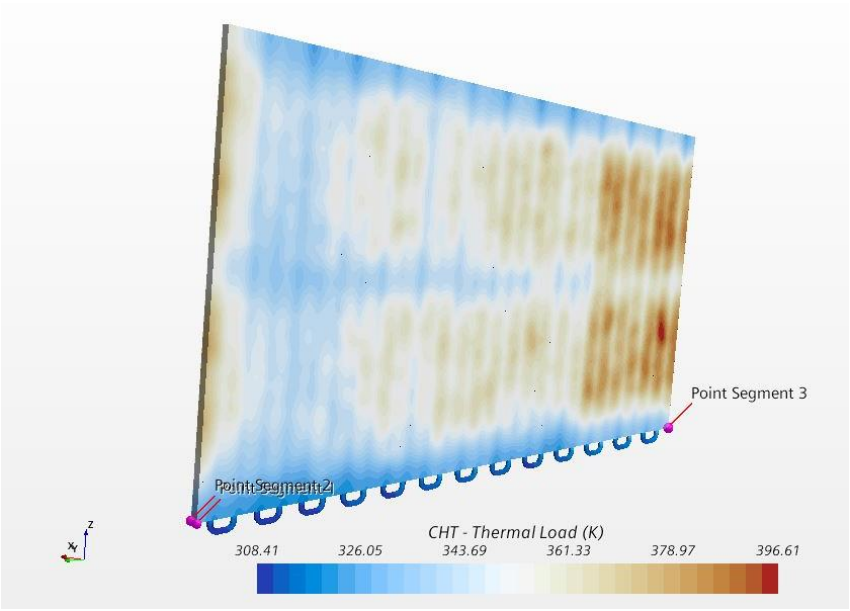


*Figure 103 Halfway 2: thermal heat load applied for thermal stress analysis and constraints*

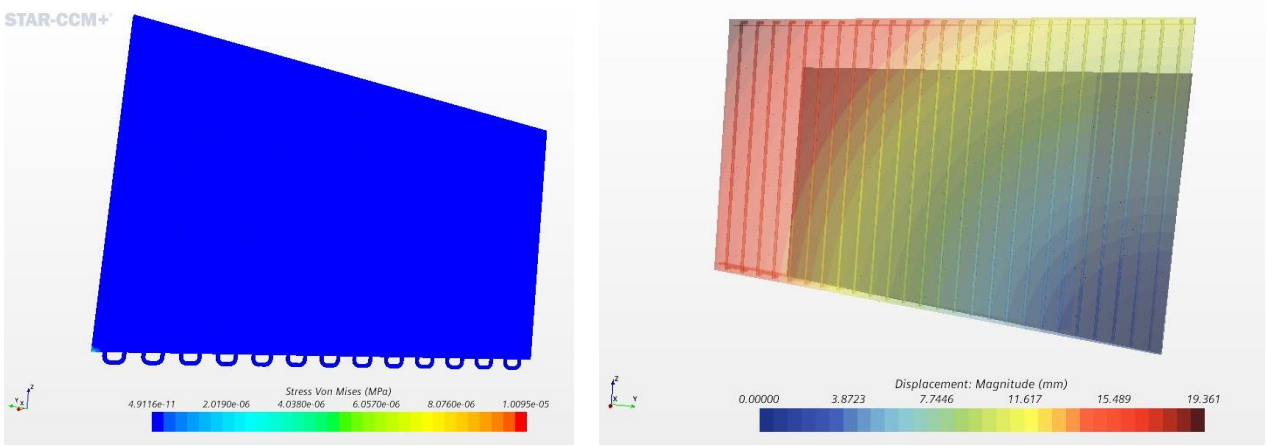


*Figure 104 Halfway 2: constraints test with uniform thermal distribution of 650K*

By prescribing the heat load from the real distribution of temperature on the solid, the computed maximum values for displacement and stress are

$$\sigma_{max} = 230MPa$$

$$displacement_{max} = 3.16mm$$

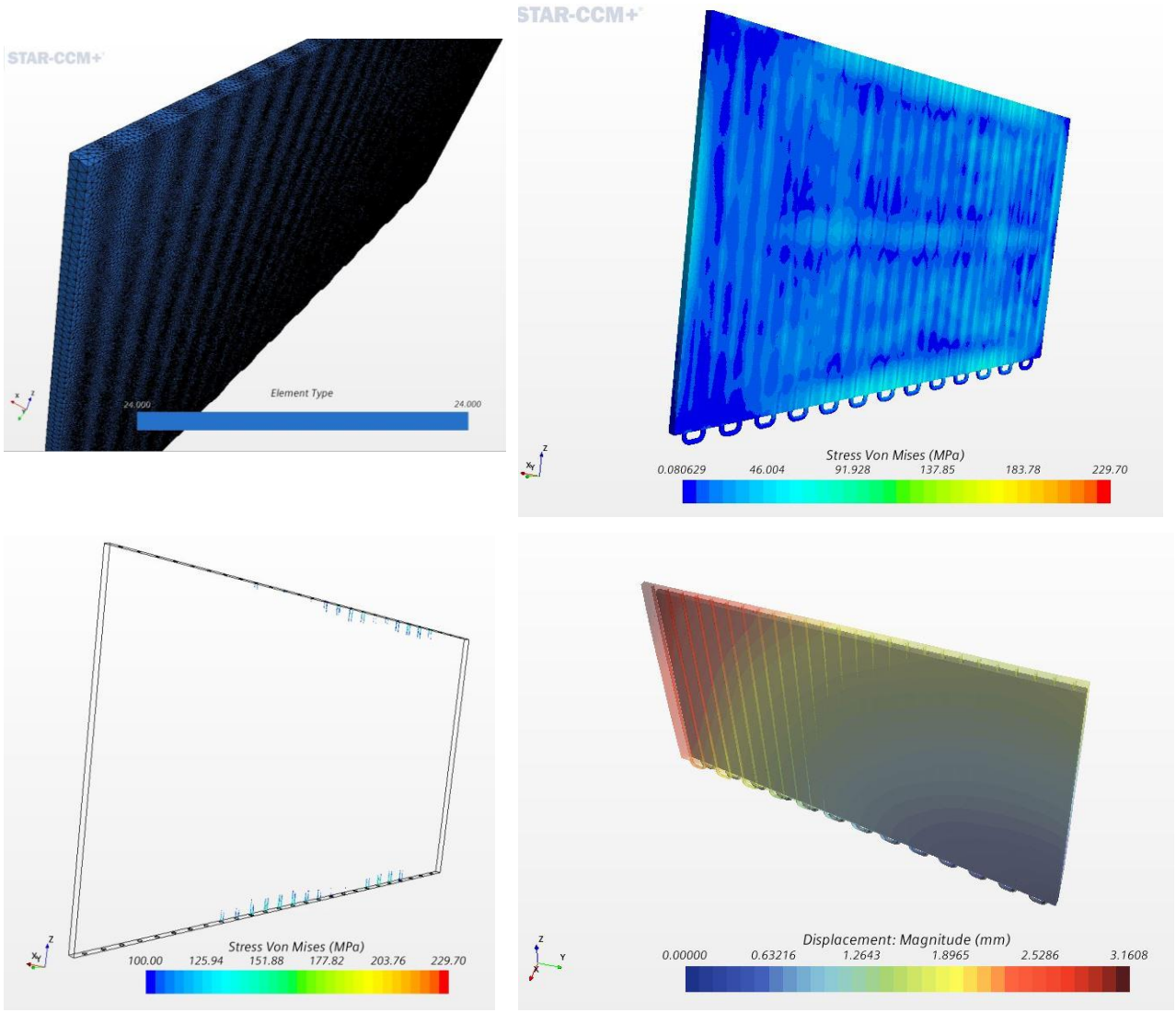


*Figure 105 Halfway 2, standalone FEM results. Mesh, 1578535 cells*

The peak of Von Mises stress is located on the external surface of the panel and, in general, higher stresses, above 100MPa, are located only on limited areas at the extremities.

For the halfway panels, the heat flux is deposited on both the two lateral surfaces. This results in a lower temperature gradient, if compared to the other typologies of panels (central and lateral), and so the deflection is relatively contained, with respect to the other two panels of the same block.

## Central panel 2

Constraints are imposed as in Table 47 and they are checked to confirm the zero stress field with a constant temperature load of 650K.

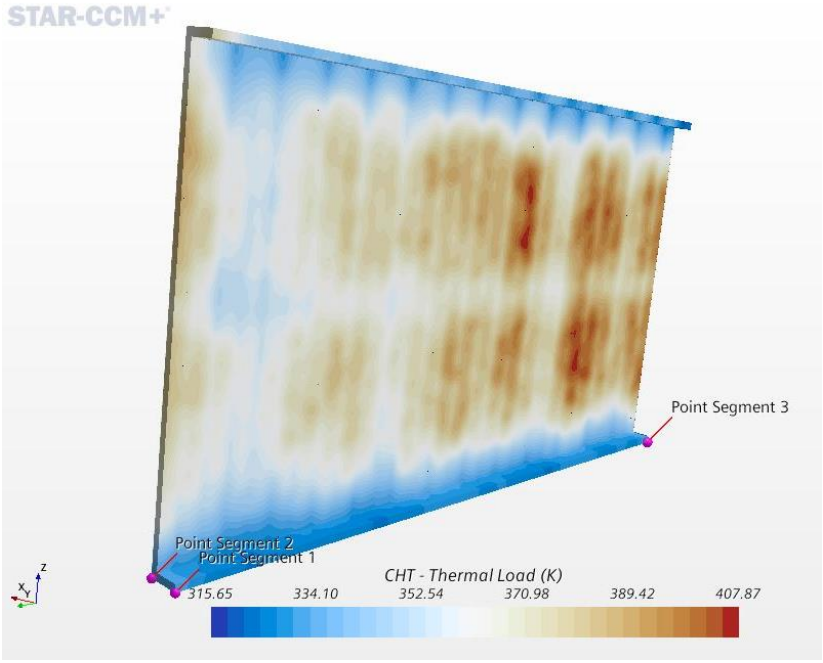


*Figure 106 Central 2: thermal heat load applied for thermal stress analysis and constraints*

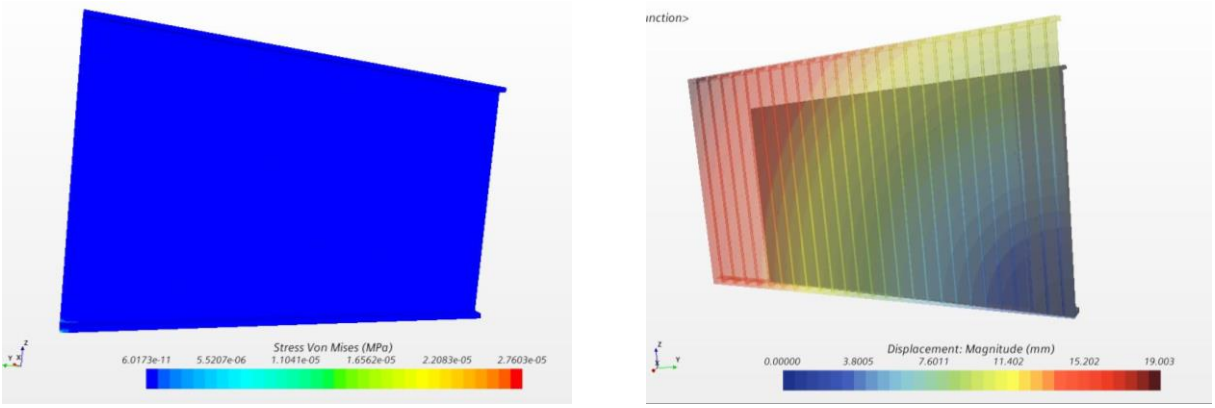


*Figure 107 Central 2: constraint test with uniform thermal distribution of 650K*

By prescribing the heat load from the real temperature distribution on the solid, the computed maximum values of displacement and stress are

$$\sigma_{max} = 276MPa$$

$$displacement_{max} = 11.77mm$$

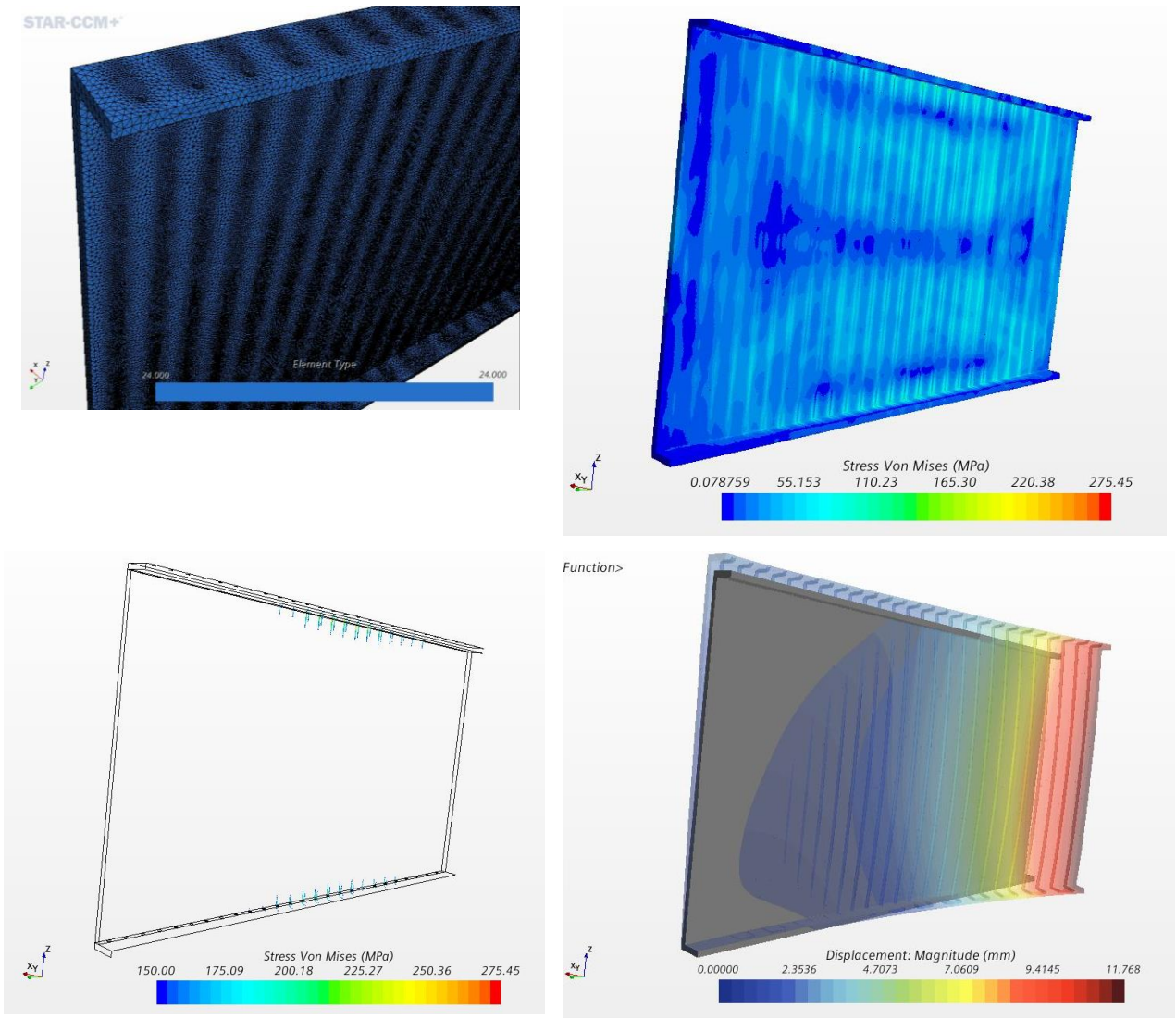


*Figure 108 Central 2, standalone FEM results*

The peaks of Von Mises stress are located on the surface and higher stresses are mainly presents on the top and on the bottom panel junctions. In general, in almost all the panel, tensions are below 150MPa.

In the central panels, the boundary heat flux is applied only on a side of the panel (the inner surfaces of the neutralizer which are directly exposed to the deuterium beam). This causes, especially in the farthest area from the ion source, a temperature difference between the two lateral sides of the central panels which is more evident if compared to the halfways, resulting in a higher inflection in the direction of the inner part of the block.

## Lateral panel 1

Constraints are imposed as in Table 47.

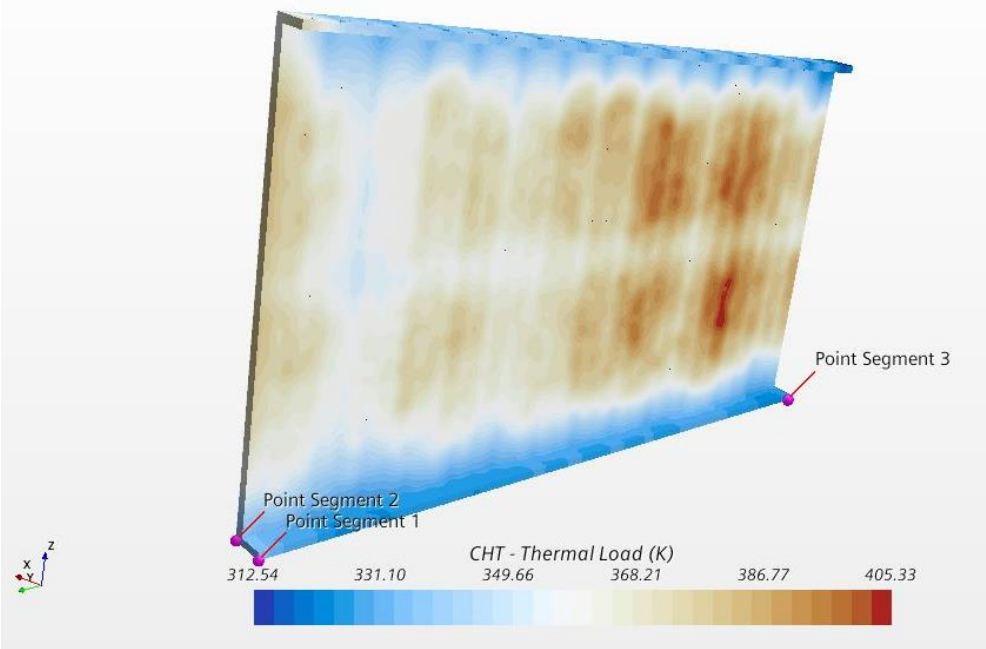


*Figure 109 Lateral 1: thermal heat load applied for thermal stress analysis and constraints*

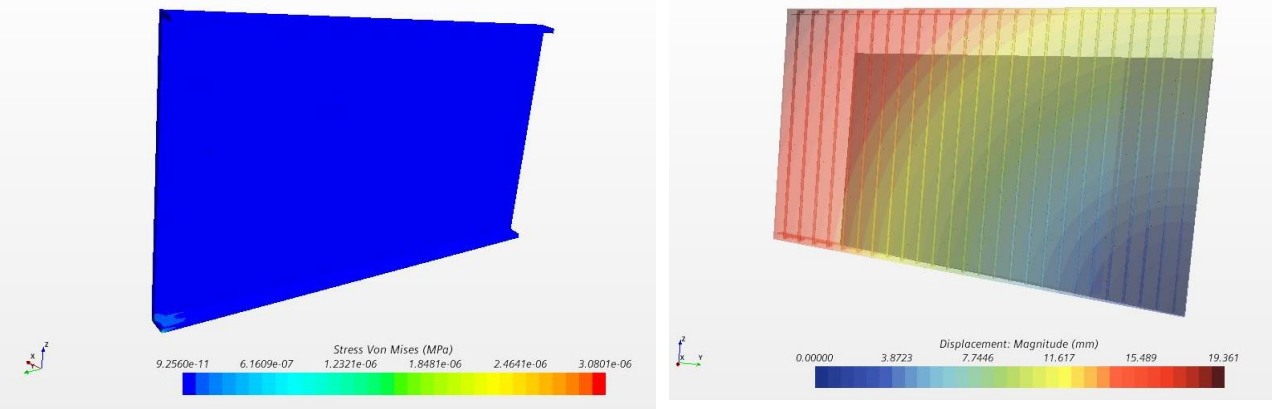


*Figure 110 Lateral 1: constraint test with uniform thermal distribution of 650K*

By prescribing the heat load from the real temperature distribution on the solid, the computed maximum values of displacement and stress are

$$\sigma_{max} = 235MPa$$

$$displacement_{max} = 9.78mm$$

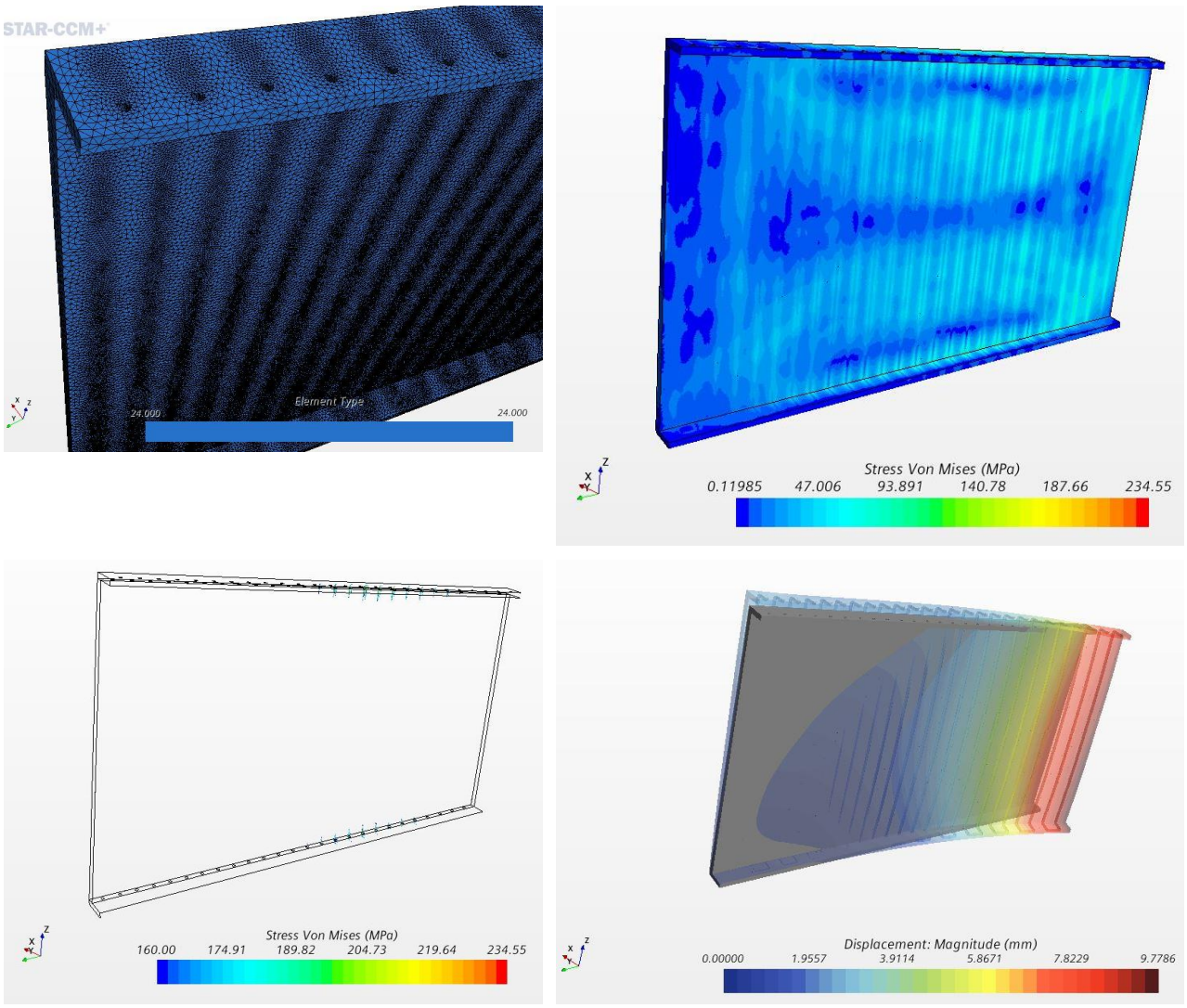


*Figure 111 Lateral 1, standalone FEM results*

Also in this case, the peaks of Von Mises stress are located on the external surface, and the highest values are limited to small areas near the top and bottom panels. In general, in almost all the panel, tensions are below 160MPa.

As discussed for the central 2, the boundary heat flux is applied only on the inner largest side directly exposed to the deuterium beam. The temperature difference between the two lateral sides, in this case, is lower than that in the central panel, and so the deflection is similar, symmetric, but smaller. As before, the highest deformation is located far from the ion source and directed to the inner part of the block.

## Conclusions

From [11], CuCrZr-IG is available in the A treatment in which solution annealing, cold work and ageing are applied. With this material, at a temperature of 423K, the minimum yield strength values is 365MPa. This means that all the critical components are below the yield limit condition.

The following results, considering all the panels, show that, if the lateral 2 panel had a symmetrical behavior in deformations with respect to lateral 1 panel, the entire block 2 should see a sort of compensation in the total displacement. In particular, lateral 2 and halfway 2 should deform mainly in negative x-direction, while central 2 should deform mainly in positive x-direction. By applying the superposition of effects, the sum of the

deformations of the first two panels is approximately the same (and opposite) of the third one: this would result in a stiffening of the neutralizer structure, if it was considered as a unique body. This observation will lead to the Scenario 2.

## 2.2.3. Final CtFD entire model

### BCs, model and material

Materials used for this simulation are listed in Table 2. Constant properties are considered for fluid part and density, in order to reduce time required, since no relevant differences have been highlighted with the more complex model accounting for temperature-dependent properties. For the single component models, variable properties were used, since the mesh required for good accuracy was characterized by a low number of cells with respect to the entire CtFD model simulation, but in this case computational cost would increase too much without adding any useful information or detail. In this model, in fact the total number of fluid cells is 93764265, with a total number of cells of 116660027.

The boundary conditions, according to what has been discussed, have been imposed as in Table 48.

| Region | Boundary conditions fluid dynamic problem | | | | Boundary conditions thermal problem | | | |
|---|---|---|---|---|---|---|---|---|
| inlet | mass flow inlet | $m_{dot}$ | 17.7 | kg/s | temperature | $T_{in}$ | 25 | °C |
| outlet | pressure outlet | $p_{out}$ | 20.21 | bar | no conduction | | dT/dn=0 | |
| non null heat flux surface | | | | | heat flux | $Q_{dot}$ | distributed | $MW/m^2$ |
| other surfaces | | | | | adiabatic | | dT/dn=0 | |

*Table 48 BCs for the entire CtFD model*

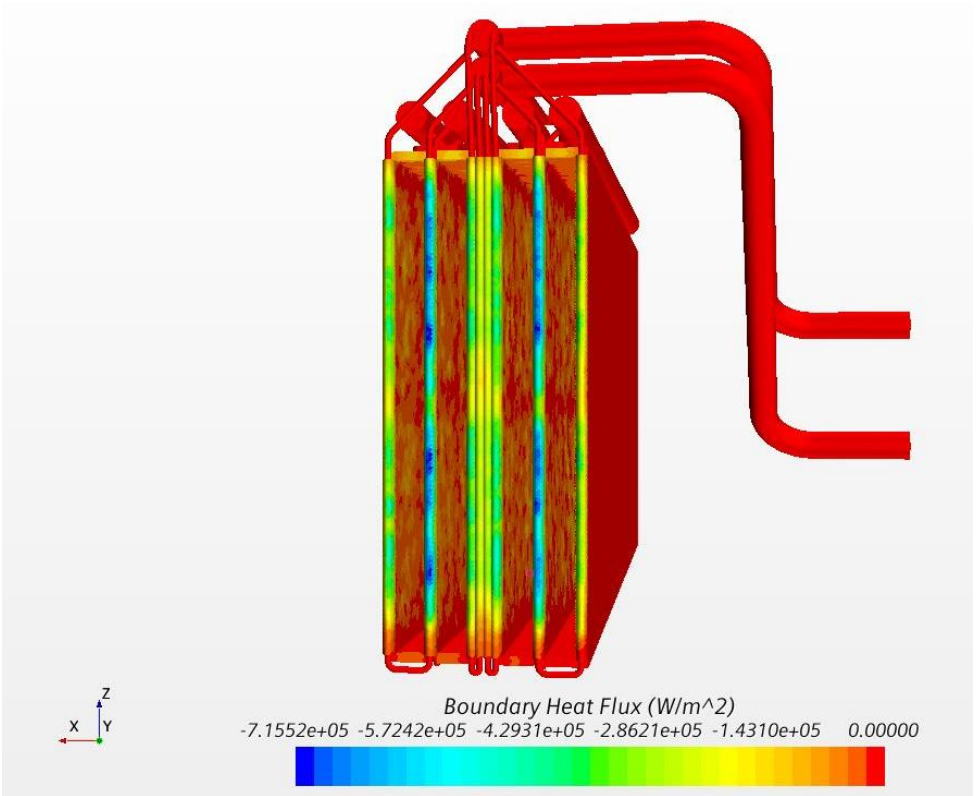


*Figure 112 Boundary heat flux applied on the entire neutralizer: only electrons and deuterium contribution*

The main stopping criteria imposed for both CFD and CtFD analyses are that the percentage errors between the total IO pressure drop and the sums of the pressure drops between the two branches in parallel (to the LEEs and to the panels) must be less than 2% and stable (asymptotic criterion). A minimum number of iterations to ensure that the residuals are stable is also needed.

## Mesh


*Figure 113 Mesh for CtFD, 94 million cells in fluid. From left to right: manifold, distributor, part of horizontal section, LEEs (top right), panels (bottom right)*

## Fluid dynamic results

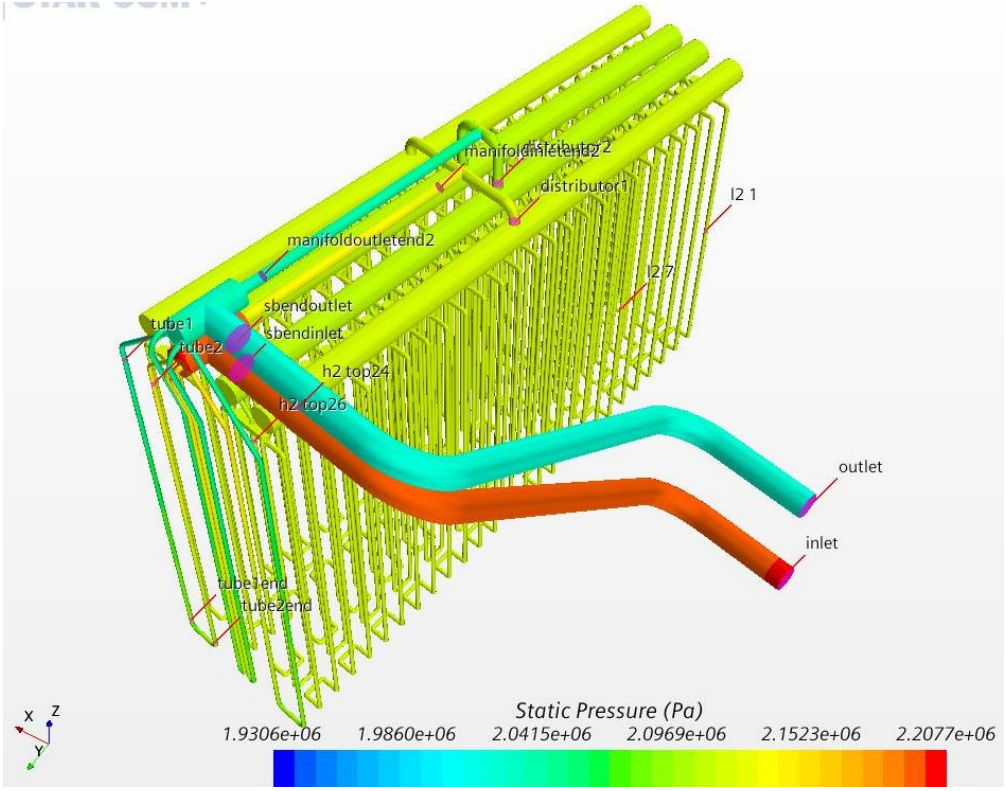


*Figure 114 CtFD pressure distribution for neutralizer, 94 million cells in fluid, 17.7kg/s at inlet, 20.21bar pressure at outlet*

| STATIC PRESSURE DIFFERENCES (bar) | | |
|---|---|---|
| inlet-sbendinlet | 0.01 | **Parallel circuit to the panels** |
| sbendinlet-manifoldinletend2 | 0.70 | |
| manifoldinletend2-distributor1 | 0.12 | |
| distributor1-distributor2 | 0.23 | |
| distributor2-manifoldoutletend2 | 0.58 | |
| manifoldoutletend2-sbendoutlet | 0.13 | |
| sbendoutlet-outlet | 0.01 | |
| sbendinlet-tube2 | 0.57 | **Parallel circuit to the LEEs** |
| tube2-tube1 | 0.93 | |
| tube1-sbendoutlet | 0.26 | |
| | | |
| sum of pressure differences from parallel circuit to the panels | 1.78 | |
| sum of pressure differences from parallel circuit to the LEEs | 1.78 | |
| **pressure drop IO** | **1.78** | |
| MASS FLOWS (kg/s) | | |
| mass flow inlet | 17.70 | |
| minimum mass flow to the LEEs (tube 3, 4, 5 and 6) | 1.80 | They vary between 1.78 and 1.91 kg/s |
| minimum mass flow for a single channel of halfway 2 (h2 13 and h2 15) | 0.18 | They vary between 0.19 and 0.24 kg/s |
| minimum mass flow for a single channel of lateral 1 (l1 13 and l1 15) | 0.08 | They vary between 0.08 and 0.09 kg/s |
| minimum mass flow for a single channel of central 2 (c2 13 and c2 15) | 0.09 | They vary between 0.08 and 0.09 kg/s |

*Table 49 Static pressure differences and mass flows from CtFD simulation of the entire neutralizer with 17.7kg/s*

Pressure at the outlet of each LEE is above 20bar, as desired. Each mass flow satisfies the minimum values calculated to avoid boiling. The model is coherent with the finest CFD one, with 175 million cells in fluid. From each LEE, in fact:

| | Mass Flows (kg/s) | Static Pressure (Surface Averaged) (Pa) | Absolute total pressure (mass flow averaged) (Pa) | Bulk temperature |
|---|---|---|---|---|
| **tube1** | 1.93 | 2.05E+06 | 2.18E+06 | 310.17 |
| **tube3** | 1.80 | 2.05E+06 | 2.18E+06 | 304.30 |
| **tube6** | 1.82 | 2.05E+06 | 2.18E+06 | 304.41 |
| **tube8** | 1.91 | 2.05E+06 | 2.19E+06 | 309.68 |

*Table 50 Mass flows and pressure at the LEEs outlets from CtFD entire model*

## Thermal results and pressure distribution details

Thermal results are given in graphic form for each single component to provide a clear idea of the difference between the standalone CtFD models already shown and the entire CtFD model[47]. The cross-shaped temperature distribution on panel surfaces reflects the boundary heat flux and is due to the shape of the ion source grid which provides the deuterium beam.

The maximum pressures, for panel channels, is located in correspondence to the holes that connect the distribution channels to the tanks in the upward part of the neutralizer, over the horizontal top panels.

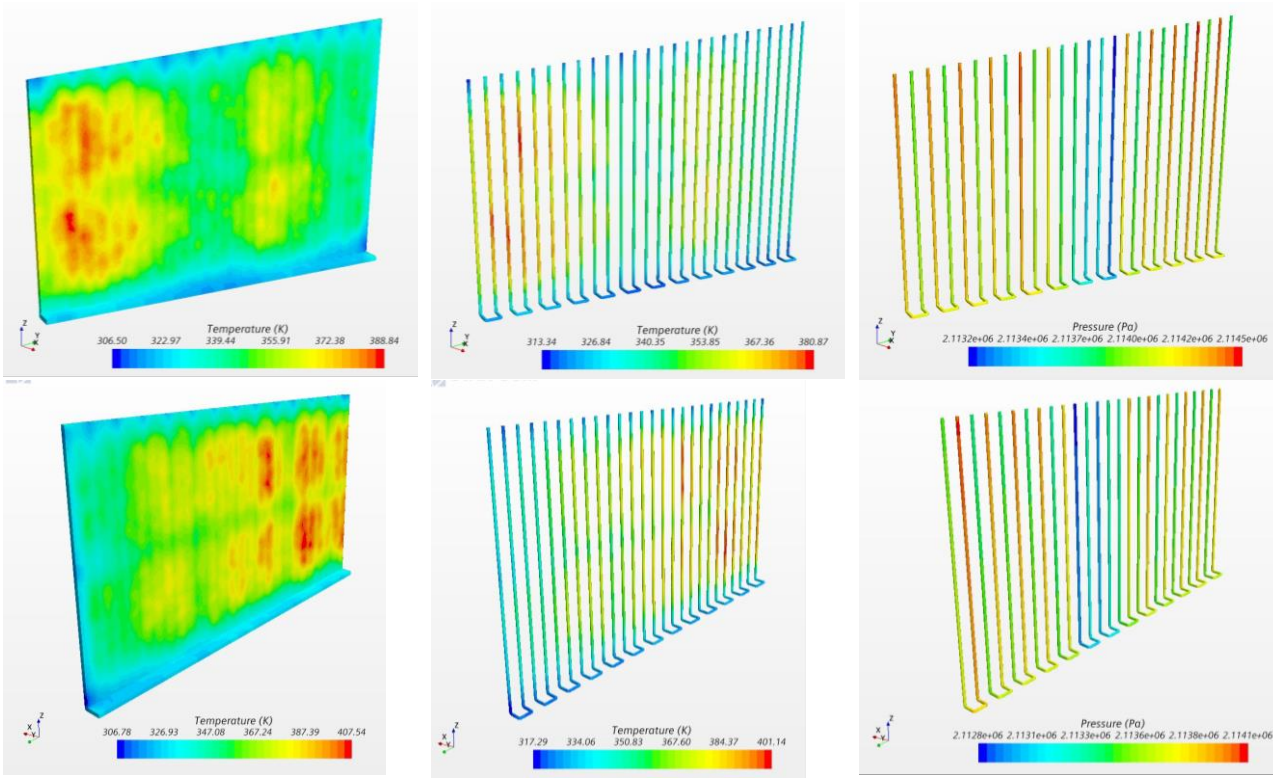


*Figure 115 Central 1 (top) and Central 2 (bottom): temperature in solid (left), temperature in fluid (center), pressure (right)*

[47] For an overall view of the temperature distribution in the entire solid region of the block of panels of the neutralizer please refer to temperature distribution reported in the following chapters in Figure 120.

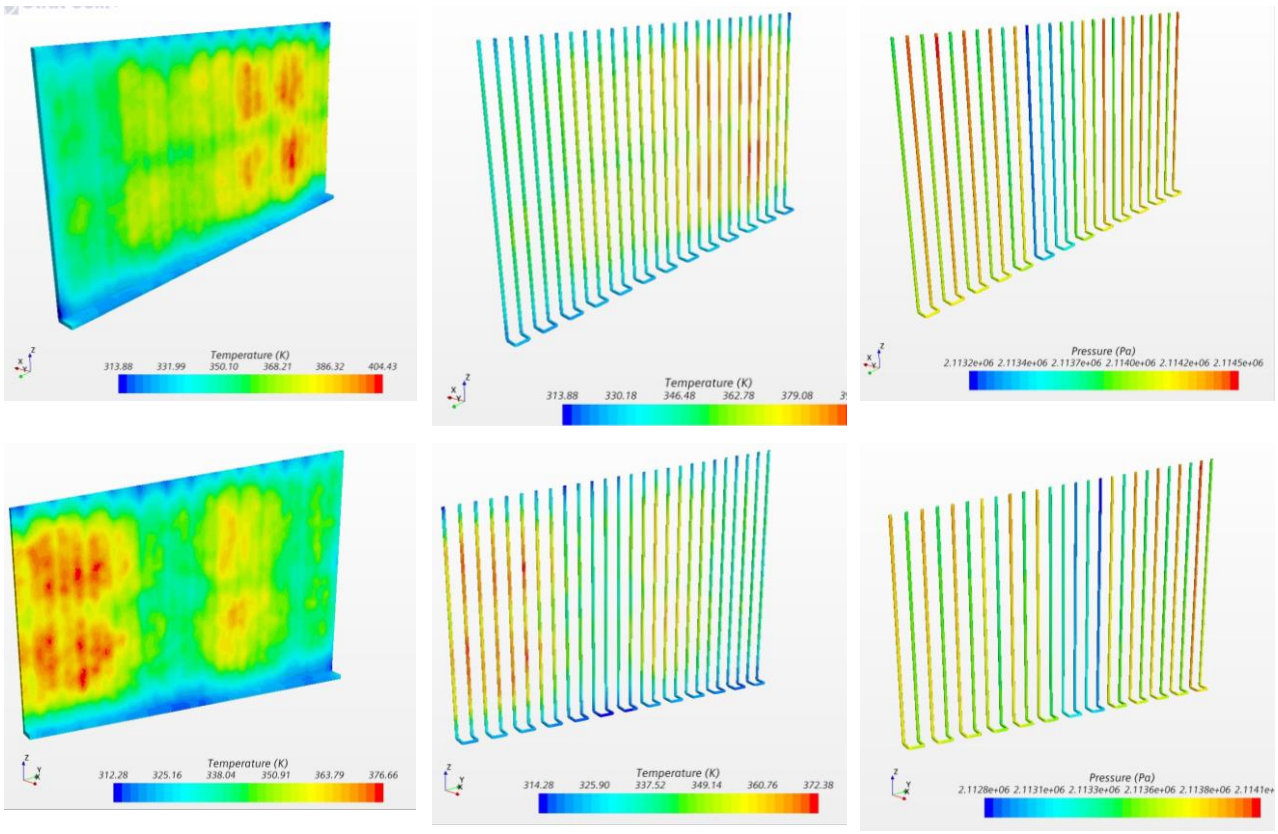


*Figure 116 Lateral 1 (top) and Lateral 2 (bottom): temperature in solid (left), temperature in fluid (center), pressure (right)*

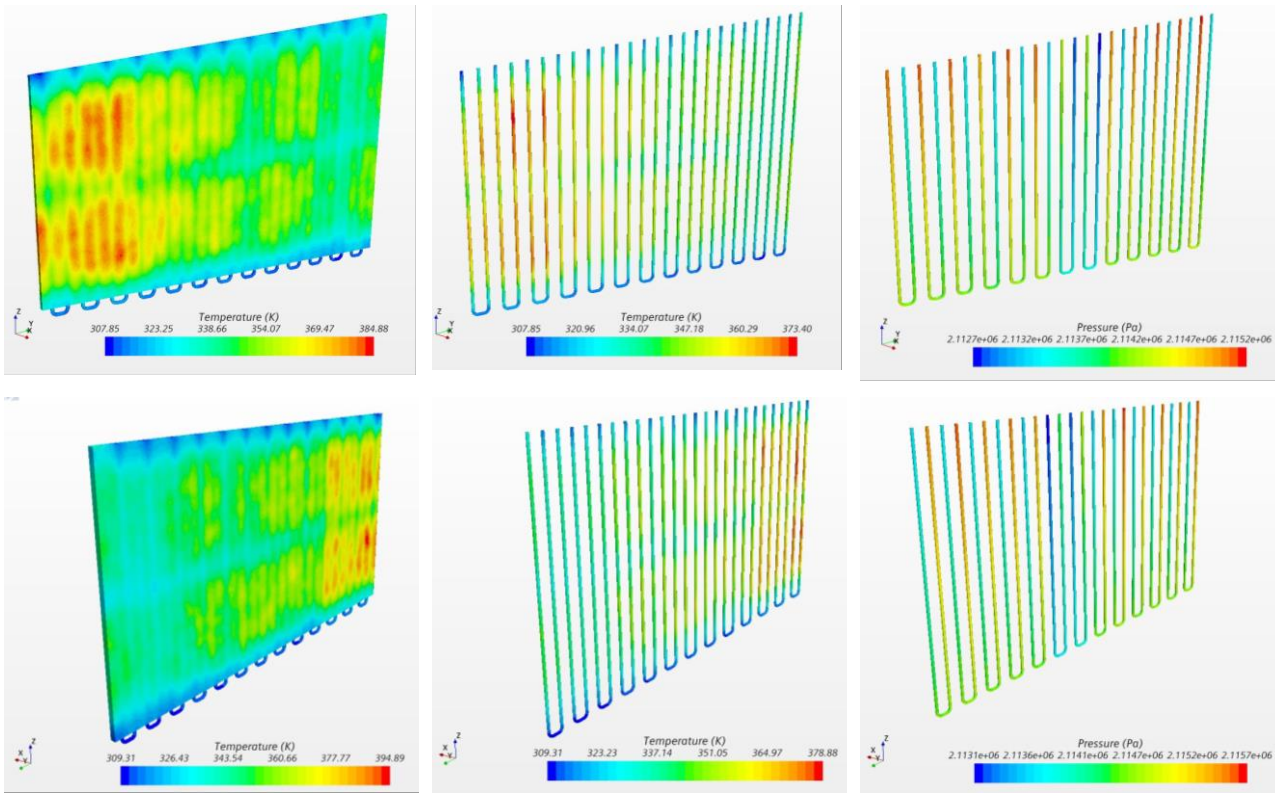


*Figure 117 Halfway 1 (top) and Halfway 2 (bottom): temperature in solid (left), temperature in fluid (center), pressure (right)*

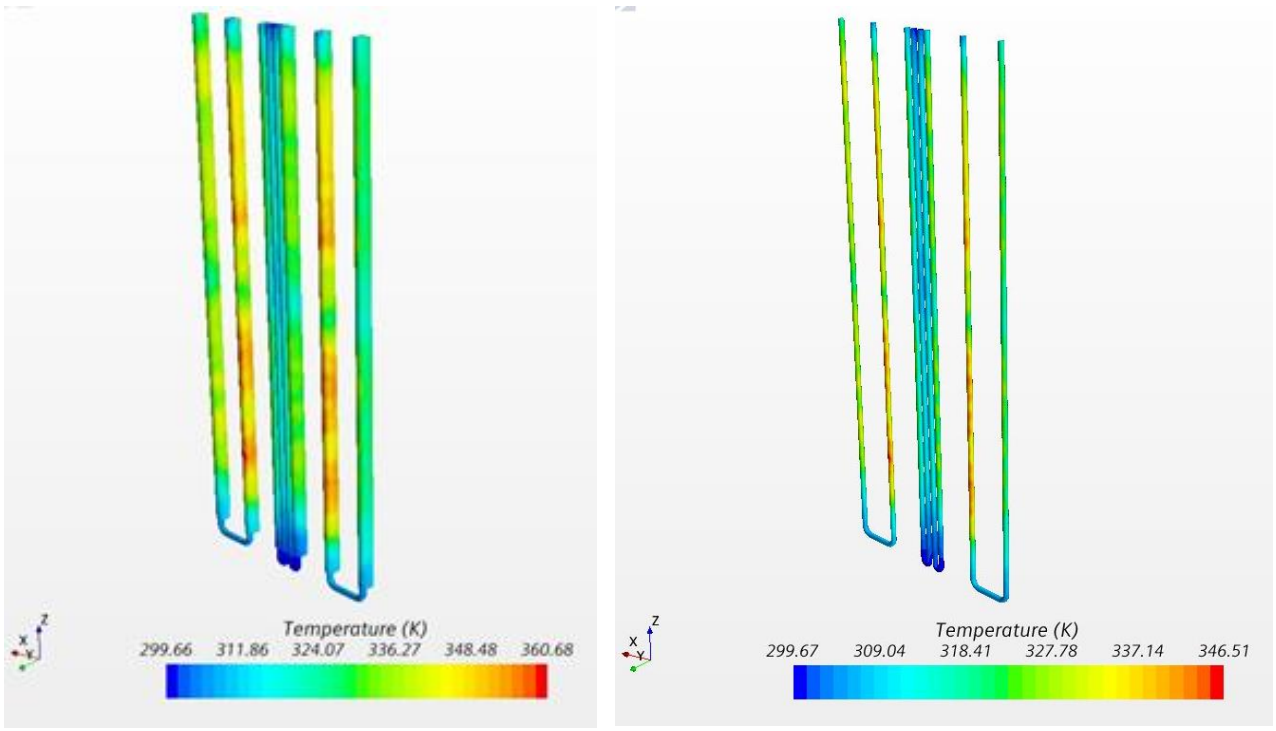


*Figure 118 LEE results: temperature in solid, temperature in fluid*

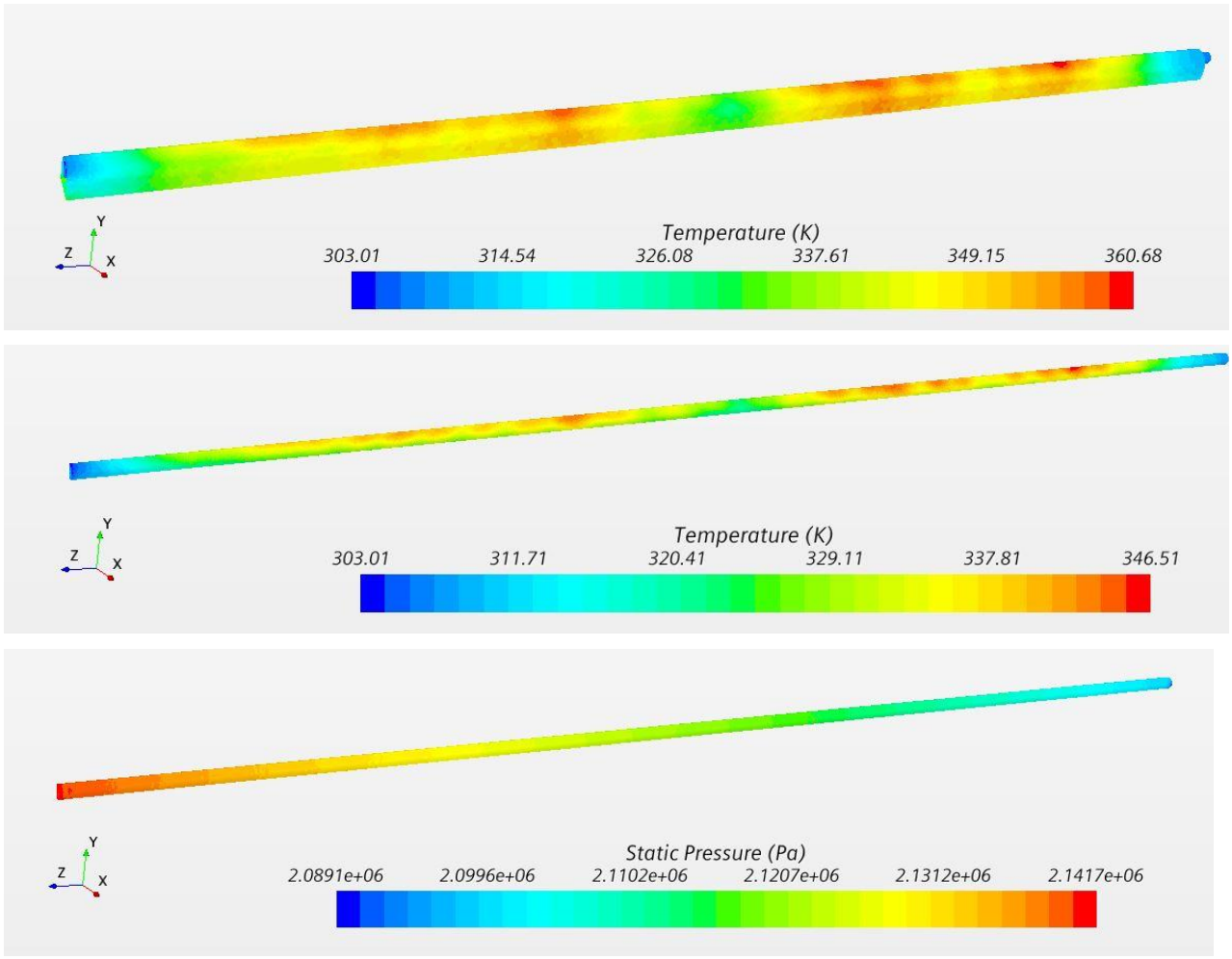


*Figure 119 LEE2, results: temperature in solid, temperature in fluid, pressure*

## Comparison between the three models and conclusions

The main conclusion of the study is that the three models (CFD, CtFD and standalone models) are substantially equivalent, in terms of mass flows, pressure and - for the CtFD - temperature distribution.

Comparison between the CFD model and the CtFD models proposed can be done by analyzing the differences for what concerns pressure and mass flows[48]: the two models seem to be, at least from the fluid dynamic point of view, equivalent, since the relative errors between the two are below 6%. Of course, it is not possible to compare them from the thermal point of view; however, if there is equivalence between the two, since the standalone models are directly derived from the CFD entire model, if also standalone models and CtFD coincide, it is possible to say that the three are substantially equivalent and provide a different level of accuracy.

Comparing results from Figure 91 to Figure 96 and from Figure 115to Figure 119, it is evident that the thermal maps are very similar, both for fluid and solid parts and for all the components: above all, minimum and maximum temperature reached in solid and fluid are approximately the same.

The pressure at the outlet of each LEEs is above 20bar, as desired and, anyway, the minimum local value of pressure is, in each point, above the 18.9bar, at which the saturation temperature limit was evaluated and used as a constraint for the preliminary optimization of the operational conditions. This means that no boiling condition should occur in the components.

For what concerns the LEEs, fluid dynamic and thermal results are reported as a direct comparison in Table 51.

| | LEE2 standalone | LEE2 from CFD (175 million cells) | LEE2 from CtFD (94 million cells in fluid) | |
|---|---|---|---|---|
| Mass flow inlet LEE2 | 1.89 | 1.89 | 1.93 | kg/s |
| Pressure inlet (static) | 2.15E+06 | 1.25E+05 | 1.20E+05 | Pa |
| Pressure outlet (static) | 2.11E+06 | 8.46E+04 | 7.92E+04 | Pa |
| Pressure difference (static) inlet-outlet | 3.94E+04 | 4.04E+04 | 4.05E+04 | Pa |
| Temperature (maximum in fluid) | 347.46 | | 346.51 | K |
| Temperature (maximum in solid) | 362.28 | | 360.68 | K |
| Temperature (surface averaged in solid) | 336.85 | | | |
| Total Pressure Drop | 3.78E+04 | | 4.02E+04 | Pa |
| Pressure inlet (absolute total, Mass Flow Averaged) | 2.27E+06 | | 2.27E+06 | Pa |
| Pressure outlet (absolute total, Mass Flow Averaged) | 2.24E+06 | | 2.23E+06 | Pa |
| fComp_Ltot | 0.015 | | | |
| fComp_section76_166 | 0.015 | | | |
| Nu medio76-166 | 669.1 | | | |
| NuComp_Ltot | 666.0 | | | |
| Temperature (bulk at outlet) | 305.82 | | | K |
| errorftot | 11.88 | | | % |
| errorNutot | 1.83 | | | % |
| errorNu | 2.31 | | | % |
| errorfriction | 10.21 | | | % |
| errorT | 0.08 | | | % |

*Table 51 LEE2: comparison between the three models*

[48] For numerical check see *Appendix*, Percentage error between CFD 175 million cells, 0bar at the outlet and CtFD with 94 million cells in fluid region.

Also for the panels all the results are similar between the three models[49], both from fluid dynamic point of view, with the direct comparisons on pressure and mass flow, and from thermal point of view, with the indirect comparisons which pass from entire CFD, to standalone components CtFD. Due to boundary conditions imposed on standalone models, the main difference that can be noticed is in the temperature distribution in the contact-area between LEEs and panels, where a Neumann condition is imposed for the standalone models. The other main difference is related to the round-off error due to the approximation in the extrapolation of mass flows from the entire model and the subsequent assignment as BCs: they are, anyway, not relevant errors, and the main behavior and key quantities and distributions remain the same for the three models.

## 2.2.4. Thermo-mechanical assessment: Scenario 2

With the same hypothesis, model and material discussed for the FEM analysis in Scenario 1, another case is presented. In Scenario 2 all the panels (i.e. the isolated components previously seen, that are vertical panels with the corresponding lower and upper horizontal panels) are welded together at the top, except for the LEEs, which are screwed on the respective panels: this condition should increase the structure stiffness and result in less deformation. The block of welded panels is free to expand upward.

For the LEEs results, the standalone FEM analysis are still valid and must be added to the following ones if the clamping system between LEEs and panels with screws remain the same and LEEs are free to expand downwards. For the remaining parts, constraints are imposed as in Table 47, but with reference to point segments indicated in Figure 120.

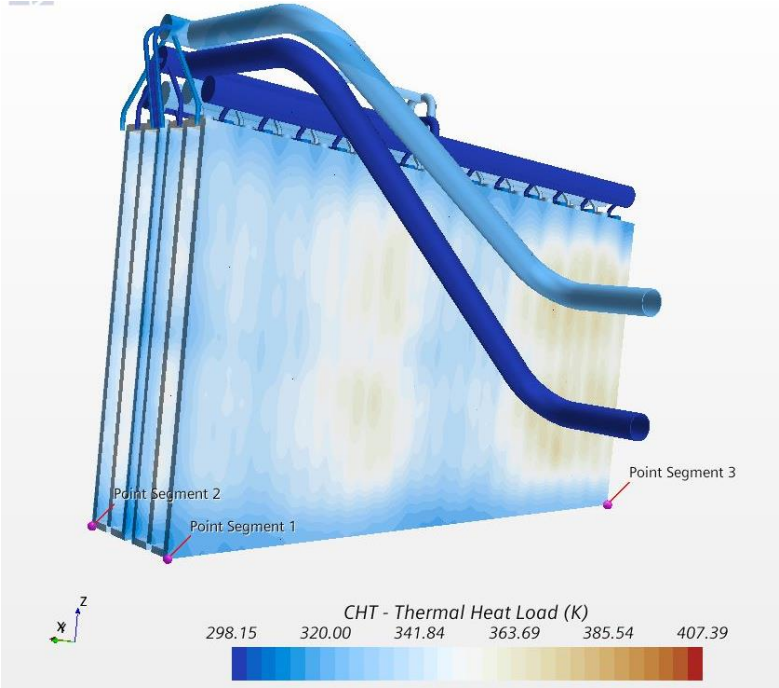


*Figure 120 Scenario 2: thermal heat load applied for thermal stress analysis and constraints*

The mesh realized is coarse (12cm base size), due to the large size of the domain, but thanks to the fact that the components have one or two predominant lengths, the tetrahedral elements used have a characteristic dimension which is small when compared to the analyzed components. The grid independence analysis

[49] Numerical values are reported in *Appendix*, Direct comparison for panels between the 3 models

should be performed to confirm the results obtained. In the present study, solutions related only to the 12cm base size FE mesh are shown.

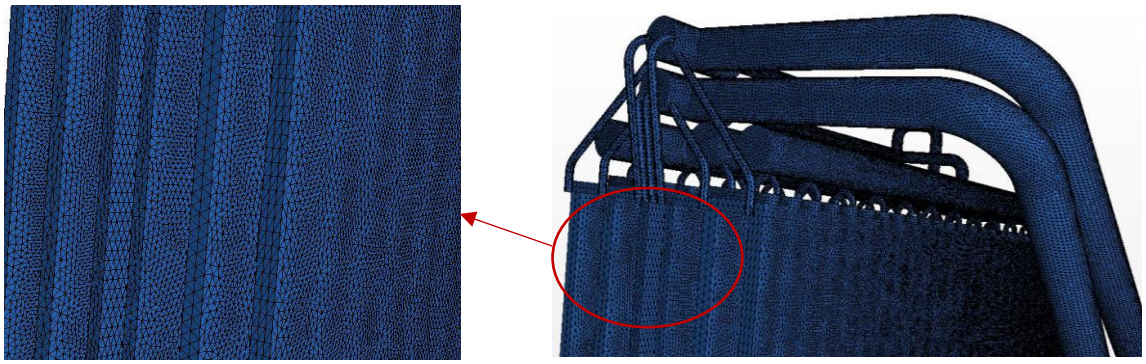

*Figure 121 Mesh realized for Scenario 2: FEM analysis, 12cm base size, 2219651 FE tetrahedral cells*

The constraints are checked in the same way as in Scenario 1, that is by applying a uniform temperature distribution of 650K. The deformation, as desired, can occur upwards: this corresponds to a structure which is mounted on a ground support. Free expansion can occur in the negative Y-direction and in positive X-direction, as represented in Figure 122.

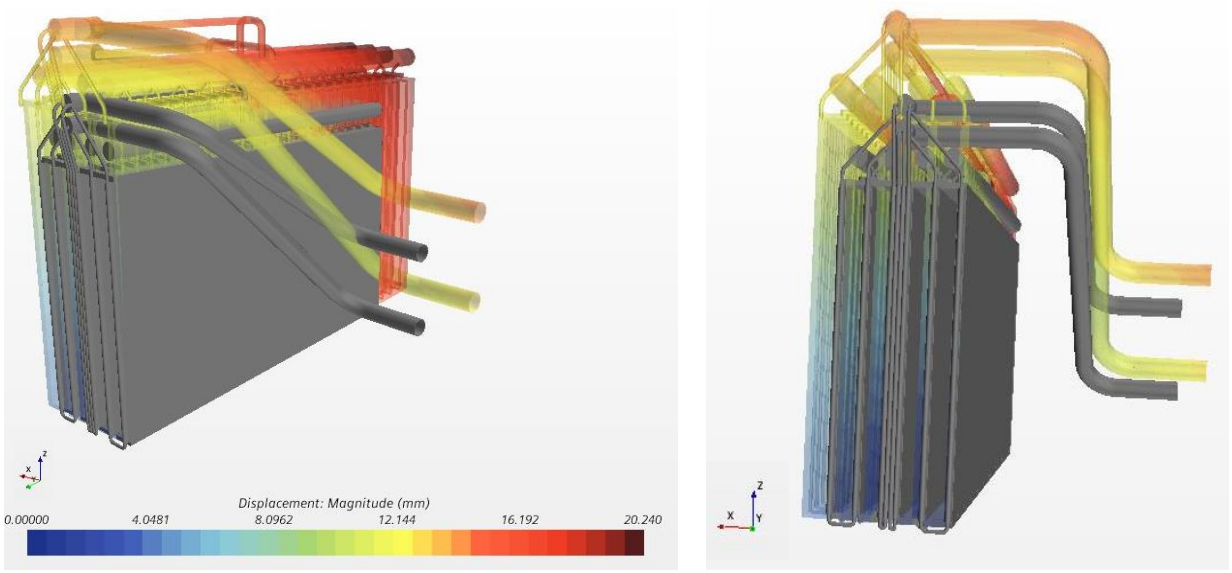


*Figure 122 Scenario 2: free expansion with uniform temperature field of 650K*

Since the test reveals that Von Mises stress are very low, also in this case constraints can be considered realistic and not too restrictive.

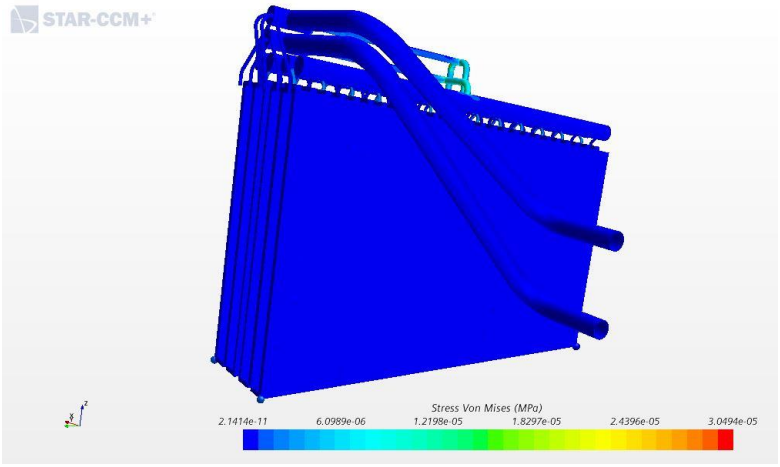


*Figure 123 Scenario 2: Von Mises stress, constraint test with uniform thermal distribution of 650K*

The temperature distribution finally obtained in the entire CtFD analysis is mapped and applied as shown in Figure 120. In the end, the results for the displacements and stress confirm the expected increase in structural rigidity, since the total maximum displacement magnitude is lower than the Scenario 1.

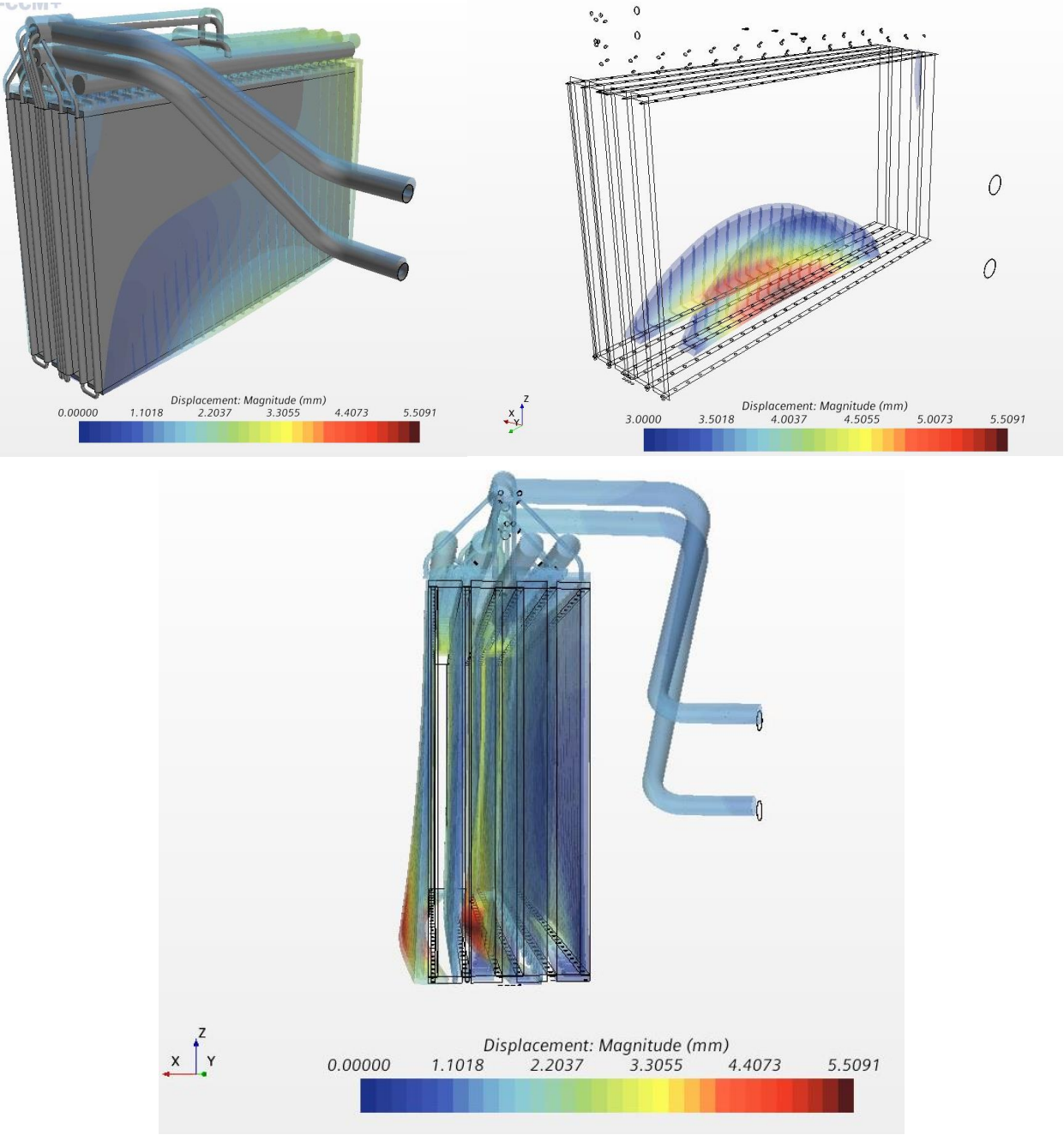


*Figure 124 Scenario 2: displacement magnitude. Colored deformed shape vs gray undeformed shape (top left), highest displacement above 3mm (top right), frontal view for planarity observations (down)*

As it can be seen, with respect to the undeformed body, the new shape causes a *barrel*-like asymmetric distortion, due to difference in temperature distribution between the two blocks and, above all to the asymmetry of the ideal constraints imposed to have an isostatic structure. Upward expansion occurs. In Figure 124, the last picture gives a qualitative idea of the flatness tolerances on the panels that should be evaluated and of the displacements of inlet and outlet holes of the entire neutralizer, whose functionalities, with this deformation, should be better investigated to understand if the deuterium beam could reach the next component of the NBI without significant problems and deflections.

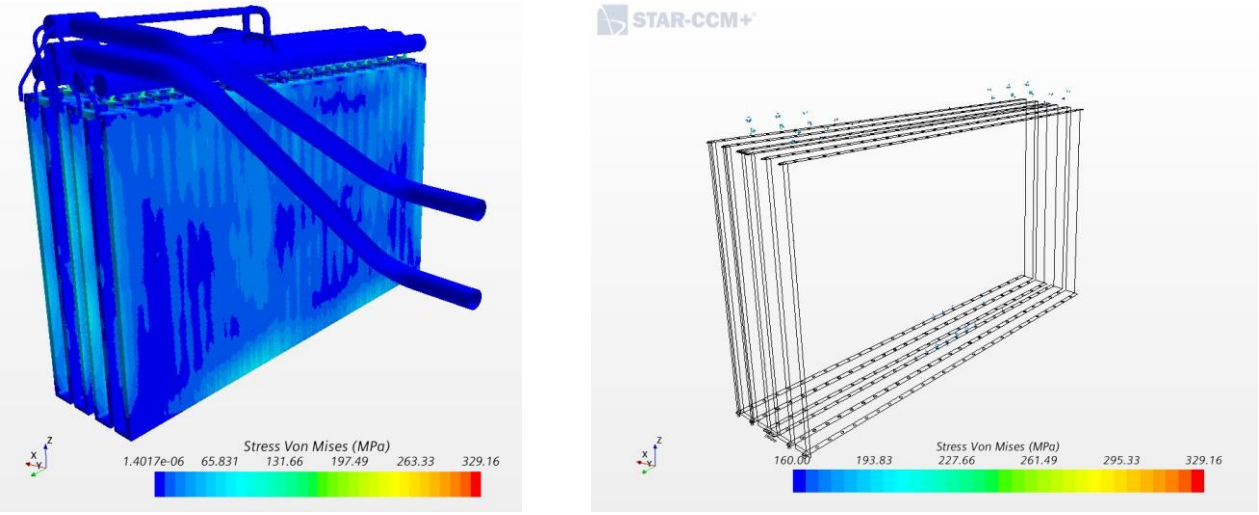


*Figure 125 Scenario 2: Von Mises stress for the block of welded panels (left), critical elements (right).The black lines outline the contours of the undeformed body.*

The maximum Von Mises stresses are located mainly on central 2 and lateral 1 panels, in the bottom areas. In general, stress above 200MPa is visible only in some of the upper *little tubes*[50] that connect the tanks to the horizontal panels and collectors. This suggests that another structural material could be used for these elements, such as AISI 304 L, as indicated in [2].

The exact selection of the material is not discussed in this context and must be accurately screened with detailed structural criteria and properties of the materials that are realistically available for the construction.

As a qualitative idea, what can be argued is that, with this constraint scenario, the most critical elements, from the mechanical point of view, are the *little tubes*, which are, anyway, subjected to a low temperature distribution and are not heated by the boundary heat flux from electrons and deuterium. Since these parts do not have particular relevance in the refrigeration – main exposed components are panels and LEEs -, but they substantially have a link and distribution function in the hydraulic circuit, they can be realized with a material which has, with respect to CuCrZr with A treatment, higher mechanical performances even if not high temperature resistant or with poor thermal conductivity properties. This choice could be cheaper and would reduce the maximum value of the tension.

In the end, maximum Von Mises stress and displacement evaluated in the Scenario 2 are

$$\sigma_{max} = 330MPa$$

$$displacement_{max} = 5.51mm$$

[50] Figure 31 for nomenclature

## 2.2.5. Thermo-mechanical assessment: Scenario 3

The last configuration proposed describes a constraint condition in which all the panels (like in Scenario 2) are welded together at the top and LEEs are totally welded to the panels to which they belong. This solution can be interesting if it is economically more convenient for the manufacturing company to produce panels and LEEs in one unique simple piece, which could then be rounded and blunt with a subsequent mechanical processing to adjust the LEE shape.

Constraints are applied as in Figure 120 and results are presented in the following pictures.

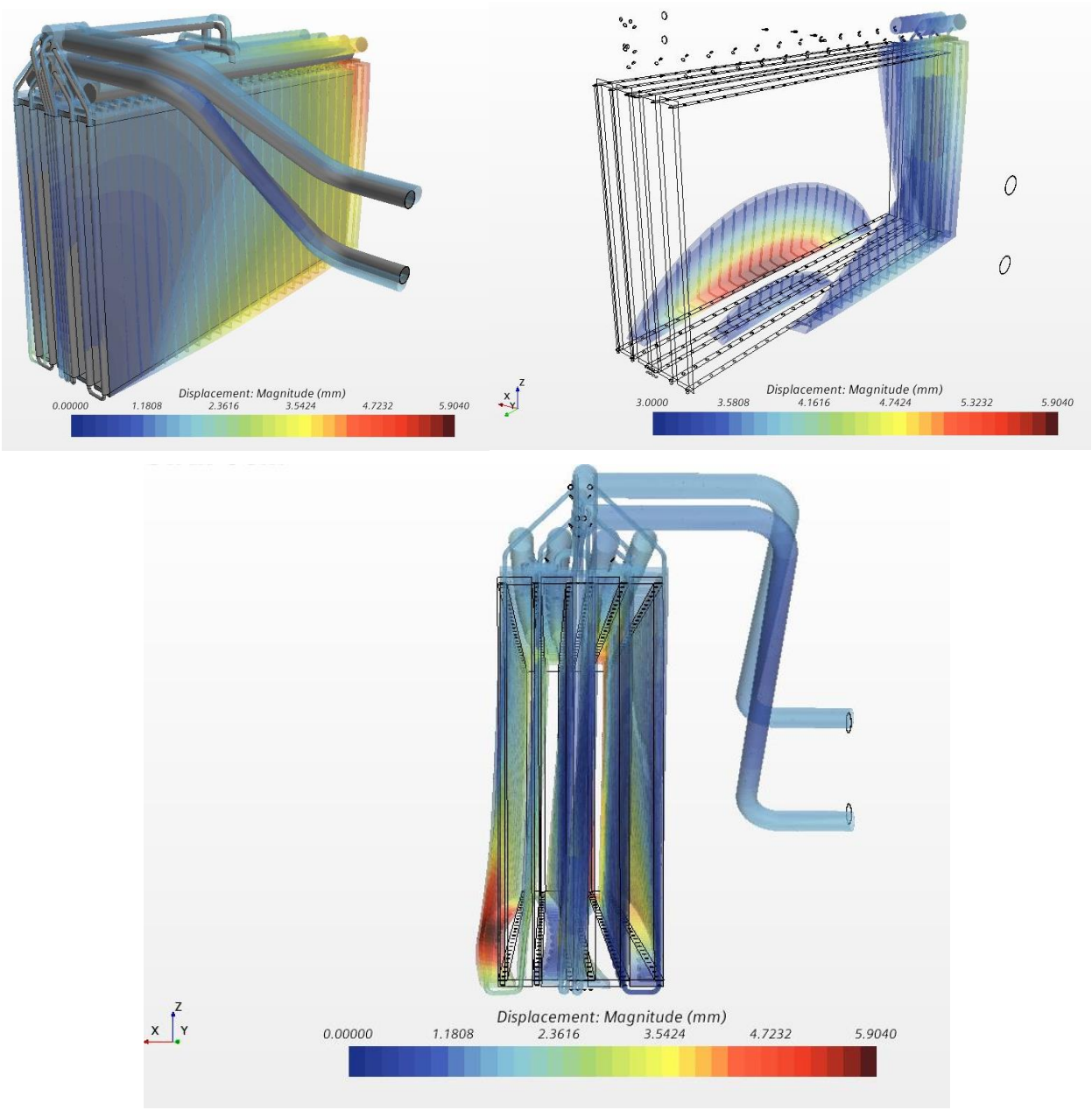


*Figure 126 Scenario 3: displacement magnitude. Colored deformed shape vs gray undeformed shape (top left), highest displacement above 3mm (top right), frontal view for planarity observations (down). The black lines outline the contours of the undeformed body.*

In this case the LEEs make the structure slightly stiffer in the frontal part. Therefore, the maximum Von Mises stress and displacement evaluated in the Scenario 3 are

$$\sigma_{max} = 301MPa$$

$$displacement_{max} = 5.90mm$$

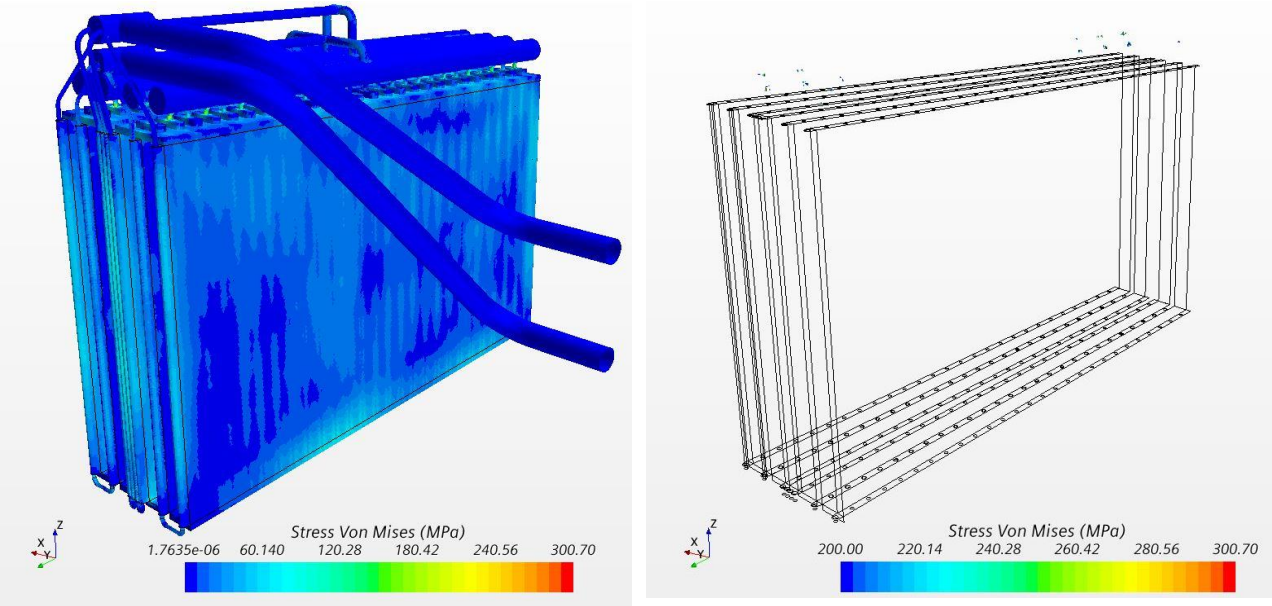


*Figure 127 Scenario 3: Von Mises stress for the block of welded panels (left), critical elements right). The black lines outline the contours of the undeformed body.*

Also in this case the most critical components are the little tubes in the upper part of the neutralizer. Except for these areas, in the rest of the structure, Von mises stresses are below 200MPa.

# 3. Conclusions

A CtFD model of the entire Neutralizer of the NBI, whose main purpose is to neutralize the accelerated ions received from the Accelerator permit gas injection from 5 points in each slit, similarly to MITICA.

The model that has been developed, has made it possible to study the mass flow and pressure distribution inside the system and the temperature field due to the high distributed heat load coming from electrons and deuterium contributions of the injected beam. From fluid dynamic and thermal analyses, thermomechanical stresses have been computed, to understand if boiling phenomena inside the fluid and structural stress inside the solid could damage the Neutralizer with certain BCs,.

Design constraints imposed by *DTT S.c.a.r.l.* on the neutralizer are satisfied with the current thermal load, which considers only electrons and deuterium contributions, neglecting the effect of stray field. The design adopted confirms the conceptual design proposed as a good alternative for the project if twisted tapes are removed from the LEE channels.

In the proposed situation, with a mass flow of 17.7kg/s provided to the refrigeration system with pressurized demineralized water at 22bar at the inlet, the maximum solid temperature is below 408 K and the margin to fluid saturation temperature is about 79K, with an estimated total pressure drop of 1.8bar. The maximum displacement evaluated is about 5.5mm, and the maximum stress approximately 330MPa with the Scenario 2 (welded blocks of panels and screwed LEEs).

CuCrZr with A treatment should be used for LEEs and panels and another structural material, with higher mechanical properties, even if with less thermal resistance, for the most stressed and least thermally loaded parts, which are, in the Scenario 2, the little tubes of connection between tanks and horizontal top panels.

Different solutions of optimizations have been qualitatively and quantitatively presented, which can supersede heavy thermal load additions due to stray field. For small increases of heat flux, higher water mass flows could be sufficient to face the load and properly feed the refrigeration system.

# Appendix

## 1.1. Mesh generation and grid independence study

### Core grid independence

Another important quantity analyzed is the maximum velocity in two different sections far from the inlet, which is a point value related to the fluid dynamic problem. An asymptotic behavior can be seen.

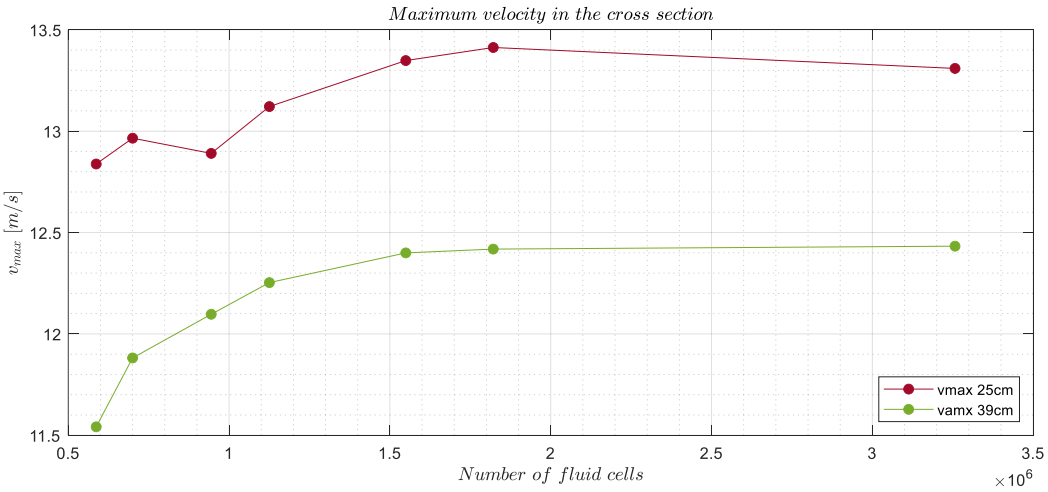


*Figure 128 Core grid independence. Maximum velocity in cross sections at 25cm and 39 cm from the inlet*

With reference to Figure 8, another point value considered is the temperature in two different point at the interface between solid and fluid, which is focused on thermal problem.

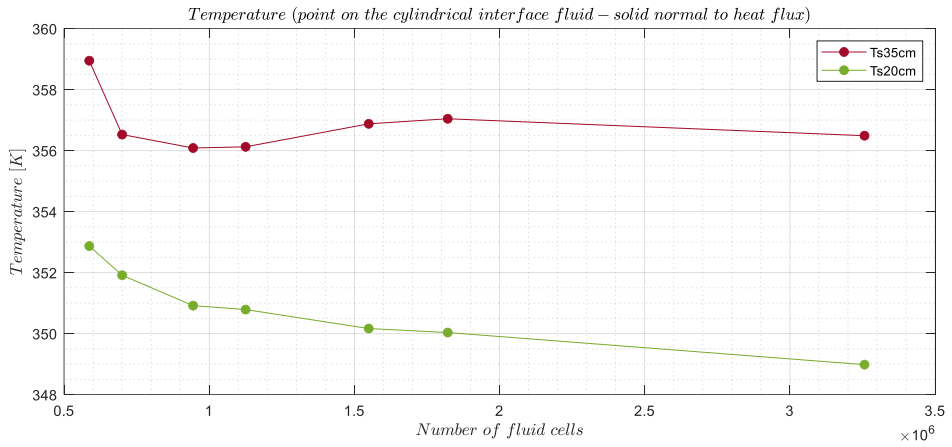


*Figure 129 Core grid independence. Temperature Ts in two point at 25cm and 20cm from the inlet, with reference to the notation in Figure 8*

Temperature along Lz line is also reported and as it can be seen the main difference on temperature, due to the base size of polyhedral mesh, occurs after the impact of the fluid with the twisted tape, where a poor quality of the mesh (i.e. big base size) cannot model accurately the effect on the flow of the geometrical curves of the tape.

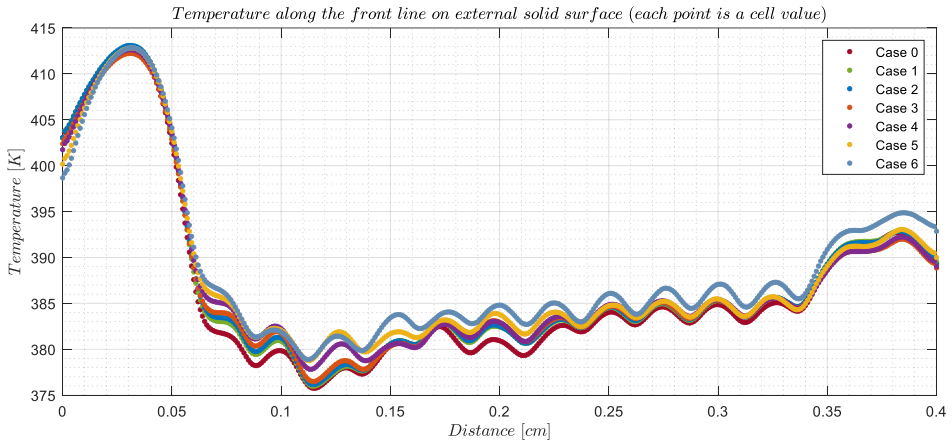


*Figure 130 Core independence. Temperature along the line Lz indicated in Figure 8*

# 1.2. Entire LEE study

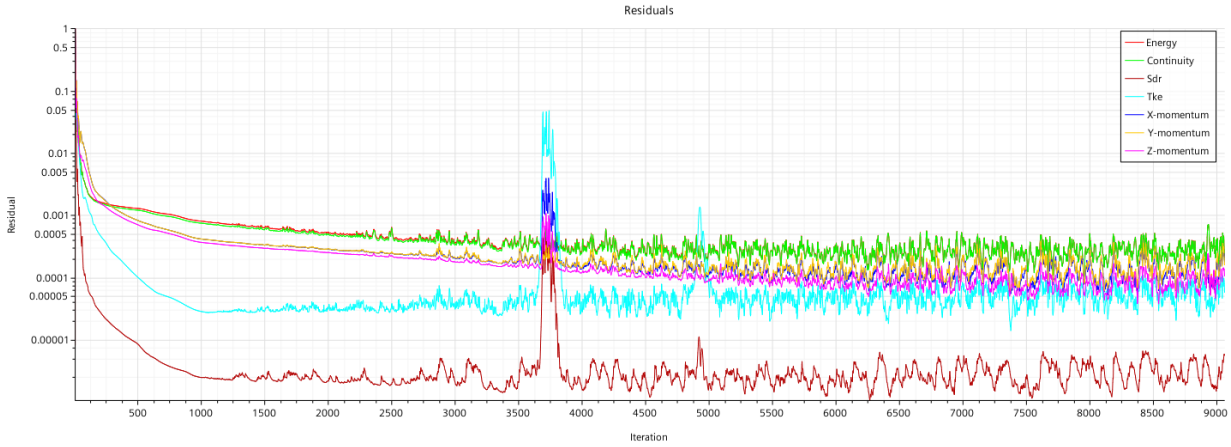


*Figure 131 Residuals for the entire LEE study simulation*

Normalized residuals are in general very low, all below at least $10^{-3}$. To check convergence, Nu and friction factors are monitored in different cross sections and for different lengths and show an asymptotic behavior.

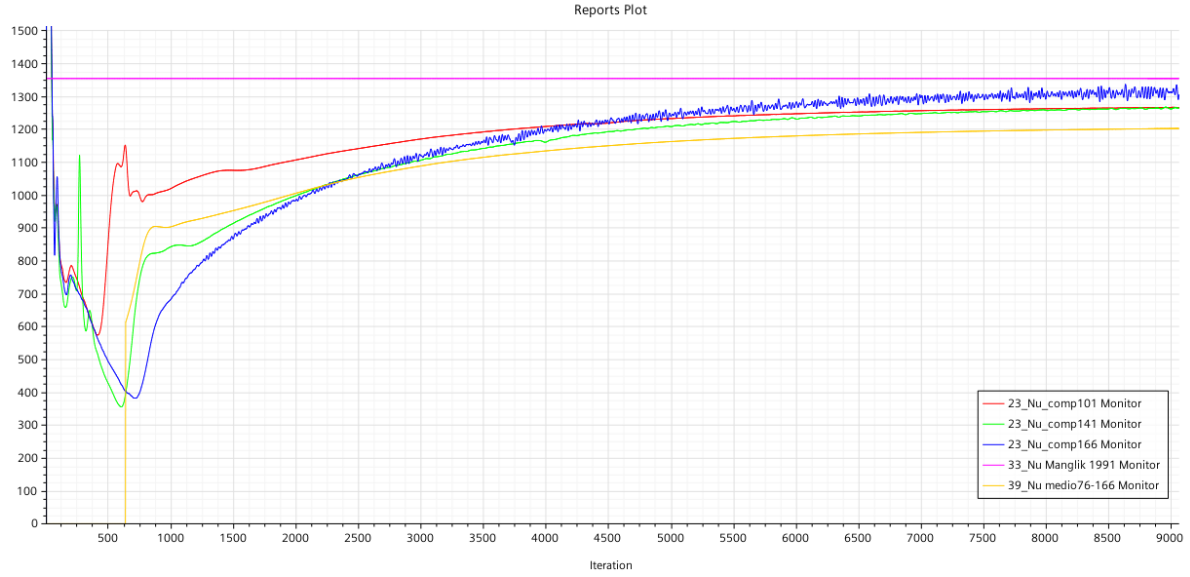


*Figure 132 Entire LEE study simulation. Nusselt number as function of the number of iterations. Nusselt number Nu_comp evaluated at 101cm, 141cm, 166cm from the inlet with equation (1.9); Nusselt number Nu_medio evaluated between 76-166cm with equation (1.11); Nusselt number from correlation Nu Manglik 1991evaluated with (1.14)*

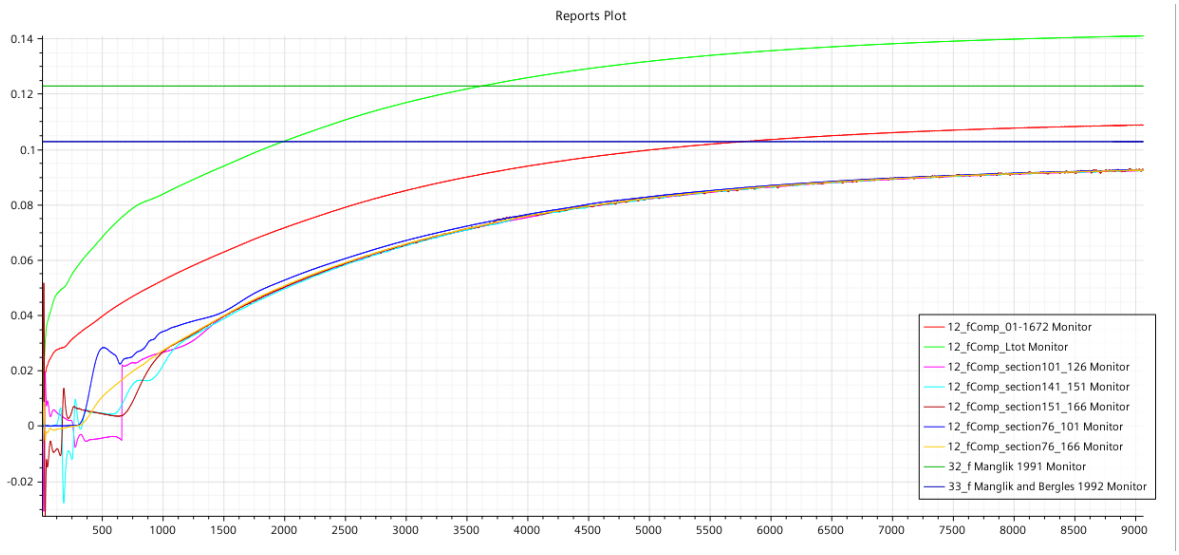


*Figure 133 Entire LEE study simulation. Friction factors as function of the number of iterations. Friction factors fComp evaluated between different cross sections at 101-126cm, 141-151cm, 151-166cm, 76-101 cm, 76-166cm from the inlet with equation (1.1); friction factors for the total length of the LEE evaluated between inlet and outlet with equation (1.1); friction factors from correlations fManglik and fManglik and Bergles evaluated with equation (1.3) and (1.6) respectively*

Also the percentage errors, evaluated with respect to literature correlations, show asymptotic trends. The mass flow error is also considered to add another check to the continuity equation.


*Figure 134 Errors on friction factor, temperature and Nusselt number as discussed*

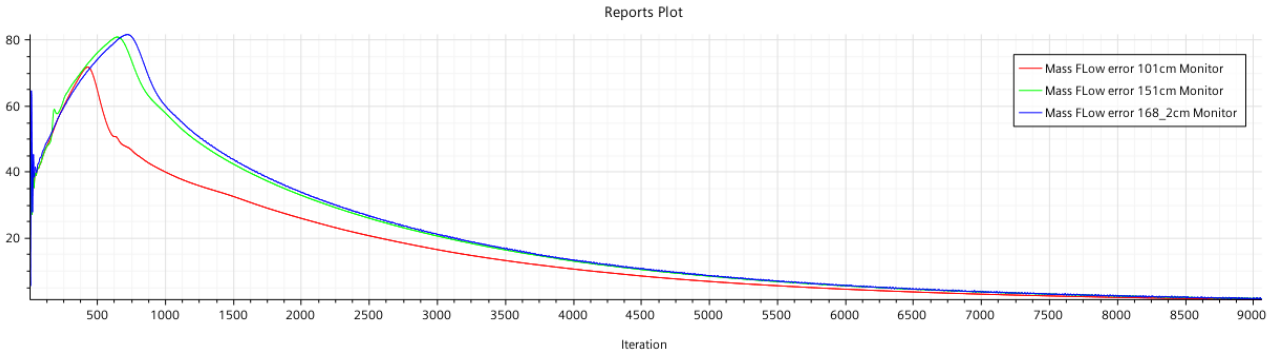


*Figure 135 Errors on mass flows at 101cm, 151cm, 168.2cm from the inlet*

# 1.4. First fluid dynamic study of the neutralizer

## CAD reconstruction

CAD reconstruction has seen the following main modifications.

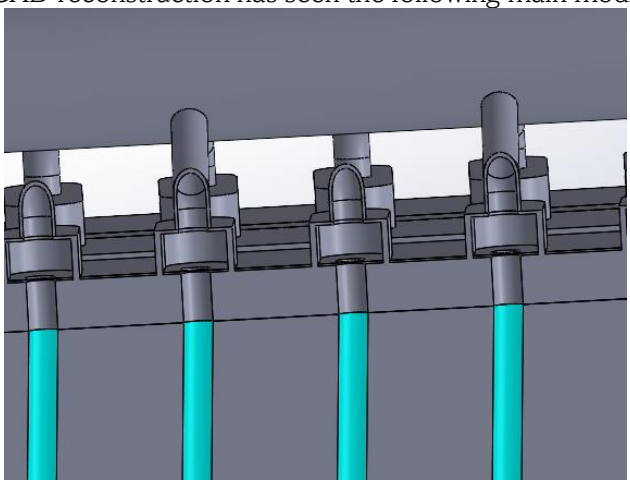

*Figure 136 Inside grooves realignment for all the panels*

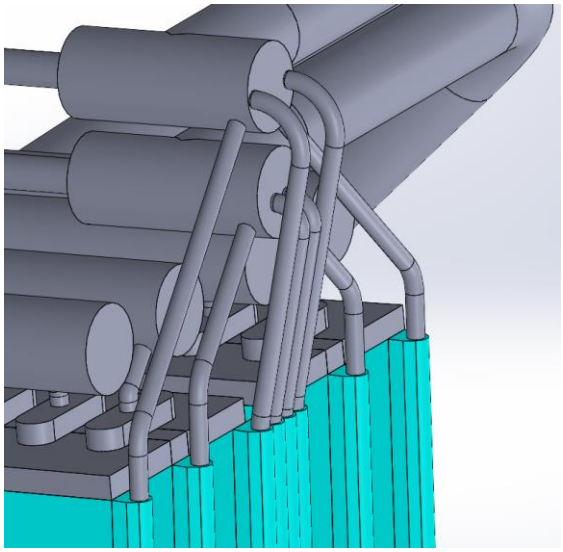

*Figure 137 Slight fitting for tubes to permit a correct realignment with LEEs holes without inner diameter variation. Panels surfaces were made coplanar.*

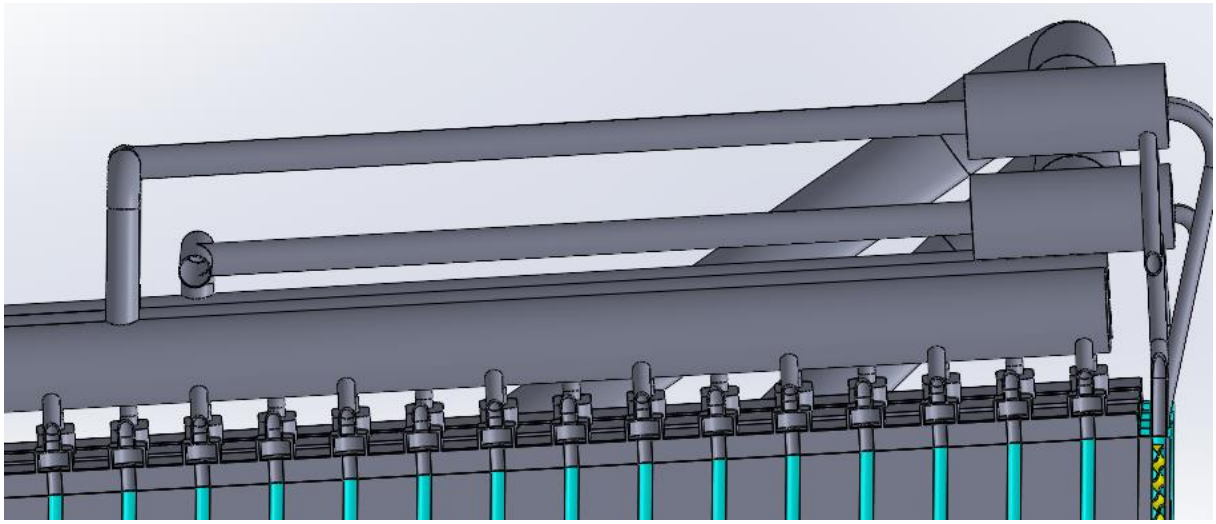

*Figure 138 Extrusion direction of initial part of the distributor has not be changed. All the dimension have been adjusted and closed holes reopened. TT has been correclty centered inside the LEEs and all inaccurate odds have been rounded.*

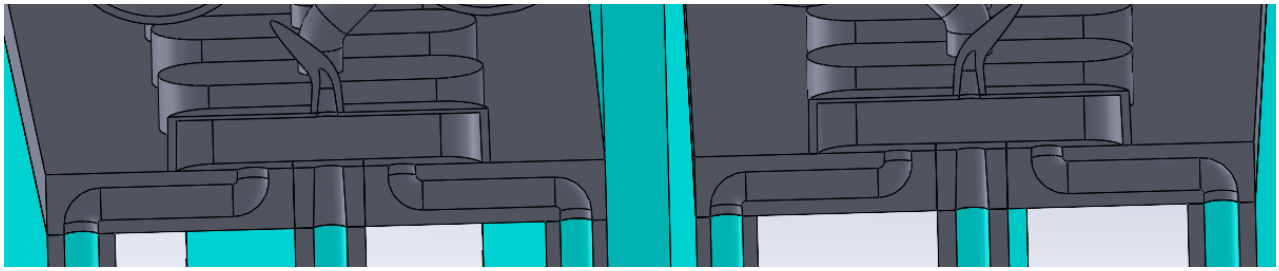

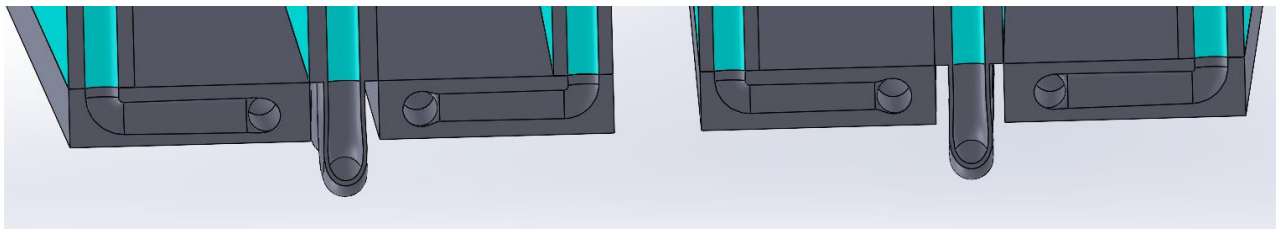

*Figure 139 Inserts have been reshaped and realigned with the main directions of top panels (top) bottom panels (bottom)*

## Detailed results for simulation for the original CAD with TT

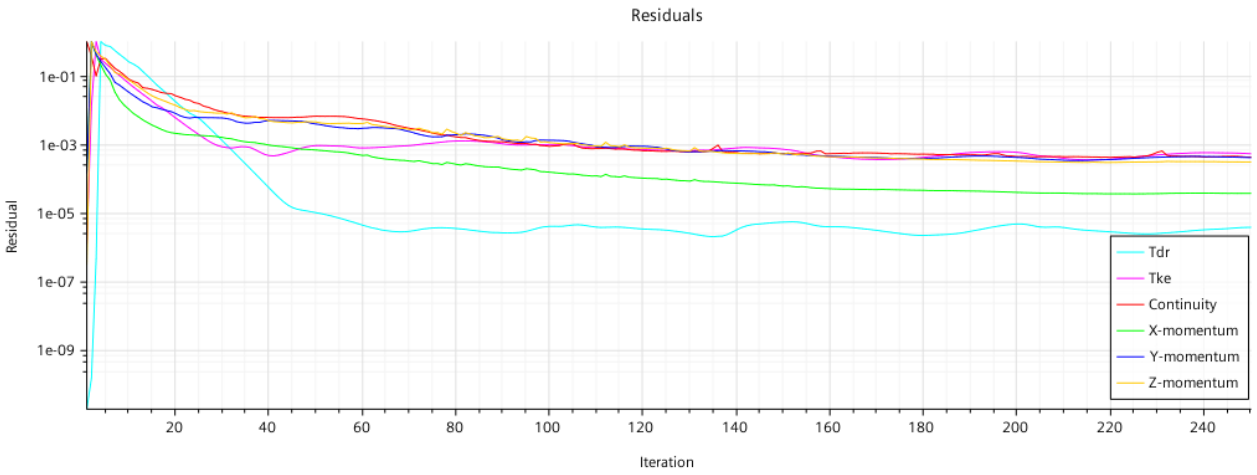


*Figure 140 Residuals for the simulation*

Residuals are kept below $10^{-3}$.

| Static pressure differences for each LEE | | Mass flows in each section | | Static pressure in each section | |
|---|---|---|---|---|---|
| Iteration | 250.00 | Iteration | 250.00 | Iteration | 250.00 |
| Pressure Drop IO Monitor (Pa) | 1.36E+06 | Mass Flow tube 1 Monitor (kg/s) | 2.06 | Pressure Static distributor1 Monitor (Pa) | 6.96E+05 |
| Pressure Drop inlet-outlet Monitor | 1.36E+06 | Mass Flow Inlet Monitor 2 (kg/s) | -40.00 | Pressure Static distributor1b Monitor (Pa) | 7.01E+05 |
| Pressure Drop tube 1 Monitor | 5.62E+05 | Mass Flow Outlet Monitor 2 (kg/s) | 39.96 | Pressure Static distributor2 Monitor (Pa) | 4.84E+05 |
| Pressure Drop tube 2 Monitor | 6.18E+05 | Mass Flow tube 2 Monitor (kg/s) | -2.07 | Pressure Static distributor2b Monitor (Pa) | 4.84E+05 |
| Pressure Drop tube 3 Monitor | 5.68E+05 | Mass Flow manifold outlet end3 Monitor (kg/s) | 31.66 | Pressure Static manifold inlet end Monitor (Pa) | 7.63E+05 |
| Pressure Drop tube 4 Monitor | 5.97E+05 | Mass Flow tube 2 end Monitor (kg/s) | -2.07 | Pressure Static manifold outlet end1 Monitor (Pa) | -2.56E+02 |
| Pressure Drop tube 5 Monitor | 5.93E+05 | Mass Flow distributor1b Monitor (kg/s) | -15.92 | Pressure Static manifold outlet end2 Monitor (Pa) | 4.40E+03 |
| Pressure Drop tube 6 Monitor | 5.69E+05 | Mass Flow manifold inlet end Monitor (kg/s) | -31.59 | Pressure Static manifold outlet end3 Monitor (Pa) | 1.50E+04 |
| Pressure Drop tube 7 Monitor | 5.97E+05 | Mass Flow distributor2b Monitor (kg/s) | 16.05 | Pressure Static tube 1 Monitor (Pa) | 9.85E+04 |
| Pressure Drop tube 8 Monitor | 5.85E+05 | Mass Flow tube 1 end Monitor (kg/s) | 2.07 | Pressure Static tube 1end Monitor (Pa) | 6.60E+05 |
| | | Mass Flow manifold outlet end Monitor (kg/s) | 31.67 | Pressure Static tube 2 Monitor (Pa) | 1.28E+06 |

| | | | | | |
|---|---|---|---|---|---|
| | | Mass Flow distributor2 Monitor (kg/s) | 15.66 | Pressure Static tube 2end Monitor (Pa) | 6.65E+05 |
| | | Mass Flow distributor1 Monitor (kg/s) | -15.70 | Pressure Static tube 3 Monitor (Pa) | 1.01E+05 |
| | | Mass Flow tube 3 end Monitor (kg/s) | 2.04 | Pressure Static tube 3end Monitor (Pa) | 6.69E+05 |
| | | Mass Flow tube 3 Monitor (kg/s) | 2.03 | Pressure Static tube 4 Monitor (Pa) | 1.29E+06 |
| | | Mass Flow tube 4 Monitor (kg/s) | -2.04 | Pressure Static tube 4end Monitor (Pa) | 6.89E+05 |
| | | Mass Flow tube 5 Monitor (kg/s) | -2.03 | Pressure Static tube 5 Monitor (Pa) | 1.28E+06 |
| | | Mass Flow tube 6 Monitor (kg/s) | 2.03 | Pressure Static tube 5end Monitor (Pa) | 6.89E+05 |
| | | Mass Flow tube 7 Monitor (kg/s) | -2.04 | Pressure Static tube 6 Monitor (Pa) | 1.01E+05 |
| | | Mass Flow tube 8 Monitor (kg/s) | 2.04 | Pressure Static tube 6end Monitor (Pa) | 6.70E+05 |
| | | | | Pressure Static tube 7 Monitor (Pa) | 1.29E+06 |
| | | | | Pressure Static tube 7end Monitor (Pa) | 6.91E+05 |
| | | | | Pressure Static tube 8 Monitor (Pa) | 9.83E+04 |
| | | | | Pressure Static tube 8end Monitor (Pa) | 6.84E+05 |
| | | | | PressureInlet Monitor 2 (Pa) | 1.36E+06 |
| | | | | PressureOutlet Monitor 2 (Pa) | -1.14E-02 |
| | | | | Pressure Static manifoldinletend2 (Pa) | 6.97E+05 |

*Table 52 Complete results: CFD entire neutralizer original model with TT, 40kg/s at inlet, 0bar outlet*

# 1.6. Optimized neutralizer design

## Detailed results for simulation for Optimization 1

| Static pressure differences for each LEE | | Mass flows in each section | | Static pressure in each section | |
|---|---|---|---|---|---|
| Iteration | 309 | Iteration | 309 | Iteration | 309 |
| Pressure Drop IO Monitor (Pa) | 7.10E+05 | Mass Flow tube 1 Monitor (kg/s) | 1.47 | Pressure Static distributor1 Monitor (Pa) | 2.36E+05 |
| Pressure Drop inlet-outlet Monitor | 7.10E+05 | Mass Flow Inlet Monitor 2 (kg/s) | -40.00 | Pressure Static distributor1b Monitor (Pa) | 2.38E+05 |
| Pressure Drop tube 1 Monitor | 2.98E+05 | Mass Flow Outlet Monitor 2 (kg/s) | 39.93 | Pressure Static distributor2 Monitor (Pa) | -9.05E+03 |
| Pressure Drop tube 2 Monitor | 3.26E+05 | Mass Flow tube 2 Monitor (kg/s) | -1.48 | Pressure Static distributor2b Monitor (Pa) | -2.18E+03 |
| Pressure Drop tube 3 Monitor | 2.87E+05 | Mass Flow manifold outlet end3 Monitor (kg/s) | 33.98 | Pressure Static manifold inlet end Monitor (Pa) | 6.85E+05 |
| Pressure Drop tube 4 Monitor | 3.27E+05 | Mass Flow tube 2 end Monitor (kg/s) | -1.48 | Pressure Static manifold outlet end1 Monitor (Pa) | 1.52E+04 |

| | | | | | |
|---|---|---|---|---|---|
| Pressure Drop tube 5 Monitor | 3.11E+05 | Mass Flow distributor1b Monitor (kg/s) | -17.07 | Pressure Static manifold outlet end2 Monitor (Pa) | 1.62E+04 |
| Pressure Drop tube 6 Monitor | 3.06E+05 | Mass Flow manifold inlet end Monitor (kg/s) | -33.84 | Pressure Static manifold outlet end3 Monitor (Pa) | 4.45E+03 |
| Pressure Drop tube 7 Monitor | 3.24E+05 | Mass Flow distributor2b Monitor (kg/s) | 16.99 | Pressure Static tube 1 Monitor (Pa) | 3.95E+04 |
| Pressure Drop tube 8 Monitor | 3.04E+05 | Mass Flow tube 1 end Monitor (kg/s) | 1.48 | Pressure Static tube 1end Monitor (Pa) | 3.37E+05 |
| | | Mass Flow manifold outlet end Monitor (kg/s) | 33.98 | Pressure Static tube 2 Monitor (Pa) | 6.69E+05 |
| | | Mass Flow distributor2 Monitor (kg/s) | 16.99 | Pressure Static tube 2end Monitor (Pa) | 3.43E+05 |
| | | Mass Flow distributor1 Monitor (kg/s) | -16.97 | Pressure Static tube 3 Monitor (Pa) | 3.96E+04 |
| | | Mass Flow tube 3 end Monitor (kg/s) | 1.46 | Pressure Static tube 3end Monitor (Pa) | 3.26E+05 |
| | | Mass Flow tube 3 Monitor (kg/s) | 1.46 | Pressure Static tube 4 Monitor (Pa) | 6.65E+05 |
| | | Mass Flow tube 4 Monitor (kg/s) | -1.46 | Pressure Static tube 4end Monitor (Pa) | 3.38E+05 |
| | | Mass Flow tube 5 Monitor (kg/s) | -1.46 | Pressure Static tube 5 Monitor (Pa) | 6.65E+05 |
| | | Mass Flow tube 6 Monitor (kg/s) | 1.46 | Pressure Static tube 5end Monitor (Pa) | 3.54E+05 |
| | | Mass Flow tube 7 Monitor (kg/s) | -1.47 | Pressure Static tube 6 Monitor (Pa) | 3.76E+04 |
| | | Mass Flow tube 8 Monitor (kg/s) | 1.47 | Pressure Static tube 6end Monitor (Pa) | 3.44E+05 |
| | | | | Pressure Static tube 7 Monitor (Pa) | 6.70E+05 |
| | | | | Pressure Static tube 7end Monitor (Pa) | 3.46E+05 |
| | | | | Pressure Static tube 8 Monitor (Pa) | 3.67E+04 |
| | | | | Pressure Static tube 8end Monitor (Pa) | 3.40E+05 |
| | | | | PressureInlet Monitor 2 (Pa) | 7.10E+05 |
| | | | | PressureOutlet Monitor 2 (Pa) | 0.00E+00 |
| | | | | Pressure Static manifoldinletend2 (Pa) | 2.09E+05 |

*Table 53 Complete results: CFD entire neutralizer Optimization 1, 40kg/s at inlet, 0bar outlet*

## Detailed results for simulation for Optimization 2

| Static pressure differences for each LEE | | Mass flows in each section | | Static pressure in each section | |
|---|---|---|---|---|---|
| Iteration | 4.97E+02 | Iteration | 497.00 | Iteration | 4.97E+02 |
| Pressure Drop IO Monitor (Pa) | 1.01E+06 | Mass Flow tube 1 Monitor (kg/s) | 1.78 | Pressure Static distributor1 Monitor (Pa) | 5.83E+05 |
| Pressure Drop inlet-outlet Monitor | 1.01E+06 | Mass Flow Inlet Monitor 2 (kg/s) | -40.00 | Pressure Static distributor1b Monitor (Pa) | 5.84E+05 |
| Pressure Drop tube 1 Monitor | 4.40E+05 | Mass Flow Outlet Monitor 2 (kg/s) | 39.98 | Pressure Static distributor2 Monitor (Pa) | 3.51E+05 |
| Pressure Drop tube 2 Monitor | 4.23E+05 | Mass Flow tube 2 Monitor (kg/s) | -1.77 | Pressure Static distributor2b Monitor (Pa) | 3.52E+05 |
| Pressure Drop tube 3 Monitor | 4.22E+05 | Mass Flow manifold outlet end3 Monitor (kg/s) | 32.83 | Pressure Static manifold inlet end Monitor (Pa) | 9.89E+05 |
| Pressure Drop tube 4 Monitor | 4.24E+05 | Mass Flow tube 2 end Monitor (kg/s) | -1.78 | Pressure Static manifold outlet end1 Monitor (Pa) | 4.45E+02 |
| Pressure Drop tube 5 Monitor | 4.40E+05 | Mass Flow distributor1b Monitor (kg/s) | -16.39 | Pressure Static manifold outlet end2 Monitor (Pa) | 8.43E+03 |
| Pressure Drop tube 6 Monitor | 4.16E+05 | Mass Flow manifold inlet end Monitor (kg/s) | -32.65 | Pressure Static manifold outlet end3 Monitor (Pa) | 3.63E+05 |

| | | | | | |
|---|---|---|---|---|---|
| Pressure Drop tube 7 Monitor | 4.53E+05 | Mass Flow distributor2b Monitor (kg/s) | 16.43 | Pressure Static tube 1 Monitor (Pa) | 9.11E+04 |
| Pressure Drop tube 8 Monitor | 4.08E+05 | Mass Flow tube 1 end Monitor (kg/s) | 1.78 | Pressure Static tube 1end Monitor (Pa) | 5.31E+05 |
| | | Mass Flow manifold outlet end Monitor (kg/s) | 32.82 | Pressure Static tube 2 Monitor (Pa) | 9.59E+05 |
| | | Mass Flow distributor2 Monitor (kg/s) | 16.39 | Pressure Static tube 2end Monitor (Pa) | 5.36E+05 |
| | | Mass Flow distributor1 Monitor (kg/s) | -16.43 | Pressure Static tube 3 Monitor (Pa) | 9.90E+04 |
| | | Mass Flow tube 3 end Monitor (kg/s) | 1.74 | Pressure Static tube 3end Monitor (Pa) | 5.21E+05 |
| | | Mass Flow tube 3 Monitor (kg/s) | 1.74 | Pressure Static tube 4 Monitor (Pa) | 9.57E+05 |
| | | Mass Flow tube 4 Monitor (kg/s) | -1.75 | Pressure Static tube 4end Monitor (Pa) | 5.34E+05 |
| | | Mass Flow tube 5 Monitor (kg/s) | -1.74 | Pressure Static tube 5 Monitor (Pa) | 9.53E+05 |
| | | Mass Flow tube 6 Monitor (kg/s) | 1.75 | Pressure Static tube 5end Monitor (Pa) | 5.13E+05 |
| | | Mass Flow tube 7 Monitor (kg/s) | -1.77 | Pressure Static tube 6 Monitor (Pa) | 8.39E+04 |
| | | Mass Flow tube 8 Monitor (kg/s) | 1.76 | Pressure Static tube 6end Monitor (Pa) | 5.00E+05 |
| | | | | Pressure Static tube 7 Monitor (Pa) | 9.60E+05 |
| | | | | Pressure Static tube 7end Monitor (Pa) | 5.07E+05 |
| | | | | Pressure Static tube 8 Monitor (Pa) | 9.25E+04 |
| | | | | Pressure Static tube 8end Monitor (Pa) | 5.01E+05 |
| | | | | PressureInlet Monitor 2 (Pa) | 1.01E+06 |
| | | | | PressureOutlet Monitor 2 (Pa) | 0.00E+00 |
| | | | | Pressure Static manifoldinletend2 (Pa) | 5.55E+05 |

*Table 54 Complete results: CFD entire neutralizer Optimization 2, 40kg/s at inlet, 0bar outlet*

## Detailed results for simulation for Optimization 3

| Static pressure differences for each LEE | | Mass flows in each section | | Static pressure in each section | |
|---|---|---|---|---|---|
| Iteration | 4.06E+02 | Iteration | 406.00 | Iteration | 4.06E+02 |
| Pressure Drop IO Monitor (Pa) | 6.61E+05 | Mass Flow tube 1 Monitor (kg/s) | 1.42 | Pressure Static distributor1 Monitor (Pa) | 2.34E+05 |
| Pressure Drop inlet-outlet Monitor | 6.62E+05 | Mass Flow Inlet Monitor 2 (kg/s) | -40.00 | Pressure Static distributor1b Monitor (Pa) | 2.34E+05 |
| Pressure Drop tube 1 Monitor | 2.80E+05 | Mass Flow Outlet Monitor 2 (kg/s) | 40.08 | Pressure Static distributor2 Monitor (Pa) | -1.02E+04 |
| Pressure Drop tube 2 Monitor | 3.09E+05 | Mass Flow tube 2 Monitor (kg/s) | -1.42 | Pressure Static distributor2b Monitor (Pa) | -1.01E+04 |
| Pressure Drop tube 3 Monitor | 2.87E+05 | Mass Flow manifold outlet end3 Monitor (kg/s) | 34.31 | Pressure Static manifold inlet end Monitor (Pa) | 6.44E+05 |
| Pressure Drop tube 4 Monitor | 2.90E+05 | Mass Flow tube 2 end Monitor (kg/s) | -1.43 | Pressure Static manifold outlet end1 Monitor (Pa) | 6.67E+03 |
| Pressure Drop tube 5 Monitor | 2.85E+05 | Mass Flow distributor1b Monitor (kg/s) | -17.16 | Pressure Static manifold outlet end2 Monitor (Pa) | 8.32E+03 |

| | | | | | |
|---|---|---|---|---|---|
| Pressure Drop tube 6 Monitor | 2.95E+05 | Mass Flow manifold inlet end Monitor (kg/s) | -32.76 | Pressure Static manifold outlet end3 Monitor (Pa) | 4.62E+01 |
| Pressure Drop tube 7 Monitor | 2.98E+05 | Mass Flow distributor2b Monitor (kg/s) | 17.18 | Pressure Static tube 1 Monitor (Pa) | 3.30E+04 |
| Pressure Drop tube 8 Monitor | 2.93E+05 | Mass Flow tube 1 end Monitor (kg/s) | 1.43 | Pressure Static tube 1end Monitor (Pa) | 3.13E+05 |
| | | Mass Flow manifold outlet end Monitor (kg/s) | 34.36 | Pressure Static tube 2 Monitor (Pa) | 6.26E+05 |
| | | Mass Flow distributor2 Monitor (kg/s) | 17.09 | Pressure Static tube 2end Monitor (Pa) | 3.18E+05 |
| | | Mass Flow distributor1 Monitor (kg/s) | -17.13 | Pressure Static tube 3 Monitor (Pa) | 3.65E+04 |
| | | Mass Flow tube 3 end Monitor (kg/s) | 1.40 | Pressure Static tube 3end Monitor (Pa) | 3.23E+05 |
| | | Mass Flow tube 3 Monitor (kg/s) | 1.41 | Pressure Static tube 4 Monitor (Pa) | 6.24E+05 |
| | | Mass Flow tube 4 Monitor (kg/s) | -1.40 | Pressure Static tube 4end Monitor (Pa) | 3.34E+05 |
| | | Mass Flow tube 5 Monitor (kg/s) | -1.40 | Pressure Static tube 5 Monitor (Pa) | 6.21E+05 |
| | | Mass Flow tube 6 Monitor (kg/s) | 1.40 | Pressure Static tube 5end Monitor (Pa) | 3.36E+05 |
| | | Mass Flow tube 7 Monitor (kg/s) | -1.41 | Pressure Static tube 6 Monitor (Pa) | 3.19E+04 |
| | | Mass Flow tube 8 Monitor (kg/s) | 1.43 | Pressure Static tube 6end Monitor (Pa) | 3.27E+05 |
| | | | | Pressure Static tube 7 Monitor (Pa) | 6.26E+05 |
| | | | | Pressure Static tube 7end Monitor (Pa) | 3.29E+05 |
| | | | | Pressure Static tube 8 Monitor (Pa) | 3.12E+04 |
| | | | | Pressure Static tube 8end Monitor (Pa) | 3.24E+05 |
| | | | | PressureInlet Monitor 2 (Pa) | 6.62E+05 |
| | | | | PressureOutlet Monitor 2 (Pa) | 0.00E+00 |
| | | | | Pressure Static manifold inlet end2 Monitor (Pa) | 2.09E+05 |

*Table 55 Complete results: CFD entire neutralizer Optimization 3, 40kg/s at inlet, 0bar outlet*

## Detailed results for simulation for Optimization 4

| Static pressure differences for each LEE | | Mass flows in each section | | Static pressure in each section | |
|---|---|---|---|---|---|
| Iteration | 5.25E+02 | Iteration | 525.00 | Iteration | 5.25E+02 |
| Pressure Drop IO Monitor (Pa) | 8.04E+05 | Mass Flow tube 1 Monitor (kg/s) | 1.52 | Pressure Static distributor1 Monitor (Pa) | 2.31E+05 |
| Pressure Drop inlet-outlet Monitor | 8.04E+05 | Mass Flow Inlet Monitor 2 (kg/s) | -40.00 | Pressure Static distributor1b Monitor (Pa) | 2.33E+05 |
| Pressure Drop tube 1 Monitor | 3.11E+05 | Mass Flow Outlet Monitor 2 (kg/s) | 40.07 | Pressure Static distributor2 Monitor (Pa) | -1.22E+04 |
| Pressure Drop tube 2 Monitor | 3.46E+05 | Mass Flow tube 2 Monitor (kg/s) | -1.53 | Pressure Static distributor2b Monitor (Pa) | -6.85E+03 |
| Pressure Drop tube 3 Monitor | 3.30E+05 | Mass Flow manifold outlet end3 Monitor (kg/s) | 33.89 | Pressure Static manifold inlet end Monitor (Pa) | 4.35E+05 |
| Pressure Drop tube 4 Monitor | 3.28E+05 | Mass Flow tube 2 end Monitor (kg/s) | -1.53 | Pressure Static manifold outlet end1 Monitor (Pa) | 1.32E+04 |

| | | | | | |
|---|---|---|---|---|---|
| Pressure Drop tube 5 Monitor | 3.29E+05 | Mass Flow distributor1b Monitor (kg/s) | -17.00 | Pressure Static manifold outlet end2 Monitor (Pa) | 1.37E+04 |
| Pressure Drop tube 6 Monitor | 3.28E+05 | Mass Flow manifold inlet end Monitor (kg/s) | -33.89 | Pressure Static manifold outlet end3 Monitor (Pa) | 1.62E+03 |
| Pressure Drop tube 7 Monitor | 3.49E+05 | Mass Flow distributor2b Monitor (kg/s) | 16.91 | Pressure Static tube 1 Monitor (Pa) | 3.38E+04 |
| Pressure Drop tube 8 Monitor | 3.08E+05 | Mass Flow tube 1 end Monitor (kg/s) | 1.53 | Pressure Static tube 1end Monitor (Pa) | 3.45E+05 |
| | | Mass Flow manifold outlet end Monitor (kg/s) | 33.94 | Pressure Static tube 2 Monitor (Pa) | 6.95E+05 |
| | | Mass Flow distributor2 Monitor (kg/s) | 16.82 | Pressure Static tube 2end Monitor (Pa) | 3.50E+05 |
| | | Mass Flow distributor1 Monitor (kg/s) | -16.89 | Pressure Static tube 3 Monitor (Pa) | 3.99E+04 |
| | | Mass Flow tube 3 end Monitor (kg/s) | 1.52 | Pressure Static tube 3end Monitor (Pa) | 3.70E+05 |
| | | Mass Flow tube 3 Monitor (kg/s) | 1.53 | Pressure Static tube 4 Monitor (Pa) | 7.08E+05 |
| | | Mass Flow tube 4 Monitor (kg/s) | -1.52 | Pressure Static tube 4end Monitor (Pa) | 3.80E+05 |
| | | Mass Flow tube 5 Monitor (kg/s) | -1.51 | Pressure Static tube 5 Monitor (Pa) | 7.03E+05 |
| | | Mass Flow tube 6 Monitor (kg/s) | 1.51 | Pressure Static tube 5end Monitor (Pa) | 3.74E+05 |
| | | Mass Flow tube 7 Monitor (kg/s) | -1.53 | Pressure Static tube 6 Monitor (Pa) | 3.59E+04 |
| | | Mass Flow tube 8 Monitor (kg/s) | 1.52 | Pressure Static tube 6end Monitor (Pa) | 3.64E+05 |
| | | | | Pressure Static tube 7 Monitor (Pa) | 7.01E+05 |
| | | | | Pressure Static tube 7end Monitor (Pa) | 3.52E+05 |
| | | | | Pressure Static tube 8 Monitor (Pa) | 3.95E+04 |
| | | | | Pressure Static tube 8end Monitor (Pa) | 3.47E+05 |
| | | | | PressureInlet Monitor 2 (Pa) | 8.04E+05 |
| | | | | PressureOutlet Monitor 2 (Pa) | 0.00E+00 |
| | | | | Pressure Static manifold inlet end2 Monitor (Pa) | 2.19E+05 |

*Table 56 Complete results: CFD entire neutralizer Optimization 4, 40kg/s at inlet, 0bar outlet*

# 2.1. Optimization of the operational conditions

## MATLAB script for heat load evaluation

```
%% deuterium
close all
clear all
clc

deuterium = load('DTT_NEU_no_field_w_LEE_deuterium.txt');
electrons = load('DTT_NEU_no_field_w_LEE_electrons.txt');
deuterium(:,4)=deuterium(:,4)*10^6;
```

```
electrons(:,4)=electrons(:,4)*10^6;

figure(1)
scatter3(deuterium(:,1), deuterium(:,2), deuterium(:,3), [], deuterium(:,4),
'filled')
title('Heat flux due to deuterium')
grid on
axis equal
ax = gca;
ax.XDir = 'reverse';
view(-31,14)
xlabel('X')
ylabel('Y')
zlabel('Z')
cb = colorbar;
cb.Label.String = 'Heat flux (W/m^2)';
%% electrons
figure(2)
scatter3(electrons(:,1), electrons(:,2),electrons(:,3), [], electrons(:,4),
'filled')
title('Heat flux due to electrons')
grid on
axis equal
ax = gca;
ax.XDir = 'reverse';
view(-31,14)
xlabel('X')
ylabel('Y')
zlabel('Z')
cb = colorbar;
cb.Label.String = 'Heat flux (W/m^2)';
%% sum
Xq = deuterium(:,1); Yq = deuterium(:,2); Zq = deuterium(:,3);
load_e = electrons(:,4);
X = electrons(:,1); Y = electrons(:,2); Z = electrons(:,3);
load_e_interp = griddata(X,Y,Z,load_e,Xq,Yq,Zq,'nearest');
ed=[Xq,Yq,Zq,load_e_interp+deuterium(:,4)];

figure(4)
scatter3(ed(:,1), ed(:,2),ed(:,3), [], ed(:,4), 'filled')
title('Heat flux due to electrons+deuterium')
grid on
axis equal
ax = gca;
ax.XDir = 'reverse';
view(-31,14)
xlabel('X')
ylabel('Y')
zlabel('Z')
cb = colorbar;
cb.Label.String = 'Heat flux (W/m^2)';
%% Peaks and locations
peak_ed=max(ed(:,4))
peak_e=max(electrons(:,4))
peak_d=max(deuterium(:,4))
peak_ed_location=ed(find(ed(:,4)==max(ed(:,4))),:)
peak_e_location=electrons(find(electrons(:,4)==max(electrons(:,4))),:)
peak_d_location=deuterium(find(deuterium(:,4)==max(deuterium(:,4))),:)
```

### Check on heat load

Check on total heat power considers percentage error between the simplified CAD (where the original boundary heat flux has been calculated by DTT S.c.a.r.l.) and the complex CAD (where simulations in this work have been performed).

| Simplified CAD | | Complex CAD | | Error |
|---|---|---|---|---|
| Heat Power bottom Monitor (W) | -5.07E+03 | Heat Power bottom Monitor (W) | -5.06E+03 | 0.23% |
| Heat Power bottomfront Monitor (W) | -3.26E+02 | Heat Power bottomfront Monitor (W) | -3.93E+02 | -20.85% |
| Heat Power central 1 Monitor (W) | -1.36E+05 | Heat Power central 1 Monitor (W) | -1.36E+05 | -0.02% |
| Heat Power central 2 Monitor (W) | -1.82E+05 | Heat Power central 2 Monitor (W) | -1.82E+05 | 0.09% |
| Heat Power halfway 1 Monitor (W) | -1.27E+05 | Heat Power halfway 1 Monitor (W) | -1.27E+05 | -0.06% |
| Heat Power halfway 1 inner Monitor (W) | -1.70E+05 | Heat Power halfway 1 inner Monitor (W) | -1.70E+05 | 0.13% |
| Heat Power halfway 2 Monitor (W) | -1.73E+05 | Heat Power halfway 2 Monitor (W) | -1.74E+05 | -0.26% |
| Heat Power halfway 2 inner Monitor (W) | -1.26E+05 | Heat Power halfway 2 inner Monitor (W) | -1.26E+05 | -0.09% |
| Heat Power LEE1 Monitor (W) | -3.13E+04 | Heat Power LEE1 Monitor (W) | -3.17E+04 | -1.33% |
| Heat Power LEE2 Monitor (W) | -5.94E+04 | Heat Power LEE2 Monitor (W) | -5.90E+04 | 0.65% |
| Heat Power LEE7 Monitor (W) | -5.80E+04 | Heat Power LEE7 Monitor (W) | -5.77E+04 | 0.42% |
| Heat Power LEE8 Monitor (W) | -2.80E+04 | Heat Power LEE8 Monitor (W) | -2.82E+04 | -0.58% |
| Heat Power LEEcentral Monitor (W) | -8.55E+04 | Heat Power LEEcentral Monitor (W) | -8.58E+04 | -0.40% |
| Heat Power lateral panel1 Monitor (W) | -1.76E+05 | Heat Power lateral panel1 Monitor (W) | -1.77E+05 | -0.20% |
| Heat Power lateral panel2 Monitor (W) | -1.32E+05 | Heat Power lateral panel2 Monitor (W) | -1.31E+05 | 0.02% |
| Heat Power top Monitor (W) | -2.21E+04 | Heat Power top Monitor (W) | -2.22E+04 | -0.03% |
| Heat Power topfront Monitor (W) | -1.94E+03 | Heat Power topfront Monitor (W) | -2.07E+03 | -6.62% |
| Total Heat Power Monitor (W) | -1.60E+06 | Total Heat Power Monitor (W) | -1.51E+06 | 5.38% |

*Table 57 Total power deposited on solid surfaces*

## 2.1.1. Minimum mass flow for LEEs

### MATLAB code developed for Tmax and pressure drop evaluation in the LEE

```
%% dati
clear all
close all
clc
```

```
m=2;%kg/s
delta=2/1000; %m
d=18/1000; %m
y=25/18;
L=1682/1000;%m
rho=997.561;%[kg/m3]
mu=8.89E-04;%[Pa*s]
cp=4181.72;%[J/(kg*K)]
k=0.620271;%[W/m*K]
A=104647.28*10^-6;%[m^2] area frontale del LEE

v=m/(rho*pi*d^2/4);
Reyno=rho*v*d/mu;
Pr=cp*mu/k;
Reyn=linspace(2*10^3,10^6,10000)';
%% friction factors and nusselt

f_Peth=@(Re)(0.790.*log(Re)-1.64).^-2; %Pethukov plain tube 3000<=Re<=5*10^6

f_ManBer=@(Re,delta,y)4*(0.0791.*Re.^-0.25).*((pi./(pi-
4*delta/d)).^1.75).*(((pi+2-2*delta/d)./(pi-
4*delta/d)).^1.25).*(1+2.06*(1+(2*y/pi)^2).^-0.74); %Manglik Bergles 1992
f_Man=@(Re,delta,y)4*(0.0791./Re.^0.25).*((pi./(pi-4*delta/d)).^1.75).*(((pi+2-
2*delta/d)./(pi-4*delta/d)).^1.25).*(1+2.752./y.^1.29); %Manglik 1991

Nu_Ditt=@(Re)0.023.*Re.^(4/5).*Pr.^0.4; %0.7<Pr<160  Re>10000  L/D>10 Dittus-
Boelter, Plain tube
phi=1;
Nu_ManBer=@(Re,delta,y)0.023.*Re.^0.8.*Pr.^0.4.*((pi./(pi-
4*delta/d)).^0.8).*(((pi+2-2*delta/d)./(pi-4*delta/d)).^0.2).*(1+0.769./y)*phi;
%twisted tape

figure(1)
subplot(2,1,1)
plot(Reyn,f_Peth(Reyn))
hold on
plot(Reyn,f_ManBer(Reyn,delta,y))
plot(Reyn,f_Man(Reyn,delta,y))
legend('Pethukov, plain tube','Manglik 1992, twisted tape','Manglik 1991,
twisted tape')
title('Friction factors from literature experimental correlations')
xlabel('Re')
ylabel('f')
subplot(2,1,2)
plot(Reyn,Nu_Ditt(Reyn))
hold on
plot(Reyn,Nu_ManBer(Reyn,delta,y))
legend('Dittus, plain tube','Manglik Bergles, twisted tape')
title('Nusselt from literature experimental correlations')
xlabel('Re')
ylabel('Nu')

%deltap_twistedtape1992=f_ManBer(Reyno)*((rho*v^2)/2)/(d/L)
% deltap_twistedtape1991=f_Man(Reyno,delta,y)*((rho*v^2)/2)/(d/L)
% deltap_plaintube=f_Peth(Reyno)*((rho*v^2)/2)/(d/L)


%% pressure drop as mdot function
vel=Reyn*mu/(rho*d);
```

```
mdot=vel*rho*(pi*d^2/4);
figure(2)
hold on

y=25/18;
deltap_tt1991=(f_Man(Reyn,delta,y).*((rho.*vel.^2)./2)./(d/L))*10^-5;
plot(mdot,deltap_tt1991,'linewidth',2,'DisplayName', ['Manglik Bergles, twisted
tape, y=', num2str(y),' delta=', num2str(delta*1000),'mm'])
for delta=[1,5]./1000
    deltap_tt1991=(f_Man(Reyn,delta,y).*((rho.*vel.^2)./2)./(d/L))*10^-5;
    plot(mdot,deltap_tt1991,'--','DisplayName', ['Manglik Bergles, twisted tape,
y=', num2str(y),' delta=', num2str(delta*1000),'mm'])
end

delta=2/1000; %m
for y=[50,100,300,400,600]./18
    deltap_tt1991=(f_Man(Reyn,delta,y).*((rho.*vel.^2)./2)./(d/L))*10^-5;
    plot(mdot,deltap_tt1991,'DisplayName', ['Manglik Bergles, twisted tape, y=',
num2str(y),' delta=', num2str(delta*1000),'mm'])
end
deltap_pt=(f_Peth(Reyn).*((rho.*vel.^2)./2)./(d/L))*10^-5;
plot(mdot,deltap_pt,'linewidth',2,'DisplayName', 'Dittus, plain tube')

xlabel('m_d_o_t (kg/s)')
ylabel('pressure drop (bar)')
title('Predicted Total pressure drop as mass flow function (from Manglik 1991
friction factor)')
legend('show')
ylim([0 1])
xlim([0 3.5])

%% Tsurface as m_dot function
Tin=(25+273.15)*ones(size(mdot,1),1); %inlet LEE temperature
q=1*10^6;%[W/m^2] %heat flux on frontal surface
Tout=q*A./(cp*mdot)+Tin; %toutlet LEE
Tpb=(Tin+Tout)/2; %average tempeature inlet outlet LEE
figure(3)
hold on

%1.5 MW/m^2
% Tplustt=30;
% Tpluspt=34;

%1 MW/m^2
Tplustt=33;
Tpluspt=27;

y=25/18;
%Tps=Tpb+(d/k).*(q./Nu_ManBer(Reyn,delta,y));%expected T_surface_ave on the
cylinder (fluid)
%Tps=Tpb+(d/k).*(q./Nu_ManBer(Reyn,delta,y))+Tplustt; %expected T_max on the
cylinder (fluid)
Tps=Tpb+(d/k).*(q./Nu_ManBer(Reyn,delta,y))-Tin+Tplustt; %expected T_max-T_min
in fluid cylindrical region
plot(mdot,Tps,'linewidth',2,'DisplayName', ['Manglik Bergles, twisted tape, y=',
num2str(y),' delta=', num2str(delta*1000),'mm'])
for delta=[1,5]./1000
    Tps=Tpb+(d/k).*(q./Nu_ManBer(Reyn,delta,y))-Tin+Tplustt;
```

```
    plot(mdot,Tps,'--','DisplayName', ['Manglik Bergles, twisted tape, y=',
num2str(y),' delta=', num2str(delta*1000),'mm'])
end

delta=2/1000; %[m]
for y=[50,100,300,400,600]./18
    Tps=Tpb+(d/k).*(q./Nu_ManBer(Reyn,delta,y))-Tin+Tplustt;
    plot(mdot,Tps,'DisplayName', ['Manglik Bergles, twisted tape, y=',
num2str(y),' delta=', num2str(delta*1000),'mm'])
end
Tps=Tpb+(d/k).*(q./Nu_Ditt(Reyn));%-Tin+Tpluspt;
plot(mdot,Tps,'linewidth',2,'DisplayName', 'Dittus, plain tube')

xlabel('m_d_o_t (kg/s)')
ylabel('T_m_a_x-T_m_i_n (°C)')
title('Predicted T_m_a_x-T_m_i_n in fluid as mass flow function (from Manglik
1991 Nusselt)')
legend('show')
ylim([70 92])
xlim([0.4 3.5])
```

### MATLAB code for alpha extrapolation from DTT data

```
clc
clear all
close all
T=[20   50  100 150 200 250 300 400 450 500 550 600]'+273.15;
alpha=10^-6*[16.7   17.0    17.3    17.5    17.7    17.8    18.0    18.1    18.2
18.4    18.5    18.6];
c=polyfit(T,alpha,4);
x=linspace(T(1),T(end),1000);
y=polyval(c,x);
figure
plot(x,y,'-',T,alpha,'o')
ylabel('coefficient of thermal expansion [K^-1]')
xlabel('Temperature [K]')
legend('fitting curve','provided data')
```

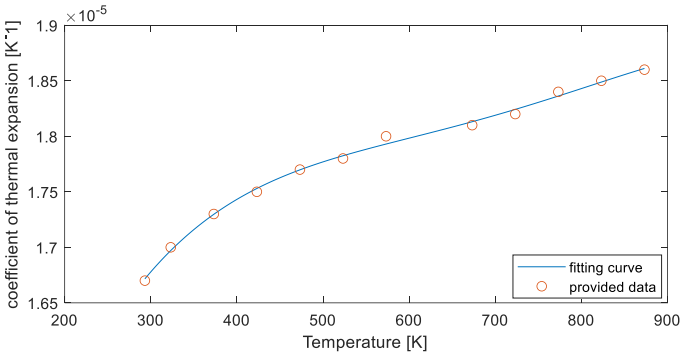


*Figure 141 CuCrZr, function for coefficient of thermal expansion*

## 2.1.2. Panels: minimum mass flow

### Rough convergence analysis on halfway panel 1

Tmax is the maximum temperature in fluid.

| | 3 prism layer | 5 prism layer | 7 prism layer | 8 prism layer |
|---|---|---|---|---|
| cells | 1.24E+07 | 1.50E+07 | 1.64E+07 | 66milioni |
| cells fluid | 7.89E+06 | 1.05E+07 | 1.22E+07 | 66000000 |
| cells solid | 4.51E+06 | 4.51E+06 | 4.17E+06 | |
| Iteration | 976 | 780 | 726 | |
| Pressure Drop 1 (Pa) | 9.67E+02 | 1.74E+03 | 1.73E+03 | 1.91E+03 |
| Pressure Drop 2 (Pa) | 9.74E+02 | 1.76E+03 | 1.75E+03 | 1.94E+03 |
| Pressure Drop 3 (Pa) | 9.99E+02 | 1.79E+03 | 1.77E+03 | 1.97E+03 |
| Pressure Drop 4 (Pa) | 1.00E+03 | 1.82E+03 | 1.80E+03 | 2.00E+03 |
| Pressure Drop 5 (Pa) | 1.02E+03 | 1.85E+03 | 1.83E+03 | 2.03E+03 |
| Pressure Drop 6 (Pa) | 1.03E+03 | 1.87E+03 | 1.84E+03 | 2.06E+03 |
| Pressure Drop 7 (Pa) | 1.04E+03 | 1.90E+03 | 1.88E+03 | 2.09E+03 |
| Pressure Drop 8 (Pa) | 1.06E+03 | 1.93E+03 | 1.91E+03 | 2.13E+03 |
| Pressure Drop 9 (Pa) | 1.07E+03 | 1.95E+03 | 1.93E+03 | 2.15E+03 |
| Pressure Drop 10 (Pa) | 1.08E+03 | 1.98E+03 | 1.96E+03 | 2.19E+03 |
| Pressure Drop 11 (Pa) | 1.10E+03 | 2.01E+03 | 1.99E+03 | 2.22E+03 |
| Pressure Drop 12 (Pa) | 1.12E+03 | 2.04E+03 | 2.02E+03 | 2.25E+03 |
| **Pressure Drop 13 (Pa)** | **1.16E+03** | **2.08E+03** | **2.05E+03** | **2.27E+03** |
| Temperature2 (K) | 322.9860412 | 322.3459249 | 322.2763107 | 3.22E+02 |
| Temperature4 (K) | 324.7147991 | 324.9341539 | 324.9493064 | 3.25E+02 |
| Temperature6 (K) | 324.8904188 | 325.4176427 | 325.4083488 | 3.25E+02 |
| Temperature8 (K) | 322.3421232 | 322.201638 | 322.1541333 | 3.22E+02 |
| Temperature10 (K) | 321.1955432 | 321.3363597 | 321.3242502 | 3.21E+02 |
| Temperature12 (K) | 319.5299328 | 319.5436453 | 319.4931367 | 3.19E+02 |
| Temperature14 (K) | 317.587958 | 317.5000742 | 317.4675434 | 3.17E+02 |
| Temperature16 (K) | 316.0322779 | 315.2748564 | 315.1993565 | 3.15E+02 |
| Temperature18 (K) | 318.2338422 | 318.6125668 | 318.6058334 | 3.19E+02 |
| Temperature20 (K) | 318.2631195 | 318.51558 | 318.4976169 | 3.18E+02 |
| Temperature22 (K) | 316.6977202 | 316.5125982 | 316.4878706 | 3.16E+02 |
| Temperature24 (K) | 316.3846308 | 315.4182989 | 315.3529449 | 3.15E+02 |
| Temperature26 (K) | 320.8219508 | 321.6989481 | 321.7570213 | 3.22E+02 |
| **Tmax (K)** | **473.7952091** | **383.3365808** | **379.9416624** | **3.73E+02** |

*Table 58 Rough convergence analysis for halfway panel 1 for minimum mass flow determination in panels*

## Panels: results for minimum mass flow determination

| | HALFWAY 1 | HALFWAY 2 | | | | LATERAL 1 | | | CENTRAL 2 | |
|---|---|---|---|---|---|---|---|---|---|---|
| | 0.25kg/s | 0.25kg/s | 0.18 kg/s | 0.15 kg/s | 0.10 kg/s | 0.25kg/s | 0.10 kg/s | 0.05 kg/s | 0.10 kg/s | 0.07kg/s |
| cells | 1.64E+07 | 1.64E+07 | | | | 2.58E+07 | | | 2.54E+07 | |

| cells fluid | 1.22E+07 | 1.22E+07 | | | | 1.95E+07 | | | 1.97E+07 | |
|---|---|---|---|---|---|---|---|---|---|---|
| cells solid | 4.17E+06 | 4.18E+06 | | | | 6.31E+06 | | | 5.75E+06 | |
| Iteration | 726 | 720 | 837 | 904 | | 805 | 1488 | 1508 | 1544 | 2006 |
| Pressure Drop 1 (Pa) | 1.73E+03 | 1.73E+03 | 9.61E+02 | 6.72E+02 | | 4.46E+03 | 8.22E+02 | 2.61E+02 | 8.21E+02 | 4.60E+02 |
| Pressure Drop 2 (Pa) | 1.75E+03 | 1.75E+03 | 9.75E+02 | 6.82E+02 | | 4.50E+03 | 8.28E+02 | 2.65E+02 | 8.29E+02 | 4.58E+02 |
| Pressure Drop 3 (Pa) | 1.77E+03 | 1.77E+03 | 9.85E+02 | 6.88E+02 | | 4.43E+03 | 8.32E+02 | 2.61E+02 | 8.67E+02 | 4.67E+02 |
| Pressure Drop 4 (Pa) | 1.80E+03 | 1.80E+03 | 1.00E+03 | 7.00E+02 | | 4.53E+03 | 8.47E+02 | 2.60E+02 | 8.56E+02 | 4.71E+02 |
| Pressure Drop 5 (Pa) | 1.83E+03 | 1.83E+03 | 1.02E+03 | 7.09E+02 | | 4.67E+03 | 8.39E+02 | 2.67E+02 | 8.65E+02 | 4.69E+02 |
| Pressure Drop 6 (Pa) | 1.84E+03 | 1.86E+03 | 1.03E+03 | 7.19E+02 | | 4.63E+03 | 8.40E+02 | 2.67E+02 | 8.76E+02 | 4.76E+02 |
| Pressure Drop 7 (Pa) | 1.88E+03 | 1.88E+03 | 1.05E+03 | 7.29E+02 | | 4.61E+03 | 8.56E+02 | 2.66E+02 | 8.52E+02 | 4.63E+02 |
| Pressure Drop 8 (Pa) | 1.91E+03 | 1.91E+03 | 1.06E+03 | 7.43E+02 | | 4.81E+03 | 8.80E+02 | 2.71E+02 | 8.97E+02 | 4.84E+02 |
| Pressure Drop 9 (Pa) | 1.93E+03 | 1.94E+03 | 1.08E+03 | 7.52E+02 | | 4.72E+03 | 8.63E+02 | 2.70E+02 | 8.74E+02 | 4.79E+02 |
| Pressure Drop 10 (Pa) | 1.96E+03 | 1.96E+03 | 1.09E+03 | 7.61E+02 | | 4.77E+03 | 8.81E+02 | 2.78E+02 | 8.92E+02 | 4.82E+02 |
| Pressure Drop 11 (Pa) | 1.99E+03 | 1.99E+03 | 1.11E+03 | 7.72E+02 | | 4.83E+03 | 8.78E+02 | 2.80E+02 | 8.93E+02 | 4.91E+02 |
| Pressure Drop 12 (Pa) | 2.02E+03 | 2.02E+03 | 1.12E+03 | 7.82E+02 | | 4.82E+03 | 8.90E+02 | 2.79E+02 | 9.11E+02 | 4.94E+02 |
| **Pressure Drop 13 (Pa)** | **2.05E+03** | **2.04E+03** | **1.14E+03** | **7.92E+02** | | **4.89E+03** | **9.11E+02** | **2.83E+02** | **9.03E+02** | **4.88E+02** |
| Temperature2 (K) | 322.28 | 326.32 | 337.10 | 344.90 | | 309.60 | 327.29 | 357.52 | 331.47 | 345.92 |
| Temperature4 (K) | 324.95 | 324.81 | 335.31 | 342.86 | | 311.95 | 332.02 | 364.49 | 331.96 | 346.71 |
| Temperature6 (K) | 325.41 | 325.63 | 335.95 | 343.18 | | 312.51 | 332.91 | 366.24 | 334.78 | 349.65 |
| Temperature8 (K) | 322.15 | 320.65 | 329.69 | 336.24 | | 310.82 | 331.13 | 363.98 | 329.35 | 343.49 |
| Temperature10 (K) | 321.32 | 320.17 | 328.79 | 334.98 | | 312.53 | 333.25 | 366.20 | 333.12 | 347.53 |
| Temperature12 (K) | 319.49 | 319.96 | 328.38 | 334.35 | | 311.01 | 330.38 | 361.68 | 331.49 | 346.04 |
| Temperature14 (K) | 317.47 | 318.26 | 326.14 | 331.79 | | 310.01 | 328.38 | 357.85 | 330.43 | 343.50 |
| Temperature16 (K) | 315.20 | 317.47 | 325.11 | 330.63 | | 308.97 | 326.21 | 354.47 | 328.02 | 341.31 |
| Temperature18 (K) | 318.61 | 318.42 | 326.27 | 331.84 | | 309.97 | 327.74 | 356.75 | 328.39 | 341.87 |
| Temperature20 (K) | 318.50 | 318.49 | 326.29 | 331.78 | | 310.63 | 328.69 | 357.56 | 330.14 | 343.12 |
| Temperature22 (K) | 316.49 | 316.19 | 323.43 | 328.67 | | 309.06 | 326.38 | 354.97 | 327.96 | 340.93 |
| Temperature24 (K) | 315.35 | 315.77 | 323.30 | 328.89 | | 308.84 | 327.21 | 357.73 | 326.93 | 340.87 |
| Temperature26 (K) | 321.76 | 325.35 | 335.38 | 342.13 | | 314.46 | 337.51 | 372.76 | 339.80 | 356.21 |
| **Tmax (K)** | **379.94** | **385.19** | **413.89** | **440.75** | **557.76** | **347.01** | **417.80** | **499.39** | **423.72** | **468.99** |

*Table 59 Iterative solution for the minimum mass flow determination in panels*

## 2.1.3 Entire neutralizer: total mass flow and real BCs calculation

Four models have been built for the rough mesh convergence on the entire neutralizer. The final selected one, as a result of convergence, is the 175 million fluid cells.

## CFD 175 million cells 17.7kg/s at inlet, 0bar outlet

Total number of cells in fluid: 174918429

| pressure drop sui singoli LEE e sul totale | | | | | |
|---|---|---|---|---|---|
| Iteration | 2000 | Iteration | 2000 | Iteration | 2000 |
| Pressure Drop IO Monitor (Pa) | 1.79E+05 | Mass Flow tube 1 Monitor (kg/s) | 1.89 | Pressure Static distributor1 Monitor (Pa) | 9.87E+04 |
| Pressure Drop inlet-outlet Monitor | 1.79E+05 | Mass Flow Inlet Monitor 2 (kg/s) | -17.70 | Pressure Static distributor1b Monitor (Pa) | 9.87E+04 |
| Pressure Drop tube 1 Monitor | 4.59E+04 | Mass Flow Outlet Monitor 2 (kg/s) | 17.74 | Pressure Static distributor2 Monitor (Pa) | 7.54E+04 |
| Pressure Drop tube 2 Monitor | 4.04E+04 | Mass Flow tube 2 Monitor (kg/s) | -1.89 | Pressure Static distributor2b Monitor (Pa) | 7.60E+04 |
| Pressure Drop tube 3 Monitor | 3.60E+04 | Mass Flow manifold outlet end3 Monitor (kg/s) | 10.34 | Pressure Static manifold inlet end Monitor (Pa) | 1.16E+05 |
| Pressure Drop tube 4 Monitor | 3.82E+04 | Mass Flow tube 2 end Monitor (kg/s) | -1.89 | Pressure Static manifold outlet end1 Monitor (Pa) | 6.74E+03 |
| Pressure Drop tube 5 Monitor | 3.57E+04 | Mass Flow distributor1b Monitor (kg/s) | -5.12 | Pressure Static manifold outlet end2 Monitor (Pa) | 8.64E+03 |
| Pressure Drop tube 6 Monitor | 3.98E+04 | Mass Flow manifold inlet end Monitor (kg/s) | -10.31 | Pressure Static manifold outlet end3 Monitor (Pa) | 2.25E+04 |
| Pressure Drop tube 7 Monitor | 3.96E+04 | Mass Flow distributor2b Monitor (kg/s) | 5.13 | Pressure Static tube 1 Monitor (Pa) | 2.84E+04 |
| Pressure Drop tube 8 Monitor | 4.78E+04 | Mass Flow tube 1 end Monitor (kg/s) | 1.89 | Pressure Static tube 1end Monitor (Pa) | 7.43E+04 |
| | | Mass Flow manifold outlet end Monitor (kg/s) | 10.34 | Pressure Static tube 2 Monitor (Pa) | 1.25E+05 |
| | | Mass Flow distributor2 Monitor (kg/s) | 5.20 | Pressure Static tube 2end Monitor (Pa) | 8.46E+04 |
| | | Mass Flow distributor1 Monitor (kg/s) | -5.19 | Pressure Static tube 3 Monitor (Pa) | 2.65E+04 |
| | | Mass Flow tube 3 end Monitor (kg/s) | 1.80 | Pressure Static tube 3end Monitor (Pa) | 6.24E+04 |
| Pressure Drop IO Monitor 2 (Pa) | 1.79E+05 | Mass Flow tube 3 Monitor (kg/s) | 1.80 | Pressure Static tube 4 Monitor (Pa) | 1.26E+05 |
| PressureMassFlowAveLEE1 Monitor (Pa) | 1.60E+05 | Mass Flow tube 4 Monitor (kg/s) | -1.80 | Pressure Static tube 4end Monitor (Pa) | 8.75E+04 |
| PressureMassFlowAveLEE1end Monitor (Pa) | 2.06E+05 | Mass Flow tube 5 Monitor (kg/s) | -1.79 | Pressure Static tube 5 Monitor (Pa) | 1.24E+05 |
| PressurMassFlowAvedistributor1 Monitor (Pa) | 2.11E+05 | Mass Flow tube 6 Monitor (kg/s) | 1.78 | Pressure Static tube 5end Monitor (Pa) | 8.87E+04 |
| PressurMassFlowAvedistributor2 Monitor (Pa) | 1.92E+05 | Mass Flow tube 7 Monitor (kg/s) | -1.91 | Pressure Static tube 6 Monitor (Pa) | 2.33E+04 |
| 1_pressure diff inlet-sbendinlet Monitor | 1.53E+03 | Mass Flow tube 8 Monitor (kg/s) | 1.90 | Pressure Static tube 6end Monitor (Pa) | 6.30E+04 |
| 2_pressure diff sbendinlet-manifoldinletend2 Monitor | 6.81E+04 | | | Pressure Static tube 7 Monitor (Pa) | 1.23E+05 |
| 2b_pressure diff sbendinlet-LEE2 Monitor | 5.23E+04 | | | Pressure Static tube 7end Monitor (Pa) | 8.31E+04 |
| 3_pressure diff manifoldinletend2-distributor1 Monitor | 1.05E+04 | | | Pressure Static tube 8 Monitor (Pa) | 2.56E+04 |
| 3b_pressure diff LEE2-LEE1 Monitor | 9.65E+04 | | | Pressure Static tube 8end Monitor (Pa) | 7.35E+04 |
| 4_pressure diff distributor1-distributor2 Monitor | 2.33E+04 | | | PressureInlet Monitor 2 (Pa) | 1.79E+05 |
| 4b_pressure diff LEE1-sbendoutlet Monitor | 2.68E+04 | | | PressureOutlet Monitor 2 (Pa) | 0.00E+00 |
| 5_pressure diff distributor2-manifoldoutletend2 Monitor | 6.68E+04 | | | PressureSbendinlet Monitor (Pa) | 1.77E+05 |

| | | | | | |
|---|---|---|---|---|---|
| 6_pressure diff manifoldoutletend2-sbendoutlet Monitor | 7.04E+03 | | | PressureSbendoutlet Monitor (Pa) | 1.60E+03 |
| 7_pressure diff sbendoutlet-outlet Monitor | 1.60E+03 | | | Pressure Static manifoldinletend2 (Pa) | 1.09E+05 |

*Table 60 Complete results: CFD entire neutralizer, 17.7kg/s at inlet, 0bar outlet. Fluid cells, 175 million*

| Iteration | 2045 | Iteration | 2045 | Iteration | 2045 |
|---|---|---|---|---|---|
| c1 1 Monitor (kg/s) | -0.09 | l1 1 Monitor (kg/s) | -0.09 | h1 1 Monitor (kg/s) | -0.23 |
| c1 3 Monitor (kg/s) | -0.09 | l1 3 Monitor (kg/s) | -0.09 | h1 3 Monitor (kg/s) | -0.23 |
| c1 5 Monitor (kg/s) | -0.09 | l1 5 Monitor (kg/s) | -0.09 | h1 5 Monitor (kg/s) | -0.23 |
| c1 7 Monitor (kg/s) | -0.09 | l1 7 Monitor (kg/s) | -0.09 | h1 7 Monitor (kg/s) | -0.23 |
| c1 9 Monitor (kg/s) | -0.09 | l1 9 Monitor (kg/s) | -0.09 | h1 9 Monitor (kg/s) | -0.23 |
| c1 11 Monitor (kg/s) | -0.09 | l1 11 Monitor (kg/s) | -0.09 | h1 11 Monitor (kg/s) | -0.22 |
| c1 13 Monitor (kg/s) | -0.09 | l1 13 Monitor (kg/s) | -0.09 | h1 13 Monitor (kg/s) | -0.20 |
| c1 15 Monitor (kg/s) | -0.08 | l1 15 Monitor (kg/s) | -0.08 | h1 15 Monitor (kg/s) | -0.18 |
| c1 17 Monitor (kg/s) | -0.09 | l1 17 Monitor (kg/s) | -0.09 | h1 17 Monitor (kg/s) | -0.22 |
| c1 19 Monitor (kg/s) | -0.09 | l1 19 Monitor (kg/s) | -0.09 | h1 19 Monitor (kg/s) | -0.22 |
| c1 21 Monitor (kg/s) | -0.09 | l1 21 Monitor (kg/s) | -0.09 | h1 21 Monitor (kg/s) | -0.21 |
| c1 23 Monitor (kg/s) | -0.09 | l1 23 Monitor (kg/s) | -0.09 | h1 23 Monitor (kg/s) | -0.21 |
| c1 25 Monitor (kg/s) | -0.09 | l1 25 Monitor (kg/s) | -0.09 | h1 25 Monitor (kg/s) | -0.21 |
| | | | | | |
| Iteration | 2045 | Iteration | 2045 | Iteration | 2045 |
| c2 1 Monitor (kg/s) | -0.09 | l2 1 Monitor (kg/s) | -0.09 | h2 1 Monitor (kg/s) | -0.23 |
| c2 3 Monitor (kg/s) | -0.09 | l2 3 Monitor (kg/s) | -0.09 | h2 3 Monitor (kg/s) | -0.23 |
| c2 5 Monitor (kg/s) | -0.09 | l2 5 Monitor (kg/s) | -0.09 | h2 5 Monitor (kg/s) | -0.23 |
| c2 7 Monitor (kg/s) | -0.09 | l2 7 Monitor (kg/s) | -0.09 | h2 7 Monitor (kg/s) | -0.22 |
| c2 9 Monitor (kg/s) | -0.09 | l2 9 Monitor (kg/s) | -0.09 | h2 9 Monitor (kg/s) | -0.23 |
| c2 11 Monitor (kg/s) | -0.09 | l2 11 Monitor (kg/s) | -0.09 | h2 11 Monitor (kg/s) | -0.22 |
| c2 13 Monitor (kg/s) | -0.09 | l2 13 Monitor (kg/s) | -0.09 | h2 13 Monitor (kg/s) | -0.20 |
| c2 15 Monitor (kg/s) | -0.08 | l2 15 Monitor (kg/s) | -0.08 | h2 15 Monitor (kg/s) | -0.19 |
| c2 17 Monitor (kg/s) | -0.09 | l2 17 Monitor (kg/s) | -0.09 | h2 17 Monitor (kg/s) | -0.22 |
| c2 19 Monitor (kg/s) | -0.09 | l2 19 Monitor (kg/s) | -0.09 | h2 19 Monitor (kg/s) | -0.21 |
| c2 21 Monitor (kg/s) | -0.09 | l2 21 Monitor (kg/s) | -0.09 | h2 21 Monitor (kg/s) | -0.21 |
| c2 23 Monitor (kg/s) | -0.09 | l2 23 Monitor (kg/s) | -0.09 | h2 23 Monitor (kg/s) | -0.21 |
| c2 25 Monitor (kg/s) | -0.09 | l2 25 Monitor (kg/s) | -0.09 | h2 25 Monitor (kg/s) | -0.21 |

*Table 61 Mass flow in panels channels. Complete results: CFD entire neutralizer, 17.7kg/s at inlet, 0bar outlet. Fluid cells, 175 million*

## CFD 44 million cells 17.7kg/s at inlet, 0bar outlet

| pressure drop sui singoli LEE e sul totale | | | | | |
|---|---|---|---|---|---|
| Iteration | 5000 | Iteration | 5000 | Iteration | 5000 |
| Pressure Drop IO Monitor (Pa) | 1.71E+05 | Mass Flow tube 1 Monitor (kg/s) | 1.92 | Pressure Static distributor1 Monitor (Pa) | 9.62E+04 |
| Pressure Drop inlet-outlet Monitor | 1.71E+05 | Mass Flow Inlet Monitor 2 (kg/s) | -17.70 | Pressure Static distributor1b Monitor (Pa) | 9.60E+04 |
| Pressure Drop tube 1 Monitor | 4.08E+04 | Mass Flow Outlet Monitor 2 (kg/s) | 17.71 | Pressure Static distributor2 Monitor (Pa) | 7.26E+04 |
| Pressure Drop tube 2 Monitor | 4.08E+04 | Mass Flow tube 2 Monitor (kg/s) | -1.92 | Pressure Static distributor2b Monitor (Pa) | 7.24E+04 |

| | | | | | |
|---|---|---|---|---|---|
| Pressure Drop tube 3 Monitor | 3.74E+04 | Mass Flow manifold outlet end3 Monitor (kg/s) | 10.23 | Pressure Static manifold inlet end Monitor (Pa) | 1.08E+05 |
| Pressure Drop tube 4 Monitor | 3.63E+04 | Mass Flow tube 2 end Monitor (kg/s) | -1.91 | Pressure Static manifold outlet end1 Monitor (Pa) | 1.02E+04 |
| Pressure Drop tube 5 Monitor | 3.75E+04 | Mass Flow distributor1b Monitor (kg/s) | -5.12 | Pressure Static manifold outlet end2 Monitor (Pa) | 1.12E+04 |
| Pressure Drop tube 6 Monitor | 3.80E+04 | Mass Flow manifold inlet end Monitor (kg/s) | -10.22 | Pressure Static manifold outlet end3 Monitor (Pa) | 1.97E+04 |
| Pressure Drop tube 7 Monitor | 3.81E+04 | Mass Flow distributor2b Monitor (kg/s) | 5.10 | Pressure Static tube 1 Monitor (Pa) | 2.31E+04 |
| Pressure Drop tube 8 Monitor | 3.85E+04 | Mass Flow tube 1 end Monitor (kg/s) | 1.92 | Pressure Static tube 1end Monitor (Pa) | 6.39E+04 |
| | | Mass Flow manifold outlet end Monitor (kg/s) | 10.23 | Pressure Static tube 2 Monitor (Pa) | 1.14E+05 |
| | | Mass Flow distributor2 Monitor (kg/s) | 5.11 | Pressure Static tube 2end Monitor (Pa) | 7.35E+04 |
| | | Mass Flow distributor1 Monitor (kg/s) | -5.11 | Pressure Static tube 3 Monitor (Pa) | 2.90E+04 |
| | | Mass Flow tube 3 end Monitor (kg/s) | 1.82 | Pressure Static tube 3end Monitor (Pa) | 6.63E+04 |
| Pressure Drop IO Monitor 2 (Pa) | 1.71E+05 | Mass Flow tube 3 Monitor (kg/s) | 1.82 | Pressure Static tube 4 Monitor (Pa) | 1.15E+05 |
| PressureMassFlowAveLEE1 Monitor (Pa) | 1.56E+05 | Mass Flow tube 4 Monitor (kg/s) | -1.82 | Pressure Static tube 4end Monitor (Pa) | 7.91E+04 |
| PressureMassFlowAveLEE1end Monitor (Pa) | 1.96E+05 | Mass Flow tube 5 Monitor (kg/s) | -1.83 | Pressure Static tube 5 Monitor (Pa) | 1.13E+05 |
| PressurMassFlowAvedistributor 1 Monitor (Pa) | 2.08E+05 | Mass Flow tube 6 Monitor (kg/s) | 1.83 | Pressure Static tube 5end Monitor (Pa) | 7.51E+04 |
| PressurMassFlowAvedistributor 2 Monitor (Pa) | 1.88E+05 | Mass Flow tube 7 Monitor (kg/s) | -1.85 | Pressure Static tube 6 Monitor (Pa) | 2.42E+04 |
| 1_pressure diff inlet-sbendinlet Monitor | 1.51E+03 | Mass Flow tube 8 Monitor (kg/s) | 1.85 | Pressure Static tube 6end Monitor (Pa) | 6.21E+04 |
| 2_pressure diff sbendinlet-manifoldinletend2 Monitor | 7.12E+04 | | | Pressure Static tube 7 Monitor (Pa) | 1.15E+05 |
| 2b_pressure diff sbendinlet-LEE2 Monitor | 5.49E+04 | | | Pressure Static tube 7end Monitor (Pa) | 7.70E+04 |
| 3_pressure diff manifoldinletend2-distributor1 Monitor | 1.76E+03 | | | Pressure Static tube 8 Monitor (Pa) | 2.95E+04 |
| 3b_pressure diff LEE2-LEE1 Monitor | 9.12E+04 | | | Pressure Static tube 8end Monitor (Pa) | 6.80E+04 |
| 4_pressure diff distributor1-distributor2 Monitor | 2.36E+04 | | | PressureInlet Monitor 2 (Pa) | 1.71E+05 |

| | | | | | |
|---|---|---|---|---|---|
| 4b_pressure diff LEE1-sbendoutlet Monitor | 2.24E+04 | | | PressureOutlet Monitor 2 (Pa) | -1.06E-03 |
| 5_pressure diff distributor2-manifoldoutletend2 Monitor | 6.14E+04 | | | PressureSbendinlet Monitor (Pa) | 1.69E+05 |
| 6_pressure diff manifoldoutletend2-sbendoutlet Monitor | 1.05E+04 | | | PressureSbendoutlet Monitor (Pa) | 7.51E+02 |

*Table 62 Complete results: CFD entire neutralizer, 17.7kg/s at inlet, 0bar outlet. Fluid cells, 44 million*

| Iteration | 5000 | Iteration | 5000 | Iteration | 5000 |
|---|---|---|---|---|---|
| c1 1 Monitor (kg/s) | -0.09 | l1 1 Monitor (kg/s) | -0.09 | h1 1 Monitor (kg/s) | -0.23 |
| c1 3 Monitor (kg/s) | -0.09 | l1 3 Monitor (kg/s) | -0.09 | h1 3 Monitor (kg/s) | -0.23 |
| c1 5 Monitor (kg/s) | -0.09 | l1 5 Monitor (kg/s) | -0.09 | h1 5 Monitor (kg/s) | -0.22 |
| c1 7 Monitor (kg/s) | -0.09 | l1 7 Monitor (kg/s) | -0.09 | h1 7 Monitor (kg/s) | -0.22 |
| c1 9 Monitor (kg/s) | -0.09 | l1 9 Monitor (kg/s) | -0.09 | h1 9 Monitor (kg/s) | -0.22 |
| c1 11 Monitor (kg/s) | -0.09 | l1 11 Monitor (kg/s) | -0.09 | h1 11 Monitor (kg/s) | -0.22 |
| c1 13 Monitor (kg/s) | -0.09 | l1 13 Monitor (kg/s) | -0.09 | h1 13 Monitor (kg/s) | -0.20 |
| c1 15 Monitor (kg/s) | -0.08 | l1 15 Monitor (kg/s) | -0.08 | h1 15 Monitor (kg/s) | -0.19 |
| c1 17 Monitor (kg/s) | -0.09 | l1 17 Monitor (kg/s) | -0.09 | h1 17 Monitor (kg/s) | -0.21 |
| c1 19 Monitor (kg/s) | -0.09 | l1 19 Monitor (kg/s) | -0.09 | h1 19 Monitor (kg/s) | -0.21 |
| c1 21 Monitor (kg/s) | -0.09 | l1 21 Monitor (kg/s) | -0.09 | h1 21 Monitor (kg/s) | -0.21 |
| c1 23 Monitor (kg/s) | -0.09 | l1 23 Monitor (kg/s) | -0.09 | h1 23 Monitor (kg/s) | -0.21 |
| c1 25 Monitor (kg/s) | -0.09 | l1 25 Monitor (kg/s) | -0.09 | h1 25 Monitor (kg/s) | -0.21 |
| | | | | | |
| Iteration | 5000 | Iteration | 5000 | Iteration | 5000 |
| c2 1 Monitor (kg/s) | -0.09 | l2 1 Monitor (kg/s) | -0.09 | h2 1 Monitor (kg/s) | -0.23 |
| c2 3 Monitor (kg/s) | -0.09 | l2 3 Monitor (kg/s) | -0.09 | h2 3 Monitor (kg/s) | -0.22 |
| c2 5 Monitor (kg/s) | -0.09 | l2 5 Monitor (kg/s) | -0.09 | h2 5 Monitor (kg/s) | -0.22 |
| c2 7 Monitor (kg/s) | -0.09 | l2 7 Monitor (kg/s) | -0.09 | h2 7 Monitor (kg/s) | -0.22 |
| c2 9 Monitor (kg/s) | -0.09 | l2 9 Monitor (kg/s) | -0.09 | h2 9 Monitor (kg/s) | -0.22 |
| c2 11 Monitor (kg/s) | -0.09 | l2 11 Monitor (kg/s) | -0.09 | h2 11 Monitor (kg/s) | -0.22 |
| c2 13 Monitor (kg/s) | -0.08 | l2 13 Monitor (kg/s) | -0.09 | h2 13 Monitor (kg/s) | -0.20 |
| c2 15 Monitor (kg/s) | -0.08 | l2 15 Monitor (kg/s) | -0.08 | h2 15 Monitor (kg/s) | -0.19 |
| c2 17 Monitor (kg/s) | -0.09 | l2 17 Monitor (kg/s) | -0.09 | h2 17 Monitor (kg/s) | -0.21 |
| c2 19 Monitor (kg/s) | -0.09 | l2 19 Monitor (kg/s) | -0.09 | h2 19 Monitor (kg/s) | -0.21 |
| c2 21 Monitor (kg/s) | -0.09 | l2 21 Monitor (kg/s) | -0.09 | h2 21 Monitor (kg/s) | -0.21 |
| c2 23 Monitor (kg/s) | -0.09 | l2 23 Monitor (kg/s) | -0.09 | h2 23 Monitor (kg/s) | -0.21 |
| c2 25 Monitor (kg/s) | -0.09 | l2 25 Monitor (kg/s) | -0.09 | h2 25 Monitor (kg/s) | -0.21 |

*Table 63 Mass flow in panels channels. Complete results: CFD entire neutralizer, 17.7kg/s at inlet, 0bar outlet. Fluid cells, 44 million*

## CFD 73 million cells 17.7kg/s at inlet, 0bar outlet

Total number of cells: 73277153

| pressure drop sui singoli LEE e sul totale | | | | | |
|---|---|---|---|---|---|
| Iteration | 2045 | Iteration | 2045 | Iteration | 2045 |
| Pressure Drop IO Monitor (Pa) | 1.62E+05 | Mass Flow tube 1 Monitor (kg/s) | 1.89 | Pressure Static distributor1 Monitor (Pa) | 8.53E+04 |
| Pressure Drop inlet-outlet Monitor | 1.62E+05 | Mass Flow Inlet Monitor 2 (kg/s) | -17.70 | Pressure Static distributor1b Monitor (Pa) | 8.68E+04 |
| Pressure Drop tube 1 Monitor | 3.70E+04 | Mass Flow Outlet Monitor 2 (kg/s) | 17.66 | Pressure Static distributor2 Monitor (Pa) | 6.16E+04 |

| | | | | | |
|---|---|---|---|---|---|
| Pressure Drop tube 2 Monitor | 3.86E+04 | Mass Flow tube 2 Monitor (kg/s) | -1.89 | Pressure Static distributor2b Monitor (Pa) | 6.39E+04 |
| Pressure Drop tube 3 Monitor | 2.66E+04 | Mass Flow manifold outlet end3 Monitor (kg/s) | 10.28 | Pressure Static manifold inlet end Monitor (Pa) | 9.72E+04 |
| Pressure Drop tube 4 Monitor | 3.42E+04 | Mass Flow tube 2 end Monitor (kg/s) | -1.89 | Pressure Static manifold outlet end1 Monitor (Pa) | 9.32E+03 |
| Pressure Drop tube 5 Monitor | 3.15E+04 | Mass Flow distributor1b Monitor (kg/s) | -5.16 | Pressure Static manifold outlet end2 Monitor (Pa) | 1.01E+04 |
| Pressure Drop tube 6 Monitor | 2.97E+04 | Mass Flow manifold inlet end Monitor (kg/s) | -10.31 | Pressure Static manifold outlet end3 Monitor (Pa) | 1.38E+04 |
| Pressure Drop tube 7 Monitor | 3.63E+04 | Mass Flow distributor2b Monitor (kg/s) | 5.09 | Pressure Static tube 1 Monitor (Pa) | 2.29E+04 |
| Pressure Drop tube 8 Monitor | 3.54E+04 | Mass Flow tube 1 end Monitor (kg/s) | 1.89 | Pressure Static tube 1end Monitor (Pa) | 5.99E+04 |
| | | Mass Flow manifold outlet end Monitor (kg/s) | 10.28 | Pressure Static tube 2 Monitor (Pa) | 1.08E+05 |
| | | Mass Flow distributor2 Monitor (kg/s) | 5.15 | Pressure Static tube 2end Monitor (Pa) | 6.89E+04 |
| | | Mass Flow distributor1 Monitor (kg/s) | -5.16 | Pressure Static tube 3 Monitor (Pa) | 2.58E+04 |
| Iteration | 2045 | Mass Flow tube 3 end Monitor (kg/s) | 1.77 | Pressure Static tube 3end Monitor (Pa) | 5.24E+04 |
| Pressure Drop IO Monitor 2 (Pa) | 1.62E+05 | Mass Flow tube 3 Monitor (kg/s) | 1.77 | Pressure Static tube 4 Monitor (Pa) | 1.11E+05 |
| PressureMassFlowAveLEE1 Monitor (Pa) | 1.55E+05 | Mass Flow tube 4 Monitor (kg/s) | -1.77 | Pressure Static tube 4end Monitor (Pa) | 7.66E+04 |
| PressureMassFlowAveLEE1end Monitor (Pa) | 1.91E+05 | Mass Flow tube 5 Monitor (kg/s) | -1.76 | Pressure Static tube 5 Monitor (Pa) | 1.09E+05 |
| PressurMassFlowAvedistributor1 Monitor (Pa) | 1.97E+05 | Mass Flow tube 6 Monitor (kg/s) | 1.76 | Pressure Static tube 5end Monitor (Pa) | 7.80E+04 |
| PressurMassFlowAvedistributor2 Monitor (Pa) | 1.77E+05 | Mass Flow tube 7 Monitor (kg/s) | -1.89 | Pressure Static tube 6 Monitor (Pa) | 2.40E+04 |
| 1_pressure diff inlet-sbendinlet Monitor | 1.47E+03 | Mass Flow tube 8 Monitor (kg/s) | 1.89 | Pressure Static tube 6end Monitor (Pa) | 5.37E+04 |
| 2_pressure diff sbendinlet-manifoldinletend2 Monitor | 7.38E+04 | | | Pressure Static tube 7 Monitor (Pa) | 1.07E+05 |
| 2b_pressure diff sbendinlet-LEE2 Monitor | 5.31E+04 | | | Pressure Static tube 7end Monitor (Pa) | 7.03E+04 |

| | | | | | |
|---|---|---|---|---|---|
| 3_pressure diff manifoldinletend2-distributor1 Monitor | 1.55E+03 | | | Pressure Static tube 8 Monitor (Pa) | 2.61E+04 |
| 3b_pressure diff LEE2-LEE1 Monitor | 8.46E+04 | | | Pressure Static tube 8end Monitor (Pa) | 6.15E+04 |
| 4_pressure diff distributor1-distributor2 Monitor | 2.37E+04 | | | PressureInlet Monitor 2 (Pa) | 1.62E+05 |
| 4b_pressure diff LEE1-sbendoutlet Monitor | 2.16E+04 | | | PressureOutlet Monitor 2 (Pa) | -1.19E-03 |
| 5_pressure diff distributor2-manifoldoutletend2 Monitor | 5.15E+04 | | | PressureSbendinlet Monitor (Pa) | 1.61E+05 |
| 6_pressure diff manifoldoutletend2-sbendoutlet Monitor | 8.80E+03 | | | PressureSbendoutlet Monitor (Pa) | 1.26E+03 |
| 7_pressure diff sbendoutlet-outlet Monitor | 1.26E+03 | | | Pressure Static manifoldinletend2 (Pa) | 8.68E+04 |

*Table 64 Complete results: CFD entire neutralizer, 17.7kg/s at inlet, 0bar outlet. Fluid cells, 73 million*

| Iteration | 2045 | Iteration | 2045 | Iteration | 2045 |
|---|---|---|---|---|---|
| c1 1 Monitor (kg/s) | -0.09 | l1 1 Monitor (kg/s) | -0.09 | h1 1 Monitor (kg/s) | -0.23 |
| c1 3 Monitor (kg/s) | -0.09 | l1 3 Monitor (kg/s) | -0.09 | h1 3 Monitor (kg/s) | -0.23 |
| c1 5 Monitor (kg/s) | -0.09 | l1 5 Monitor (kg/s) | -0.09 | h1 5 Monitor (kg/s) | -0.23 |
| c1 7 Monitor (kg/s) | -0.09 | l1 7 Monitor (kg/s) | -0.09 | h1 7 Monitor (kg/s) | -0.23 |
| c1 9 Monitor (kg/s) | -0.09 | l1 9 Monitor (kg/s) | -0.09 | h1 9 Monitor (kg/s) | -0.23 |
| c1 11 Monitor (kg/s) | -0.09 | l1 11 Monitor (kg/s) | -0.09 | h1 11 Monitor (kg/s) | -0.22 |
| c1 13 Monitor (kg/s) | -0.09 | l1 13 Monitor (kg/s) | -0.09 | h1 13 Monitor (kg/s) | -0.20 |
| c1 15 Monitor (kg/s) | -0.08 | l1 15 Monitor (kg/s) | -0.08 | h1 15 Monitor (kg/s) | -0.18 |
| c1 17 Monitor (kg/s) | -0.09 | l1 17 Monitor (kg/s) | -0.09 | h1 17 Monitor (kg/s) | -0.22 |
| c1 19 Monitor (kg/s) | -0.09 | l1 19 Monitor (kg/s) | -0.09 | h1 19 Monitor (kg/s) | -0.22 |
| c1 21 Monitor (kg/s) | -0.09 | l1 21 Monitor (kg/s) | -0.09 | h1 21 Monitor (kg/s) | -0.21 |
| c1 23 Monitor (kg/s) | -0.09 | l1 23 Monitor (kg/s) | -0.09 | h1 23 Monitor (kg/s) | -0.21 |
| c1 25 Monitor (kg/s) | -0.09 | l1 25 Monitor (kg/s) | -0.09 | h1 25 Monitor (kg/s) | -0.21 |
| | | | | | |
| Iteration | 2045 | Iteration | 2045 | Iteration | 2045 |
| c2 1 Monitor (kg/s) | -0.09 | l2 1 Monitor (kg/s) | -0.09 | h2 1 Monitor (kg/s) | -0.23 |
| c2 3 Monitor (kg/s) | -0.09 | l2 3 Monitor (kg/s) | -0.09 | h2 3 Monitor (kg/s) | -0.23 |
| c2 5 Monitor (kg/s) | -0.09 | l2 5 Monitor (kg/s) | -0.09 | h2 5 Monitor (kg/s) | -0.23 |
| c2 7 Monitor (kg/s) | -0.09 | l2 7 Monitor (kg/s) | -0.09 | h2 7 Monitor (kg/s) | -0.22 |
| c2 9 Monitor (kg/s) | -0.09 | l2 9 Monitor (kg/s) | -0.09 | h2 9 Monitor (kg/s) | -0.23 |
| c2 11 Monitor (kg/s) | -0.09 | l2 11 Monitor (kg/s) | -0.09 | h2 11 Monitor (kg/s) | -0.22 |
| c2 13 Monitor (kg/s) | -0.09 | l2 13 Monitor (kg/s) | -0.09 | h2 13 Monitor (kg/s) | -0.20 |
| c2 15 Monitor (kg/s) | -0.08 | l2 15 Monitor (kg/s) | -0.08 | h2 15 Monitor (kg/s) | -0.19 |
| c2 17 Monitor (kg/s) | -0.09 | l2 17 Monitor (kg/s) | -0.09 | h2 17 Monitor (kg/s) | -0.22 |
| c2 19 Monitor (kg/s) | -0.09 | l2 19 Monitor (kg/s) | -0.09 | h2 19 Monitor (kg/s) | -0.21 |
| c2 21 Monitor (kg/s) | -0.09 | l2 21 Monitor (kg/s) | -0.09 | h2 21 Monitor (kg/s) | -0.21 |
| c2 23 Monitor (kg/s) | -0.09 | l2 23 Monitor (kg/s) | -0.09 | h2 23 Monitor (kg/s) | -0.21 |
| c2 25 Monitor (kg/s) | -0.09 | l2 25 Monitor (kg/s) | -0.09 | h2 25 Monitor (kg/s) | -0.21 |

*Table 65 Mass flow in panel channels. Complete results: CFD entire neutralizer, 17.7kg/s at inlet, 0bar outlet. Fluid cells, 73 million*

## CtFD 94 million cells in fluid 17.7kg/s at inlet, 0bar outlet

Total number of cells in solid: 22895762

Total number of cells in fluid: 93764265

| | | | | |
|---|---|---|---|---|
| pressure drop sui singoli LEE e sul totale | | | | |

| | | Iteration | 2000 | Iteration | 2000 |
|---|---|---|---|---|---|
| | | Mass Flow tube 1 Monitor (kg/s) | 1.93 | Pressure Static distributor1 Monitor (Pa) | 1.02E+05 |
| | | Mass Flow Inlet Monitor 2 (kg/s) | -17.70 | Pressure Static distributor1b Monitor (Pa) | 1.02E+05 |
| | | Mass Flow Outlet Monitor 2 (kg/s) | 17.69 | Pressure Static distributor2 Monitor (Pa) | 7.83E+04 |
| | | Mass Flow tube 2 Monitor (kg/s) | -1.93 | Pressure Static distributor2b Monitor (Pa) | 7.83E+04 |
| | | Mass Flow manifold outlet end3 Monitor (kg/s) | 10.24 | Pressure Static manifold inlet end Monitor (Pa) | 1.26E+05 |
| | | Mass Flow tube 2 end Monitor (kg/s) | -1.93 | Pressure Static manifold outlet end1 Monitor (Pa) | 1.37E+04 |
| | | Mass Flow distributor1b Monitor (kg/s) | -5.11 | Pressure Static manifold outlet end2 Monitor (Pa) | 1.54E+04 |
| | | Mass Flow manifold inlet end Monitor (kg/s) | -10.25 | Pressure Static manifold outlet end3 Monitor (Pa) | 2.73E+04 |
| | | Mass Flow distributor2b Monitor (kg/s) | 5.13 | Pressure Static tube 1 Monitor (Pa) | 2.80E+04 |
| | | Mass Flow tube 1 end Monitor (kg/s) | 1.93 | Pressure Static tube 1end Monitor (Pa) | 7.40E+04 |
| | | Mass Flow manifold outlet end Monitor (kg/s) | 10.24 | Pressure Static tube 2 Monitor (Pa) | 1.30E+05 |
| | | Mass Flow distributor2 Monitor (kg/s) | 5.12 | Pressure Static tube 2end Monitor (Pa) | 8.49E+04 |
| | | Mass Flow distributor1 Monitor (kg/s) | -5.14 | Pressure Static tube 3 Monitor (Pa) | 3.32E+04 |
| | | Mass Flow tube 3 end Monitor (kg/s) | 1.80 | Pressure Static tube 3end Monitor (Pa) | 7.31E+04 |
| Pressure Drop IO Monitor 2 (Pa) | 1.90E+05 | Mass Flow tube 3 Monitor (kg/s) | 1.80 | Pressure Static tube 4 Monitor (Pa) | 1.35E+05 |
| PressureMassFlowAveLEE1 Monitor (Pa) | 1.61E+05 | Mass Flow tube 4 Monitor (kg/s) | -1.80 | Pressure Static tube 4end Monitor (Pa) | 9.55E+04 |
| PressureMassFlowAveLEE1end Monitor (Pa) | 2.06E+05 | Mass Flow tube 5 Monitor (kg/s) | -1.82 | Pressure Static tube 5 Monitor (Pa) | 1.32E+05 |
| PressurMassFlowAvedistributor1 Monitor (Pa) | 2.14E+05 | Mass Flow tube 6 Monitor (kg/s) | 1.82 | Pressure Static tube 5end Monitor (Pa) | 9.10E+04 |
| PressurMassFlowAvedistributor2 Monitor (Pa) | 1.95E+05 | Mass Flow tube 7 Monitor (kg/s) | -1.90 | Pressure Static tube 6 Monitor (Pa) | 2.79E+04 |
| 1_pressure diff inlet-sbendinlet Monitor | 1.81E+03 | Mass Flow tube 8 Monitor (kg/s) | 1.90 | Pressure Static tube 6end Monitor (Pa) | 6.73E+04 |
| 2_pressure diff sbendinlet-manifoldinletend2 Monitor | 7.72E+04 | | | Pressure Static tube 7 Monitor (Pa) | 1.31E+05 |
| 2b_pressure diff sbendinlet-LEE2 Monitor | 5.83E+04 | | | Pressure Static tube 7end Monitor (Pa) | 8.94E+04 |
| 3_pressure diff manifoldinletend2-distributor1 Monitor | 9.41E+03 | | | Pressure Static tube 8 Monitor (Pa) | 3.55E+04 |
| 3b_pressure diff LEE2-LEE1 Monitor | 1.02E+05 | | | Pressure Static tube 8end Monitor (Pa) | 7.90E+04 |
| 4_pressure diff distributor1-distributor2 Monitor | 2.36E+04 | | | PressureInlet Monitor 2 (Pa) | 1.90E+05 |

| | | | | | |
|---|---|---|---|---|---|
| 4b_pressure diff LEE1-sbendoutlet Monitor | 2.68E+04 | | | PressureOutlet Monitor 2 (Pa) | 0.00E+00 |
| 5_pressure diff distributor2-manifoldoutletend2 Monitor | 6.29E+04 | | | PressureSbendinlet Monitor (Pa) | 1.89E+05 |
| 6_pressure diff manifoldoutletend2-sbendoutlet Monitor | 1.41E+04 | | | PressureSbendoutlet Monitor (Pa) | 1.28E+03 |
| 7_pressure diff sbendoutlet-outlet Monitor | 1.28E+03 | | | Pressure Static manifoldinletend2 (Pa) | 1.11E+05 |

*Table 66 Complete results: CFD entire neutralizer, 17.7kg/s at inlet, 0bar outlet. Fluid cells, 94 million*

| 2000 | Iteration | 2000 | Iteration | 2000 |
|---|---|---|---|---|
| -0.09 | l1 1 Monitor (kg/s) | -0.09 | h1 1 Monitor (kg/s) | -0.23 |
| -0.09 | l1 3 Monitor (kg/s) | -0.09 | h1 3 Monitor (kg/s) | -0.22 |
| -0.09 | l1 5 Monitor (kg/s) | -0.09 | h1 5 Monitor (kg/s) | -0.22 |
| -0.09 | l1 7 Monitor (kg/s) | -0.09 | h1 7 Monitor (kg/s) | -0.22 |
| -0.09 | l1 9 Monitor (kg/s) | -0.09 | h1 9 Monitor (kg/s) | -0.22 |
| -0.09 | l1 11 Monitor (kg/s) | -0.09 | h1 11 Monitor (kg/s) | -0.22 |
| -0.09 | l1 13 Monitor (kg/s) | -0.09 | h1 13 Monitor (kg/s) | -0.19 |
| -0.08 | l1 15 Monitor (kg/s) | -0.08 | h1 15 Monitor (kg/s) | -0.18 |
| -0.09 | l1 17 Monitor (kg/s) | -0.09 | h1 17 Monitor (kg/s) | -0.21 |
| -0.09 | l1 19 Monitor (kg/s) | -0.09 | h1 19 Monitor (kg/s) | -0.21 |
| -0.09 | l1 21 Monitor (kg/s) | -0.09 | h1 21 Monitor (kg/s) | -0.21 |
| -0.09 | l1 23 Monitor (kg/s) | -0.09 | h1 23 Monitor (kg/s) | -0.21 |
| -0.09 | l1 25 Monitor (kg/s) | -0.09 | h1 25 Monitor (kg/s) | -0.21 |
| | | | | |
| 2000 | Iteration | 2000 | Iteration | 2000 |
| -0.09 | l2 1 Monitor (kg/s) | -0.09 | h2 1 Monitor (kg/s) | -0.22 |
| -0.09 | l2 3 Monitor (kg/s) | -0.09 | h2 3 Monitor (kg/s) | -0.23 |
| -0.09 | l2 5 Monitor (kg/s) | -0.09 | h2 5 Monitor (kg/s) | -0.22 |
| -0.09 | l2 7 Monitor (kg/s) | -0.09 | h2 7 Monitor (kg/s) | -0.22 |
| -0.09 | l2 9 Monitor (kg/s) | -0.09 | h2 9 Monitor (kg/s) | -0.22 |
| -0.09 | l2 11 Monitor (kg/s) | -0.09 | h2 11 Monitor (kg/s) | -0.22 |
| -0.09 | l2 13 Monitor (kg/s) | -0.09 | h2 13 Monitor (kg/s) | -0.19 |
| -0.08 | l2 15 Monitor (kg/s) | -0.08 | h2 15 Monitor (kg/s) | -0.18 |
| -0.09 | l2 17 Monitor (kg/s) | -0.09 | h2 17 Monitor (kg/s) | -0.21 |
| -0.09 | l2 19 Monitor (kg/s) | -0.09 | h2 19 Monitor (kg/s) | -0.21 |
| -0.09 | l2 21 Monitor (kg/s) | -0.09 | h2 21 Monitor (kg/s) | -0.21 |
| -0.09 | l2 23 Monitor (kg/s) | -0.09 | h2 23 Monitor (kg/s) | -0.21 |
| -0.09 | l2 25 Monitor (kg/s) | -0.09 | h2 25 Monitor (kg/s) | -0.21 |

*Table 67 Mass flow in panel channels. Complete results: CFD entire neutralizer, 17.7kg/s at inlet, 0bar outlet. Fluid cells, 94 million*

## Mesh convergence for 4 entire models of the neutralizer

With the notation introduced, the 4 different models are listed. All the models have the same BCs and materials of 2.1.3. Entire neutralizer: total mass flow and real BCs calculation. A CtFD model is added too, with the same pressure conditions (thermal BCs and results for this are omitted, since not relevant for the purpose of this analysis).

| | CFD | CFD | CtFD | CFD |
|---|---|---|---|---|
| Notes on the meshes | | | Finer areas for manifold and distributors, coarser for panels and remaining parts | Finer areas everywhere, but manifolds are slightly coarser with respect to CtFD |
| Number of cells in fluid | 4.40E+07 | 7.33E+07 | 9.38E+07 | 1.75E+08 |

| pressure drop (bar) | | | | |
|---|---|---|---|---|
| inlet-sbendinlet | 0.02 | 0.01 | 0.02 | 0.02 |
| sbendinlet-manifoldinletend2 | 0.71 | 0.74 | 0.77 | 0.68 |
| manifoldinletend2-distributor1 | 0.02 | 0.02 | 0.09 | 0.11 |
| distributor1-distributor2 | 0.24 | 0.24 | 0.24 | 0.23 |
| distributor2-manifoldoutletend2 | 0.61 | 0.52 | 0.63 | 0.67 |
| manifoldoutletend2-sbendoutlet | 0.10 | 0.09 | 0.14 | 0.07 |
| sbendoutlet-outlet | 0.01 | 0.01 | 0.01 | 0.02 |
| | | | | |
| sbendinlet-tube2 | 0.55 | 0.53 | 0.58 | 0.52 |
| tube2-tube1 | 0.91 | 0.85 | 1.02 | 0.96 |
| tube1-sbendoutlet | 0.22 | 0.22 | 0.27 | 0.27 |
| | | | | |
| pressure drop IO | 1.71 | 1.62 | 1.90 | 1.79 |
| MASS FLOWS (kg/s) | | | | |
| mass flow LEE 2 | -1.92 | -1.89 | -1.93 | -1.89 |
| h2 15 Monitor (kg/s) | -0.19 | -0.19 | -0.18 | -0.19 |

*Table 68 Mesh convergence for 4 entire model of the neutralizer*

## 2.2. Design verification

### CtFD 94 million cells in fluid, 17.7kg/s at inlet 20.21bar at outlet

| pressure drop sui singoli LEE e sul totale | | | | | |
|---|---|---|---|---|---|
| Iteration | 2000 | Iteration | 2000 | Iteration | 2000 |
| Pressure Drop IO Monitor (Pa) | 1.78E+05 | Mass Flow tube 1 Monitor (kg/s) | 1.93 | Pressure Static distributor1 Monitor (Pa) | 2.12E+06 |
| Pressure Drop inlet-outlet Monitor | 1.78E+05 | Mass Flow Inlet Monitor 2 (kg/s) | -17.70 | Pressure Static distributor1b Monitor (Pa) | 2.12E+06 |
| Pressure Drop tube 1 Monitor | 4.28E+04 | Mass Flow Outlet Monitor 2 (kg/s) | 17.70 | Pressure Static distributor2 Monitor (Pa) | 2.09E+06 |
| Pressure Drop tube 2 Monitor | 4.05E+04 | Mass Flow tube 2 Monitor (kg/s) | -1.93 | Pressure Static distributor2b Monitor (Pa) | 2.09E+06 |
| Pressure Drop tube 3 Monitor | 3.40E+04 | Mass Flow manifold outlet end3 Monitor (kg/s) | 10.24 | Pressure Static manifold inlet end Monitor (Pa) | 2.14E+06 |
| Pressure Drop tube 4 Monitor | 3.58E+04 | Mass Flow tube 2 end Monitor (kg/s) | -1.92 | Pressure Static manifold outlet end1 Monitor (Pa) | 2.03E+06 |
| Pressure Drop tube 5 Monitor | 3.83E+04 | Mass Flow distributor1b Monitor (kg/s) | -5.11 | Pressure Static manifold outlet end2 Monitor (Pa) | 2.03E+06 |
| Pressure Drop tube 6 Monitor | 3.47E+04 | Mass Flow manifold inlet end Monitor (kg/s) | -10.23 | Pressure Static manifold outlet end3 Monitor (Pa) | 2.04E+06 |
| Pressure Drop tube 7 Monitor | 3.86E+04 | Mass Flow distributor2b Monitor (kg/s) | 5.12 | Pressure Static tube 1 Monitor (Pa) | 2.05E+06 |

| | | | | | |
|---|---|---|---|---|---|
| Pressure Drop tube 8 Monitor | 3.94E+04 | Mass Flow tube 1 end Monitor (kg/s) | 1.92 | Pressure Static tube 1end Monitor (Pa) | 2.09E+06 |
| | | Mass Flow manifold outlet end Monitor (kg/s) | 10.23 | Pressure Static tube 2 Monitor (Pa) | 2.14E+06 |
| | | Mass Flow distributor2 Monitor (kg/s) | 5.12 | Pressure Static tube 2end Monitor (Pa) | 2.10E+06 |
| | | Mass Flow distributor1 Monitor (kg/s) | -5.12 | Pressure Static tube 3 Monitor (Pa) | 2.05E+06 |
| Iteration | 2000 | Mass Flow tube 3 end Monitor (kg/s) | 1.81 | Pressure Static tube 3end Monitor (Pa) | 2.09E+06 |
| Pressure Drop IO Monitor 2 (Pa) | 1.78E+05 | Mass Flow tube 3 Monitor (kg/s) | 1.81 | Pressure Static tube 4 Monitor (Pa) | 2.14E+06 |
| PressureMassFlowAveLEE1 Monitor (Pa) | 2.18E+06 | Mass Flow tube 4 Monitor (kg/s) | -1.80 | Pressure Static tube 4end Monitor (Pa) | 2.11E+06 |
| PressureMassFlowAveLEE1end Monitor (Pa) | 2.22E+06 | Mass Flow tube 5 Monitor (kg/s) | -1.82 | Pressure Static tube 5 Monitor (Pa) | 2.14E+06 |
| PressurMassFlowAvedistributor1 Monitor (Pa) | 2.23E+06 | Mass Flow tube 6 Monitor (kg/s) | 1.82 | Pressure Static tube 5end Monitor (Pa) | 2.10E+06 |
| PressurMassFlowAvedistributor2 Monitor (Pa) | 2.21E+06 | Mass Flow tube 7 Monitor (kg/s) | -1.91 | Pressure Static tube 6 Monitor (Pa) | 2.05E+06 |
| | | Mass Flow tube 8 Monitor (kg/s) | 1.91 | Pressure Static tube 6end Monitor (Pa) | 2.08E+06 |
| | | | | Pressure Static tube 7 Monitor (Pa) | 2.14E+06 |
| | | | | Pressure Static tube 7end Monitor (Pa) | 2.10E+06 |
| | | | | Pressure Static tube 8 Monitor (Pa) | 2.05E+06 |
| | | | | Pressure Static tube 8end Monitor (Pa) | 2.09E+06 |
| | | | | PressureInlet Monitor 2 (Pa) | 2.20E+06 |
| | | | | PressureOutlet Monitor 2 (Pa) | 2.02E+06 |
| | | | | PressureSbendinlet Monitor (Pa) | 2.20E+06 |
| | | | | PressureSbendoutlet Monitor (Pa) | 2.02E+06 |
| | | | | Pressure Static manifoldinletend2 (Pa) | 2.13E+06 |

*Table 69 Complete results: CFD entire neutralizer, 17.7kg/s at inlet, 20.21bar outlet. Fluid cells, 94 million*

| Iteration | 2000.00 | Iteration | 2000.00 | Iteration | 2000.00 |
|---|---|---|---|---|---|
| c1 1 Monitor (kg/s) | -0.09 | l1 1 Monitor (kg/s) | -0.09 | h1 1 Monitor (kg/s) | -0.22 |
| c1 3 Monitor (kg/s) | -0.09 | l1 3 Monitor (kg/s) | -0.09 | h1 3 Monitor (kg/s) | -0.22 |
| c1 5 Monitor (kg/s) | -0.09 | l1 5 Monitor (kg/s) | -0.09 | h1 5 Monitor (kg/s) | -0.22 |
| c1 7 Monitor (kg/s) | -0.09 | l1 7 Monitor (kg/s) | -0.09 | h1 7 Monitor (kg/s) | -0.22 |
| c1 9 Monitor (kg/s) | -0.09 | l1 9 Monitor (kg/s) | -0.09 | h1 9 Monitor (kg/s) | -0.22 |

| | | | | | |
|---|---|---|---|---|---|
| c1 11 Monitor (kg/s) | -0.09 | l1 11 Monitor (kg/s) | -0.09 | h1 11 Monitor (kg/s) | -0.22 |
| c1 13 Monitor (kg/s) | -0.08 | l1 13 Monitor (kg/s) | -0.08 | h1 13 Monitor (kg/s) | -0.19 |
| c1 15 Monitor (kg/s) | -0.08 | l1 15 Monitor (kg/s) | -0.08 | h1 15 Monitor (kg/s) | -0.18 |
| c1 17 Monitor (kg/s) | -0.09 | l1 17 Monitor (kg/s) | -0.09 | h1 17 Monitor (kg/s) | -0.21 |
| c1 19 Monitor (kg/s) | -0.09 | l1 19 Monitor (kg/s) | -0.09 | h1 19 Monitor (kg/s) | -0.21 |
| c1 21 Monitor (kg/s) | -0.09 | l1 21 Monitor (kg/s) | -0.09 | h1 21 Monitor (kg/s) | -0.21 |
| c1 23 Monitor (kg/s) | -0.09 | l1 23 Monitor (kg/s) | -0.09 | h1 23 Monitor (kg/s) | -0.21 |
| c1 25 Monitor (kg/s) | -0.09 | l1 25 Monitor (kg/s) | -0.09 | h1 25 Monitor (kg/s) | -0.21 |
| | | | | | |
| Iteration | 2000.00 | Iteration | 2000.00 | Iteration | 2000.00 |
| c2 1 Monitor (kg/s) | -0.09 | l2 1 Monitor (kg/s) | -0.09 | h2 1 Monitor (kg/s) | -0.22 |
| c2 3 Monitor (kg/s) | -0.09 | l2 3 Monitor (kg/s) | -0.09 | h2 3 Monitor (kg/s) | -0.22 |
| c2 5 Monitor (kg/s) | -0.09 | l2 5 Monitor (kg/s) | -0.09 | h2 5 Monitor (kg/s) | -0.22 |
| c2 7 Monitor (kg/s) | -0.09 | l2 7 Monitor (kg/s) | -0.09 | h2 7 Monitor (kg/s) | -0.22 |
| c2 9 Monitor (kg/s) | -0.09 | l2 9 Monitor (kg/s) | -0.09 | h2 9 Monitor (kg/s) | -0.22 |
| c2 11 Monitor (kg/s) | -0.09 | l2 11 Monitor (kg/s) | -0.09 | h2 11 Monitor (kg/s) | -0.22 |
| c2 13 Monitor (kg/s) | -0.09 | l2 13 Monitor (kg/s) | -0.09 | h2 13 Monitor (kg/s) | -0.20 |
| c2 15 Monitor (kg/s) | -0.08 | l2 15 Monitor (kg/s) | -0.08 | h2 15 Monitor (kg/s) | -0.18 |
| c2 17 Monitor (kg/s) | -0.09 | l2 17 Monitor (kg/s) | -0.09 | h2 17 Monitor (kg/s) | -0.21 |
| c2 19 Monitor (kg/s) | -0.09 | l2 19 Monitor (kg/s) | -0.09 | h2 19 Monitor (kg/s) | -0.21 |
| c2 21 Monitor (kg/s) | -0.09 | l2 21 Monitor (kg/s) | -0.09 | h2 21 Monitor (kg/s) | -0.21 |
| c2 23 Monitor (kg/s) | -0.09 | l2 23 Monitor (kg/s) | -0.09 | h2 23 Monitor (kg/s) | -0.21 |
| c2 25 Monitor (kg/s) | -0.09 | l2 25 Monitor (kg/s) | -0.09 | h2 25 Monitor (kg/s) | -0.21 |

*Table 70 Mass flow in panel channels. Complete results: CFD entire neutralizer, 17.7kg/s at inlet, 20.21bar outlet. Fluid cells, 94 million*

## Percentage error between CFD 175 million cells, 0bar at the outlet and CtFD with 94 million cells in fluid region at 20.21bar outlet

| LEE | | |
|---|---|---|
| | Static pressure difference (Pa) | Mass Flows (kg/s) |
| tube2 | -4.1% | 1.9% |
| tube2end | -6.3% | 1.7% |
| tube1 | -6.5% | |

*Table 71 Percentage error for LEE2: results from entire CFD 175million cells vs CtFD 94million cells*

| | Central2 | | Halfway 2 | | Lateral 1 | |
|---|---|---|---|---|---|---|
| | Static pressure difference (Pa) | Mass Flows (kg/s) | Static pressure difference (Pa) | Mass Flows (kg/s) | Static pressure difference (Pa) | Mass Flows (kg/s) |
| top1 | -4.2% | 1.0% | -4.2% | -5.7% | -3.3% | 3.4% |
| top2 | -4.2% | 3.5% | -4.1% | -5.2% | -3.5% | 4.5% |
| top3 | -3.9% | 1.1% | -3.9% | -5.6% | -3.4% | 3.8% |
| top4 | -3.9% | 2.0% | -3.9% | -5.3% | -3.5% | 2.5% |
| top5 | -3.9% | 2.2% | -3.9% | -5.9% | -3.3% | 4.0% |
| top6 | -3.9% | 1.7% | -3.9% | -5.4% | -3.4% | 2.4% |
| top7 | -4.1% | 1.5% | -4.2% | -5.0% | -3.4% | 2.0% |
| top8 | -4.1% | 0.7% | -4.1% | -4.7% | -3.5% | 3.9% |

| | | | | | | |
|---|---|---|---|---|---|---|
| top9 | -3.9% | 1.1% | -3.9% | -4.7% | -3.3% | 3.6% |
| top10 | -4.0% | 2.2% | -4.0% | -4.9% | -3.5% | 3.3% |
| top11 | -4.0% | 1.6% | -3.8% | -3.1% | -3.5% | 3.7% |
| top12 | -4.0% | -0.1% | -3.9% | -3.4% | -3.6% | 5.0% |
| top13 | -4.3% | 2.0% | -4.2% | -1.4% | -3.5% | 1.7% |
| top14 | -4.1% | -2.7% | -4.1% | -2.3% | -3.5% | -0.6% |
| top15 | -3.8% | 2.3% | -3.7% | -1.6% | -3.6% | 0.3% |
| top16 | -3.9% | -0.2% | -3.9% | -2.3% | -3.5% | 0.9% |
| top17 | -3.9% | 2.1% | -3.9% | -4.1% | -3.6% | 1.7% |
| top18 | -3.9% | 0.9% | -4.0% | -4.6% | -3.6% | 2.3% |
| top19 | -3.9% | 2.5% | -4.0% | -4.2% | -3.6% | 2.6% |
| top20 | -3.9% | 2.5% | -3.9% | -3.7% | -3.6% | 0.9% |
| top21 | -3.9% | 0.1% | -3.9% | -1.9% | -3.5% | 2.3% |
| top22 | -4.0% | -0.1% | -4.0% | -3.7% | -3.6% | 1.2% |
| top23 | -4.0% | 1.5% | -4.0% | -5.6% | -3.4% | 3.5% |
| top24 | -4.0% | 3.9% | -4.0% | -5.1% | -3.5% | 4.2% |
| top25 | -3.9% | 0.9% | -3.9% | -4.6% | -3.9% | 4.8% |
| top26 | -3.9% | 2.7% | -3.9% | -4.8% | -3.7% | -1.7% |

*Table 72 Percentage error for panels: results from entire CFD 175million cells vs CtFD 94million cells*

## Direct comparison for panels between the 3 models

| | Halfway2 standalone | Halfway2 da CFD a 175 milioni di celle | Halfway2 da CFTD a 94 milioni di celle | |
|---|---|---|---|---|
| **Static Pressure difference (surface averaged) (Pa)** | | | | |
| top hole 1-2 | 1.86E+03 | 1.93E+03 | 1.73E+03 | Pa |
| top hole 3-4 | 1.91E+03 | 1.90E+03 | 1.83E+03 | Pa |
| top hole 5-6 | 1.95E+03 | 1.88E+03 | 1.82E+03 | Pa |
| top hole 7-8 | 1.81E+03 | 1.81E+03 | 1.63E+03 | Pa |
| top hole 9-10 | 1.84E+03 | 1.83E+03 | 1.82E+03 | Pa |
| top hole 11-12 | 1.87E+03 | 1.86E+03 | 1.87E+03 | Pa |
| top hole 13-14 | 1.51E+03 | 1.64E+03 | 1.46E+03 | Pa |
| top hole 15-16 | 1.39E+03 | 1.31E+03 | 1.46E+03 | Pa |
| top hole 17-18 | 1.80E+03 | 1.81E+03 | 1.78E+03 | Pa |
| top hole 19-20 | 1.83E+03 | 1.88E+03 | 1.78E+03 | Pa |
| top hole 21-22 | 1.85E+03 | 1.84E+03 | 1.84E+03 | Pa |
| top hole 23-24 | 1.87E+03 | 1.93E+03 | 1.85E+03 | Pa |
| top hole 25-26 | 1.90E+03 | 1.95E+03 | 1.82E+03 | Pa |
| **Temperature (bulk, mass flow averaged) (K)** | | | | |
| Temperature2 | 327.45 | | 329.22 | K |
| Temperature4 | 325.92 | | 327.82 | K |
| Temperature6 | 326.97 | | 329.10 | K |
| Temperature8 | 322.44 | | 323.56 | K |
| Temperature10 | 322.12 | | 322.93 | K |
| Temperature12 | 322.32 | | 323.33 | K |
| Temperature14 | 322.82 | | 323.48 | K |
| Temperature16 | 322.67 | | 323.43 | K |
| Temperature18 | 321.59 | | 322.51 | K |
| Temperature20 | 321.28 | | 322.07 | K |
| Temperature22 | 318.54 | | 319.38 | K |

| | | | | |
|---|---|---|---|---|
| Temperature24 | 317.52 | | 318.12 | K |
| Temperature26 | 322.78 | | 319.98 | K |
| **Temperature** | | | | |
| Temperature (maximum in fluid) | 381.11 | K | 378.88 | K |
| Temperature (maximum in solid) | 396.74 | K | 394.89 | K |
| Temperature (surface averaged in solid) | 352.45 | K | | |

*Table 73 Halfway 2. Main thermal and fluid dynamic results: comparison between standalone, CFD, CtFD model*

| | central2 standalone | central2 da CFD a 175 milioni di celle | central2 da CFTD a 94 milioni di celle | |
|---|---|---|---|---|
| **Static Pressure difference (surface averaged)** | | | | |
| top hole 1-2 | 8.92E+02 | 4.78E+02 | 3.97E+02 | Pa |
| top hole 3-4 | 8.94E+02 | 4.93E+02 | 4.72E+02 | Pa |
| top hole 5-6 | 8.98E+02 | 4.58E+02 | 4.90E+02 | Pa |
| top hole 7-8 | 9.04E+02 | 4.64E+02 | 4.62E+02 | Pa |
| top hole 9-10 | 9.18E+02 | 4.48E+02 | 5.14E+02 | Pa |
| top hole 11-12 | 9.26E+02 | 5.67E+02 | 5.48E+02 | Pa |
| top hole 13-14 | 7.47E+02 | 7.07E+02 | 4.48E+02 | Pa |
| top hole 15-16 | 7.51E+02 | 3.90E+02 | 5.13E+02 | Pa |
| top hole 17-18 | 9.32E+02 | 5.24E+02 | 5.18E+02 | Pa |
| top hole 19-20 | 9.33E+02 | 5.64E+02 | 5.56E+02 | Pa |
| top hole 21-22 | 9.34E+02 | 5.77E+02 | 5.95E+02 | Pa |
| top hole 23-24 | 9.47E+02 | 5.78E+02 | 6.00E+02 | Pa |
| top hole 25-26 | 9.58E+02 | 6.27E+02 | 5.82E+02 | Pa |
| **Temperature (bulk, mass flow averaged) (K)** | | | | |
| Temperature2 | 335.37 | | 339.64 | K |
| Temperature4 | 336.13 | | 340.62 | K |
| Temperature6 | 339.43 | | 344.38 | K |
| Temperature8 | 332.45 | | 336.15 | K |
| Temperature10 | 337.60 | | 341.75 | K |
| Temperature12 | 336.15 | | 338.99 | K |
| Temperature14 | 337.26 | | 339.01 | K |
| Temperature16 | 334.44 | | 336.67 | K |
| Temperature18 | 332.87 | | 335.72 | K |
| Temperature20 | 334.07 | | 336.81 | K |
| Temperature22 | 331.14 | | 333.09 | K |
| Temperature24 | 328.21 | | 327.86 | K |
| Temperature26 | 334.54 | | 323.97 | K |
| **Temperature** | | | | |
| Temperature (maximum in fluid) | 402.76 | K | 401.14 | K |
| Temperature (maximum in solid) | 408.00 | K | 407.54 | K |
| Temperature (surface averaged in solid) | 364.13 | K | | |

*Table 74 Central 2. Main thermal and fluid dynamic results: comparison between standalone, CFD, CtFD models*

| | lateral1 standalone | lateral1 da CFD a 175 milioni di celle | lateral1 da CFTD a 94 milioni di celle | |
|---|---|---|---|---|
| **Static Pressure difference (surface averaged)** | | | | |
| top hole 1-2 | 8.88E+02 | 3.44E+02 | 5.17E+02 | Pa |
| top hole 3-4 | 8.90E+02 | 4.79E+02 | 5.11E+02 | Pa |
| top hole 5-6 | 9.00E+02 | 4.65E+02 | 5.12E+02 | Pa |

| | | | | |
|---|---|---|---|---|
| top hole 7-8 | 9.07E+02 | 4.61E+02 | 5.48E+02 | Pa |
| top hole 9-10 | 9.21E+02 | 4.16E+02 | 5.82E+02 | Pa |
| top hole 11-12 | 9.25E+02 | 4.88E+02 | 5.27E+02 | Pa |
| top hole 13-14 | 7.48E+02 | 5.90E+02 | 5.00E+02 | Pa |
| top hole 15-16 | 7.45E+02 | 5.01E+02 | 3.75E+02 | Pa |
| top hole 17-18 | 9.29E+02 | 5.45E+02 | 5.74E+02 | Pa |
| top hole 19-20 | 9.48E+02 | 6.15E+02 | 5.82E+02 | Pa |
| top hole 21-22 | 9.43E+02 | 5.81E+02 | 5.93E+02 | Pa |
| top hole 23-24 | 9.51E+02 | 4.65E+02 | 5.93E+02 | Pa |
| top hole 25-26 | 9.58E+02 | 8.10E+02 | 6.04E+02 | Pa |
| **Temperature (bulk, mass flow averaged) (K)** | | | | |
| Temperature2 | 330.35 | | 333.17 | K |
| Temperature4 | 335.61 | | 339.57 | K |
| Temperature6 | 337.29 | | 341.06 | K |
| Temperature8 | 334.35 | | 337.80 | K |
| Temperature10 | 337.10 | | 340.52 | K |
| Temperature12 | 334.79 | | 337.33 | K |
| Temperature14 | 334.49 | | 335.74 | K |
| Temperature16 | 331.94 | | 333.54 | K |
| Temperature18 | 331.97 | | 333.97 | K |
| Temperature20 | 332.35 | | 334.49 | K |
| Temperature22 | 329.24 | | 330.56 | K |
| Temperature24 | 328.84 | | 328.29 | K |
| Temperature26 | 335.61 | | 326.87 | K |
| **Temperature** | | | | |
| Temperature (maximum in fluid) | 396.81 | K | 395.38 | K |
| Temperature (maximum in solid) | 405.39 | K | 404.43 | K |
| Temperature (surface averaged in solid) | 361.85 | K | | |

*Table 75 Lateral 1. Main thermal and fluid dynamic results: comparison between standalone, CFD, CtFD model*

# References


[1] R. Martone, A. R. F. Crisanti, P. Martin and A. Pizzuto, "Divertor Tokamak Test facility Interim Design Report," ENEA, 2019.

[2] DTT S.c.a.r.l., "Technical summary of the injector for the DTT NBI system," 23 April 2021.

[3] SIEMENS, "SIEMENS Support Center," [Online]. Available: https://support.sw.siemens.com/en-US/product/226870983/knowledge-base/KB000034612_EN_US?pid=sc%3Apc-typeahead&index=content-external&audience=external.

[4] D. C. Wilcox, Turbulence Modeling for CFD, 2nd edition ed., DCW Industries Inc., 1998.

[5] F. R. Menter, Two-equation eddy-viscosity turbulence modeling for engineering applications, vol. 32(8), AIAA Journal, 1994, pp. 1598-1605.

[6] R. M. Manglik and A. E. Bergles, "Heat Transfer and Pressure Drop Correlations for Twisted-Tape Insertes in Isothermal Tubes: Part II-Transition and Turbulent Flows," 1993.

[7] B. R. Munson, T. H. Okiishi, W. W. Huebsch and A. P. Rothmayer, "Viscous Flow in Pipes," in *Fundamentals of Fluid Mechanics*, 7 ed., John Wiley & Sons, Inc., 2012, pp. 416-431.

[8] F. P. Incropera, D. DeWItt, T. L. Bergman and A. S. Lavine, "Internal Flow," in *Fundamentals of Heat and Mass Transfer*, 6 ed., John Wiley & Sons Inc., pp. 490-528.

[9] R. M. Manglik, "Heat Transfer Enhancement of Intube Flows in," Troy, NY, 1991.

[10] R. M. Manglik and A. E. Bergles, Heat Transfer Enhancement and Pressure Drop in Viscous Liquid Flows in Isothermal Tubes With Twisted-Tape Inserts, vol. 27, Warme-und Stoffubertragung, pp. 249-257.

[11] DTT S.c.a.r.l., "Structural design criteria for ITER in-vessell components (SDC-IC)".

[12] Y. A. Çengel and J. M. Cimbala, Fluid Mechanics, McGraw-Hill, 2006, p. 888.

[13] S. Ponnadaa, T. Subrahmanyam and S. Naidu, "A comparative study on the thermal performance of water in a circular tube with twisted tapes, perforated twisted tapes and perforated twisted tapes with alternate axis," *International Journal of Thermal Sciences 136 (2019) 530–538.*

[14] B. S. Petukhov, Advances in Heat Transfer, vol. 6, E. T. F. Irvine and J. P. Hartnett, Ed., New York: Academic Press, 1970.

[15] R. H. S. Winterton, Int. J. Heat Mass Transfer, 1998, p. 809.

[16] P. E. Shashi Menon, Piping Calculations Manual, McGraw-Hill, pp. 28-31.

[17] Neutrium, "https://neutrium.net/fluid-flow/pressure-loss-from-fittings-expansion-and-reduction-in-pipe-size/?web=1&wdLOR=c2171D5F8-4275-452F-A38D-CAC8DFD34C25," [Online].

[18] SIEMENS, "https://docs.sw.siemens.com/documentation/external/PL20201113103827399/en-US/userManual/userguide/html/index.html#page/STARCCMP%2FGUID-8275C96D-5FCB-4467-A139-70ADADACE8F3.html%23," [Online].

[19] T. Frank, C. Lifante, H. Prasser and F. Menter, "Simulation of turbulent and thermal mixing in T-junctions using URANS and scale-resolving turbulence models in ANSYS CFX," vol. 240, pp. 2313-2328, 2010.

[20] L. Xin and W. Shaoping, "Flow field and pressure loss analysis of junction and its structure optimization of aircraft hydraulic pipe systemChinese Journal of Aeronautics," *Chinese Journal of Aeronautics,* vol. 26, no. 4, pp. 1080-1092, 2013.

[21] M. Rossetto, C. Delprete, T. Berruti and E. Brusa, *Appunti per le lezioni di CM del corso di Elementi di costruzione e disegno di macchine,* 2019.

[22] B. A. D. and D. Allan, "10.7.3 Twisted-Tape Inserts," in *Heat Transfer Handbook*, John Wiley & Sons, 2003.

[23] ASHRAE, ASHRAE Handbook - Fundamentals (SI Edition), American Society of Heating, Refrigerating and Air-Conditioning Engineers, Inc. (ASHRAE), 2013.

[24] "www.synecom.it," [Online]. Available: https://www.synecom.it/en/nuclear-fusion-project-by-iter/.

[25] R. Manglik, "503.10.5.2 Turbulent Flow," in *Heat Transfer and Fluid Flow Data Books*, Genium Publishing Corporation, 1980, pp. 21-34.

[26] S. H., Boundary-Layer Theory, McGraw-Hill.

[27] S. P. S. 2019.3, "Simcenter STAR-CCM+®," SIEMENS, 2019.

[28] "www.dtt-project.it," [Online]. Available: https://www.dtt-project.it/index.php.

[29] "www.iter.org," [Online]. Available: https://www.iter.org/.